JOURNAL OF SCIENCE

PART A: ENGINEERING AND INNOVATION

Year | Yıl: 2021 **Volume | Cilt: 8** **Issue | Sayı: 4**

e-ISSN 2147-9542

Gazi University
Journal of Science
PART A: ENGINEERING AND INNOVATION

e-ISSN 2147-9542

YEAR YIL 2021 VOLUME CİLT 8 ISSUE SAYI 4

Gazi University
Journal of Science
PART A: ENGINEERING AND INNOVATION

e-ISSN 2147-9542

YEAR YIL 2021 VOLUME CİLT 8 ISSUE SAYI 4

Editorial Board | Editörler Kurulu

Gazi University
Journal of Science
PART A: ENGINEERING AND INNOVATION

e-ISSN 2147-9542

YEAR YIL 2021 VOLUME CİLT 8 ISSUE SAYI 4

Editorial Board | Editörler Kurulu

Gazi University
Journal of Science
PART A: ENGINEERING AND INNOVATION

e-ISSN 2147-9542

YEAR YIL 2021 VOLUME CİLT 8 ISSUE SAYI 4

Technical Editors | Teknik Editörler

Dr. Fatih UÇAR
Akdeniz University | Akdeniz Üniversitesi

Dr. Silver GÜNEŞ
Gazi University | Gazi Üniversitesi

Murat AKIN
Gazi University | Gazi Üniversitesi

Correspondence Address

Gazi University Graduate School of Natural and Applied Sciences
Emniyet Neighborhood, Bandırma Avenue, No:6/20B, 06560, Yenimahalle - ANKARA
B Block, Auxiliary Building

Yazışma Adresi

Gazi Üniversitesi Fen Bilimleri Enstitüsü
Emniyet Mahallesi, Bandırma Caddesi, No:6/20B, 06560, Yenimahalle - ANKARA
B Blok, Ek Bina

e-mail | e-posta

gujsa06@gmail.com

web page | web sayfası

https://dergipark.org.tr/tr/pub/gujsa

Gazi University Journal of Science Part A: Engineering and Innovation is a peer-reviewed journal.

Gazi Üniversitesi Fen Bilimleri Dergisi Bölüm A: Mühendislik ve İnovasyon hakemli bir dergidir.

Gazi University
Journal of Science
PART A: ENGINEERING AND INNOVATION

e-ISSN 2147-9542

YEAR YIL 2021 VOLUME CİLT 8 ISSUE SAYI 4

INDEXING | DİZİNLENME

ACCESSIBILITY | ERİŞİLEBİLİRLİK

Gazi University
Journal of Science
PART A: ENGINEERING AND INNOVATION

e-ISSN 2147-9542

YEAR YIL 2021 VOLUME CİLT 8 ISSUE SAYI 4

CONTENTS | İÇİNDEKİLER

Page | Sayfa	Articles | Makaleler
391-401	**Explanation of the Sutlegen Bauxites to Some REE Contents by Statistical Approach and Inequality Expressions** *Ozge OZER ATAKOGLU, Mustafa Gurhan YALCIN* *Research Article* — *Araştırma Makalesi* *Geological Engineering* — *Jeoloji Mühendisliği*
402-410	**Formulae to Fubini Type Numbers emerge from Application of p-adic Integrals** *Neslihan KILAR, Yilmaz SIMSEK* *Research Article* — *Araştırma Makalesi* *Mathematics* — *Matematik*
411-423	**Bioactivities from Novel Toxins of Pterois volitans: A Bioinformatics Approach** *Levent CAVAS, Yagmur BILGIN* *Research Article* — *Araştırma Makalesi* *Fisheries and Aquaculture Engineering* — *Su Ürünleri Mühendisliği*
424-434	**Effect of Wood-Based Panels and Varnish Types on VOC Emissions in Furniture Production** *Hamza ÇINAR, Kemal YILDIRIM, Mustafa HAMARAT* *Research Article* — *Araştırma Makalesi* *Wood Works Industrial Engineering* — *Ağaç İşleri Endüstri Mühendisliği*
435-450	**Data Mining and Application of Decision Tree Modelling on Electrochemical Data Used for Damaged Starch Detection** *Nilufer YILDIRIM, Niyazi Alper TAPAN* *Research Article* — *Araştırma Makalesi* *Chemical Engineering* — *Kimya Mühendisliği*
451-458	**On Prime Ideals Related to an Ideal in a Commutative Ring** *Ortaç ÖNEŞ* *Research Article* — *Araştırma Makalesi* *Mathematics* — *Matematik*
459-481	**LPG Stoklama Terminalinde Risk Değerlendirilmesi** *Risk Assessment in an LPG Storage Terminal* *Baharsu AKDAĞ, Saliha ÇETİNYOKUŞ* *Araştırma Makalesi* — *Research Article* *Kimya Mühendisliği* — *Chemical Engineering*

Gazi University
Journal of Science
PART A: ENGINEERING AND INNOVATION

e-ISSN 2147-9542

YEAR YIL 2021 VOLUME CİLT 8 ISSUE SAYI 4

CONTENTS | İÇİNDEKİLER

Page | Sayfa	Articles | Makaleler
482-493	**Thermal and Computational Fluid Dynamics (CFD) Analysis of a Modified Two Stroke Spark Ignition Engine Block** *Sunday BAKO, Jacob Nonom DOGO, Muhammed Bello UMAR, Ige BORI* *Research Article* — *Araştırma Makalesi* *Automotive Engineering* — *Otomotiv Mühendisliği*
494-504	**Artificial Neural Network Predictive Modelling of luffa cylindrica Seed Oil Antioxidant Yield** *Kenechi NWOSU-OBIEOGU* *Research Article* — *Araştırma Makalesi* *Chemical Engineering* — *Kimya Mühendisliği*
505-514	**Rh_2CoX (X=Al, Ga ve In) Bileşiklerinin Yapısal, Elastik, Elektronik ve Manyetik Özellikleri** *Rh_2CoX (X=Al, Ga and In) Compounds Structural, Elastic, Electronic and Magnetic Properties* *Ziya MERDAN, Fadime I. BALMUMCU* *Araştırma Makalesi* — *Research Article* *Fizik* — *Physics*
515-528	**Evaluation of Student Attitudes Using Multivariate Statistical Analysis** *Nurfer CIZMECI, Fusun YALCIN* *Research Article* — *Araştırma Makalesi* *Statistics* — *İstatistik*
529-536	**Synthesis, Spectroscopic and Thermal Characterization of a New Sustainable Polymer** *Nevin ÇANKAYA, & Nevin TURAN* *Research Article* — *Araştırma Makalesi* *Chemistry* — *Kimya*
537-550	**Chromitite Ore Types and Geochemical Investigation of Pozantı-Karsanti Ophiolite in Mazmılı Region (Turkey)** *Ali TÜMÜKLÜ* *Research Article* — *Araştırma Makalesi* *Geological Engineering* — *Jeoloji Mühendisliği*
551-569	**Determination of the Bed Hydrodynamics by MFIX-PIC in the Biomass Gasification Process of Circulating Fluidized Bed** *Yelda ALTINSOY, Ahmet KEÇECİ, Hüseyin TOPAL* *Research Article* — *Araştırma Makalesi* *Mechanical Engineering* — *Makine Mühendisliği*

Research Article / Araştırma Makalesi GU J Sci, Part A, 8(4): 391-401 (2021) https://doi.org/10.54287/gujsa.987102

Gazi University
Journal of Science
PART A: ENGINEERING AND INNOVATION
http://dergipark.org.tr/gujsa

Explanation of the Sutlegen Bauxites to Some REE Contents by Statistical Approach and Inequality Expressions

Ozge OZER ATAKOGLU[1], Mustafa Gurhan YALCIN[1*]

[1]*Department of Geological Engineering, Akdeniz University, 07058 Antalya, Turkey*

Keywords

Bauxite
Statistical Analysis
Inequalities Expression
Chemical Property

Abstract

Bauxite formation is usually possible in humid and tropical weather conditions with the enrichment of minerals containing Al_2O_3 in the environment. These minerals are found in chemical compositions that are rich in major and trace elements, and REEs. Karst-type bauxites have different characteristics in terms of REE and trace elements since they undergo alteration processes. Various correlations can be evaluated using geostatistical methods to reveal the behavior of these elements in bauxitization processes. The REE contents of the Sutlegen bauxite deposits were obtained by conducting ICP-MS analysis. The inequality expressions of the La element, which is in the lanthanide group of the periodic table and is included in the light rare earth elements, with Y element, the heavy and transition metal, has provided information about the formation conditions of bauxite. The arithmetic mean of the La/Y ratios of bauxites was found to be 0.25, and the ore formation condition was interpreted as acidic. Therefore, ∑REE concentrations of the Sutlegen bauxite deposits were associated with ∑LREE/HREE and La/Y ratios. ∑REE concentration was found to be positively correlated with the ∑LREE/HREE and La/Y ratios, and the correlation coefficients were found to be 0.89 and 0.44, respectively. The positive correlation between ∑REE concentration and La/Y ratio can be interpreted that the pH in the bauxite formation environment has a positive effect on REEs. Under the acidic conditions of ore formation, the bauxites were enriched in REEs.

Cite

Atakoglu, O. O., & Yalcin, M. G. (2021). Explanation of the Sutlegen Bauxites to Some REE Contents by Statistical Approach and Inequality Expressions. *GU J Sci, Part A, 8*(4), 391-401.

Author ID (ORCID Number)

O. Ozer Atakoglu, 0000-0003-2678-1194
M. G. Yalcin, 0000-0002-8011-5371

Article Process

Submission Date 25.08.2021
Revision Date 29.09.2021
Accepted Date 05.10.2021
Published Date 06.10.2021

1. INTRODUCTION

In bauxite formation processes, the rare earth element (REE) concentrations, as well as the characteristics of the environment, vary due to chemical alteration processes (Maksimovic & Panto, 1991; Yalcin & Temur, 2006; Yalcin & Ilhan, 2008; 2013; Kansun et al., 2010; Nyamsari & Yalcin, 2017; Nyamsari et al., 2019; 2020; Sidibe & Yalcin, 2019; Yalcin et al., 2012; 2016a). Rare earth elements are studied under two groups: light rare earth elements (LREEs) and heavy rare earth elements (HREEs). Bauxite formation depends on ambient conditions (Atakoglu & Yalcin, 2021). For bauxite formation, the upper soil horizon is enriched with trace elements such as Fe, Al. Acidic or alkaline conditions with pH varying between 4-5 are provided (Yang et al., 2019). With the effect of erosion, the chemical decomposition of the elements in the soil increases, trace and REE group elements decrease or increase, thus providing acidic or alkaline conditions. In order to understand these conditions that develop in the bauxite formation environment, the concentrations and ratios of some REE and trace elements should be looked at. The relationship of Y element, one of the transition metals, with lanthanides provides information about the pH conditions in the formation of bauxite (Maksimovic & Panto, 1991). In bauxite formation processes, chemical decomposition reactions and the concentrations of REEs are affected by the other major and trace elements (Yalcin & Ilhan, 2013; Yalcin et al., 2013; 2015; 2019a; 2020;

*Corresponding Author, e-mail: gurhanyalcin@akdeniz.edu.tr

Ozer & Yalcin, 2019; 2020). Several studies in the literature on associating the behavior of REEs with the ore formation environment are as follows:

In the study conducted in four selected bauxite deposits in former Yugoslavia and Greece, the La, Y, and REE concentrations were determined by Maksimovic & Panto (1991). The characteristics of the ore formation environment were revealed using the La/Y ratios, and the findings were evaluated using the ∑REE concentrations. REE concentrations and the values of the elements of Y and La-Lu were analyzed for 4 different karstic bauxite deposits in former Yugoslavia and Greece. The formation patterns in bauxite deposits were suggested based on the values of the chemical concentrations (Maksimovic & Panto, 1991).

In the study conducted on Henan Baofeng bauxite deposit in China, major elements, trace elements, and REE concentrations were analyzed. The value of La/Y inequality was investigated to interpret the conditions of the ore formation environment. The rare earth element behavior of the ore, whose formation environment was interpreted, was associated with the value of La/Y inequality (Yang et al., 2019).

In the study on the Mandan and Deh-Now bauxite deposits, the REE concentrations were revealed and correlated with the pH conditions of the environment. According to the results of the study, the relationships between the major and trace elements and REEs that played a role in the formation were evaluated, and the sedimentary environment conditions were interpreted (Zarasvandi et al., 2012).

The study area covers the Sutlegen bauxite deposits in the Kas district of the province of Antalya. Interpretation of the origin and formation conditions is important for the bauxite raw material, which has economic value. Therefore, the formation conditions of bauxite were interpreted using the inequality expressions in the present study.

In the literature, no study was found on the interpretation of the ore deposit formation conditions using statistical approaches. In this context, the study was carried out for the statistical explanation of the correlation between the La/Y ratios and REE concentrations of the bauxite deposits. Besides, the correlation between pH conditions and REE concentrations was also evaluated statistically in the study.

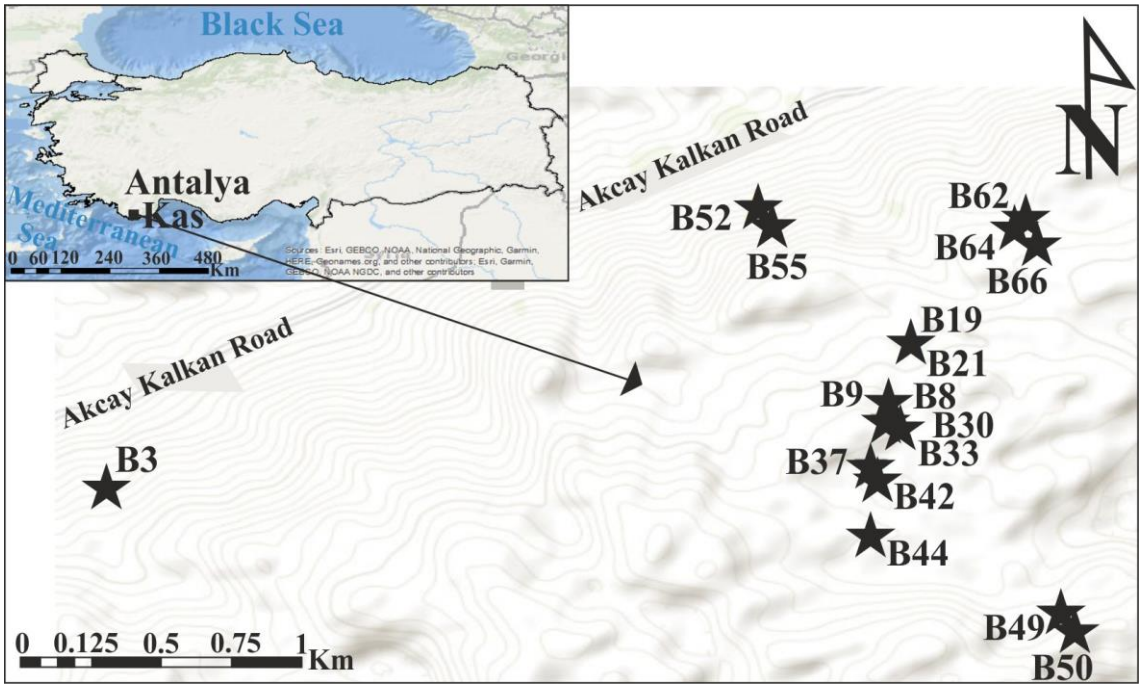

Figure 1. *Site Location Map of the Study Area*

2. MATERIAL AND METHOD

Inductively Coupled Plasma Mass Spectrometry (ICP-MS) method was used to determine La, Y and REE concentrations of the Sutlegen bauxite deposits. Then, the statistical analysis of the findings of the ICP-MS method was conducted using the SPSS23 software package. The coordinate information of the samples collected from the Sutlegen was processed on the Turkey map using Arcmap 10.7 program and distribution maps were created.

3. REGIONAL GEOLOGY

The study area is located within the boundaries of Beydaglari carbonate rock association and Katran Mountain (Figure 2). Beydaglari autochthonous, which is composed of rocks showing angular unconformity, consists of neritic limestones and clastic units deposited in the Upper Cretaceous-Miocene age range (Keser & Ozel, 2008). The units belonging to the Beydaglari autochthon on the exposed surfaces of the study area are listed as follows; Beydaglari formation consisting of Jurassic-Upper Cretaceous neritic limestones, Gomuce member which is Burdigalian aged algal unit, Caybogazi member as Burdigalian aged clayey unit, Kibrisdere member consisting of clayey limestones, Sinekci formation which is Burdigalian aged consisting of claystones, Kasaba formation which is Upper Burdigalian-Lower Langhian sandstone and conglomerate, Felenkdagi conglomerate which is Upper Langhian-Serravallian aged siltstone unit (Keser & Ozel, 2008). Allochthonous units in tectonic relationship on Beydaglari are Elmali formation consisting of Upper Lutetian-Lower Burdigalian aged neritic limestones and Mandirkaya formation consisting of Liassic-Upper-Cretaceous clastic units. The youngest units in the region are represented by alluvium and slope debris (Keser & Ozel, 2008) (Figure 3).

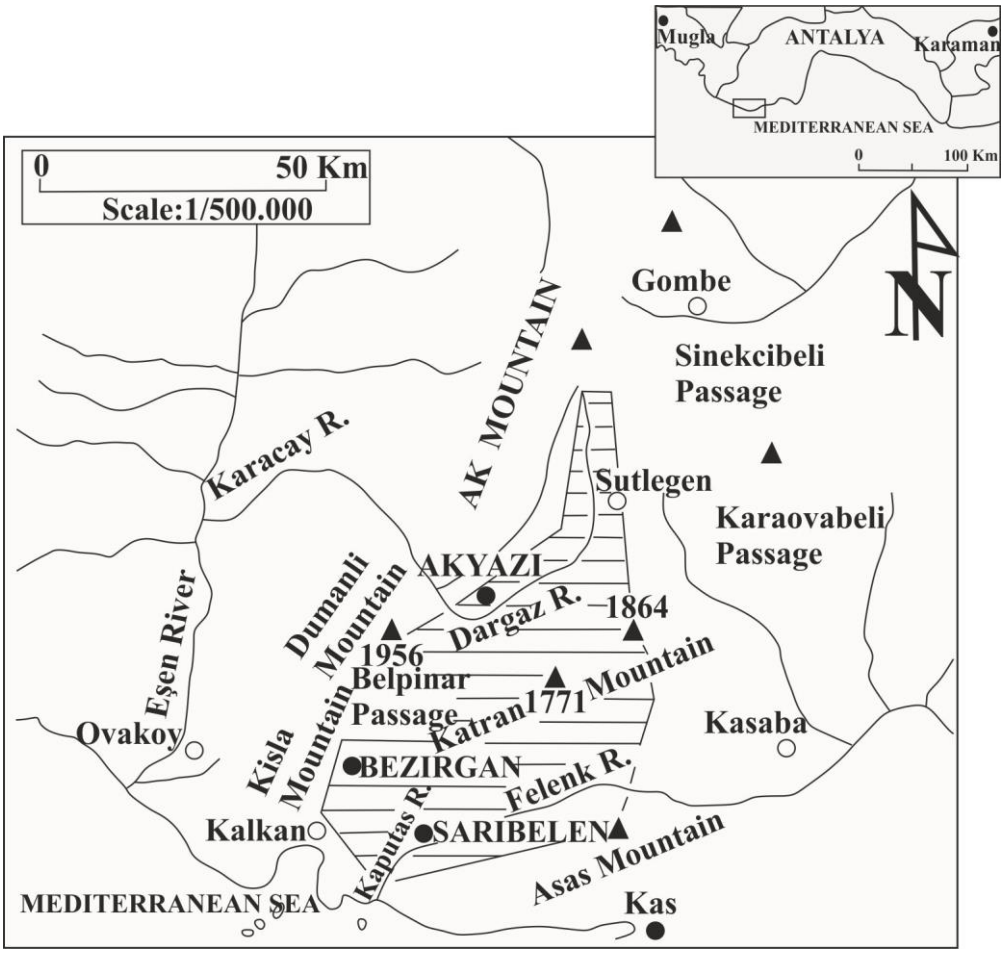

Figure 2. *Boundaries Map of the Study Area (modified after Keser & Ozel, 2008)*

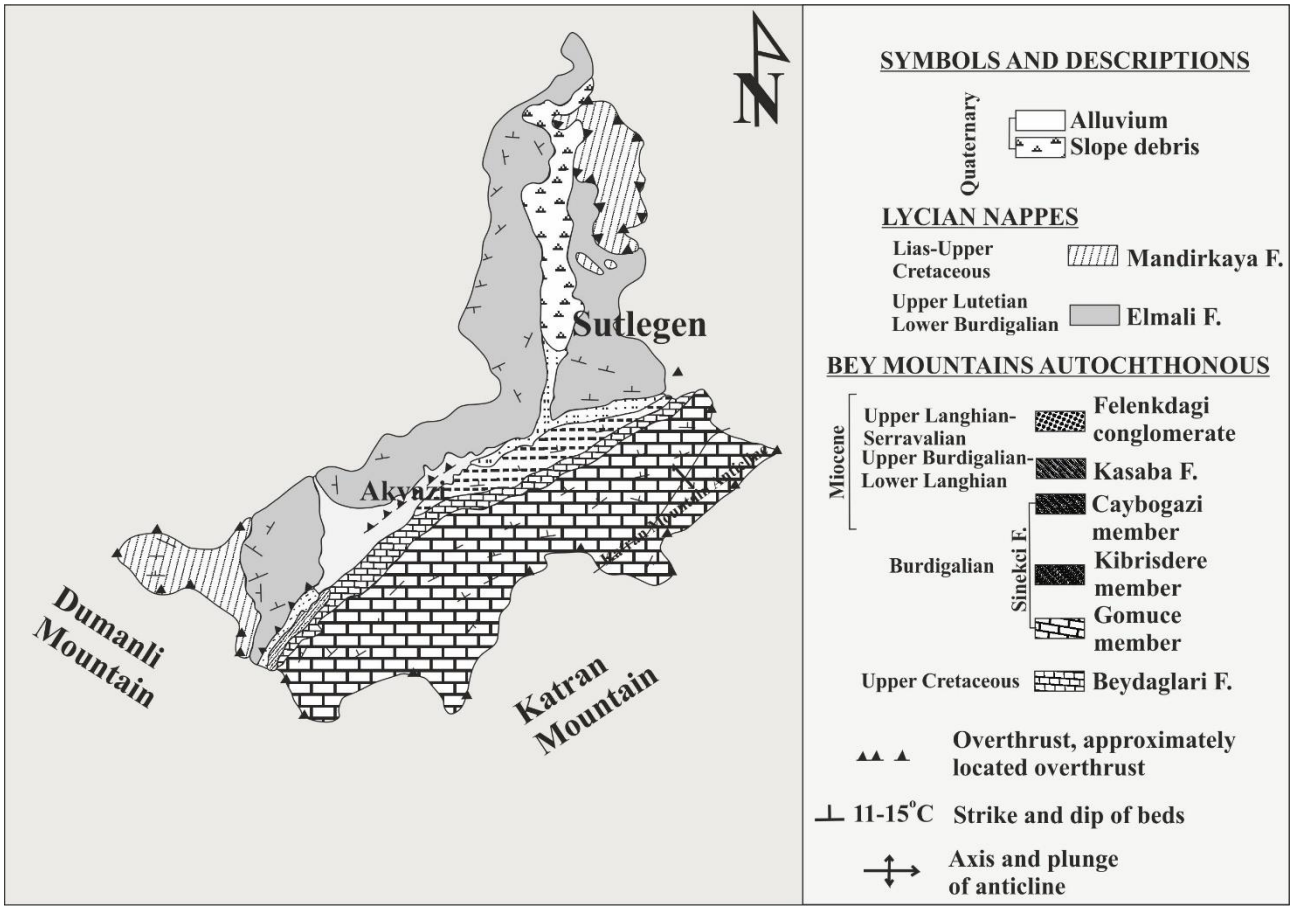

Figure 3. *Regional Geologic Map of the Study Area (modified after Keser & Ozel, 2008)*

4. RESULTS AND DISCUSSION

REE element contents of 17 samples collected from the study area were revealed by conducting ICP-MS analysis (Table 1). The inequality expressions suggested for the La/Y concentrations by Maksimovic & Panto (1991) and Zarasvandi et al. (2012) are as follows (1), (2):

La/Y < Acidic conditions (1)

La/Y > Alkaline conditions (2)

The findings were compared with the values of other karstic-type bauxite deposits in the literature. On the other hand, in the study conducted on the Henan karstic-type bauxite deposits in China, the bauxite formation condition was found to be generally alkaline (Yang et al., 2019). The La/Y ratio of the Grebnik karstic bauxite deposit was found to vary between 0.5 and 4; thus, it was interpreted that the transition from acidic to alkaline conditions could be possible by a carbonate contact (Maksimovic & Panto, 1991). The box plot used for descriptive statistics is given in Figure 4.

ΣREE, ΣLREE (La-Sm), ΣHREE (Gd-Lu), and ΣLREE/HREE values are given in Table 2. In the study conducted on Baofeng bauxite deposits, the value of the coefficient of determination (R^2) of the model which was designed to explain ∑REE using the ∑LREE/∑HREE ratio was found to be 0.57. On the other hand, the R^2 value of the model which was established to explain ∑REE using the La/Y ratio was found to be 0.55. The positive correlation found was associated with source rocks that played a role in the ore formation. It was interpreted that pH played a critical role in ∑REEs, and it increased in total ∑REE concentration under alkaline conditions (Yang et al., 2019).

Table 1. *REE Elements Results and La/Y Ratios of the Sutlegen Bauxites (ppm) (Ozer, 2020)*

Sample Code	Latitude	Longitude	Ce	Dy	Er	Eu	Gd	Hf	Ho	La	Lu	Nd	Pr	Sc	Sm	Tb	Th	Tm	U	Y	Yb	La/Y
B3	36.3928	29.5553	81.80	21.30	11.40	3.90	17.70	1.90	4.30	22.00	1.60	70.00	11.80	26.40	18.60	3.30	2.60	1.80	1.50	104.30	10.20	0.21
B8	36.5591	29.5628	52.10	14.70	7.90	2.80	13.40	5.10	2.90	9.10	1.20	46.50	7.70	36.60	11.50	2.40	20.60	1.10	3.50	138.80	7.10	0.06
B9	36.5591	29.5628	20.90	15.80	8.00	3.20	16.10	1.60	3.20	9.80	1.10	52.50	6.90	20.40	14.50	2.60	22.70	1.20	5.00	85.60	7.10	0.19
B19	36.3995	29.5928	48.40	21.20	12.60	2.80	13.20	3.50	4.60	17.60	1.80	19.30	3.40	24.40	10.20	3.00	31.30	2.10	4.70	88.40	11.20	0.11
B21	36.3995	29.5928	6.20	4.00	2.50	0.40	2.40	2.70	0.80	5.20	0.40	4.20	0.90	21.70	1.20	0.50	20.60	0.40	6.10	17.90	2.70	0.72
B30	36.3959	29.5917	13.70	2.70	1.90	0.30	1.50	1.50	0.70	4.60	0.30	5.30	1.20	10.20	1.40	0.40	15.30	0.30	2.90	11.90	2.20	0.29
B33	36.3956	29.5922	60.80	14.30	8.40	2.30	9.70	2.60	3.00	12.40	1.30	27.40	4.40	19.50	9.20	2.00	24.40	1.40	2.20	58.70	8.60	0.21
B37	36.3938	29.5908	46.30	23.60	13.10	3.70	18.80	3.60	5.00	12.50	1.80	32.50	4.20	25.40	14.00	3.50	28.20	2.10	2.70	130.40	11.60	0.05
B42	36.3936	29.5908	9.00	6.30	4.10	0.80	4.60	0.90	1.50	2.90	0.50	5.70	0.90	14.00	2.80	0.90	8.30	0.60	4.20	50.10	3.40	0.37
B44	36.3906	29.5908	45.00	9.30	5.60	1.60	6.30	2.70	1.90	11.80	1.00	22.30	3.50	24.10	7.40	1.40	21.80	1.00	4.30	31.60	6.60	0.48
B49	36.3870	29.5997	39.20	4.10	2.40	0.70	2.70	6.50	0.80	4.90	0.60	9.50	1.60	26.80	3.20	0.50	15.60	0.40	2.10	19.10	2.90	0.25
B50	36.3870	29.5997	31.70	4.60	2.90	0.80	2.90	2.80	1.00	9.30	0.60	12.60	2.50	23.90	3.60	0.60	28.10	0.60	3.00	19.00	4.00	0.09
B52	36.4058	29.5856	10.40	15.30	9.70	1.70	9.10	4.00	3.40	8.30	1.50	9.10	1.70	21.50	5.20	2.10	33.60	1.60	3.90	73.40	9.50	0.46
B55	36.4058	29.5856	10.00	10.60	6.60	1.10	6.00	3.10	2.40	8.00	1.00	7.40	1.40	25.90	3.40	1.40	27.90	1.10	8.50	71.10	6.80	0.24
B62	36.4053	29.5981	5.20	1.10	0.60	0.20	0.90	1.50	0.20	2.70	<0.1	3.70	0.70	10.10	1.10	0.20	27.50	<0.1	2.10	3.70	0.60	0.11
B64	36.4053	29.5981	105.10	16.10	8.40	3.40	14.60	2.80	3.20	22.50	1.20	64.10	11.70	18.50	16.30	2.60	26.80	1.40	2.60	48.10	8.10	0.38
B66	36.4053	29.5981	104.50	20.20	10.10	3.90	16.80	3.10	3.90	18.00	1.40	64.10	11.20	20.50	18.00	3.20	28.20	1.70	2.20	73.80	9.50	0.11
																					Mean	0.25
																					Std. Deviation	0.18

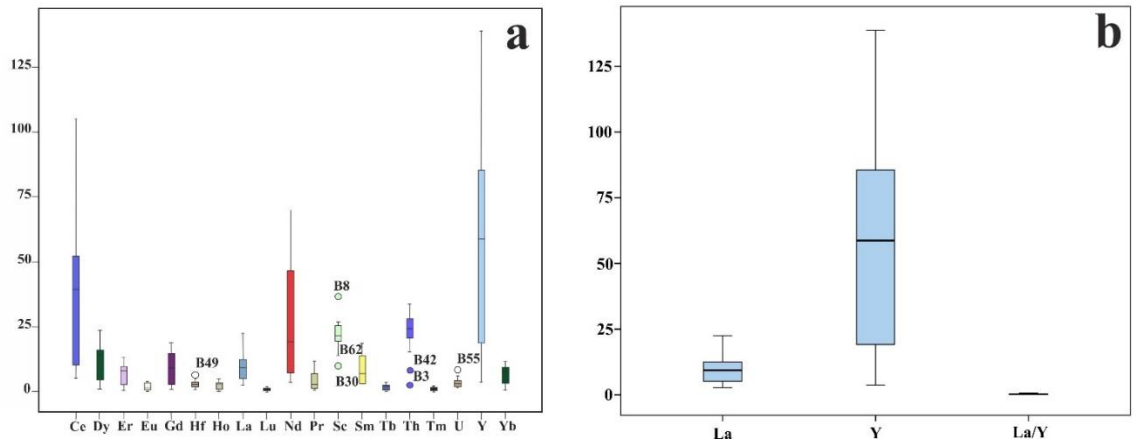

Figure 4. *Box Plot of the* ***a)*** *REE of Bauxite Samples,* ***b)*** *La, Y and La/Y*

As seen in Figure 5, the REE content was found to have a positive correlation with the ∑LREE/HREE ratio, and the correlation coefficient was calculated as 0.89. The ∑REE behavior was observed to increase based on the ∑LREE content. Furthermore, it was observed that the ∑REE contents were positively correlated also with La/Y ratios, and the coefficient of correlation was found to be 0.44 (Figure 6).

The explained variance (coefficient of correlation) (R^2) of the model that was designed to explain ∑REE values using La/Y and ∑LREE/∑HREE ratios was found to be 0.57 (Table 3). In other words, it is possible to explain about 57% of the variability of ∑REE with La/Y and ∑LREE/∑HREE ratios. In addition, the error rate of this model was found to be 0 (Table 4). Therefore, explaining ∑REE with La/Y and ∑LREE/∑HREE ratios is statistically significant (Ozer & Yalcin, 2019; 2020; Aydin et al., 2020; Ozer et al., 2020, Atakoglu et al., 2021; Ince et al., 2021; Yalcin et al., 2021).

Table 2. *The Results of ΣREE, ΣLREE, ΣHREE and ΣLREE/ΣHREE Calculations of the Bauxite Samples in the Study Area (Atakoglu & Yalcin, 2021)*

Sample Code	**∑REE**	**∑LREE**	**∑HREE**	**∑LREE/∑HREE**
B3	295.9	185.6	103.4	1794.00
B8	209.9	115.4	93.6	12329.00
B19	184.6	88.7	101.6	0.87303
B55	86.3	44069	71.4	0.3753501
B62	44038	43902	16.00	0.76875
B21	50.8	43967	41.9	0.3937947
B33	176.1	105	72.7	14442916
B42	54.6	4396	40.9	0.4523227
B44	142.2	82.6	63.1	13090333
B50	97.6	56.1	44.9	12494432
B49	97.4	55.2	44	12545455
B37	206,00	95.5	111	0.85
B64	289.1	203.4	80.1	25393258
B66	297.5	197.8	93.4	2117773
B52	100.6	43980	79.3	0.372005
B30	44.5	440670	43944	10598291
B9	176.2	90.1	83.7	10764636
Mean	14920	82576	685117	11277575
Std. Dvd.	8981668	6347113	28885240	0.6123101

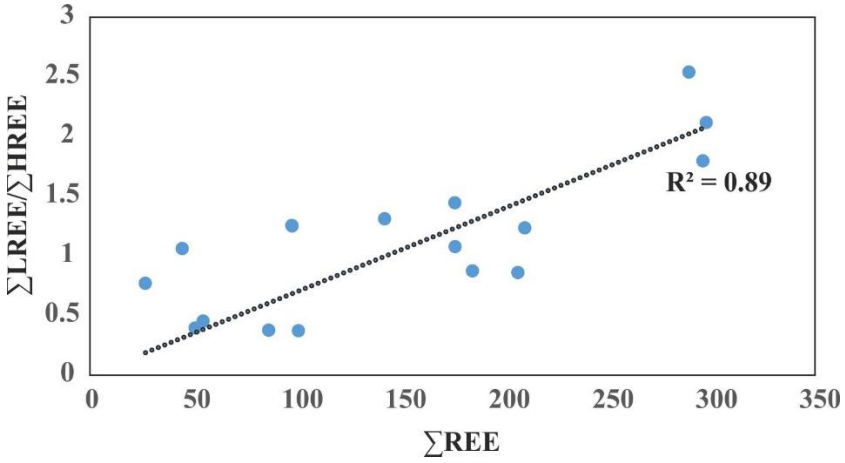

Figure 5. *Simple Regression Scatter Diagrams of ΣREE versus ΣLREE/ΣHREE Ratio*

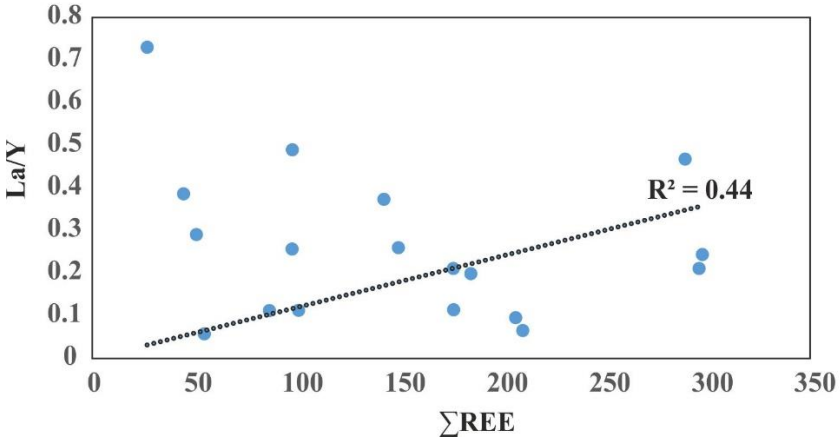

Figure 6. *Simple Regression Scatter Diagrams of ΣREE versus the La/Y Ratio*

Table 3. *Determination Coefficient of the Model Explaining ΣREE using the ΣLREE/ΣHREE and La/Y Ratios*

Model Summary[b]				
Model	R	**R Square**	Adjusted R Square	Std. Error of the Estimate
1	0.76[a]	**0.57**	0.51	0.12
a. Predictors: (Constant), ∑REE, ∑LREE b. Dependent Variable: La/Y				

Table 4. *Error Data of the Model Explaining ΣREE using the ΣLREE/ΣHREE and La/Y Ratios*

ANOVA[a]						
Model		Sum of Squares	df	Mean Square	F	**P-value**
1	Regression	0.30	2	0.15	0.63	**0[b]**
	Residual	0.22	14	0.01		
	Total	0.52	16			
a. Dependent Variable: La/Y b. Predictors: (Constant), ∑REE, ∑LREE						

The results of the correlation analysis performed according to La, Y and La/Y values are given in Table 5. Factor analysis was performed to determine the variance ratios of La, Y and La/Y values and to understand the relationships they established (Yalcin & Unal, 2018; Ozer et al., 2019; Tarinc et al., 2019a, b; Yalcin et al., 2007; 2008; 2019b; Yazici et al., 2021) (Table 6).

Table 5. *Pearson's Correlation Coefficients Calculated using the Results of La, Y and La/Y*

	La	**Y**	**La/Y**
La	1		
Y	0.463	1	
La/Y	-0.060	-0.719**	1

Table 6. *Total Variance Explained According to Factor Analysis*

Total Variance Explained						
Component	Initial Eigenvalues			Extraction Sums of Squared Loadings		
	Total	% of Variance	Cumulative %	Total	% of Variance	**Cumulative %**
1	**1.88**	62.78	62.78	1.88	62.78	**62.78**
2	0.94	31.51	94.29			
3	0.17	5.70	100			
Extraction Method: Principal Component Analysis.						

The province polygon with the coordinates was selected and converted to raster data format in Arcmap 10.7 program. Distribution maps were created using the Krigging interpolation method with La, Y and the calculated La/Y ratio values from REE group elements in raster data format (Yalcin et al., 2016b, c, d) (Figure 7).

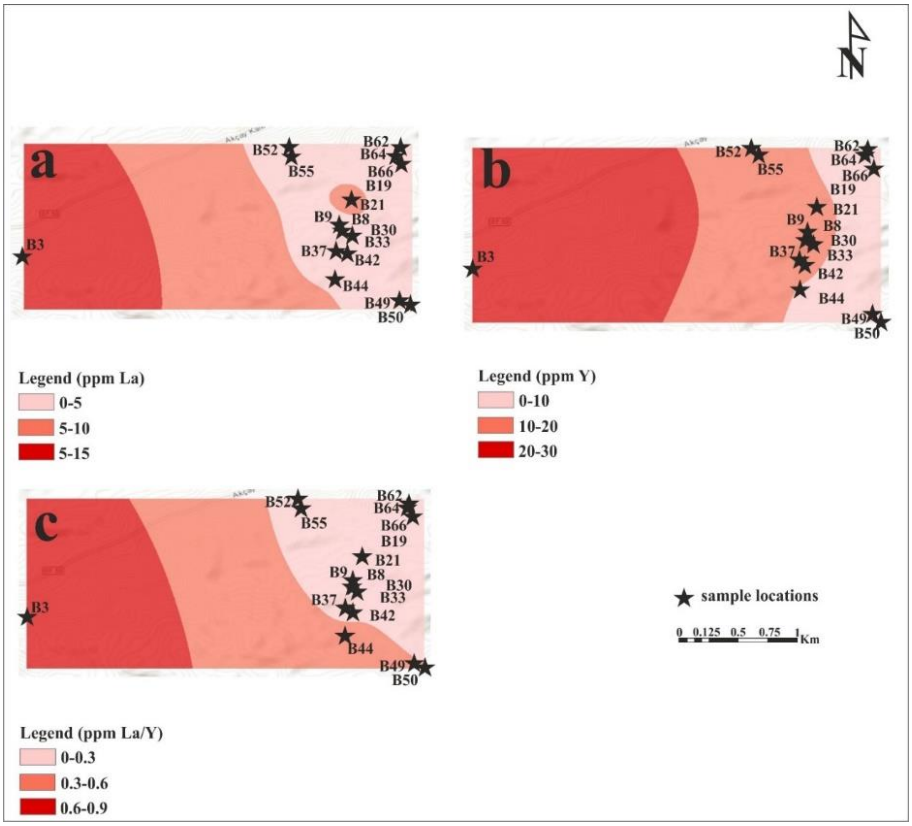

Figure 7. *Spatial Distribution Maps of* ***a)*** *La,* ***b)*** *Y,* ***c)*** *La/Y*

5. CONCLUSION

In this study, the arithmetic mean of La/Y ratios for the Sutlegen bauxites was calculated as 0.25 while the standard deviation was found to be 0.18. It was interpreted that the formation conditions of bauxites were acidic. The positive correlation of La/Y ratios, which were associated with the pH values of the ore formation environment, with ∑REE provided the information that bauxites that were formed under acidic conditions were also enriched in REEs. The positive correlation of La/Y ratios, which were associated with the pH values of the ore formation environment, with ∑REE provided the information that bauxites that were formed under acidic conditions were also enriched in REEs. In the case of the Sutlegen bauxites, it was found that the ∑REE concentrations increased under acidic conditions (pH <1), and the established model was statistically significant. According to the correlation analysis, there is a high-order negative-intermediate correlation between Y and La/Y. The data were collected under 1 factor with an eigenvalue greater than 1, and it was seen that the 1st factor explained 62.78% of the total variance.

The distribution maps obtained by the Krigging interpolation method; La and Y distributions of REE group elements are similar in the study area. The distribution of the La/Y ratio calculated in this context is similar in the study area.

ACKNOWLEDGEMENT

This paper is a part of the M.Sc. thesis of Atakoglu Ozer O., the first author.

CONFLICT OF INTEREST

The authors declare no conflict of interest.

REFERENCES

Atakoglu, O. O., & Yalcin, M. G. (2021). Geochemical characterization of the Sutlegen bauxite deposit, SW Antalya. *Mining of Mineral Deposits*, *15*(3), 108-121. doi:10.33271/mining15.03.108

Atakoglu, O. O., Yalcin, M. G., & Ozmen, S. F. (2021). Determination of radiological hazard parameters and radioactivity concentrations in bauxite samples: the case of the Sutlegen Mine Region (Antalya, Turkey). *Journal of Radioanalytical and Nuclear Chemistry*, *329*(2), 701-715. doi:10.1007/s10967-021-07826-5

Aydin, B., Yalcin, F., Ozer, O., & Yalcin, M. G. (2020). Regression analysis and statistical examiantion of knoop hardness on abrasion resistance in Lyca beige marbles. *Filomat*, *34*(2), 609-614. doi:10.2298/FIL2002609A

Ince, Z., Atakoglu, O. O., & Yalcin, M. G. (2021). Multivariate and spatial statistical analysis of geochemical data of dolomite: the case of ındustrial raw materials' differentiation. *Montes Taurus J Pure Appl Math*, *3*(2), 8-28.

Kansun, G., Yalcin, M. G., & Copuroglu, I. (2010). Bolkardagi bauxite deposits at Ayranci, Karaman, central Turkey. Part 2. Mineralogical and petrographical studies. XIX Congress of the Carpathian-Balkan Geological Association Thessaloniki, Greece, 23-26 September, *39*(1-2), 177.

Keser, N., & Ozel, A. (2008). Three Examples to Explain the Formation and Development Mechanism of West Taurus Poljes. In: Natural Environment and Culture in Mediterranean Region, Cambridge Scholars Publishing, Part I, Chapter Fourteen, 197-214.

Maksimovic, Z., & Panto, G. Y. (1991). Contribution to the geochemistry of the rare earth elements in the karst-bauxite deposits of Yugoslavia and Greece. *Geoderma*, *51*(1-4), 93-109. doi:10.1016/0016-7061(91)90067-4

Nyamsari, D. G., & Yalcin, M. G. (2017). Statistical analysis and source rock of the Minim-Martap plateau bauxite, Cameroon. *Arabian Journal of Geosciences*, *10*(18), 415. doi:10.1007/s12517-017-3172-0

Nyamsari, D. G., Yalcin, F., Mboh, M. T., Alfred, F. G., & Yalcin, M. G. (2019). Natural radioactive risk assessment in topsoil and possible health effect in Minim and Martap villages, Cameroon: using radioactive risk index and statistical analysis. *Kerntechnik*, *84*(2), 115-122. doi:10.3139/124.110927

Nyamsari, D. G., Yalçin, M. G., & Wolfson, I. (2020). Alteration, Chemical Processes, and Parent Rocks of Haléo-Danielle Plateau Bauxite, Adamawa–Cameroon. *Lithology and Mineral Resources*, *55*, 231-243. doi:10.1134/S0024490220030049

Ozer, O. (2020). The genesis and economic characteristics of the Sütleğen region (Kaş, Antalya) bauxite deposits. MSc Thesis, Akdeniz University, Antalya, 125 p. (Turkish).

Ozer, O., & Yalcin, M. G. (2019). Modeling of elemental distribution of Kas (Antalya) bauxite deposit. In: II. International Conference of Numerical Analysis and Applied Mathematics (ICNAAM), Rhodes, Greece, 23-28 September, 24-25.

Ozer, O., & Yalcin, M. G. (2020). Correlation of chemical contents of Sutlegen (Antalya) bauxites and regression analysis. *AIP Conference Proceedings*, *2293*(1), 180008. doi:10.1063/5.0026731

Ozer, O., Yalcin, F., Nyamsari, D. G., Yalcin, M. G. (2019). Appraisal of metal accumulation in beach sand using contamination indices and multivariate statistical analysis. In: Proceedings Book of the 2nd Mediterranean International Conference of Pure Applied Mathematics and Related Areas, Paris, France, 28-31 August, 1-5.

Ozer, O., Yalcin, F., Tarinc, O. K., & Yalcin, M. G. (2020). Investigation of suitability of marbles to standards with inequality expressions and statistical approach using some physical and mechanical properties. *Journal of Inequalities and Applications*, 97, 1-15. doi:10.1186/s13660-020-02360-6

Sidibe, M., & Yalcin, M. G. (2019). Petrography, mineralogy, geochemistry and genesis of the Balaya bauxite deposits in Kindia region, Maritime Guinea, West Africa. *Journal of African Earth Sciences*, *149*, 348-366. doi:10.1016/j.jafrearsci.2018.08.017

Tarinc, O. K., Ozer, O., Aydin, B., & Yalcin, M. G. (2019a). Comparison of physical-mechanical properties of Clova and Lyca marbles in Akcay (Antalya) region by using independent-samples T-test statistics. In: Proceedings Book of the 2nd Mediterranean International Conference of Pure Applied Mathematics and Related Areas, Paris, France, 28-31 August.

Tarinc, O. K., Ozer, O., Yalcin, F., & Yalcin, M. G. (2019b). Statistical evaluation of the chemical characteristics on marble in Akcay village (Elmali, Antalya) region. In: International Symposium on Advanced Engineering Technologies, Kahramanmaras, Turkey, 1333-1338.

Yalcin, M. G., & Ilhan, S. (2008). Major and trace element geochemistry of Terra Rossa soil in the Kucukkoras region, Karaman, Turkey. *Geochemistry International*, *46*(10), 1038-1054. doi:10.1134/S001670290810008X

Yalcin, M. G., & Ilhan, S. (2013). Major and trace element geochemistry of bauxites of Ayranci, Karaman, central Bolkardag, Turkey. *Asian Journal of Chemistry*, *25*(5), 2893-2904, doi:10.14233/ajchem.2013.14275

Yalcin, M. G., & Temur, S. (2006). Geochemistry of the terra rossa from Ayranci, Central Turkey. *Geochmica et Cosmochimica Acta*, *70*(18), doi:10.1016/j.gca.2006.06.1285

Yalcin, M. G., & Unal, S. (2018). Natural radioactivity levels and associated radiation hazards in ophiolites around Tekirova, Kemer, and Kumluca Touristic Regions in Antalya, Turkey. *Journal of Radioanalytical and Nuclear Chemistry*, *316*(1), 321–330. doi:10.1007/s10967-018-5760-1

Yalcin, M. G., Battaloglu, R., Ilhan, S., Tumuklu, A., & Topuz, D. (2007). Heavy metal contamination along the Nigde-Adana highway, Turkey. *Asian Journal of Chemistry*, *19*(2), 1506-1518.

Yalcin, M. G., Aydin, O., & Elhatip, H. (2008). Heavy metal contents and the water quality of Karasu Creek in Nigde, Turkey. *Environmental Monitoring and Assessment*, *137*, 169. doi:10.1007/s10661-007-9737-8

Yalcin, M. G., Karaman, M. E., & Alagoz, Z. (2012). Origin of the red soils in the Bolkardag regıon: Pınarkaya-Kayaonu case. (Karaman. Turkey). In: International Multidisciplinary Scientific GeoConference: SGEM: Surveying Geology Mining Ecology Management, 4, 149.

Yalcin, M. G., Cevik, O., & Karaman, M. E. (2013). Use of multivariate statistics methods to determine grain size, heavy metal distribution and origins of heavy metals in Mersin Bay (Eastern Mediterranean) coastal sediments. *Asian Journal of Chemistry*, *25*(5), 2696-2702. doi:10.14233/ajchem.2013.13683

Yalcin, M. G., Setti, M., Karakaya, F., Sacchi, E., & Ilbeyli, N. (2015). Geochemical and mineralogical characteristics of beach sediments along the coast between Alanya and Silifke (southern Turkey). *Clay Minerals*, *50*(2), 233-248. doi:10.1180/claymin.2015.050.2.07

Yalcin, M. G., Nyamsari, D. G., Paksu, E., & Yalcin, F. (2016a). Statistical assessment of rare earth elements of bauxite deposits of Minim-Martap Plateau. Cameroon. In: International Multidisciplinary Scientific GeoConference: SGEM: Surveying Geology Mining Ecology Management, 2, 819-825.

Yalcin, F., Kilic, S., Nyamsari, D. G., Yalcin, M. G., & Kilic, M. (2016b). Principal component analysis of integrated metal concentrations of bogacayi riverbank sediments in Turkey. *Polish Journal of Environmental Studies*, *25*(2), 471-485. doi:10.15244/pjoes/61009

Yalcin, M. G., Akturk, O., & Paksu, E. (2016c). The contribution of west mediterranean cities (Antalya, Isparta and Burdur) to Turkey's natural stones-marble export. In: International Multidisciplinary Scientific GeoConference: SGEM: Surveying Geology & Mining Ecology Management, 2, 875-880.

Yalcin, F., Nyamsari, D. G., Paksu, E., & Yalcin, M. G. (2016d). Statistical assessment of heavy metal distribution and contamination of beach sands of Antalya-Turkey: an approach to the multivariate analysis techniques. *Filomat*, *30*(4). 945-952. doi:10.2298/FIL1604945Y

Yalcin, M. G., Coskun, B., Nyamsari, D. G., & Yalcin, F. (2019a). Geomedical, ecological risk, and statistical assessment of hazardous elements in shore sediments of the Iskenderun Gulf, Eastern Mediterranean, Turkey. *Environmental Earth Sciences*, *78*(15), 438. doi:10.1007/s12665-019-8435-5

Yalcin, F., Ozer, O., Nyamsari, D. G., & Yalcin, M. G. (2019b). Statistical evaluation of the geochemical content of beach sand along the Sarisu-Kemer coastline of Antalya, Turkey. *AIP Conference Proceedings*, *2116*(1), 100005. doi:10.1063/1.5114081

Yalcin, F., Unal, S., Yalcin, M. G., Akturk, O., Ocak, S. B., & Ozmen, S. F. (2020). Investigation of the Effect of Hydrothermal Waters on Radionuclide Activity Concentrations in Natural Marble with Multivariate Statistical Analysis. *Symmetry*, *12*(8), 1219. doi:10.3390/sym12081219

Yalcin, M. G., Nyamsari, D. G., Atakoglu, O. O., & Yalcin, F. (2021). Chemical and statistical characterization of beach sand sediments: implication for natural and anthropogenic origin and paleo-environment. *International Journal of Environmental Science and Technology*. doi:10.1007/s13762-021-03280-8

Yang, S., Wang, Q., Deng, J., Wang, Y., Kang, W., Liu, X., & Li, Z. (2019). Genesis of karst bauxite-bearing sequences in Baofeng. Henan (China) and the distribution of critical metals. *Ore Geology Reviews*, *115*, 103161. doi:10.1016/j.oregeorev.2019.103161

Yazici, I., Yalcin, M. G., Atakoglu, O. O., & Yalcin, F. (2021) Multivariate Statistical Evaluation of Geochemical Properties of “Alanya Emperador Dark” Marbles. *Gazi University Journal of Science Part A: Engineering and Innovation*, *8*(3), 361-372.

Zarasvandi, A., Carranza, E. J. M., & Ellahi, S. S. (2012). Geological, geochemical, and mineralogical characteristics of the Mandan and Deh-now bauxite deposits, Zagros Fold Belt, Iran. *Ore Geology Reviews*, *48*, 125-138. doi:10.1016/j.oregeorev.2012.02.010

Research Article / Araştırma Makalesi GU J Sci, Part A, 8(4): 402-410 (2021) https://doi.org/10.54287/gujsa.980263

Gazi University
Journal of Science
PART A: ENGINEERING AND INNOVATION
http://dergipark.org.tr/gujsa

Formulae to Fubini Type Numbers emerge from Application of p-adic Integrals

Neslihan KILAR[1*], Yilmaz SIMSEK[2]

[1]*Niğde Ömer Halisdemir University, Bor Vocational School, Department of Computer Technologies, Niğde TR-51700 Turkey*
[2]*Akdeniz University, Faculty of Science, Department of Mathematics, Antalya TR-07058, Turkey*

Keywords

Bernoulli Polynomials and Numbers

Fubini Type Polynomials and Numbers

Special Polynomials and Numbers

Generating Function

p-adic Integral

Abstract

The aim of this manuscript is to examine and survey various formulae for Fubini type numbers and polynomials with application of the p-adic integrals to some special polynomials. Relations and formulae related to the Fubini type numbers and polynomials, the Bernoulli numbers, the Euler numbers, Stirling type numbers, and combinatorial numbers are given. Moreover, by using generating functions with their functional equations, some new formulae including the Hermite polynomials, the Fubini type polynomials, and the Lah numbers are given. Finally, remarks on the results of this manuscript are presented.

Cite

Kilar, N., & Simsek, Y. (2021). Formulae to Fubini Type Numbers emerge from Application of p-adic Integrals. *GU J Sci, Part A, 8*(4), 402-410.

Author ID (ORCID Number)

N. Kilar, 0000-0001-5797-6301
Y. Simsek, 0000-0002-0611-7141

Article Process

Submission Date 08.08.2021
Revision Date 14.10.2021
Accepted Date 15.10.2021
Published Date 18.10.2021

1. INTRODUCTION

In "The On-Line Encyclopedia of Integer Sequences" (OEIS, 2021) (https://oeis.org/A000670), it is well-know that the Fubini numbers are related to the number of preferential arrangements of n labeled elements, and also the number of ordered partitions of $[n]$. The Fubini numbers are also called the ordered Bell numbers. Later, by Comtet (1974), these numbers were also called the Fubini numbers.

Kilar & Simsek (2017) modified these numbers and defined new generalized Fubini type numbers and polynomials. They also gave very different and interesting applications of these numbers and polynomials with aid of the generating functions and their functional equations. Recently, it is known that these type numbers and polynomials have been studied by many mathematicians using different methods and fields (Belbachir et al., 2011; Kilar, 2017; 2021; Kilar & Simsek, 2017; 2019a,b; Kim et al., 2018; Srivastava & Kızılateş, 2019).

Some definitions and notations connected with special polynomials and numbers and their generating functions are presented as follows:

Let $\mathbb{N} = \{1,2,3,\dots\}$ and $\mathbb{N} \cup \{0\} = \mathbb{N}_0$. Let $\mathbb{Z} = \mathbb{N} \cup \{0,-1,-2,-3,\dots\}$. Let $\mathbb{C}$ indicate the set of complex numbers and $\mathbb{Z}_p$ indicate the set of p-adic integers.

$$\binom{u}{c} = \frac{u(u-1)\dots(u-c+1)}{c!} = \frac{(u)_c}{c!},$$

*Corresponding Author, e-mail: neslihankilar@ohu.edu.tr; neslihankilar@gmail.com

where $c \in \mathbb{N}$, $u \in \mathbb{C}$ and $(u)_0 = 1$ (Belbachir et al., 2011;-; Srivastava & Choi, 2012).

Generating function of the classical Bernoulli polynomials is given by

$$\frac{z}{e^z - 1} e^{tz} = \sum_{\mathrm{m}=0}^{\infty} B_m(t) \frac{z^m}{m!}, \tag{1}$$

where $|z| < 2\pi$ (Comtet, 1974;-; Srivastava & Choi, 2012).

Setting $t = 0$ in (1), we see that

$$B_m(0) = B_m,$$

denoted the classical Bernoulli numbers (Comtet, 1974;-; Srivastava & Choi, 2012).

Generating function of the classical Euler polynomials is given by

$$\frac{2}{e^z + 1} e^{tz} = \sum_{m=0}^{\infty} E_m(t) \frac{z^m}{m!}, \tag{2}$$

where $|z| < \pi$ (Comtet, 1974;-; Srivastava & Choi, 2012).

Setting $t = 0$ in (2), we observe that

$$E_m(0) = E_m,$$

denoted the classical Euler numbers (Comtet, 1974;-; Srivastava & Choi, 2012).

Generating function of the Hermite polynomials is given by

$$G_H(z, \mathrm{t}) = e^{2tz - z^2} = \sum_{m=0}^{\infty} H_m(t) \frac{z^m}{\mathrm{m!}}, \tag{3}$$

(Rainville, 1960).

Using equation (3), we have

$$t^n = \sum_{k=0}^{\left[\frac{n}{2}\right]} \frac{n!\, H_{n-2k}(t)}{2^n k!\, (n-2k)!} \tag{4}$$

(Rainville, 1960).

Let $c \in \mathbb{N}_0$ and $a \in \mathbb{C}$. Generating function of Stirling type numbers is given by

$$\frac{(ae^z - 1)^c}{c!} = \sum_{d=0}^{\infty} S_2(d, c; a) \frac{z^d}{d!} \tag{5}$$

(Simsek, 2013; 2019).

Generating function of the Stirling numbers of the second kind is given by

$$\frac{(e^z-1)^c}{c!}=\sum_{d=0}^{\infty}S_2(d,c)\frac{z^d}{d!} \tag{6}$$

and

$$t^c=\sum_{m=0}^{c}S_2(c,m)(t)_m \tag{7}$$

(Comtet, 1974;-; Srivastava & Choi, 2012).

Substituting $a=1$ into (5), we have

$$S_2(d,c;1)=S_2(d,c).$$

For $c>d$, one has

$$S_2(d,c)=0$$

(Comtet, 1974;-; Srivastava & Choi, 2012).

An explicit formula for the Lah numbers is given by

$$L(c,s)=\frac{(-1)^c c!\binom{c-1}{s-1}}{s!}, \tag{8}$$

where $c\geq s\geq 1$, $L(0,0)=1$ and $L(c,s)=0$ for all $s>c$ (Riordan, 1958; Comtet, 1974). Here note that this numbers are so called signed Lah numbers.

By the aid of the equation (8), we have

$$(r)_c=\sum_{s=0}^{c}L(c,s)(-r)_s \tag{9}$$

(Riordan, 1958 (p.43); Comtet, 1974 (p.156)).

The Daehee numbers are given by

$$\frac{\ln(1+z)}{\mathrm{z}}=\sum_{m=0}^{\infty}D_m\frac{z^m}{m!} \tag{10}$$

(Kim & Kim, 2013; 2018; Simsek, 2016; 2019).

By using (10), we get

$$D_v=\frac{(-1)^v v!}{v+1}$$

(Kim & Kim, 2013; 2018; Simsek, 2016; 2019).

The Changhee numbers Ch_m are given by

$$\frac{2}{\mathrm{z}+2}=\sum_{m=0}^{\infty} Ch_m \frac{z^m}{\mathrm{m!}} \tag{11}$$

(Kim et al., 2013; Simsek, 2019). By using (11), we have

$$Ch_v=\frac{(-1)^v v!}{2^v}$$

(Kim et al., 2013; Simsek, 2019).

Generating function of the Fubini type polynomials of order c is given by

$$G_a(z,t,c)=\frac{2^c}{(2-e^z)^{2c}}e^{tz}=\sum_{m=0}^{\infty} a_m^{(c)}(t)\frac{z^m}{m!}, \tag{12}$$

where $|z|<\ln 2$ and $c \in \mathbb{N}_0$ (Kilar & Simsek, 2017; see also Kilar, 2017; Kilar & Simsek, 2019a,b).

Setting $t=0$ in (12), we have the Fubini type numbers of order c:

$$a_m^{(c)}(0)=a_m^{(c)}$$

(Kilar & Simsek, 2017; see also Kilar, 2017; Kilar & Simsek, 2019a,b).

Using (12), we get

$$a_d^{(c)}(t)=\sum_{k=0}^{\mathrm{d}} \binom{d}{k} a_k^{(c)} t^{d-k} \tag{13}$$

(Kilar & Simsek, 2017; Kilar, 2017).

1.1. Formulas for p-adic Integrals and Some Special Numbers

Here, we give some formulas including the p-adic integrals involving the Volkenborn integral and the p-adic Fermionic integral and special numbers. These formulas have many applications in physics and in engineering besides in mathematics.

Let C^1 ($\mathbb{Z}_p \rightarrow$K) denotes the set of the uniformly differential function f on $\mathbb{Z}_p$.

The Volkenborn integral (or the bosonic p-adic integral) of the uniformly differential function f on $\mathbb{Z}_p$ is given by

$$\int_{\mathbb{Z}_p} f(x)d\mu_1(x)=\lim_{N\rightarrow\infty}\frac{1}{p^N}\sum_{x=0}^{p^N-1} f(x), \tag{14}$$

where $f \in$($\mathbb{Z}_p \rightarrow$K) and

$$\mu_1(x)=\mu_1\left(x+p^N\mathbb{Z}_p\right)=p^{-N}$$

(Schikhof, 1984; Kim, 2002a; 2005; Kim & Kim, 2013; Simsek, 2019; 2021).

Using (14), the Bernoulli numbers B_m is also given by

$$\int_{\mathbb{Z}_p} x^m d\mu_1(x) = B_m \tag{15}$$

(Schikhof, 1984; Kim, 2002a; Kim & Kim, 2013; Simsek, 2019).

Using (14), the Daehee numbers D_m is also given by

$$\int_{\mathbb{Z}_p} (x)_m d\mu_1(x) = D_m \tag{16}$$

(Kim, 2002b; Kim & Kim, 2013; Simsek, 2019).

Let $f \in(\mathbb{Z}_p \rightarrow \mathbb{K})$. The p-adic Fermionic integral of the uniformly differential function f on $\mathbb{Z}_p$ is given by

$$\int_{\mathbb{Z}_p} f(x) d\mu_{-1}(x) = \lim_{N\rightarrow\infty} \sum_{x=0}^{p^N-1} (-1)^x f(x), \tag{17}$$

Where

$$\mu_{-1}(x) = (-1)^x$$

(Kim, 2007; Simsek, 2019).

Using (17), the Euler numbers E_m is also given by

$$\int_{\mathbb{Z}_p} x^m d\mu_{-1}(x) = E_m \tag{18}$$

(Kim, 2007; Simsek, 2019).

Using (17), the Changhee numbers Ch_m is also given by

$$\int_{\mathbb{Z}_p} (x)_m d\mu_{-1}(x) = Ch_m \tag{19}$$

(Kim et al., 2013; Simsek, 2019).

2. FORMULAE FOR FUBINI TYPE NUMBERS: APPROACH TO APPLICATION OF *P*-ADIC INTEGRALS

By using the p-adic integrals and functional equations of the generating functions, we give some formulae and finite sums including the Fubini type polynomials and numbers of higher order, the Bernoulli numbers, the Euler numbers, the Lah numbers, the Stirling type numbers, combinatorial numbers, and also the Hermite polynomials.

For $v \in \mathbb{N}_0$, Kilar (2017; Corollary 4.2, p. 28) gave the following identity:

$$x^v = (2c)!\, 2^c \sum_{r=0}^{v} \binom{v}{r} S_2\left(r, 2c; \frac{1}{2}\right) a_{v-r}^{(c)}(x). \tag{20}$$

By using (20) and (7), the following result is derived:

Corollary 2.1. Let $v \in \mathbb{N}_0$. Then we have

$$\sum_{s=0}^{v} S_2(v,s)(x)_s = (2c)!\,2^c \sum_{r=0}^{v} \binom{v}{r} S_2\left(r, 2c; \frac{1}{2}\right) a_{v-r}^{(c)}(x). \tag{21}$$

Combining (21) with (9), we derive the following relation involving the Lah numbers, the Stirling type numbers, and the Fubini type polynomials of higher order:

Theorem 2.2. Let $v \in \mathbb{N}_0$. Then we have

$$\sum_{s=0}^{v} \sum_{d=0}^{s} S_2(v,s) L(s,d)(-x)_d = (2c)!\,2^c \sum_{r=0}^{v} \binom{v}{r} S_2\left(r, 2c; \frac{1}{2}\right) a_{v-r}^{(c)}(x).$$

Theorem 2.3. Let $v \in \mathbb{N}_0$. Then we have

$$a_v^{(c)}(2x) = \sum_{r=0}^{\left[\frac{v}{2}\right]} \sum_{s=0}^{v-2r} \binom{v-2r}{s} \binom{v}{2r} a_s^{(c)} H_{v-2r-s}(x).$$

Proof. Multiplying the function $\frac{2^c}{(2-e^z)^{2c}}$ on the both-sides of (3), after that using the resulting equation and (12), we obtain

$$G_a(z, 2x, c) = e^{z^2} G_a(z, 0, c) G_H(z, x).$$

With the help of the above functional equation, we get

$$\sum_{v=0}^{\infty} a_v^{(c)}(2x) \frac{z^v}{v!} = \sum_{v=0}^{\infty} \frac{z^{2v}}{v!} \sum_{v=0}^{\infty} a_v^{(c)} \frac{z^v}{v!} \sum_{v=0}^{\infty} H_v(x) \frac{z^v}{v!}.$$

Thus

$$\sum_{v=0}^{\infty} a_v^{(c)}(2x) \frac{z^v}{v!} = \sum_{v=0}^{\infty} \sum_{r=0}^{\left[\frac{v}{2}\right]} \sum_{s=0}^{v-2r} \binom{v-2r}{s} \binom{v}{2r} a_s^{(c)} H_{v-2r-s}(x) \frac{z^v}{v!}.$$

Therefore, we arrive at the desired result.

Applying the Volkenborn integral to (20), then make use of the final equation with (13) and (15), we obtain the following result:

Theorem 2.4. Let $v \in \mathbb{N}_0$. Then we have

$$B_v = (2c)!\,2^c \sum_{r=0}^{v} \binom{v}{r} S_2\left(r, 2c; \frac{1}{2}\right) \sum_{l=0}^{v-r} \binom{v-r}{l} a_l^{(c)} B_{v-r-l}. \tag{22}$$

Applying the Volkenborn integral to (21), after that using the resulting equation with (15) and (16), we have the following result:

Theorem 2.5. Let $v \in \mathbb{N}_0$. Then we have

$$\sum_{s=0}^{v} S_2(v,s)D_s = (2c)!\,2^c \sum_{r=0}^{v} \binom{v}{r} S_2\left(r, 2c; \frac{1}{2}\right) \sum_{l=0}^{v-r} \binom{v-r}{l} a_l^{(c)} B_{v-r-l} \tag{23}$$

or, equivalently,

$$\sum_{s=0}^{v} (-1)^s \frac{s!\,S_2(v,s)}{s+1} = (2c)!\,2^c \sum_{r=0}^{v} \binom{v}{r} S_2\left(r, 2c; \frac{1}{2}\right) \sum_{l=0}^{v-r} \binom{v-r}{l} a_l^{(c)} B_{v-r-l}.$$

Remark 2.6. Combining (23) with (22), we get

$$\sum_{s=0}^{v} S_2(v,s)D_s = B_v,$$

where $v \in \mathbb{N}_0$ (Kim & Kim, 2013; Simsek, 2019).

Applying the p-adic Fermionic integral to (20), then using final equation and equations (13) and (18), we get Theorem 2.7 as follows.

Theorem 2.7. Let $v \in \mathbb{N}_0$. Then we have

$$E_v = (2c)!\,2^c \sum_{r=0}^{v} \binom{v}{r} S_2\left(r, 2c; \frac{1}{2}\right) \sum_{l=0}^{v-r} \binom{v-r}{l} a_l^{(c)} E_{v-r-l}. \tag{24}$$

Applying the p-adic Fermionic integral to (21), then make use of the final equation with (18) and (19), we derive Theorem 2.8 below.

Theorem 2.8. Let $v \in \mathbb{N}_0$. Then we have

$$\sum_{s=0}^{v} S_2(v,s)Ch_s = (2c)!\,2^c \sum_{r=0}^{v} \binom{v}{r} S_2\left(r, 2c; \frac{1}{2}\right) \sum_{l=0}^{v-r} \binom{v-r}{l} a_l^{(c)} E_{v-r-l} \tag{25}$$

or, equivalently,

$$\sum_{s=0}^{v} (-1)^s \frac{s!\,S_2(v,s)}{2^s} = (2c)!\,2^c \sum_{r=0}^{v} \binom{v}{r} S_2\left(r, 2c; \frac{1}{2}\right) \sum_{l=0}^{v-r} \binom{v-r}{l} a_l^{(c)} E_{v-r-l}.$$

Remark 2.9. Combining (25) with (24), we have

$$\sum_{s=0}^{v} S_2(v,s)Ch_s = E_v,$$

where $v \in \mathbb{N}_0$ (Kim et al., 2013; Simsek, 2019).

3. CONCLUSION

Generating functions and p-adic integrals have been widely investigated by many mathematicians, physicists, engineers, and other scientists. In particular, the applications of p-adic integrals have been frequently used in many different areas. For this reason, here, we gave some interesting formulae for the Fubini type polynomials and numbers by the aid of p-adic integrals. These formulae are involved in the Fubini type numbers of higher

order, the Bernoulli polynomials and numbers, the Euler polynomials and numbers, the Lah numbers, the Stirling type numbers, the combinatorial numbers, and the Hermite polynomials. Consequently, the results of this paper may be usefulness in many areas such as mathematics, engineering and physics.

ACKNOWLEDGEMENT

The second-named author was supported by the Scientific Research Project Administration of the University of Akdeniz.

CONFLICT OF INTEREST

The authors declare no conflict of interest.

REFERENCES

Belbachir, H., Rahmani, M., & Sury, B. (2011). Sums involving moments of reciprocals of binomial coefficients. *Journal of Integer Sequences*, *14*(6), Article 11.6.6.

Comtet, L. (1974). Advanced Combinatorics: The Art of Finite and Infinite Expansions. Dordrecht and Boston: D. Reidel Publishing.

Kilar, N. (2017). Fubini Type Numbers and Their Generating Functions. MSc Thesis in Mathematics, Akdeniz University, Antalya.

Kilar, N. (2021). Combinatorial sums and identities associated with functional equations of generating functions for Fubini type polynomials. Preprint.

Kilar, N., & Simsek, Y. (2017). A new family of Fubini numbers and polynomials associated with Apostol-Bernoulli numbers and polynomials. *Journal of the Korean Mathematical Society*, *54*(5), 1605–1621.

Kilar, N., & Simsek, Y. (2019a). Some relationships between Fubini type polynomials and other special numbers and polynomials. *AIP Conference Proceedings*, *2116*(100017), 100017.1–100017.4

Kilar, N., & Simsek, Y. (2019b). Identities and relations for Fubini type numbers and polynomials via generating functions and p-adic integral approach. *Publications de l'Institut Mathématique*, *106*(120), 113–123.

Kilar, N., & Simsek, Y. (2021). Formulas and relations of special numbers and polynomials arising from functional equations of generating functions. *Montes Taurus Journal of Pure and Applied Mathematics*, *3*(1), 106–123.

Kim, T. (2002a). q-Volkenborn integration. *Russian Journal of Mathematical Physics*, *19*, 288–299.

Kim, T. (2002b). An invariant p-adic integral associated with Daehee numbers. *Integral Transforms and Special Functions*, *13*(1), 65–69.

Kim, T. (2005). A note on q-Volkenborn integration. *Proceedings of the Jangjeon Mathematical Society*, *8*(1), 13–17.

Kim, T. (2007). On the analogs of Euler numbers and polynomials associated with p-adic q-integral on $\mathbb{Z}_p$ at $q = -1$. *Journal of Mathematical Analysis and Applications*, *331*(2), 779–792.

Kim, D. S., & Kim, T. (2013). Daehee numbers and polynomials. *Applied Mathematical Sciences (Ruse)*, *7* (120), 5969–5976.

Kim, D. S., & Kim, T. (2018). Some p-adic integrals on $\mathbb{Z}_p$ associated with trigonometric functions. *Russian Journal of Mathematical Physics*, *25*(3), 300–308.

Kim, D. S., Kim, T., & Seo, J. (2013). A note on Changhee numbers and polynomials. *Advanced Studies in Theoretical Physics*, *7*, 993–1003.

Kim, T., Kim, D.S., Jang, G.-W., & Kwon, J. (2018). Symmetric identities for Fubini polynomials. *Symmetry*, *10*, 219.

OEIS, The On-Line Encyclopedia of Integer Sequences (2021). (Accessed: 14/10/2021) oeis.org/A000670.

Rainville, E. D. (1960). Special Functions. New York: The Macmillan Company.

Riordan, J. (1958). An Introduction to Combinatorial Analysis. New York: John Wiley Sons Inc.

Schikhof, W. H. (1984). Ultrametric Calculus: An Introduction to p-adic Analysis. Cambridge Studies in Advanced Mathematics 4, Cambridge: Cambridge University Press.

Simsek, Y. (2013). Generating functions for generalized Stirling type numbers, Array type polynomials, Eulerian type polynomials and their applications. *Fixed Point Theory and Applications*, *87*(2013), 1–28.

Simsek, Y. (2016). Apostol type Daehee numbers and polynomials. *Advanced Studies in Contemporary Mathematics*, *26*, 555–566.

Simsek, Y. (2019). Explicit formulas for p-adic integrals: Approach to p-adic distributions and some families of special numbers and polynomials. *Montes Taurus Journal of Pure and Applied Mathematics*, *1*(1), 1–76.

Simsek, Y. (2021). Interpolation functions for new classes special numbers and polynomials via applications of p-adic integrals and derivative operator. *Montes Taurus Journal of Pure and Applied Mathematics*, *3*(1), 38–61.

Srivastava, H. M., & Choi, J. (2012). Zeta and q-Zeta Functions and Associated Series and Integrals. Amsterdam: Elsevier.

Srivastava, H. M., & Kızılateş, C. (2019). A parametric kind of the Fubini-type polynomials. *Revista de la Real Academia de Ciencias Exactas, Físicas y Naturales. Serie A. Matemáticas (RACSAM) 113*, 3253–3267.

Research Article / Araştırma Makalesi GU J Sci, Part A, 8(4): 411-423 (2021) https://doi.org/10.54287/gujsa.1002703

Gazi University
Journal of Science
PART A: ENGINEERING AND INNOVATION
http://dergipark.org.tr/gujsa

Bioactivities from Novel Toxins of *Pterois volitans*: A Bioinformatics Approach

Levent CAVAS[12*], Yagmur BILGIN[1]

[1]*Department of Chemistry, Faculty of Science, Dokuz Eylül University, İzmir, Turkey 35390, Kaynaklar Campus*
[2]*Department of Biotechnology, Graduate School of Natural and Applied Sciences, Dokuz Eylül University, İzmir, Turkey 35390, Kaynaklar Campus*

Keywords

Angiotensin Converting Enzyme

Bioactive Peptides

Dipeptidyl Peptidase-IV

Pterois volitans

Abstract

Pterois volitans (Linnaeus, 1758), native of the Indo-Pacific Ocean, is an invasive fish species in the Western-Atlantic. Due to the very long venomous spines, they increase their populations in newly invaded habitats. No validated eradication method has been existed for this species yet. Therefore, there is an urgent need for alternative utilization methods for this fish species. Bioactive peptides are of great importance for human health since they exhibit excellent inhibitory properties for some medicinally important enzymes in human metabolisms such as angiotensin converting enzyme (ACE) and dipeptidyl peptidase-IV (DPP-IV). In this study, the bioactive peptides in protein-based venom of *P. volitans*, Pvtoxin-a and Pvtoxin-b, were investigated by using in silico tools. Total number of negatively charged residues (Asp + Glu) for Pvtoxin-a and Pvtoxin-b were found as 21 and 18, respectively. Total number of positively charged residues (Arg + Lys) for Pvtoxin-a and Pvtoxin-b were observed to be 22 and 24, respectively. According to BIOPEP results, A_E values for ACE and DPP-IV were found to be 0.0305 and 0.0666 for Pvtoxin-a and Pvtoxin-b as 0.0333 and 0.0569, respectively. It is very interesting to note that A_E values related to antioxidant property were observed to be 0.0083 for both Pvtoxin-a and Pvtoxin-b. Although A_E value for alpha-glucosidase inhibitor was found to be 0.0014 for Pvtoxin-a, no A_E value was obtained for Pvtoxin-b. In conclusion, the BIOPEP results clearly show that after a possible eradication study, protein-based venoms from *P. volitans* can be evaluated in the production of bioactive peptides. A possible economical value may create a pressure on its increasing population in newly invaded areas.

Cite

Cavas, L., & Bilgin, Y. (2021). Bioactivities from Novel Toxins of *Pterois volitans*: A Bioinformatics Approach. *GU J Sci, Part A, 8*(4), 411-423.

Author ID (ORCID Number)

L. Cavas, 0000-0003-2136-6928
Y. Bilgin, 0000-0002-1999-6050

Article Process

Submission Date 30.09.2021
Revision Date 01.11.2021
Accepted Date 08.11.2021
Published Date 12.11.2021

1. INTRODUCTION

The entry of invasive species has been increasing and becoming a major problem in the Mediterranean Sea (Carballo-Cárdenas, 2015; Bédry et al., 2021). The name "lionfish" is given for the members of the genera *Pterois*, *Parapterois* and *Dendrochirus*. Among this large family, *Pterois volitans* (Linnaeus, 1758) and *P. miles* (Bennett, 1828) (Actinoptery: Scorpaeniformes: Scorpaenidae) are of great importance due to their invasive properties. The lionfish invasion is one of the important concerns for marine ecosystems since they have an ability to alter native fish populations and damage to the native biodiversity (Sutherland et al., 2010; Andradi-Brown, 2019). Although *P. volitans* are native to the western parts of the Indo-Pacific Ocean, they have so far been reported from western Atlantic (Schofield, 2009; 2010), USA (Meister et al., 2005) and southeast Brazil (Ferreira et al., 2015). The invasion of lionfish has still been confused for the Mediterranean Sea due to some published reports in the scientific journals. As an example, although some authors (Gürlek et al., 2016; Turan et al., 2017; 2020, Ayas et al., 2018) previously identified the lionfish in the Mediterranean Sea coastline of Turkey as *P.volitans*, according to the recent papers by Ulman et al. (2020) and Cinar et al. (2021), the lionfish off the Turkish coastline is defined as *P. miles*. The reason of the confusion is based on the misinterpretation of the samples due to i) morphological properties cannot be enough to distinguish *P.volitans*

*Corresponding Author, e-mail: levent.cavas@deu.edu.tr

and *P.miles*, ii) correct bio-sequences should be selected to identify correct taxon in the genetic studies (Ulman et al., 2020; Cinar et al., 2021, Kovačić et al., 2021). Lionfish invasion along Turkish coastline is in increasing trend. It is very important to note that the lionfish is also mentioned in the recent novel of Zülfü Livaneli, one of the famous writers in Turkey, titled "*Balıkçı ve Oğlu*" (Livaneli, 2021). The lionfish has venomous dorsal spiky rays and pectoral fins (Dağhan & Demirhan, 2020). Therefore, hunting of lionfish through spear fishing is dangerous and also risky because of its venomous spines. On the other hand, spear fishing tournaments specific to lionfish organized by various local organizations to reduce their numbers on the shores (Antalya Büyükşehir Belediyesi, 2021). However, this kind of organizations must be carried out by experts. Yuzvik et al. (2018) developed a submarine robot which has properties of hunting lionfish to control of *P. volitans* population in the Caribbean. Therefore, it could be stated that lionfish may harm the ecosystem due to their huge appetites and preferences for native species, however they may also present economic benefits through development of commercial fisheries for them (Kleitou et al., 2019). It has maroon or brown and white stripes (Davis, 2016) also it has 13 back, 3 anal spines and one on each pelvic fin (Galloway & Porter, 2019). *P. volitans* uses its back spines to present itself larger and stronger (Galloway & Porter, 2019). Its spines contain non-protein based ichthyotoxin with low molecular mass. This venom can be isolated from only alive fishes (Nair et al., 1985). Toxins can cause to symptoms that last for a few days as a result of contact with humans. Burning symptom is observed within the first 15-20 minutes after the spines come into contact. Also, tachycardia, hypertension, and numbness can be observed. After 3 hours, the venom spreading into the body can cause limb paralysis (Vetrano et al., 2002). Therefore, it is dangerous if the spines penetrate humans, but once their spines are removed, they are safe to consume and are considered a very delicious fish. The lionfish is at the top of the underwater food chain and is a major threat to native fish. *P. volitans* is observed in the ecosystem where it skillfully hunts smaller fish and crustaceans. It damages native biodiversity. Especially, the Mediterranean Sea and the Caribbean are under the threat since lionfish has widely distributed areas in these marine ecosystems (Carballo-Cárdenas, 2015; Ulman et al., 2020).

Bioactive peptides are obtained from food proteins. They are component of the functional foods and nutraceuticals and therefore they play important roles in human health (Liu et al., 2020). Hyperlipidemia, inflammation, diabetes, cancer, immune disorder can be given as example disorders in which bioactive peptides can show effectiveness (Agyei & Danquah, 2012). They are related with biological activities such as antimicrobial, antioxidant, antihypertensive, immunomodulatory, antidiabetes, anti-cancer (Daroit & Brandelli, 2021). Bioactive peptides consist of 2-20 amino acid residues. Long peptides are inactive without hydrolysis. They are activated via hydrolysis methods such as fermentation (proteolytic enzymes, microbial or vegetable proteolytic enzymes) (Weaver, 2014). Compared to proteins, bioactive peptides are absorbed by the intestine completely due to their sizes (Zhou et al., 2020). Bioactive peptides are new to humans but safety studies have been limited yet for commercial use although they are derived from foods. There has so far been no information yet about if new bioactive peptides carry sequences with allergenic or even toxic (Liu et al., 2020). The origin of bioactive peptides can be plant or animal. Grains and legumes are peptide rich sources (Jang & Lee, 2005). According to Chakrabarti et al. (2018), there are three challenges on the utilization of food-derivated bioactive peptides and they are production, oral consumption and regulation. Bioactive peptides may be used for the chronic diseases but further studies are required.

Kiriake & Shiomi (2011) discovered two proteinaceous toxins from two lionfish species (*Pterois antennata* and *Pterois volitans*). The authors investigated the toxin structures via cDNA cloning using primers designed from the highly conserved sequences of the stonefish toxins. Since these toxins homologous are most probably existed in Scorpaeniformes members (Kiriake & Shiomi, 2011), *P. miles* which has a second colonization in the Mediterranean Sea may have these toxins and may show similar symptoms when preys are exposed to these toxins. *P. miles* is also widely distributed within the Mediterranean Sea, we wanted to investigate bioactive peptides in Pvtoxin-a and Pvtoxin-b in *P.volitans* by using bioinformatics tools developed for identification of bioactive peptides within protein sequences.

2. MATERIALS AND METHODS

The proteins related to *P. volitans* were searched by using UniProt.org and 560 proteins were listed. The longest protein was Pvtoxin-a (F2ZAF0) with 699 amino acids and the shortest protein was ATP synthase protein 8 (A0A0U1WQN3) with 55 amino acids (Morgat et al., 2020). In this study, Pvtoxin-a (F2ZAF0) and

Pvtoxin-b (F2ZAF1) were selected as model proteins. FASTA formats of proteins were obtained from UniProt.org. In order to obtain protein parameters, Protparam tool was used (Gasteiger et al., 2005). Pairwise sequence alignment was carried out by using Clustal Omega (Sievers et al., 2011). BIOPEP-UWM (http://www.uwm.edu.pl/biochemia/index.php/en/biopep) was used to estimate bioactive peptides in Pvtoxin-a and Pvtoxin-b. Chymotrypsin, trypsin and pepsin (pH = 1.3) were used for in silico digestions. The reason for selection of these 3 proteolytic enzymes was their importance in human protein digestion system (Minkiewicz et al., 2019). The analytical parameters with respect to bioactive peptides were estimated from BIOPEP-UWM and then they were compared. The Basic Local Alignment Search Tool (BLAST) was used to find similar proteins in the protein database.

3. RESULTS

3.1. Protparam Results

Protein parameters in Pvtoxin-a and -b were studied in this paper by using Protparam tool (Gasteiger et al., 2005). According to Table 1, most two abundant amino acids in Pvtoxin-a were leucin (% 8.8) and valine (% 7.7). Maximum percentages of amino acids in Pvtoxin-b were found as leucine (% 7.8) and glycine and lysine (% 7.3). From the results, it could be said that essential amino acid leucine is very high in both studied proteins. Theoretical pI value was found for Pvtoxin-a as 7.89 and for Pvtoxin-b as 9.14. Total number of negatively charged residues (Asp + Glu) for Pvtoxin-a and Pvtoxin-b were found as 21 and 18, respectively. Total number of positively charged residues (Arg + Lys) for Pvtoxin-a and Pvtoxin-b were observed to be 22 and 24, respectively. It is very interesting to note that the net charges of the proteins studied, Pvtoxin-a and Pvtoxin-b, were found as 1 and 6, respectively.

Table 1. *Number, Percentages and Theoretical pI, Total Number of Positively & Negatively Charged Residues and Net Charge of Amino Acids of Pvtoxin-a and Pvtoxin-b Proteins of Pterois volitans (aa: amino acids)*

	Pvtoxin-a		**Pvtoxin-b**	
	#aa	**aa%**	**#aa**	**aa%**
Ala (A)	6	3.1	10	5.2
Arg (R)	8	4.1	10	5.2
Asn (N)	14	7.2	8	4.1
Asp (D)	10	5.2	11	5.7
Cys (C)	3	1.5	4	2.1
Gln (Q)	5	2.6	10	5.2
Glu (E)	11	5.7	7	3.6
Gly (G)	14	7.2	14	7.3
His (H)	8	4.1	6	3.1
Ile (I)	9	4.6	10	5.2
Leu (L)	17	8.8	15	7.8
Lys (K)	14	7.2	14	7.3
Met (M)	3	1.5	1	0.5
Phe (F)	10	5.2	1	5.7
Pro (P)	10	5.2	10	5.2
Ser (S)	14	7.2	12	6.2
Thr (T)	10	5.2	12	6.2
Trp (W)	5	2.6	8	4.1
Tyr (Y)	8	4.1	8	4.1
Val (V)	15	7.7	12	6.2
Theoretical pI	7.89		9.14	
Total number of negatively charged residues (Asp + Glu):	21		18	
Total number of positively charged residues (Arg + Lys):	22		24	
Net charge	1		6	

3.2. Pairwise Sequence Alignment results

Clustal Omega tool was used to determine the similarity of Pvtoxin-a and -b (Siever et al., 2011). According to Figure 1, their both N-terminals are methionine (M) and their C-terminals are leucine (L), respectively. There is very high similarity in the amino acid sequences of the proteinous toxins, Pvtoxin-a and –b.

```
tr|F2ZAF0|      MSSEILIVAALGRPFTLGALYDSRKDRLIPGFTLWEDDVLQANTVESRQPSSAFEIIASD   60
tr|F2ZAF1|      MSSQILVVAALGRPFTLGTLYDARKVRLIPGFTLWEDDVLQANTVESRQPSSAFEIIASD   60
                ***:**:**********:***:** ********************************

tr|F2ZAF0|      SIEDKSSLMDIEASLKASFLGGLVEVGGSAKYLDDRKKFKNQSRVTLQYKATTSFKQLMT   120
tr|F2ZAF1|      SIEDKSSLMDIEASLKASFLGGLVEVGGSAKYLDDRKKFKNQSRVTLQYKATTSFKQLMT   120
                ************************************************************

tr|F2ZAF0|      NLETKHVEYSEYFQNLEATHVVIGILYGANAFFVFDSAKTESSNVQDIQGSMEAAIKKIP   180
tr|F2ZAF1|      NLETKHVEYSEYFQNLEATHVFIGILYGANAFFVFDSAKTESSNVQDIQGSMEAAIKKIP   180
                ********************.***************************************

tr|F2ZAF0|      SVEISGQGSVKLTSEDSAITDRFSCKFHGDVLLPSNPTTFEDAVQTYQQLPQMMGKENAV   240
tr|F2ZAF1|      SVEISGKGEVKLTSEDSAITSGFSCKFHGDFFLPSNPTTFEDAVQTYQQLPQMMGKENAV   240
                ******:*.**********. ********.:****************************

tr|F2ZAF0|      PMKVWLVPLVHFYSEAPKLMADSSISILRRVRNTLEAMRELEMRCNDALEDNTVKLFPLM   300
tr|F2ZAF1|      PMTVWLVPLVNFYSEAPKLMADSSTPILRKVRNTLEAMRELEMRCNDALEDNTVKLFPLI   300
                **.*******:************  ***:****************************:

tr|F2ZAF0|      VKKLNNFQNLFGVYMSNLRRSIAEKLQSIRSGSEDQSAMLQLFQENLKSPFNTDSLNMWM   360
tr|F2ZAF1|      EKKLNNFKNFFGDYMLNLRRTIAEKLQSIRSGSENESAMLQLFQENLKSPFNIDSLNMWM   360
                 ******:*:** ** ****:************::**************** *******

tr|F2ZAF0|      DCAEREINVLRSCIDIIEEARHKVVLSESEMFRELLDSNVKHAVCYVFTFVTDQDPFLKV   420
tr|F2ZAF1|      DCAEREINVLRSCIDIIEEARHKVVLSESEMFRELLDPNVKHAVCYVFTFVTDQDPFLNV   420
                ************************************ ******************:*

tr|F2ZAF0|      LTDYLDSPDSRPKRTRPPATEYWYASDTIPEMMRDKAHIFYNLAKEMDNRRVRFLVASIV   480
tr|F2ZAF1|      LSDFLDSPTSKPKKLRPSTKDYWYISDDIPEMMRAKAHHFRNLALDMDNRCVRFLVASIG   480
                *:*:**** *:**: ** :.:*** ** ****** *** * *** :**** ********

tr|F2ZAF0|      NPKQEGAGIHYYRENILIEQEFLQPKMNPVEKIVDRRDLLWCDCELTLDPVTAHPALTLS   540
tr|F2ZAF1|      NPKQEGAGIHYYREGIQIIDEFTKPWIPPVETIQDRRELLWCDCELTLDPDTAQPALTLS   540
                **************.* * :** :* : ***.* ***:************ **:******

tr|F2ZAF0|      EGNKKAVSGKPKPSDNNPERFEHFQYVLCKKQLIRRHYWEIKWSGFVGAGVIRNSIHPKS   600
tr|F2ZAF1|      EGNKKAVSGTAKPFDNQQRRFQCYQQVLCNKGLSRRHYWEVEWSGYVRAGVTYKGISRRT   600
                *********. ** **: .**: :* ***:* * ******::***:* ***  :.*  ::

tr|F2ZAF0|      SQVDSSLGGSDKSWVFEYNPNTGYRQIFKNTPENVNVSSTGFDRLGVYLDWLGGTLSYYM   660
tr|F2ZAF1|      WNQDSSLGHNKISWVFDYFPKSGYNHIFDAKKTKVNVSSPGFKKLGIYLDWPAGTLSFYM   660
                 : ***** .. ****:* *::**.:**. .  :***** **.:**:**** .****:**

tr|F2ZAF0|      INNNFVTHLHTFHTLFKEAVYPAFMIGDKQNVHGEIELL 699
tr|F2ZAF1|      VDTIWVTHIHTFKARFQEAVFPAFLIGHGPD-NGQIKLL 698
                ::. :***:***:: *:***:***:**.  : :*:*:**
```

Figure 1. *Clustal Omega Results of Pvtoxin-a and Pvtoxin-b. ('*****' symbol is used to show conserved residues, '**:**' symbol used to show very similar amino acids in terms of physicochemical characters and '**.**' symbol is used to show similar amino acids in terms of physicochemical characters. Empty spaces are used for deleted or inserted amino acids)*

3.3. BIOPEP-UWM Results

BIOPEP-UWM was used for in silico hydrolysis of bioactive peptides which are obtained from Pvtoxin-a and -b (Minkiewicz et al., 2019). When Table 2 is examined, DHt value of Pvtoxin-a was found as 40.1389. A_E value corresponds to the frequency of release of fragments by selected enzymes. A_E values related to dipeptidyl peptidase-III and -IV inhibitors were as 0.0042 and 0.066, respectively. A_E values of Angiotensin converting Enzyme (ACE) inhibitor as 0.0305. The A_E values related to other bioactivities such as stimulating, antioxidative, renin inhibitor, CaMPDE inhibitor and alpha-glucosidase inhibitor can also be found in Table 2. According to Table 3, DHt value of Pvtoxin-b was found as 39.7775. The A_E values were found for dipeptidyl peptidase-III and –IV inhibitors to be 0.0069 and 0.0569, respectively. The A_E values with respect to ACE inhibitor as 0.0333. The other bioactivities such as antiamnestic, stimulating, antioxidative and renin inhibitor were depicted in Table 3.

Table 2. *In Silico Hydrolysis of Pvtoxin-a Protein of Pterois volitans Using BIOPEP-UWM Database*

DHt [%] 40.1389					
No	Activity	**A_E**	**W**	**B_E**	**V**
1	ACE inhibitor	0.0305	0.0830	0.0023	0.1357
2	Stimulating	0.0055	0.1134	0	Nd
3	Antioxidative	0.0083	0.1273	0	0
4	renin inhibitor	0.0042	0.1317	0.0002	0.3332
5	CaMPDE inhibitor	0.0014	0.1687	0	nd
6	dipeptidyl peptidase IV inhibitor	0.0666	0.1109	0.0001	0.2552
7	alpha-glucosidase inhibitor	0.0014	0.0530	6.1370E-5	0.9683
8	dipeptidyl peptidase III inhibitor	0.0042	0.0445	0	nd

Table 3. *In Silico Hydrolysis of Pvtoxin-b Protein of Pterois volitans Using BIOPEP-UWM Database*

DHt [%] 39.7775					
No	**Activity**	**A_E**	**W**	**B_E**	**V**
1	antiamnestic	0.0014	0.2500	2.9551E-5	1
2	stimulating	0.0028	0.0695	0	
3	ACE inhibitor	0.0333	0.0885	0.0010	0.0905
4	antioxidative	0.0083	0.1390	0	0
5	dipeptidyl peptidase IV inhibitor	0.0569	0.0962	0.0001	0.2193
6	renin inhibitor	0.0042	0.1317	8.9606E-7	0.0058
7	dipeptidyl peptidase III inhibitor	0.0069	0.0776	0	

3.4. BLAST Results

In order to find similar proteins, BLAST-p analysis was carried out by using BLAST server (Altschul et al., 1990). Blast-p results of Pvtoxin-a and -b were given in Figure 2 and Figure 3, respectively. Pvtoxin-a like proteins were also existed in the member of same genus such as *P.lunulata* and *P.antennata*. However, similar proteins are also existed in different genus such as *Scorpaenopsis, Sebastapistes, Dendrochrius* and *Hypodytes*. The Pvtoxin-a is highlighted as yellow in Figure 2. The BLAST-p results for Pvtoxin-b were given Figure 3. Contrary to Pvtoxin-a, Tx gamma-subunit from *Dendrochrius zebra* was in the same clade with Pvtoxin-b. Very similar proteins with most probably same bioactivities are existed in the genus of *Inimicus, Sebastepisces, Scorpaenopsis, Scorpaena, Sebastes, Sebastiscus, Dendrochrius* and *Hypodytes* (Figure 3). The Pvtoxin-b is highlighted as yellow in Figure 3. Table 4-5 show codes and names of the proteins in the phylogenetic tree. Since Pvtoxin-a and –b are searched, the original sequences were also found after BLAST search.

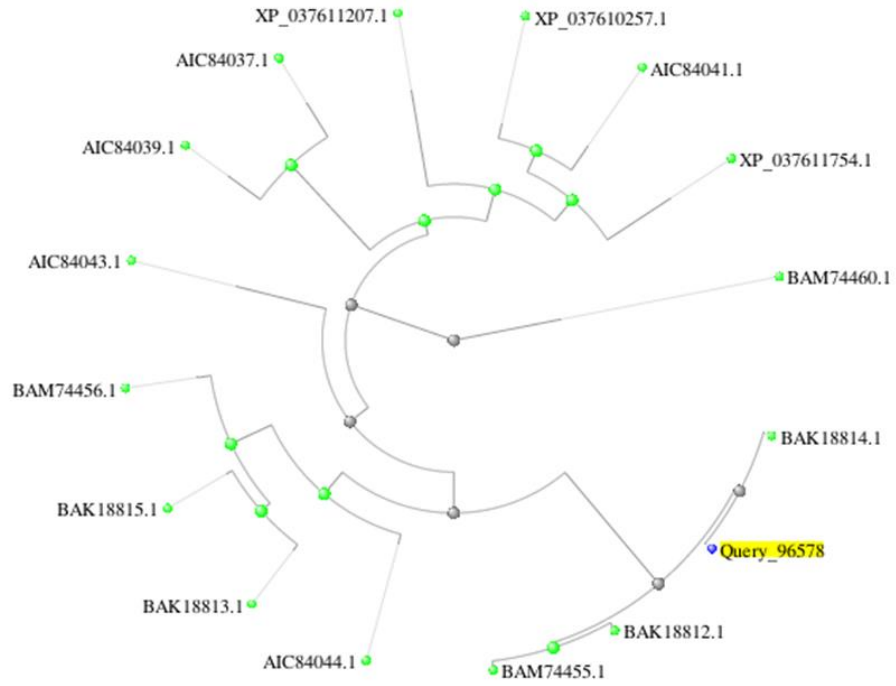

Figure 2. *BLAST-p Analysis Results for Pvtoxin-a*
(The Codes and Names of the Proteins are Explained in the Table 4)

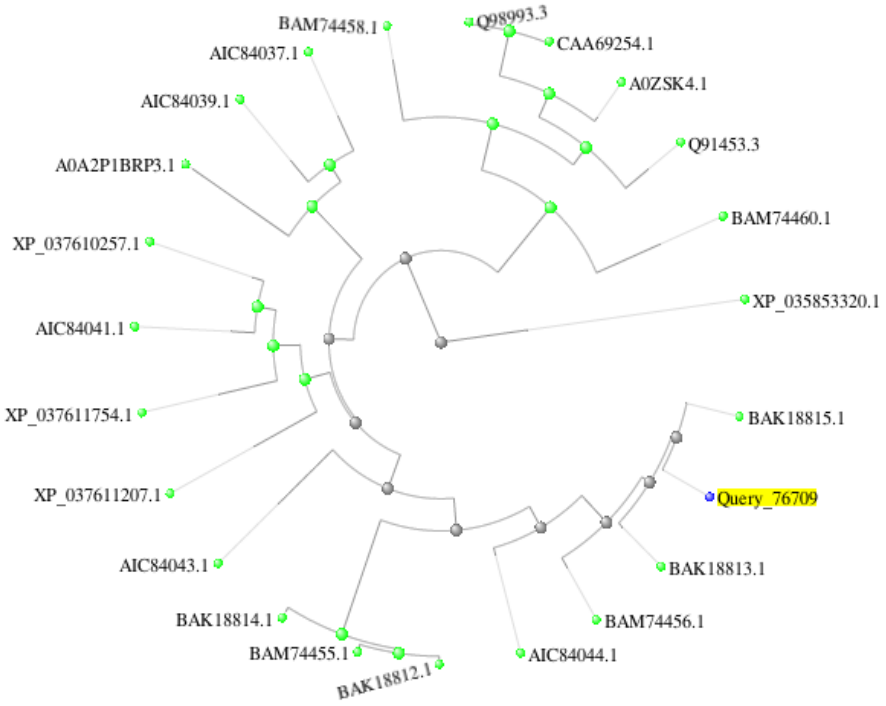

Figure 3. *BLAST-p Analysis Results for Pvtoxin-b*
(The Codes and Names of the Proteins are Explained in the Table 5)

Table 4. *A list of the codes and names of proteins obtained for Pvtoxin-a from BLAST-p*

The Codes	**The Name of The Proteins**
Query_96578	pvtoxin-a [*Pterois volitans*]
BAK18814.1	pvtoxin-a [*Pterois volitans*]
BAM74455.1	pltoxin-a subunit [*Pterois lunulata*]
BAK18812.1	patoxin-a subunit [*Pterois antennata*]
BAM74456.1	pltoxin-b subunit [*Pterois lunulata*]
BAK18815.1	pvtoxin-b [*Pterois volitans*]
BAK18813.1	patoxin-b subunit [*Pterois antennata*]
XP_037611754.1	stonustoxin subunit beta-like [*Sebastes umbrosus*]
AIC84041.1	Tx beta-subunit [*Sebastiscus marmoratus*]
AIC84037.1	Tx beta-subunit [*Sebastapistes strongia*]
XP_037610257.1	stonustoxin subunit beta-like [*Sebastes umbrosus*]
XP_037611207.1	stonustoxin subunit beta-like [*Sebastes umbrosus*]
AIC84039.1	Tx beta-subunit [*Scorpaenopsis oxycephala*]
AIC84044.1	Tx gamma-subunit [*Dendrochirus zebra*]
BAM74460.1	hrtoxin-b subunit [*Hypodytes rubripinnis*]
AIC84043.1	Tx beta-subunit [*Dendrochirus zebra*]

Table 5. *A list of the codes and names of proteins obtained for Pvtoxin-b from BLAST-p*

The Codes	**The Name of The Proteins**
Query_76709	pvtoxin-b [*Pterois volitans*]
BAK18815.1	pvtoxin-b [*Pterois volitans*]
BAK18813.1	patoxin-b subunit [*Pterois antennata*]
BAM74456.1	pltoxin-b subunit [*Pterois lunulata*]
XP_037610257.1	stonustoxin subunit beta-like [*Sebastes umbrosus*]
AIC84041.1	Tx beta-subunit [*Sebastiscus marmoratus*]
AIC84037.1	Tx beta-subunit [*Sebastapistes strongia*]
BAK18814.1	pvtoxin-a [*Pterois volitans*]
AIC84044.1	Tx gamma-subunit [*Dendrochirus zebra*]
BAM74455.1	pltoxin-a subunit [*Pterois lunulata*]
XP_037611207.1	stonustoxin subunit beta-like [*Sebastes umbrosus*]
BAK18812.1	patoxin-a subunit [*Pterois antennata*]
AIC84039.1	Tx beta-subunit [*Scorpaenopsis oxycephala*]
XP_037611754.1	stonustoxin subunit beta-like [*Sebastes umbrosus*]
BAM74460.1	hrtoxin-b subunit [*Hypodytes rubripinnis*]
Q91453.3	RecName: Full=Stonustoxin subunit beta; Short=SNTX subunit beta; AltName: Full=DELTA-synanceitoxin-Sh1b; Short=DELTA-SYTX-Sh1b; AltName: Full=Trachynilysin subunit beta; Short=TLY subunit beta [*Synanceia horrida*]
A0ZSK4.1	RecName: Full=Neoverrucotoxin subunit beta; Short=NeoVTX subunit beta [*Synanceia verrucosa*]
XP_035853320.1	LOW QUALITY PROTEIN: stonustoxin subunit beta-like [*Sander lucioperca*]
BAM74458.1	ijtoxin-b subunit [*Inimicus japonicus*]
A0A2P1BRP3.1	RecName: Full=Cytolytic toxin-beta; Short=Sp-CTx-beta [*Scorpaena plumieri*]
AIC84043.1	Tx beta-subunit [*Dendrochirus zebra*]
CAA69254.1	verrucotoxin alpha [*Synanceia verrucosa*]
Q98993.3	RecName: Full=Verrucotoxin subunit beta; Short=VTX subunit beta [*Synanceia verrucosa*]

4. DISCUSSION

Introduction of alien or non-indigenous species into a new habitat may not always harm to ecosystem. In order to define an alien species as an invasive species, alien species must negatively impact the biodiversity, economy or human health (Ulman et al., 2020). As an example, *P.miles* invasion in the Mediterranean Sea coastline of Turkey impressed not only scientists, but also writers. Lionfish invasion and its social effects from the eyes of a local fisherman in Turkey are described in the recent novel of Zülfü Livaneli (Livaneli, 2021). The current situation of *P.volitans* in Turkey is also complicated due to previously published and confused papers where the lionfish is defined as *P.volitans* (Gürlek et al., 2016; Turan et al., 2017; 2020, Ayas et al., 2018), on the other hand, recent papers underline that the lionfish in Turkish coastlines is *P.miles* (Ulman et al., 2020; Çinar et al., 2021). Bioactive peptides are obtained via wet lab studies. The bioinformatic tools are also used for discovering of bioactive peptides (Agirbasli & Cavas, 2017; Kandemir-Cavas et al., 2019). In this study, Pvtoxin-a and Pvtoxin-b from *P. volitans* were studied as model proteins. Amino acid sequences were compared by using well-known bioinformatics tools such as Protparam and multiple sequence alignment. The novelty of the paper is to study BIOPEP parameters of Pvtoxin-a and Pvtoxin-b from *P. volitans*. There are some differences in protein parameters in Pvtoxin-a and Pvtoxin-b from *P. volitans* such as theoretical pI, net charge and total number of negatively and positively charged residues (Table 1). These differences are caused by the amino acid sequence variations in these proteins (Figure 1). These toxins are still classified as unreviewed proteins in the uniprot.org. However, based on the sequence homology, it is said that these proteins show their functions outside the cell membranes since they are toxin-based proteins. Since they are long protein, consisted of more than 698 amino acids, their short-bioactive peptides are worthwhile to study. Among bioactive peptides, ACE inhibitors are of great importance in terms of hypertension. Since the hypertension is very common not only in developing countries but also in developed countries, it is very important to propose the ACE inhibitors for the production of functional food-based inhibitors. From this perspectives, isolated *P. volitans* toxins can be an alternative source of ACE inhibitors. After partial purification of these toxins, ACE-inhibitors based bioactive peptide cocktails can be prepared. The stimulating is one of the parameters that BIOPEP provided. The stimulating in BIOPEP is defined as the peptides stimulating various biological processes (Minkiewicz et al., 2019). The information related to specific biological activities are also given for each individual protein. When two proteins are compared, it is clear from Table 2 and 3 that Pvtoxin-a has remarkable stimulating activities than Pvtoxin-b. Specific biological activities can be accessed from BIOPEP web page after enzymatic in silico digestion of these proteins. For example, after enzymatic digestion of Pvtoxin-a via trypsin, chymotrypsin and pepsin, VPL was found as a stimulating peptide. Its biological activities are matched with stimulating release of vasoactive substance with 327.41 chemical mass value. The antioxidative term in BIOPEP is defined as peptides inhibiting oxidation. When Pvtoxin-a and -b were compared, the differences in the W values were observed. On the other hand, their A_E values were the same. According to Table 3, Pvtoxin-b has more antioxidative activities than Pvtoxin-a. After digestion of Pvtoxin-b, SDF was found as an antioxidative peptide. AH and EL can also be given as examples for this activity. W and A_E values of Pvtoxin-a and -b for Renin inhibitor were found same. SF and TF were found as renin inhibitor peptides after digestion of Pvtoxin-b. DPP-IV is a serine protease which catalyzes amide bonds. It is reported that DPP-4 inhibitors have an effect on diabetes type-II. Diabetes is a very common health issue and it is very common among 35-40 aged people (Misumi & Ikehara, 2013). According to Table 2 and 3, when A_E and W values were compared for the two proteins, Pvtoxin-a has more DPP-IV inhibitors than Pvtoxin-b. VP, PL, AF, AH, DN can be given as examples as DPP-IV inhibitor peptides. Dipeptidyl peptidase III (DPP-III) is a zinc-dependent hydrolase involved in degrading oligopeptides with 4–12 amino acid residues (Jha et al., 2020). When two proteins were compared, Pvtoxin-b had noticeably more DPP-III inhibitors than Pvtoxin-a. TF and PF can be given as examples for DPP-III inhibitor peptides. BLAST-p was used to find similar proteins. According to Figure 2, *Pterois lunulata, Pterois antennata, Sebastes umbrosus, Sebastastiscus marmoratus, Sebastapistes strongia, Scorpaenopsis oxycephala, Dendrochirus zebra* and *Hypodytes rubripinnis* have Pvtoxin-a like protein. Their percent identities were found to be between 98.57 and 70.67%. The shortest sequence was found to be 583 in *D. zebra* and the longest sequence was 752 in *S. umbrosus*. According to Figure 3, Pvtoxin-b like protein was found in the genus *Inimicus, Sebastepisces, Scorpaenopsis, Scorpaena, Sebastes, Sebastiscus, Dendrochrius* and *Hypodytes*. When two proteins were compared, Tx gamma-subunit from *D. zebra, Synanceia horrida, Synanceia verrucose, Sander lucioperca and Inimicus japonicus* were observed for Pvtoxin-b. Most of these fishes belong to the Scorpaenidae family and they are distributed in tropical waters.

Harris et al. (2020) tested the collapsible trap (Gittings trap) for mitigation of *P. volitans*. The trap technology is very important since SCUBA divers may not always access the depth limits of *P. volitans*. The authors tested their trap in the northern Gulf of Mexico. It is reported that 327 lionfish and 28 native fish were trapped. On the other hand, removal efficacy was given between as 12-24%. According to the authors, even if this range is lower than that of spearfishing, more studies are recommended to develop the traps.

Sommeng et al. (2019) studied the antiviral activity of *P.volitans* phospholipase A2 (PLA2) from Indonesia for its effects on the human immunodeficiency virus. The authors reported that PLA2 from *P.volitans* showed strong inhibition on the SRV2-A549 cell lines, therefore, they suggested to evaluate their effects *in vivo*. Sommeng et al. (2020) also investigated the coagulant activity of *P.volitans* spine venom. The authors studied the coagulant activity via prothrombin time and activated partial thromboplastin time. They found out that the responsible procoagulant molecule in *P.volitans* venom is Nomega-nitro-L-arginine methyl ester. Becerra-Amezcua et al. (2020) investigated the effects of the venom of *P.volitans* on the cholinergic and dopaminergic systems via nicotinic acetylcholine receptors and dopaminergic neurons. Zebra fish was used as a model organisms in their study and it was found by the authors that the venom from *P.volitans* significantly affected the dopaminergic neurons and retarded embryonic development due to the venom also affects growth hormone secretion. The authors also concluded that lionfish venom should be further studied for its possible pharmaceutical effects on the Alzheimers' disease.

Hoo Fung et al. (2013) investigated concentrations of essential, non-essential and toxic elements in the tissues of *P. volitans* collected from Jamaican waters. While the muscular tissues of the *P. volitans* (lionfish) were evaluated, researchers demonstrated that it might make a significant contribution as an alternative nutrition source since it did not reveal conceivably hazardous substances. This study appears partly to confirm the findings of our study. Cavas et al. (2020), in our previous study, proposed that the toxins of *Lagocephalus sceleratus* can be removed and the residues including toxins could be exploited in some industries such as pharmacy inasmuch as their analgesic and anti-cancer effects have been reported for these toxins. From the study of Cavas et al. (2020), it could be said that the removed toxins of *L. sceleratus* may also be evaluated in different industries such as pharmacy inasmuch as their analgesic and anti-cancer effects.

Galloway & Porter (2019) studied the mechanical properties of *P. volitans* spines by quantifying the impacts of shape and tapering on the mechanical properties of the spine. Well-known mechanical properties such as Young's modulus, elastic energy store and flexural stiffness were studied by Galloway & Porter (2019). Bending properties of the spines are also investigated in their study. The authors suggested that the mechanical properties of the spines are important in many functions such as defense, protection and intimidation.

5. CONCLUSION

From the published papers, it could be said that the systematic of the genera *Pterois* is very complex. Even if there has so far been a confusion in the taxonomic identification, the toxins mentioned in this paper most probably exist in P. *miles* which has colonized the Mediterranean Sea. After carefully removal of the venomous spines, the rest of the lionfish tissues can be consumed. From the results of the present study, it could be said that bioactive peptides exist in proteinaceous toxins of *P. volitans* and these bioactive peptides can be used as an alternative protein source. A possible economical values assigned to these invasive fishes may create extra stress on their populations and may help to control their populations. More studies on lionfish species, are strongly warranted to evaluate their values in the preparation of functional foods.

CONFLICT OF INTEREST

The authors declare no conflict of interest.

REFERENCES

Agirbasli, Z., & Cavas, L. (2017). In silico evaluation of bioactive peptides from the green algae *Caulerpa*. *Journal of Applied Phycology*, *29*, 1635–1646. doi:10.1007/s10811-016-1045-7

Agyei, D., & Danquah, M. K. (2012). Rethinking food-derived bioactive peptides for antimicrobial and immunomodulatory activities. *Trends in Food Science and Technology*, *23*(2), 62–69. doi:10.1016/j.tifs.2011.08.010

Altschul, S. F., Gish, W., Miller, W., Myers, E. W., & Lipman, D. J. (1990). Basic local alignment search tool. *Journal of Molecular Biology*, *215*(3), 403–410. doi:10.1016/S0022-2836(05)80360-2

Andradi-Brown, D. A. (2019). Invasive Lionfish (*Pterois volitans* and *P. miles*): Distribution, Impact, and Management. In: Y. Loya, K. A. Puglise, & T. C. L. Bridge (Eds.) *Mesophotic Coral Ecosystems* (pp. 931-941) *Coral Reefs of the World book series (CORW, 12)*. Springer, Cham. doi:10.1007/978-3-319-92735-0_48

Antalya Büyükşehir Belediyesi. (2021, July 11) *Akdeniz'de aslan balığı avı*. (Accessed:10/09/2021) www.antalya.bel.tr/Haberler/HaberDetay/3294/akdenizde-aslan-baligi-avi

Ayas, D., Ağılkaya, G. Ş., & Yağlıoğlu, D. (2018). New record of the red lionfish, *Pterois volitans* (Linnaeus, 1758), in the Northeastern Mediterranean Sea. *Düzce Üniversitesi Bilim ve Teknoloji Dergisi*, *6*(4), 871–877. doi:10.29130/dubited.362703

Becerra-Amezcua, M. P., Hernández-Sámano, A. C., Puch-Hau, C., Aguilar, M. B., & Collí-Dulá, R. C. (2020). Effect of *Pterois volitans* (lionfish) venom on cholinergic and dopaminergic systems. *Environmental Toxicology and Pharmacology*, *77*, 103359. doi:10.1016/j.etap.2020.103359

Bédry, R., de Haro, L., Bentur, Y., Senechal, N., & Galil, B. S. (2021). Toxicological risks on the human health of populations living around the Mediterranean Sea linked to the invasion of non-indigenous marine species from the Red Sea: A review. *Toxicon*, *191*, 69–82. doi:10.1016/j.toxicon.2020.12.012

Carballo-Cárdenas, E. C. (2015). Controversies and consensus on the lionfish invasion in the western atlantic ocean. *Ecology and Society*, *20*(3), 24. doi:10.5751/ES-07726-200324

Cavas, L., Bilgin, Y., & Yilmaz-Abeska, Y. (2020). Can bioactive peptides of *Lagocephalus sceleratus* be evaluated in the functional food industry? *Biotech Studies*, *29*(2), 77–84. doi:10.38042/biost.2020.29.02.04

Chakrabarti, S., Guha, S., & Majumder, K. (2018). Food-derived bioactive peptides in human health: Challenges and opportunities. *Nutrients*, *10*(11), 1–17. doi:10.3390/nu10111738

Çinar, M. E., Bilecenoğlu, M., Yokeş, M. B., Öztürk, B., Taşkin, E., Bakir, K., Doğan, A., & Açik, Ş. (2021). Current status (as of end of 2020) of marine alien species in Turkey, *PLoS ONE*, *16*(5), 1-46, e0251086. doi:10.1371/journal.pone.0251086

Dağhan, H., & Demirhan, S. A. (2020). Some bio-ecological characteristics of lionfish *Pterois miles* (Bennett, 1828) in Iskenderun Bay. *Marine Life Science*, *2*(1), 28–40.

Daroit, D. J., & Brandelli, A. (2021). *In vivo* bioactivities of food protein-derived peptides – a current review. *Current Opinion in Food Science*, *39*, 120–129. doi:10.1016/j.cofs.2021.01.002

Davis, A. (2016). The Consumption of Lionfish as a Control of an Invasive Species in Bermuda. *Undergraduate Honors Theses*, 1045.

Ferreira, C. E. L., Luiz, O. J., Floeter, S. R., Lucena, M. B., Barbosa, M. C., Rocha, C. R., & Rocha, L. A. (2015). First record of invasive lionfish (*Pterois volitans*) for the Brazilian coast. *PLoS ONE*, *10*(4), 1-5, e0123002. doi:10.1371/journal.pone.0123002

Galloway, K. A., & Porter, M. E. (2019). Mechanical properties of the venomous spines of *Pterois volitans* and morphology among lionfish species. *Journal of Experimental Biology*, *222*(6). doi:10.1242/jeb.197905

Gasteiger, E., Hoogland, C., Gattiker, A., Duvaud, S., Wilkins, M. R., Appel, R. D., & Bairoch, A. (2005). Protein identification and analysis tools on the ExPASy server. In: J. M. Walker (Eds.) *The Proteomics Protocols Handbook* (pp. 571-607). Humana Press.

Gürlek, M., Ergüden, D., Uyan, A., Doğdu, S. A., Yağlıoğlu, D., Öztürk, B., & Turan, C. (2016). First record red lionfish *Pterois volitans* (Linnaeus, 1785) in the Mediterranean Sea. *Natural and Engineering Sciences*, *4*(1), 64–75. doi:10.28978/nesciences.286308

Harris, H. E., Fogg, A. Q., Gittings, S. R., Ahrens, R. N. M., Allen, M. S., & Patterson, W. F. (2020). Testing the efficacy of lionfish traps in the northern Gulf of Mexico. *PLoS ONE*, *15*(8), 1-20, e0230985. doi:10.1371/journal.pone.0230985

Hoo Fung, L. A., Antoine, J. M. R., Grant, C. N., & Buddo, D. S. A. (2013). Evaluation of dietary exposure to minerals, trace elements and heavy metals from the muscle tissue of the lionfish *Pterois volitans* (Linnaeus 1758). *Food and Chemical Toxicology*, *60*, 205–212. doi:10.1016/j.fct.2013.07.044

Jang, A., & Lee, M. (2005). Purification and identification of angiotensin converting enzyme inhibitory peptides from beef hydrolysates. *Meat Science*, *69*(4), 653–661. doi:10.1016/j.meatsci.2004.10.014

Jha, S., Taschler, U., Domenig, O., Poglitsch, M., Bourgeois, B., Pollheimer, M., Pusch, L. M., Malovan, G., Frank, S., Madl, T., Gruber, K., Zimmermann, R., & Macheroux, P. (2020). Dipeptidyl peptidase 3 modulates the renin–Angiotensin system in mice. *Journal of Biological Chemistry*, *295*(40), 13711–13723. doi:10.1074/jbc.RA120.014183

Kandemir-Cavas, C., Pérez-Sánchez, H., Mert-Ozupek, N., & Cavas, L. (2019). In Silico Analysis of Bioactive Peptides in Invasive Sea Grass *Halophila stipulacea*. *Cells*, *8*(6), 557. doi:10.3390/cells8060557

Kleitou, P., Savva, I., Kletou, D., Hall-Spencer, J. M., Antoniou, C., Christodoulides, Y., Chartosia, N., Hadjioannou, L., Dimitriou, A. C., Jimenez, C., Petrou, A., Sfenthourakis, S., & Rees, S. (2019). Invasive lionfish in the Mediterranean: Low public awareness yet high stakeholder concerns. *Marine Policy*, *104*, 66–74. doi:10.1016/j.marpol.2019.02.052

Kiriake, A., & Shiomi, K. (2011). Some properties and cDNA cloning of proteinaceous toxins from two species of lionfish (*Pterois antennata* and *Pterois volitans*). *Toxicon*, *58*(6-7), 494-501. doi:10.1016/j.toxicon.2011.08.010

Kovačić, M., Lipej, L., Dulčić, J., Iglesias, S. P., & Goren, M. (2021). Evidence-based checklist of the Mediterranean Sea fishes. *Zootaxa*, *4998*(1), 1-115. doi:10.11646/zootaxa.4998.1.1

Liu, L., Li, S., Zheng, J., Bu, T., He, G., & Wu, J. (2020). Safety considerations on food protein-derived bioactive peptides. *Trends in Food Science and Technology*, *96*, 199–207. doi:10.1016/j.tifs.2019.12.022

Livaneli, Z. (2021). *Balıkçı ve Oğlu* (1st ed.). İnkılap Kitabevi. İstanbul.

Meister, H. S., Wyanski, D. M., Loefer, J. K., Ross, S. W., Quattrini, A. M., & Sulak, K. J. (2005). Further evidence for the invasion and establishment of *Pterois volitans* (Teleostei: Scorpaenidae) along the Atlantic Coast of the United States. *Southeastern Naturalist*, *4*(2), 193–206. doi:10.1656/1528-7092(2005)004[0193:FEFTIA]2.0.CO;2

Minkiewicz, P., Iwaniak, A., & Darewicz, M. (2019). BIOPEP-UWM database of bioactive peptides: Current opportunities. *International Journal of Molecular Sciences*, *20*(23). doi:10.3390/ijms20235978

Misumi, Y., & Ikehara, Y. (2013). Dipeptidyl-peptidase IV. In: N. D. Rawlings, & G. Salvesen (Eds.) *Handbook of Proteolytic Enzymes* (Vol. 3), (3rd ed., pp. 3374–3379). doi:10.1016/B978-0-12-382219-2.00745-6

Morgat, A., Lombardot, T., Coudert, E., Axelsen, K., Neto, T. B., Gehant, S., Bansal, P., Bolleman, J., Gasteiger, E., de Castro, E., Baratin, D., Pozzato, M., Xenarios, I., Poux, S., Redaschi, N., Bridge, A., & The UniProt Consortium. (2020). Enzyme annotation in UniProtKB using Rhea. *Bioinformatics*, *36*(6), 1896–1901. doi:10.1093/bioinformatics/btz817

Nair, M. S. R., Cheung, P., Leong, I., & Ruggieri, G. D. (1985). A non-proteinaceous toxin from the venomous spines of the Lionfish *Pterois volitans* (Linnaeus). *Toxicon*, *23*(3), 525–527. doi:10.1016/0041-0101(85)90037-6

Sievers, F., Wilm, A., Dineen, D., Gibson, T. J., Karplus, K., Li, W., Lopez R., McWilliam H., Remmert M., Söding J., & Thompson, J. D. (2011). Fast, scalable generation of high-quality protein multiple sequence alignments using Clustal Omega. *Molecular Systems Biology*, *7*(1), 539. doi:10.1038/msb.2011.75

Sommeng, A. N., Arya, R. M. Y., Ginting, M. J., Pratami, D. K., Hermansyah, H., Sahlan, M., & Wijanarko, A. (2019). Antiretroviral activity of *Pterois volitans* (red lionfish) venom in the early development of human immunodeficiency virus/acquired immunodeficiency syndrome antiretroviral alternative source. *Veterinary World*, *12*(2), 309–315. doi:10.14202/vetworld.2019.309-315

Sommeng, A. N., Eka, A. K., Ramadhan, M. Y. A., Ginting, M. J., Sahlan, M., Hermansyah, H., & Wijanarko, A. (2020). Protein isolation and identification of *Pterois volitans* spine venom coagulant activity. *IOP Conference Series: Earth and Environmental Science*, *462*, 012039. doi:10.1088/1755-1315/462/1/012039

Schofield, P. J. (2009). Geographic extent and chronology of the invasion of non-native lionfish (*Pterois volitans* [Linnaeus 1758] and *P. miles* [Bennett 1828]) in the western North Atlantic and Caribbean Sea. *Aquatic Invasions*, *4*(3), 473–479. doi:10.3391/ai.2009.4.3.5

Schofield, P. J. (2010). Update on geographic spread of invasive lionfishes (*Pterois volitans* [Linnaeus, 1758] and *P. miles* [Bennett, 1828]) in the western North Atlantic Ocean, Caribbean Sea and Gulf of Mexico. *Aquatic Invasions*, *5*, 117–122. doi:10.3391/ai.2010.5.S1.024

Sutherland, W. J., Clout, M., Côté, I. M., Daszak, P., Depledge, M. H., Fellman, L., Fleishman, E., Garthwaite, R., Gibbons, D. W., De Lurio, J., Impey, A. J., Lickorish, F., Lindenmayer, D., Madgwick, J., Margerison, C., Maynard, T., Peck, L. S., Pretty, J., Prior, S., Redford, K. H., Scharlemann, J. P. W., Spalding, M., & Watkinson, A. R. (2010). A horizon scan of global conservation issues for 2010. *Trends in Ecology & Evolution*, *25*(1), 1–7. doi:10.1016/J.TREE.2009.10.003

Turan, C., Uygur, N., & İğde, M. (2017). Lionfishes *Pterois miles* and *Pterois volitans* in the North-eastern Mediterranean Sea: Distribution, habitation, predation and predators. *Natural and Engineering Sciences*, *2*(1), 35–43. doi:10.28978/nesciences.292355

Turan, C., Uyan, A., Gürlek, M., & Doğdu, S. A. (2020). DNA Barcodes for Identifications of Two Lionfish Species *Pterois miles* (Bennett, 1828) and *Pterois volitans* (Linnaeus, 1758) in the Mediterranean. *FishTaxa*, *16*, 29–36.

Ulman, A., Tunçer, S., Kizilkaya, I. T., Zilifli, A., Alford, P., & Giovos, I. (2020). The lionfish expansion in the Aegean Sea in Turkey: A looming potential ecological disaster. *Regional Studies in Marine Science*, *36*, 101271. doi:10.1016/j.rsma.2020.101271

Vetrano, S. J., Lebowitz, J. B., & Marcus, S. (2002). Lionfish envenomation. *Journal of Emergency Medicine*, *23*(4), 379–382. doi:10.1016/s0736-4679(02)00572-3

Weaver, C. M. (2014). Bioactive foods and ingredients for health. *Advances in Nutrition*, *5*(3), 306S-311S. doi:10.3945/an.113.005124

Yuzvik, A., Kelly, B. R., Lombardi, J. P., Uvarov, N. A., & Godsey, W. G. (2018). Autonomous Lionfish Harvester. Worcester Polytechnic Institute. https://digitalcommons.wpi.edu/mqp-all/2499

Zhou, J., Chen, M., Wu, S., Liao, X., Wang, J., Wu, Q., Zhuang, M., & Ding, Y. (2020). A review on mushroom-derived bioactive peptides: Preparation and biological activities. *Food Research International*, *134*, 109230. doi:10.1016/j.foodres.2020.109230

Research Article / Araştırma Makalesi GU J Sci, Part A, 8(4): 424-434 (2021) https://doi.org/10.54287/gujsa.1012834

Gazi University
Journal of Science
PART A: ENGINEERING AND INNOVATION
http://dergipark.org.tr/gujsa

Effect of Wood-Based Panels and Varnish Types on VOC Emissions in Furniture Production

Hamza ÇINAR[1], Kemal YILDIRIM[1*], Mustafa HAMARAT[2]

[1]*Department of Wood Products Industrial Engineering, Faculty of Technology, Gazi University, Ankara / Turkey*
[2]*Ankara Metropolitan Municipality, Ankara / Turkey*

Keywords

Wood-Based Boards
Furniture
Emission
Varnish
VOC

Abstract

This study investigated the effects of varnishes on VOCs emissions from wood-based panels of standard particle panels (PB) and medium density fiber panels (MDF) which are covered by beech veneer and varnished by three different types of varnishes. The highest value was 624,90 ppm for Toluene, while the lowest was 0,30 ppm for Para xylene in respect to the Particleboards which were covered by beech veneered and varnished with cellulosic varnish. However, samples of beech veneered and varnished with synthetic and polyurethane varnishes yielded less gas emission than cellulosic varnish. The samples of MDF, covered with beech veneer and varnished polyurethane varnished yielded gas emission more than the synthetic (100%) and cellulosic varnishes (220%). All values show that gas emission reduces its effect within time in respect to the manufacturing time, after drying period, 15- and 30-days measurements.

Cite

Çınar, H., Yıldırım, K., & Hamarat, M. (2021). Effect of Wood-Based Panels and Varnish Types on VOC Emissions in Furniture Production. *GU J Sci, Part A, 8*(4), 424-434.

Author ID (ORCID Number)

H. Çınar, 0000-0003-2607-852X
K. Yıldırım, 0000-0001-5447-1201
M. Hamarat, 0000-0003-0699-191X

Article Process

Submission Date 21.10.2021
Revision Date 03.11.2021
Accepted Date 16.11.2021
Published Date 25.11.2021

1. INTRODUCTION

Air quality is very significant in terms of having healthy life in all aspects of lives and eco design becomes more important day by day. For example, 5 million liters of air as known of oxygen and nitrogen and are inspired by human beings in every year. On the other hand, almost fifty thousand liters of other gases (argon, carbon-dioxide i.e.) are dangerously presented into human body each year with impressive effects on the health issues regarding to the composition. Particularly in doors; offices, houses, hospitals, schools, and so on people mostly spend their time and a particular attention have been paid to the air quality of indoors (Bulian & Fragassa, 2016).

Nowadays, many non-environmentally friendly and polluting building materials can be used in indoor architectural spaces, sometimes knowingly or unknowingly. A number of studies has been carried out on furniture and interiors livable (Subaşı et al., 2017; Hidayetoglu & Müezzinoglu, 2018; Yıldırım et al., 2020; 2021). However, there are few studies on the effect of volatile organic compounds (VOCs) emitted from furniture to the environment. All these pollutants emitted from furniture and equipment elements might have a negative impression on air quality, health issues of people and indoor-outdoor environments (Kephalopoulos et al., 2012). The emission of VOCs for furniture and indoors, coated with paints, varnishes, waxes, and solvents, are discussed by the authors of Missia et al. (2010), Bartzis et al. (2015), Cacho et al. (2013), Nandan et al. (2020) and Ulker et al. (2021). In addition to that, alongside with other sources; other household chemicals, cleaning agents and heating furnaces, cooking appliances and candles also contribute to air concentration of VOCs in living areas. In the last thirty years, the topic of sick building syndrome

*Corresponding Author, e-mail: kemaly@gazi.edu.tr

(SBS) becomes to the attention concerned with VOC concentrations and seriously suspected to be adjuvant factors for asthma, allergy and various symptoms (Andersson et al., 1997; Fechter et al., 2006).

Studies show that people working in the construction industry and in environments where furniture and other wood products are manufactured, repaired or restored are frequently exposed to hazardous chemicals (Cinar & Erdogdu, 2018). In recent years, from indoor building materials, a significant approach here were raised with the exposure to VOCs. European Union (EU) Directive No 320 of 29 May 2002 puts limits on the discharge of VOCs from industrial materials, and subsequently, furniture producers have been forced to move toward alternative coating methods for wood and wood-based materials that use fewer volatile organic solvents (Akkuş et al., 2021). Even though the emissions from indoor materials decrease over time (Cinar, 2005; 2018; Brockmann et al., 1998; Benotto et al., 2009; Yu & Kim, 2012; Cinar & Erdogdu, 2018; Cinar et al., 2018), many building materials are repeatedly and periodically being used as interior architectural coatings, remodeling and renovation so on.

Related to the furniture industry regarding ecological concerns, there is a significant tendency for ecological production. The stricter regulations, Kyoto protocol and Paris Climate Changes Agreement and public pressures have accelerated the manufacturers how they do the business. Another significant push was conscious consumers who were aware of the raising need for more ecofriendly products. These movements have pushed the industry for timber harvesting and management, has begun to differentiate products through ecological processes. Moreover, the consumption for wood-based production has greatly affected due to the wood-based panel production to meet the demands from the building and furniture industries. Increased demand has influenced investors, consumers, regulatory agencies, and shareholders to develop their production strategies (Cinar et al., 2018). Not surprisingly, these attempts affect the furniture industry regarding the furniture and wood-based panel productions.

Varnishes and coatings have been used for furniture and wood protection in wider aspects since very ancient times. The use of resin based-based varnishes can be historically traced back to the ancient time such as Egyptian, Persian, Chinese, Greek or Indian culture (Cortina & Carbo, 2004). In the industry, varnishes are classified by ASTM (2019) into four types. These are oil-based (film primarily chemical reaction), bituminous, spirit and spar varnishes. Varnishes are also classified for the polarity as oil or water-based varnishes (Wu et al., 2015; Cheng et al., 2018) and is the highest for ozone formation (Li et al., 2018).

A number of studies on the emissions concerned with varnishes for indoor air pollution (WHO, 1989; Clausen et al., 1991; Howard et al., 1998; McCrillis et al., 1999) shows that cyclic hydrocarbons, saturated aliphatic, oxygenated hydrocarbon and aromatic hydrocarbon have been identified both spirit varnishes and oil-based varnishes (Silva et al., 1998). The major VOCs for oil-based varnishes were identified as ethylbenzene, isobutanol, o-xylene, formaldehyde and m,p-xylene (Howard et al., 1998; Guo et al., 2002; Shun-Cheng et al., 2003).

The literature provides useful information concerned with the facts for the varnish selection when coating wood products and furniture. Experience for the ecological impression for furniture and wood products is a crucial agent for manufactures to develop the production strategies from ecologically approaches for “green” products. In the light of the above information, the hypotheses of this study are given below.

H1: There are significant differences between measurements of VOCs emission values on particleboard (PB) and medium density fiberboard (MDF) wood-based boards covered with varnish.

H2: There are significant differences for the values of VOCs emission in the wood-based panels concerning three different varnish types.

H3: There are differences between the measurement values of VOCs emissions in the wood-based boards at four different times.

2. MATERIAL AND METHOD

2.1. Wood Based Panels

Standard particle panels (PB) with 18 mm thicknesses, manufactured in accordance with TS EN 312 (TSE, 2012) and MDF with 18 mm thicknesses, manufactured in accordance with TS EN 622-5 (TSE, 2011) were analyzed. The samples were veneered by beech with a thickness of 1,0mm and varnished with three types of varnishes; respectively, cellulosic varnish, synthetic varnish and polyurethane varnish. These two types of wood-based panels and three types of varnishes are being commonly used in the furniture industry. The samples for the experiments were supplied from boards of 210x280x0.18 cm in accordance with TS EN 326-1 (TSE, 1999).

2.2. Preparation of Samples

Twenty specimens were prepared from PB and MDF with 18 mm thicknesses. They were dimensioned by cutting into 500 x 500 mm, weighed out with Precia Gravimetrics 312_6200C, in accordance with TS EN 326-1 (TSE, 1999), and each sample was numbered from 1 to 20, varnished with cellulosic, synthetic and polyurethane varnishes respectively. After drying, they were covered with nylon for avoiding emissions (Figure 1), and left at the temperature of 20ºC and 60/65 percent relative humidity in order to obtain a moisture value equal to the internal environmental conditions according to TS EN 2471 (TSE, 1976).

Figure 1. *Number of Samples at Positions and Keeping Samples for Experiment*

2.3. Experiment Implementation

Gas emissions were measured from newly veneered and edge covered PB and MDF, were left in store less than three days. Specimens were put into the Climatic Test Cabinet TK600NUVE (2012) at 20ºC and 65 % relative humidity for the 1st measurements, which were taken by a multi- RAE multiple gas analyzer at 1, 2, and 3 hours over the test specimen prepared from boards supplied immediately from the factory in accordance with TS EN 13986 (TSE, 2015) and test method TS EN 717-1 (TSE, 2006). The measurements of TK600NUVE cabinet were 75 by 75 by 132 cm, and a multi-RAE multiple gas analyzers were installed to the cabinet (Figure 2 and 3).

Figure 2. *Climatic Test Cabinet*

Figure 3. *FTIR Spectrum Two ™ Gas Analyzer*

This study determined the effects of varnishes on nButylacetate, Toluene, Acetone, Isopropanol, Isobutylacetate and Paraxylene emissions for cellulosic, synthetic and polyurethane varnishes were determined and synthesized with the accepted limit values as ppm (per million particular part). Eco-Indicator 99 (Goedkoop & Spriensma, 2000) was used to check the quantitative data representing VOC emission, which was measured according to TS EN 717-1 (TSE, 2006) by a FTIR SpectrumTwo ™ Gas analyser.

2.4. Statistical Analysis

In order to carry out the effects of VOCs emission on varnished wood-based panels, data obtained from the measurements were summarized for understanding and comparing with the eco indicator results. Measurements of the VOCs emission in two different types of varnished wood-based boards (PB and MDF) were accepted as "dependent variables", whereas, the measurement time with wood-based board type and the varnish type were accepted as "independent variables." Afterwards, multivariate analysis of variance (MANOVA) was used to measure the effects of interactions between independent variables (board type X varnish type X time) depending on the measurement values of VOCs emission for the dependent variables. In addition, one-way analysis of variance (ANOVA) was used to examine the effect of differences in board type, varnish type, and measurement time (production moment, after drying, on the 15th day and 30th day) on VOCs emission in wood-based boards. The mean values found to be important in the analysis of variance are presented in graphic form.

3. RESULTS

Cronbach's Alpha test was used for reliability of dependent variables, and evaluations of values for VOCs emissions for examining. A coefficient of internal consistency of the Cronbach for two scales based on the VOC emissions measurement values are as follows: Particleboard (PB): 0.66; and Medium Density Fiberboard (MDF): 0.67. The reliability of the scale, which covers the measurement values of all dependent variables, is 0.67. Studies of Cronbach (1951) and Panayides (2013) state that the alpha reliability coefficients for all dependent variables could be accepted as 'reliable' while it is above 0.60. This scale is reliable.

According to data obtained from the study, the differences among each independent variable evaluated and VOCs emission values variance analyzes were carried out and performed to determine the differences between board type * VOCs emission values, varnish type * VOCs emission values and time * VOCs emission values.

First, the effects of interactions for independent variables (board type X varnish type X time) depending on the measurement values of the VOC emission for dependent variables (nButylacetate, Toluene, Acetone,

Isopropanol, Isobutylacetate and Paraxylene) were tested by using the multivariate analysis of variance (MANOVA) and given in Table 1.

Table 1. *MANOVA, Independent Variables*

Independent Variables	F	df	Sig.
Board type	1.305	6	0.0263^{ns}
Varnish type	37.314	12	0.000*
Time	7.424	18	0.000*
Board type*Varnish type	0.823	12	0.627^{ns}
Board type*Time	0.703	18	0.808^{ns}
Varnish type*Time	7.091	36	0.000*
Board type*Varnish type*Time	0.808	36	0.782^{ns}

Note: * α: 0.001 is the level of significance, ^{ns}: Not significant.

According to Table 1, the main effects (varnish type and time) and the two-way interaction for varnish type*time were found to be significant at a level of $p < 0.001$. However, the main effect of board type, board type*varnish type and board type*time two-way interactions with board type*varnish type*time triple interaction were insignificant (at a level of $p < 0.05$). Accordingly, binary and triple comparisons of board type do not influence VOCs emission measurement values. In other words, changing any varnish type or time factor in any board type did not significantly affect the total VOCs emission measurement value.

In another analysis, the ANOVA test results for the categorical averages, values of standard deviation and data obtained for differences for the measurement values of the VOCs emissions in the wood-based panels coated with varnish (PB and MDF) are given in Table 2.

Table 2. *The ANOVA, Average Values, Standard Deviation and the Dependent Variables Related to the VOCs Emissions According to Wood-Based Panels*

Dependent Variables	Wood-Based Boards				ANOVA Results		
	Particleboard (PB)		Fiberboard (MDF)				
	M	SD	M	SD	F	df	Sig.
nButylacetate	35,696	66,452	35,609	72,045	0,000	1	0,995^{ns}
Toluene	94,051	182,463	85,537	180,128	0,066	1	0,797^{ns}
Acetone	10,734	50,268	11,157	38,463	0,003	1	0,959^{ns}
Isopropanol	2,655	27,719	2,443	32,549	0,001	1	0,970^{ns}
Isobutylacetate	5,948	11,625	5,539	11,514	0,038	1	0,846^{ns}
Paraxylene	2,173	3,094	1,776	2,704	0,555	1	0,458^{ns}

Notes: ns: The differences among the groups are not significant at the level of p<0.05.
M: Average value, SD: Standard deviation, F: F value, df: Degree of freedom.

According to Table 2, the differences for the dependent variables including the measurement values of the VOCs emissions in the panels were not found statistically significant (at a level of $p < 0.05$) in terms of all the dependent variables related to the scale. These results show that the board type has no effect on the

VOCs emission values measured from both wood-based boards covered with varnish. Figure 4 shows the graphical results.

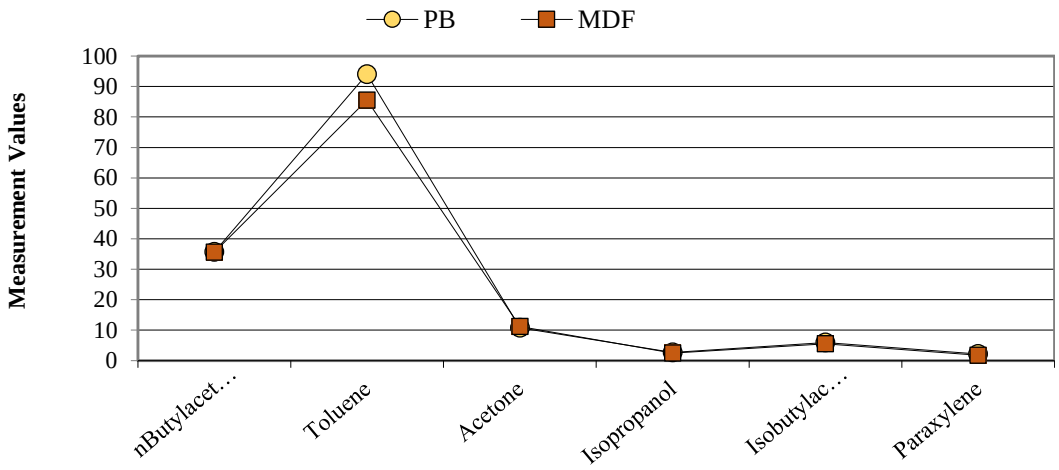

Figure 4. *Effect of the Wood-Based Board Types on the VOC Emissions*

According to Figure 4, the average measurement values of the VOC emissions in the boards covered with varnish are very close to each other for all the dependent variables related to the scale. There is no difference between the VOC emission measurements of both boards. This result shows that the H1 hypothesis, "*There are significant differences between measurements of VOCs emission values on particleboard (PB) and medium density fiberboard (MDF) wood-based boards covered with varnish*" was not supported.

The ANOVA test results for the data obtained for the differences between the measurement values of the VOCs emissions in boards using three different varnish types (cellulosic, synthetic and polyurethane varnish) are given in Table 3.

Table 3. *ANOVA Test Results of the Dependent Variables Related to the VOCs Emissions According to Varnish Type*

Dependent Variables	**Varnish Type**						**ANOVA Results**		
	Cellulosic Varnish		Synthetic Varnish		Polyurethane Varnish				
	M	SD	M	SD	M	SD	F	df	Sig.
nButylacetate	31,093	43,321	4,369	9,039	71,495	101,151	11,243	2	0,000*
Toluene	191,977	267,658	12,582	15,068	64,822	100,876	12,452	2	0,000*
Acetone	38,469	66,045	-0,344	1,453	-5,287	22,780	14,112	2	0,000*
Isopropanol	21,337	42,206	-2,065	3,823	-11,624	19,477	15,864	2	0,000*
Isobutylacetate	10,503	15,599	-0,074	1,323	6,802	10,046	9,991	2	0,000*
Paraxylene	0,688	0,492	1,700	1,616	3,507	4,299	11,250	2	0,000*

Notes: *: The differences among the groups are significant at the level of p<0.001.
M: Average value, SD: Standard deviation, F: F value, df: Degree of freedom.

According to Table 3, the differences for the dependent variables including the measurement values of the VOCs emissions in the boards using three different varnish types were found to be statistically significant at a level of $p < 0.001$ in terms of all the dependent variables related to the scale. These results show that the

varnish type has effect on the VOCs emission values measured from both boards covered with varnish. The result is given Figure 5.

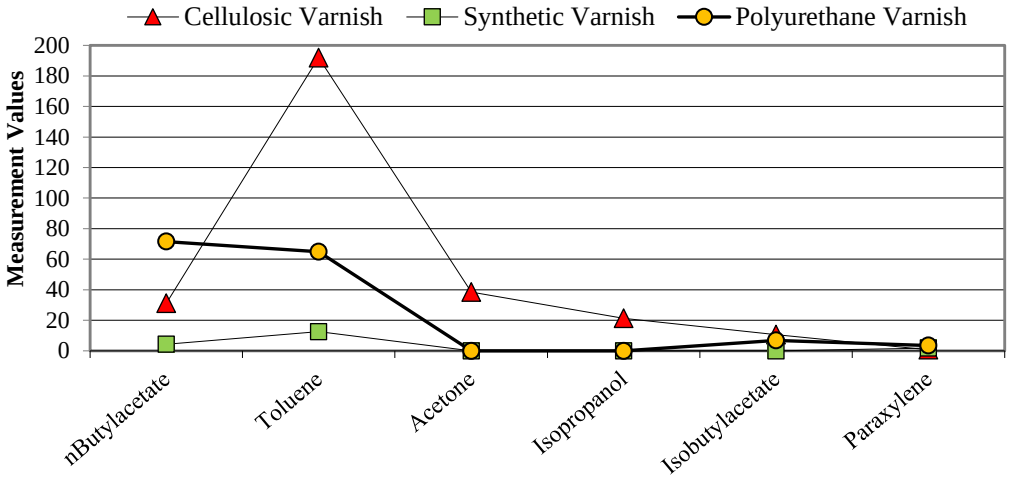

Figure 5. *Effect of the Varnish Types on the VOC Emissions*

According to Figure 5, the average measurement values of the VOCs emissions in the boards using three different varnish types were found to be quite different for all the dependent variables related to the scale. The figure shows that there are significant differences for the average measurement values of VOCs emissions in the boards using three different varnish types. This result supports the H2 hypothesis, which asserts "*There are significant differences between for the values of VOCs emission from wood-based panels using three different varnish types*". According to these results, it can be said that the board using cellulosic varnish gives more toluene gas release compared to the panels using other varnishes.

Table 4 gives ANOVA test results of the differences for the measurement values of VOC emissions in the panels at four different times (production moment, after drying, on the 15th day and 30th day).

Table 4. *The Average, Standard Deviation and ANOVA Test Results of the Dependent Variables Related to the VOC Emissions According to Measurement Time*

Dependent Variables	**Measurement Time**								**ANOVA Results**		
	Production Moment		After Drying		15th Day		30th Day				
	M	SD	M	SD	M	SD	M	SD	F	df	P
nButylacetate	106,469	106,242	28,690	28,009	6,144	10,107	1,307	3,274	23,354	3	0,000*
Toluene	282,877	268,754	68,928	84,522	6,126	8,561	1,243	1,744	26,461	3	0,000*
Acetone	38,395	83,075	6,947	12,903	-0,901	1,475	-0,658	0,629	5,909	3	0,001*
Isopropanol	14,847	57,456	-3,117	13,435	-1,646	4,376	-0,112	1,956	2,361	3	0,075*
Isobutylacetate	18,309	16,367	5,036	5,998	0,035	1,849	-0,406	0,928	29,704	3	0,000*
Paraxylene	4,5819	4,530	1,981	1,512	0,799	0,749	0,492	0,489	17,313	3	0,000*

Notes: *: The differences among the groups are significant at the levels of $p<0.10$ and $p<0.001$.
M: Average value, SD: Standard deviation, F: F value, df: Degree of freedom.

Table 4 gives ANOVA results for the differences for the dependent variables including the values for VOCs emissions in the panels at four different times, were found to be statistically significant at a level of $p < 0.001$ in terms of all the dependent variables. These results show that the measurement time has effect on the VOCs

emission values measured from both boards covered with varnish. Figure 6 gives the values after drying, 15th day and 30th day results.

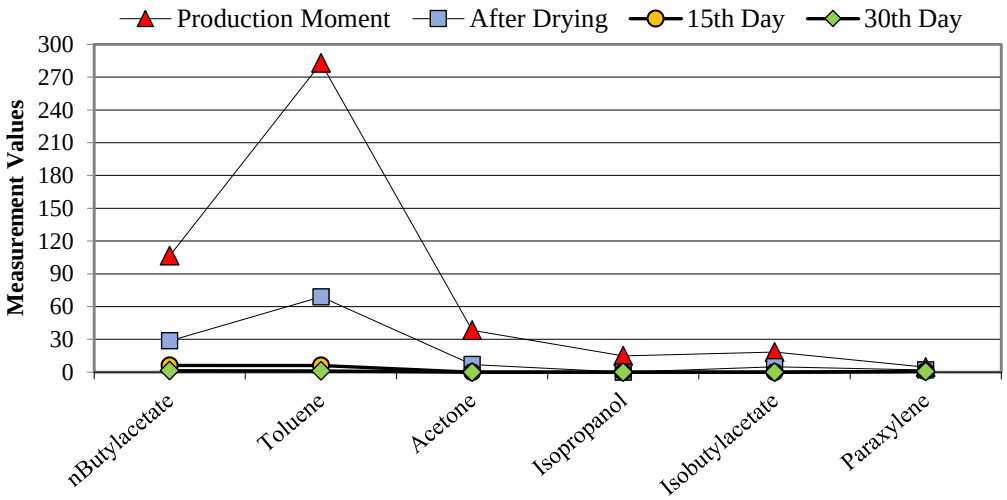

Figure 6. *Effect of the Measurement Time on the VOCs Emissions*

The average values of VOCs emissions in the boards using three different varnish types were found to be quite different for all the dependent variables related to the scale according to Figure 6. The figure shows that there are significant differences for the average measurement values of VOCs emissions in the boards at four different times. The H3 hypothesis, is supported, asserts "*There are differences between the measurement values of VOCs emissions in the wood-based boards at four different times*". According to these results, it is seen that the VOCs emission value is reset on the 30th day in the measurements made on the boards.

4. CONCLUSION

This paper analyzed the effects of varnishes on nButylacetate, Toluene, Acetone, Isopropanol, Isobutylacetate and Paraxylene emissions for cellulosic, synthetic and polyurethane varnishes for VOCs. The following conclusion can be made:

- ✓ The highest value was **624,90 ppm for Toluene**, while the lowest was **0,30 ppm for Para xylene** in respect to the Particleboards which were covered by beech veneered and varnished with cellulosic varnish. However, samples of beech veneered and varnished with synthetic and polyurethane varnishes yielded less gas emission than cellulosic varnish.
- ✓ The samples of MDF, covered with beech veneer and varnished polyurethane varnished yielded gas emission more than the synthetic (100%) and cellulosic varnishes (220%).
- ✓ In accordance with the results, it can be said that cellulosic, synthetic and polyurethane varnishes, which are widely used in the sector in terms of protection and visual appearance, are not considered as environmentally friendly.

Considering manufacturing furniture, raw materials and semi-finished materials in line with the product life cycle, selection and application of varnishes used for protection are significantly important in terms of environmentally friendly products. All values show that gas emission reduces its effect within time in respect to the manufacturing time, after drying period, 15- and 30-days measurements. After the application of varnishes, it is important to make ventilation frequently daily and to ensure air circulation in closed environments.

Giving a thought into the number of products, components, elements and agents in the furniture industry and interiors for design projects, it is possible to say that there is a high responsibility for designers in order to be aware of the consequence of their work for ecological aspects for the eco-friendly and sustainable production and are supposed to start taking into account eco design issues concerned with the impacts on the environment.

CONFLICT OF INTEREST

The authors declare no conflict of interest.

REFERENCES

Akkuş, M., Akbulut, T., & Candan, Z. (2021). Formaldehyde emission, combustion behavior, and artificial weathering characteristics of electrostatic powder coated wood composite panels. *Wood Material Science & Engineering*. doi:10.1080/17480272.2021.1901142

Andersson, K., Bakke, J. V., Bjørseth, O., Bornehag, C-G., Clausen, G., Hongslo, J. K., Kjellman, M., Kjærgaard, S., Levy, F., Mølhave, L., Skerfving, S., & Sundell, J. (1997). TVOC and health in non-industrial indoor environments. *INDOOR AIR International Journal of Indoor Air Quality and Climate*, *7*(2), 78-91. doi:10.1111/j.1600-0668.1997.t01-2-00002.x

ASTM, American Society for Testing and Materials. (2019). Standard Specification for Standard Environment for Conditioning and Testing Paint, Varnish, Lacquer, and Related Materials (D3924-16, Active Standart), Philadelphia, PA. (Accessed:19/11/2021) https://www.astm.org/Standards/D3924.htm

Bartzis, J., Wolkoff, P., Stranger, M., Efthimiou, G., Tolis, E. I., Maes, F., Nørgaard, A. W., Ventura, G., Kalimeri, K. K., Goelen, E., & Fernandes, O. (2015). On organic emissions testing from indoor consumer products' use. *Journal of Hazardous Materials*, *285*, 37-45. doi:10.1016/j.jhazmat.2014.11.024

Benotto, E., Becker, M., & Welfring, J. (2009). Life cycle assessment of oriented strand boards (OSB): From process innovation to eco-design. *Environmental Science Technology Journal*, *43*(15), 6003-6009. doi:10.1021/es900707u

Brockmann, C. M., Sheldon, L. S., Whitaker., D. A., & Baskir, J. N. (1998). *The Application of Pollution Prevention Techniques to Reduce Indoor Air Emissions from Engineered Wood Products* (Report No. EPA-600/R-98-146), U.S. Environmental Protection Agency, Washington, DC.

Bulian, F., & Fragassa, C. (2016). VOC emissions from wood products and furniture: A survey about legislation, standards and measures referred to different materials. *FME* Transactions, *44*(4), 358-364. doi:10.5937/fmet1604358B

Cacho, C., Ventura Silva, G., Martins, A. O., Fernandes, E. O., Saraga, D. E., Dimitroulopoulou, C., Bartzis, J. G., Rembges, D., Barrero-Moreno, J., & Kotzias, D. (2013). Air pollutants in office environments and emissions from electronic equipment: A review. *Fresenius Environmental Bulletin*, *22*(9), 2488-2497.

Cheng, K., Hao, W-W., Yi, P., Zhang, Y., & Zhang, J-Y. (2018). Volatile organic compounds emission from chinese wood furniture coating industry: Activity-based Emission factor, speciation profiles, and provincial emission inventory. *Aerosol and Air Quality Research*, *18*(11), 2813-2825. doi:10.4209/aaqr.2018.02.0044

Cinar, H. (2005). Eco design and furniture: Environmental impacts of wood-based panels, surface and edge finishes. *Forest Products Journal*, *55*(11), 27-33.

Cinar, H. (2018). Effects of temperature and thickness of wood-based boards on formaldehyde emission. *Wood Research*, *63*(5), 895-908.

Cinar, H., & Erdogdu, M. (2018). Eco-Design: Effects of thickness and time in service for wood-based boards on formaldehyde emission. *Forest Products Journal*, *68*(4), 405-413. doi:10.13073/FPJ-D-17-00027

Cinar, H., Ozturk, Y., & Yıldırım, K. (2018). Effects of surface veneering, edge banding, drilling holes for handles and hinges of wood-based boards on formaldehyde emission. *Forest Products Journal*, *68*(3), 264-271.

Clausen, P. A., Wolkoff, P., Host, E., & Nielsen, P. A. (1991). Long-term emission of volatile organic compounds from waterborne paints. *INDOOR AIR International Journal of Indoor Air Quality and Climate*, *1*(4), 562-576. doi:10.1111/j.1600-0668.1991.00019.x

Climatic Test Cabinet (2012). NÜVE Industrial Materials for production and Trade IC. Model TK 600 (W). Volume 600 Lt. Max. Temp. -10/60°C. Ankara, Turkey.

Cronbach, L. J. (1951). Coefficient alpha and the internal structure of tests. *Psychometrika*, *16*(3), 297-334. doi:10.1007/BF02310555

Fechter, J-O., Englund, F., & Lundin, A. (2006) Association between temperature, relative humidity and concentration of volatile organic compounds from wooden furniture in a model room. *Wood Material Science & Engineering*, *1*(2), 69-75. doi:10.1080/17480270600900551

Goedkoop, M., & Spriensma, R. (2000). *The Eco-Indicator 99: A Damage Oriented Method for Life Cycle Impact Assessment* (Methodology Report, nr.1999/36A), Product Ecology Consultants B. V., Amersfoort, Netherlands.

Guo, H., Lee, S. C., & Kwok, N-H. (2002). Modeling of VOCS emissions from a varnish. *Proceedings*: *Indoor Air*, 226-231. (Accessed:19/11/2021) https://www.irbnet.de/daten/iconda/CIB7084.pdf

Hidayetoglu, M. L., & Muezzinoglu, K. M. (2018). User-involved universal design experience in the space, product and service development process. *ICONARP International Journal of Architecture and Planning*, *6*, 41-62. doi:10.15320/ICONARP.2018.48

Howard, E. M., McCrillis, R. C., Krebs, K. A., Fortmann, R., Lao, H. C., & Guo, Z. (1998). Indoor emissions from conversion varnishes. *Journal of Air & Waste Management Association*, *48*(10), 924-930.

Kephalopoulos, S., Crump, D., Däumling, C., Funch, L. W., Horn, W., Keirsbulck, M., Maupetit, F., Sateri, J., Saarela, K., Scutaru, A. M., Tirkkonen, T., Witterseh, T., & Sperk, C. (2012). Harmonisation framework for indoor products labelling schemes in the EU (European Collaborative Action Report no. 27). European Commission Joint Research Centre. Publications Office of the European Union, Luxembourg. doi:10.2788/20292

Li, G., Wei, W., Shao, X., Nie, L., Wang, H., Yan, X., & Zhang, R. (2018). A comprehensive classification method for VOC emission sources to tackle air pollution based on VOC species reactivity and emission amounts. *Journal of Environmental Sciences*, *67*, 78-88. doi:10.1016/j.jes.2017.08.003

McCrillis, R. C., Howard, E. M., Guo, Z., Krebs, K. A., Fortmann, R., & Lao, H. C. (1999). Characterization of curing emissions from conversion varnishes. *Journal of Air & Waste Management Association*, *49*(1), 70-75.

Missia, D. A., Demetriou, E., Michael, N., Tolis, E. I., & Bartzis, J. G. (2010). Indoor exposure from building materials: A field study. *Atmospheric Environment*, *44*(35), 4388-4395. doi:10.1016/j.atmosenv.2010.07.049

Nandan, A., Siddiqui, N. A. & Kumar, P. (2020). Estimation of indoor air pollutant during photocopy/printing operation: A computational fluid dynamics (CFD)-based study. *Environmental Geochemistry and Health*, *42*, 3543-3573. doi:10.1007/s10653-020-00589-0

Panayides, P. (2013). Coefficient Alpha: Interpret with caution. *Europe's Journal of Psychology*, *9*(4), 687-696. doi:10.5964/ejop.v9i4.653

Subaşı, T., Çınar, H., & Çağatay, K. (2017). Mobilya sektöründe kullanılan kompozit malzemelerin insan yaşamına ve çevreye etkileri. *İleri Teknoloji Bilimleri Dergisi*, *6*(3), 557-571.

TSE, Turkish Standards Institution (1976). Wood, Determination of Moisture Content for Physical and Mechanical Tests (TS 2471, Active Standart), Ankara.

TSE, Turkish Standards Institution (1999). Wood- Based panels- Sampling, cutting and inspection- Part 1: Sampling test pieces and expression of test results (TS EN 326-1, Active Standart), Ankara.

TSE, Turkish Standards Institution (2006). Wood - based panels - Determination of formaldehyde release - Part 1: Formaldehyde emission by the chamber method (TS EN 717-1, Active Standart), Ankara, Turkey.

TSE, Turkish Standards Institution (2011). Fibreboards - Specifications - Part 5: Requirements for dry process boards (MDF) (TS EN 622-5, Active Standart), Ankara.

TSE, Turkish Standards Institution (2012). Particleboards- Specification (TS EN 312, Active Standart), Ankara.

TSE, Turkish Standards Institution (2015). Wood-based panels for use in construction - Characteristics, evaluation of conformity and marking (TS EN 13986:2004+A1, Active Standart), Ankara.

Ulker, O. C., Ulker, O., & Hiziroglu, S. (2021). Volatile organic compounds (VOCs) emitted from coated furniture units. *Coatings*, *11*(7), 806. doi:10.3390/coatings11070806

WHO, World Health Organization (1989). Indoor Air Quality: Organic Pollutants, WHO Regional Office for Europe, EURO Reports and Studies No. 111, Copenhagen.

Wu, X., Huang, W., Zhang, Y., Zheng, C., Jiang, X., Gao, X., & Cen, K. (2015). Characteristics and uncertainty of industrial VOCs emissions in China. *Aerosol and Air Quality Research*, *15*(3), 1045-1058. doi:10.4209/aaqr.2014.10.0236

Yıldırım, K., Müezzinoğlu, M. K., & Bozkurt, O. (2020). Konutlarda Döşemeli Mobilyaların Değiştirilme Süreçlerinin İncelenmesi. *Selçuk-Teknik Dergisi*, *19*(2), 68-83.

Yıldırım, K., Müezzinoğlu, M. K., & Türkdal, S. (2021). Fiziksel Engelli Kullanıcıların İç Mekân Donatı Elemanlarına Yönelik Tercihlerinin Belirlenmesi. *Uluslararası Disiplinlerarası ve Kültürlerarası Sanat*, *6*(12), 193-213.

Yu, C. W. F., & Kim, J. T. (2012). Long-term impact of formaldehyde and VOC emissions from wood-based products on indoor environments; and issues with recycled products. *Indoor and Built Environment*, *21*(1), 137-149. doi:10.1177/1420326X11424330

Research Article / Araştırma Makalesi GU J Sci, Part A, 8(4): 435-450 (2021) https://doi.org/10.54287/gujsa.997123

Gazi University
Journal of Science
PART A: ENGINEERING AND INNOVATION
http://dergipark.org.tr/gujsa

Data Mining and Application of Decision Tree Modelling on Electrochemical Data Used for Damaged Starch Detection

Nilufer YILDIRIM[1*], Niyazi Alper TAPAN[1]

[1]*Department of Chemical Engineering, Faculty of Engineering, Ankara, Turkey*

Keywords

Decision Tree
Damaged Starch
Electrochemical
Machine Learning

Abstract

In this study, unsupervised and supervised machine learning techniques, principal component analysis and classification tree modelling which could be improved with additional input variables were applied on iodine oxidation voltammetric data in order to determine routes and extract information about the electrochemical conditions leading to different damaged starch ratios in flour. For this purpose a database of 3542 observations which was normalized and filtered from outliers was used. It was seen that although it was almost impossible to generalize information or determine correlations from voltammetric data at different conditions, principal component analysis indicate that on platinum electrode UCD values of 16.5 mostly seen at high potentials, optimized decision tree indicate that the impact of variables on UCD values can be ordered as current density > potential > electrode type > KI concentration and give routes to UCD values with high class membership leaf nodes. Therefore machine learning with decision tree modelling could open perspectives for practical and fast prediction of damaged starch ratio which would help food industry to speed up and economize costs for analysis in flour.

Cite

Yıldırım, N. & Tapan, N. A. (2021). Data Mining and Application of Decision Tree Modelling on Electrochemical Data Used for Damaged Starch Detection. *GU J Sci, Part A, 8*(4), 435-450.

Author ID (ORCID Number)

N. Yıldırım, 0000-0003-0666-3182
N. A. Tapan, 0000-0001-8599-0450

Article Process

Submission Date 17.09.2021
Revision Date 10.11.2021
Accepted Date 28.11.2021
Published Date 01.12.2021

1. INTRODUCTION

In the world and in our country, most important flour based nutritional products like bread are brought to our daily lives by highly technological processes. In addition, there is an increasing demand on high quality food products and on development of standards every day. Therefore, it is utmost important to launch food product on the market from correctly processed flour.

During industrial flour production, one of the most important processing step is milling. In the milling process, the endosperm (nutritional tissue) is separated from the wheat bran and then the endosperm is ground as flour. The grinding process takes place in two stages as on gear and flat steel rollers, and the proper adjustment of the flat rolls during the grinding stage determines the damaged starch ratio in the ground wheat (Liu et al., 2017). If the chemical structure of starch which is a critical component and quality indicator of flour is analyzed, it is seen that starch is composed of straight and branched chain structures as amylose and amylopectin. Studies demonstrate that the application of mechanical energy or milling process deteriorate mostly the crystal structure of amylopectin rather than straight chain amylose molecules (Dhital et al., 2011; Li et al., 2014). The change of amylopectin / amylose ratio during wheat milling also affects the texture of the final product. In general, the damage of the starch structure during the milling of wheat is not only due to the size of the molecules but also depends on the branching structure. High branching density and short branch length in starch is also more prone to damage. A study on corn starch has shown that; the amylopectin is damaged more than amylose during milling not only due to the size of molecule but more short branches of

*Corresponding Author, e-mail: nilufer.yildirim@gazi.edu.tr

amylopectin (Liu et al., 2010). In addition, studies on types of starches with different amounts of amylopectin (99%, 75%, 20%) indicate that, after 15 min milling process of starch, damaged starch ratio reaches to 40% for 99% amylopectin ratio and the amylose ratio increase (Liu et al., 2017). Therefore, from the structural point of view, high damaged starch ratio which is affected by milling process time means high amylose content in the final wheat product. Beside the effect on the chemical structure, since the high or low proportion of damaged starch could cause quality defects like low volume and low viscosity in dough due to inefficient amylolytic activity during and after grinding process, fast and accurate determination and continuous monitoring of damaged starch in flour from a wide variety of wheat is very important for the desired end product (Zhu, 2016; Liu et al., 2017).

Today, for the determination of damaged starch, amperometric (or iodimetric) method (Medcalf and Gilles principle) which is based on the amount of iodine absorbed by starch granules is used (Medcalf & Gilles, 1965). In the amperometry technique which is based on iodine absorption kinetics and which the iodine absorption index is recorded as units of UCD (Chopin Dubois Unit (UCD) scales the Ai % (percentage of iodine absorption)), residual current after iodine fixing on the damaged starch is determined which takes about 7 to 10 minutes in a 120 ml electrolyte volume. Although the amperometry procedure and technique is well established, continuous and frequent analysis of damaged starch by this conventional method could bring burden of cost in the food industries in the world. At this point, in order to decrease analysis time and the amount of chemicals used for determination damaged starch during amperometry, it could be possible to use machine learning techniques based on the electrochemical data acquired by short electrochemical experiments like cyclic voltammetry of iodine oxidation in flour containing electrolyte. By the extraction of cyclic voltametric data performed on different type of electrodes, in different electrolyte concentrations and with different type of flours (with different UCD values), the degree of iodine absorption or UCD value can be modelled by supervised machine learning techniques like decision trees to determine routes and conditions leading to different damaged starch ratios. In addition, supervised learning procedure could help researchers to analyze damaged starch content with different experimental conditions easily and quickly.

Therefore, in this study, it is aimed to apply a decision tree machine learning strategy on determination of UCD values by selection of electrochemical features like electrode type, iodine concentration in the electrolyte, oxidation current density and applied potential. It is believed that machine learning strategy in this study can be extended and developed with the addition of more experimental variables like the wheat type or with different electrochemical techniques to increase the applicability or performance of the decision tree model.

2. MATERIAL AND METHOD

In this study, cyclic voltammetry technique in a three-electrode system were used to extract electrochemical data for decision tree analysis. During cyclic voltammetry, two different working electrodes as polycrystalline platinum (Pt) and glassy carbon (GC) discs, platinum counter electrode and standard calomel reference electrode were used for iodine oxidation in a three-electrode set up. For the electrolyte, sulphuric acid and 1.5 gr of boric acid (Merck Inc.) as an emulsifier, 1.5gr KI (Merck Inc.) as and iodine source and 60 ml of deionized water as a solvent were used in three neck glass electrochemical cell. In order to prevent formation of elemental iodine 1 drop of 0.1 M sodium thiosulphate (Merck Inc.) was added to the mixture. After stirring the electrolyte for 5 min, 15 ml electrolyte was transferred to a three-neck glass cell. Voltammetric scans were performed with and without flour addition to the electrolyte. After the first scan at 50 mV/sec between 0-1 V vs. SCE in flour free electrolyte, 0.5 gr of flour was added to the electrolyte and voltammetric scan was repeated. Cyclic voltammetric experiments were performed with different KI concentrations as 0.15M and 0.075M in the electrolyte with flour samples of three different UCD values of 16.5, 25 and 30 as well. Flour samples with different UCD values were collected from the local flour factories in central Anatolia region in Turkey. For the computations in machine learning only forward scan between 0-1V vs. SCE at different UCD values, KI concentrations and with different electrode types were used.

2.1. Principle Component Analysis (PCA) of Voltammetry Data

As a famous type of unsupervised machine learning where there is no training of the model with observed data, exploratory analysis and dimensionality reduction helps researchers to propose trends and provide initial insights in the data with less number of variables than during observations. At this point techniques like PCA

which is based on the covariance or correlation matrix can be used to assign latent variables that are linearly related with original variables with maximum variance (Comon, 1994).

For PCA analysis, initially a dataset of n observations with p numerical input variables is needed. During PCA, linear combinations of p vectors that would give us maximum variance (how wide the experimental data is distributed around mean value) is searched. The variance of linear combinations of p vectors is represented by a'Sa where a is a coefficient vector with dimensions p, a' is transpose of a and S is the covariance matrix (joint variability) between each pair of input variables which should be maximized (Jolliffe & Cadima, 2016).

To allow for interpretation of voltammetry data, we have taken into account 4 input variables of potential, ln(1+current density), KI concentration and type of electrode (0 for glassy carbon, 1 for platinum electrode). Therefore, PCA identified new variables, principal components as linear combinations of these four electrochemical variables. In Matlab environment "score" together with "pca" command give principal components by centering each input variable to zero average level. For instance one principle component can be expressed as a_{11}*potential$_{centered}$ + a_{12}*ln(1+current density)$_{centered}$ + a_{13}*KI concentration$_{centered}$ + a_{14}*presence of Pt electrode$_{centered}$, where a_{11}, a_{12}, a_{13}, a_{14} are coefficients for the first principal component (Ringnér, 2008). After determination of the percentage of variances, principal components with highest variances were used for explanatory analysis of the voltammetric data.

2.2. Construction of Decision Tree

A decision tree is a model that shows routes to output by the help of input variables or features partitioned and predicts new data based on the trained tree. In decision tree, the subsets that are formed in the leaves of the tree by splitting observed data set should have a desired purity. In order to have a desired purity the three main splitting criteria used in decision tree are information gain, gini index and node error. In the decision tree the partition value is selected based on maximum information gain, minimum gini index or minimum node error. Information gain is given in equation 1.

$$\text{InfoGain} = \text{Info}(\text{Parent node}) - \sum_k(p_k)\text{Info}(\text{Childnode}_k) \quad (1)$$

Info and p_k in equation 1 is the information of the feature subspace (node), and the proportion of samples passed to the *k*th subspace (or node) as given in equation 2.

$$Info = -\sum_k \left(\frac{N_j(t)}{N(t)}\right) \cdot \ln \frac{N_j(t)}{N(t)} \quad (2)$$

In equation 2 where *N(t)* is the number of samples in node t, and $N_j(t)$ is the number of class *j* samples in node *t*. The other split criterion Gini index is an indication of node impurity as given in equation 3.

$$1 - \sum_i p^2(i) \quad (3)$$

In equation 3 above, the sum is over the classes *i* at the node, and *p(i)* is the observed fraction of classes with class *i* that reach the node. A node with just one class (a pure node) has Gini index 0; otherwise, the Gini index is positive, therefore minimum Gini index is desired for node purity. And finally, node error shows the fraction of misclassified observations at the node. *p(j)* in equation 4 below is the observed fraction of largest class (with largest number of observations).

$$1 - p(j) \quad (4)$$

In Matlab environment, other than Gini (diversity) index, two different split criterions 'twoing' and 'deviance' are used similar to equations 1-4. The deviance of a node is given in equation 5 below where a pure node has deviance 0; otherwise, the deviance is positive.

$$-\sum_k \left(\frac{N_j(t)}{N(t)}\right) \cdot ln \frac{N_j(t)}{N(t)} \quad (5)$$

As given in equation 6, twoing is expressed in terms of *L(i)* which denotes the fraction of members of class *i* in the left child node after a split, and *R(i)* which denotes the fraction of members of class *i* in the right child node after a split and *P(L)* and *P(R)* are the fractions of observations that are split to the left and right leaf nodes respectively. It is desired to maximize twoing to make child node purer.

$$P(L)P(R)(\sum_i |L(i) - R(i)|)^2 \quad (6)$$

A very important point about the splitting criterions mentioned above is that the choice of the criterion may affect the choice of best features for the root or branch nodes which may lead to different decision trees. Therefore, it is necessary to compare decision tree models from different scoring criteria and to identify certain features with more or less significance.

Since the decision tree algorithm is a recursive technique, running of algorithm continues until the selected criterion is optimized by selecting optimum partition of predictors (input variables) (Quinlan, 1986). Of course, there are different algorithms like ID3, CART, C4.5, C5.0 etc. in the computing history used for decision trees with different advantages of high classifying speed, strong learning ability and simple construction (Breiman et al., 1984). Although different algorithms exist, researchers still face difficulties during modeling like low accuracy and try to make improvements on the existing algorithms (Han et al., 2011). Matlab software environment (8.4.0.150421 (R2014b)) uses non-parametric CART (Classification and regression tree) algorithm (Breiman et al., 1984). This algorithm can canconstruct binary classification trees for categorical output variables. CART algorithm can be represented as a flow diagram as seen in Figure 1. In Matlab environment (8.4.0.150421 (R2014b)), binary decision trees for classification are built using "fitctree" command.

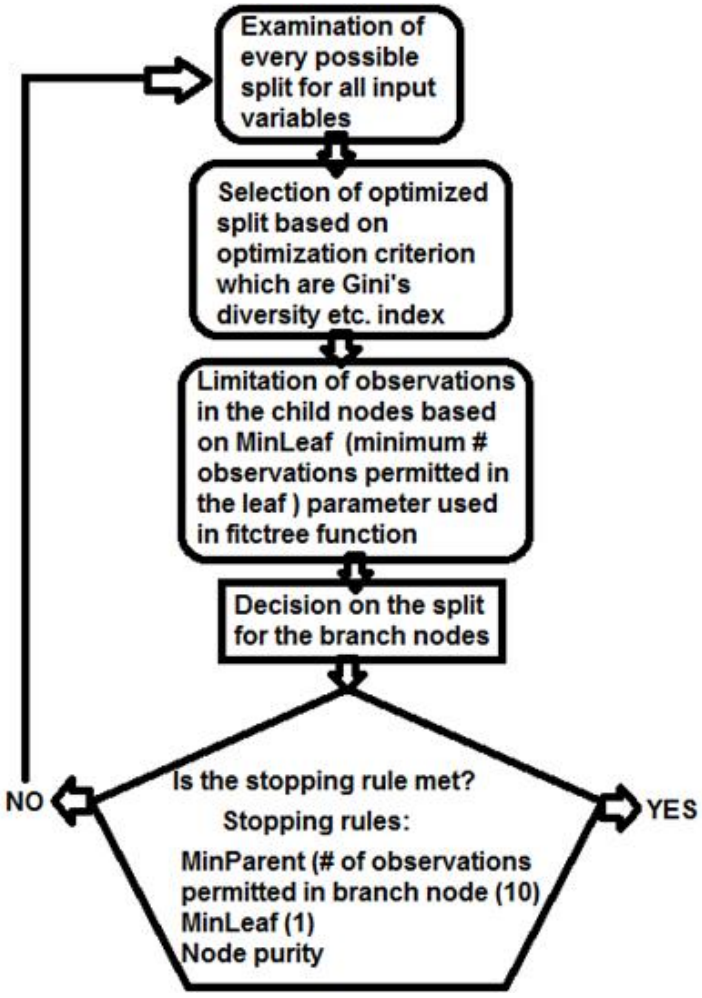

Figure 1. *Simple Representation of CART Algorithm in MATLAB Environment*

In this study, binary classification tree was used for the determination of routes to UCD values with potential, current density, KI concentration and type of electrode (platinum or glassy carbon disc electrode) as input variables. For the decision tree, a testing procedure was used to observe the accuracy of the model. First the database was randomly separated into training and testing subsets after shuffling the observations of the database randomly. Shuffling of observations was done in order to sample observations from the database in a wide range of input variables during training of the decision tree. The testing subset included 10% of the total number of observations. After the selection of splitting criterion, testing and training errors were compared at different tree sizes by the pruning the decision tree incrementally. The pruned tree size with the minimum testing error was selected as the optimal tree (Larose & Larose, 2014; Tapan et al., 2016; Baysal et al., 2017; Günay et al., 2018). Since it is known that the choice of optimization criterion may affect the choice of best features for the root or branch nodes which lead to different decision trees and therefore may affect the testing error, the testing procedure mentioned in Figure 1 was repeated to compare testing accuracy with different splitting criterion (Myles et al., 2004).

3. RESULTS AND DISCUSSION

3.1. Cyclic Voltammetry

As can be seen from the cyclic voltammetry experiments in Figure 2, oxidation and reduction peaks corresponding to triiodide/iodide redox couple (Boschloo & Hagfeldt, 2009) as given by the one step electrochemical reaction below in equation 7 appear close to 0.45 V and 0.25 V vs. SCE.

$$I_3^- + 2e^- \rightarrow 3I^- \quad (7)$$

Upon performing cyclic voltammetric experiments on 2 different types of electrodes, in two different electrolyte concentrations and with three different values of UCD, it is clearly seen that it is not possible to separate and analyze the effect of electrochemical features on current density or applied potential or to observe electrochemical conditions leading to different UCD values.

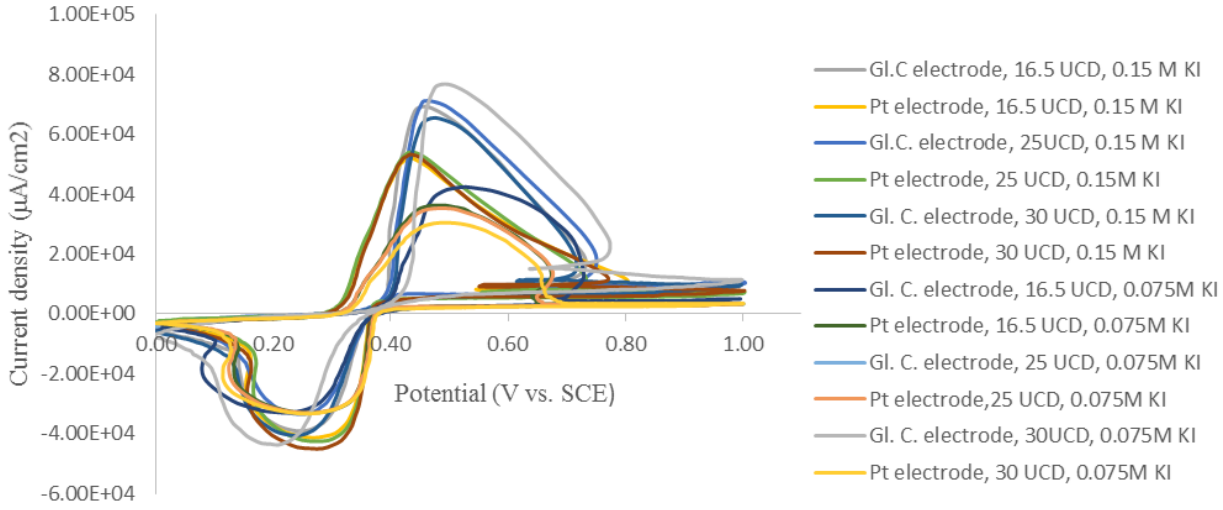

Figure 2. *Cyclic Voltammetry Experiments Performed with Pt and GC Disc Electrodes in Electrolytes with 0.075 M and 0.15M KI and with Flours of 16.5, 25 and 30 UCD Values (Scan Rate:50 mV/sec)*

For the purpose of extracting some general information and better visualization of electrochemical data used for computational purposes, voltammetry experiments were also classified with respect electrode type, UCD values and KI concentration in the electrolyte by the use of data visualization tool, ggplot2 package in R environment as seen in Figure 3. It was seen that although it not possible to differentiate UCD values in voltammetric data , higher oxidation peak current densities were observed on glassy carbon electrode and drop in KI concentration decreases peak oxidation currents for UCD values of 16.5 and 25 on both electrodes and secondly at UCD value of 30 highest oxidation peak current densities were seen on GC electrode which is just

the opposite of platinum electrode and which may indicate the different oxidation mechanisms on the two electrodes.

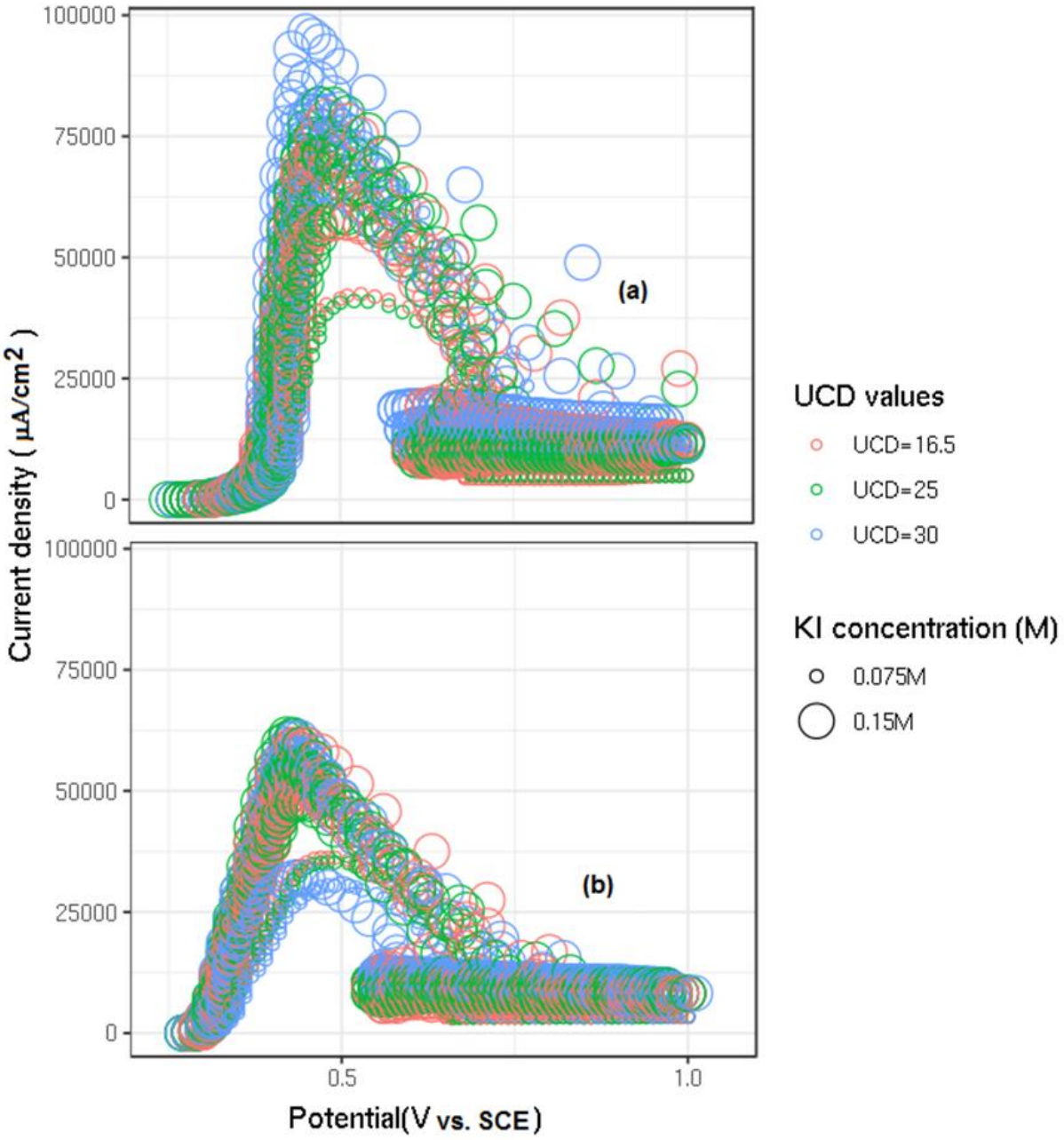

Figure 3. *Visualization of Voltammetric Experiments by Classifying with Respect to Electrode Type, UCD Values and KI Concentration* ***a)*** *glassy carbon electrode,* ***b)*** *platinum electrode (Scan Rate:50 mV/sec)*

3.2. Construction, Filtering and Analysis of Electrochemical Database

After cyclic voltammetry experiments, voltammetric data in the forward potential scan in range of 0 to 1V vs. SCE was filtered from outliers by analyzing box and whisker plots. In addition, in order to remove outliers from the voltammograms, Matlab code (MATLAB environment, version number 8.4; R2014b) was used and box and whisker plots (Walpole et al., 2012) before and after removal of outliers from the voltammetric data were compared as seen in Figure 4. After removal outliers from current density data, a filtered database of 3542 observations was used for the construction of decision trees. In Figure 4 natural logarithm transformation of current density data (ln (1+current density)) was performed in order to normalize data as much as possible after filtering from outliers.

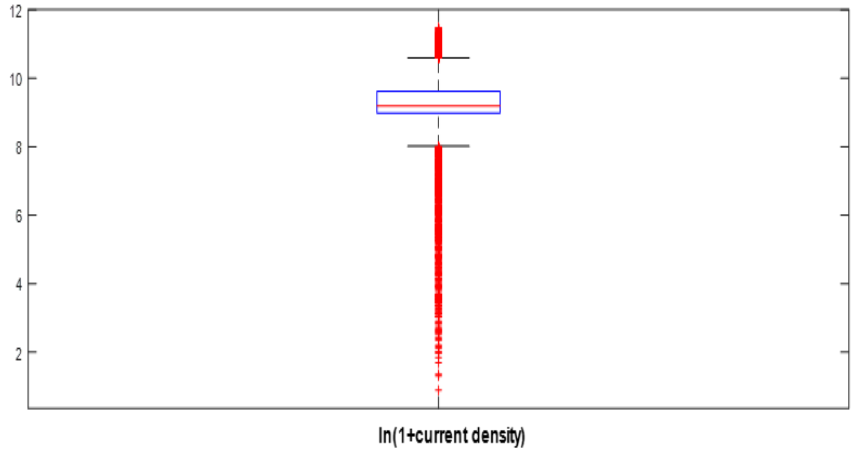

(a)

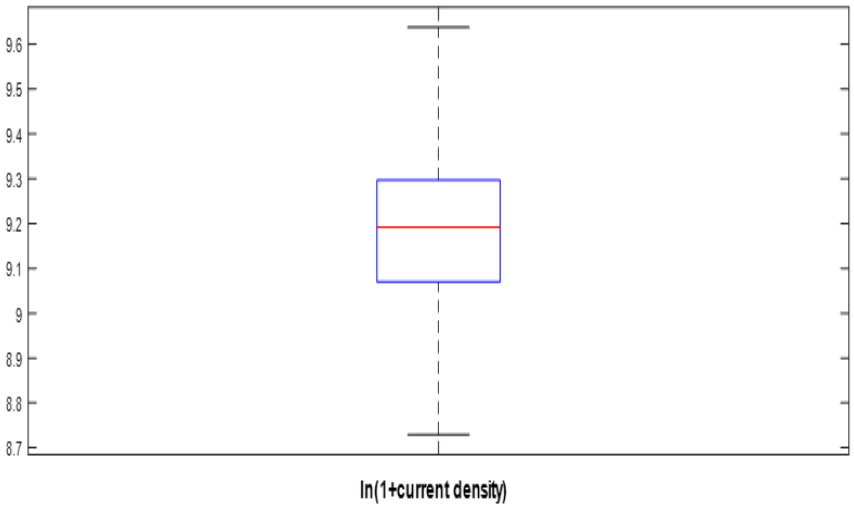

(b)

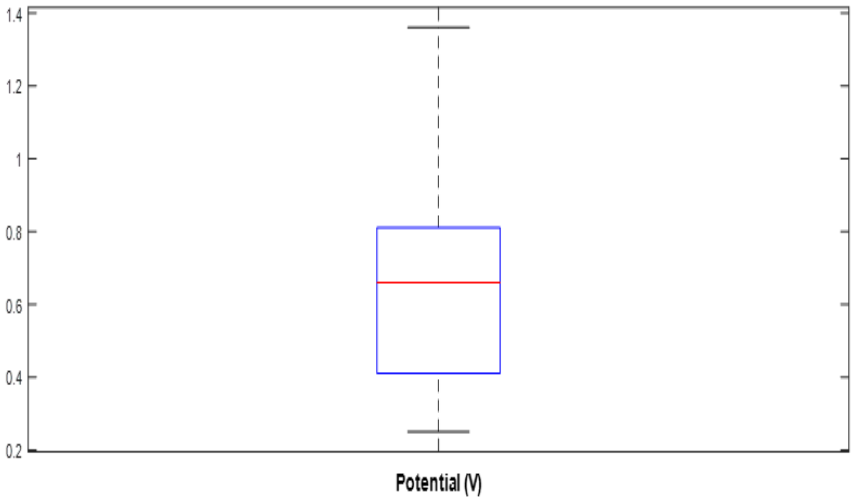

(c)

Figure 4. *Box and Whisker Plots of Electrochemical Features Before and After Removal of Outlier from the Current Density Data. Current Density Analysis were performed as the Natural Logarithm of (1+current density) [ln (1+current density)]* ***a)*** *before,* ***b)*** *after potential;* ***c)*** *before* ***d)*** *after UCD values;* ***e)*** *before,* ***f)*** *after removal of outliers*

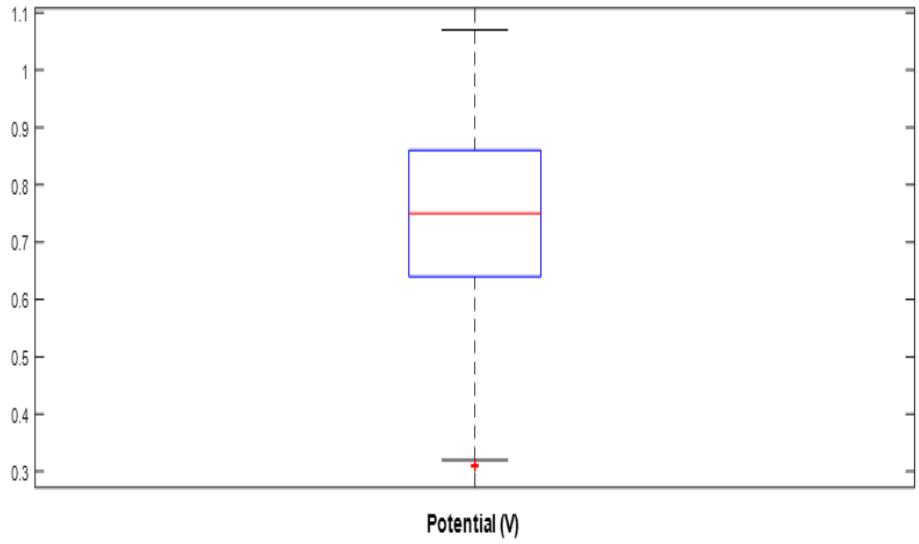

(d)

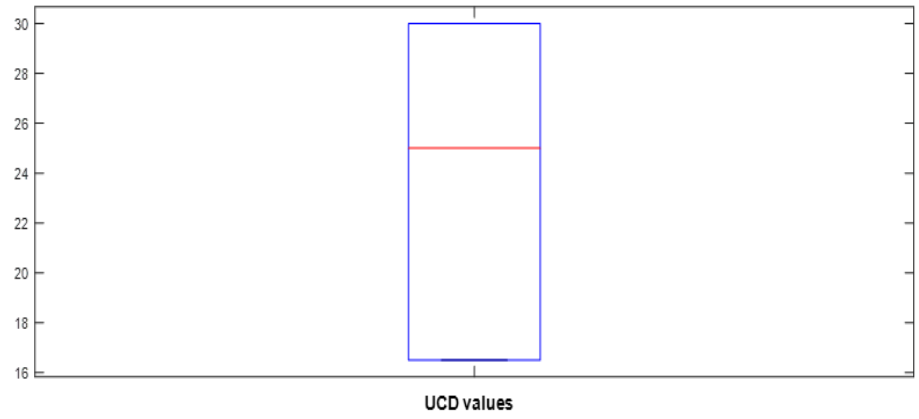

(e)

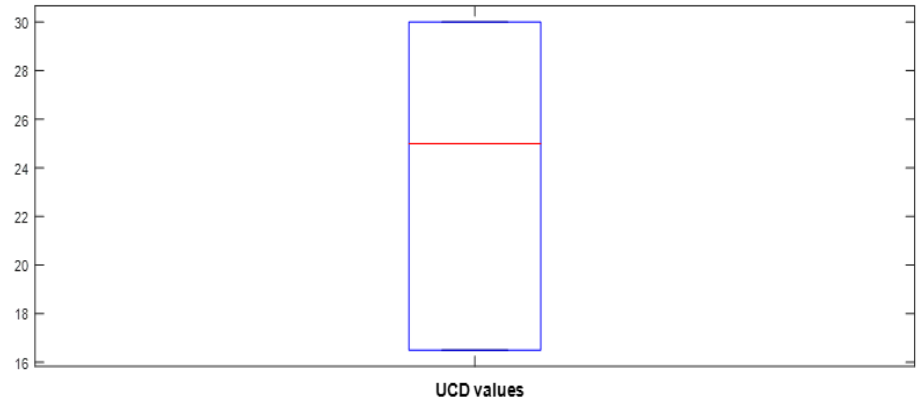

(f)

Figure 4. *Continued*

It can be seen from Figure 4 that after removal of outliers which are the data points outside the whiskers, current density data was also normally distributed since the line in the box which shows the median of observations is almost in the middle of the box and the position of the box is almost in the center of upper and lower whiskers. Like current density, almost the similar behavior was observed for potential and UCD values. Therefore, after removal of outliers, no skewness in the filtered observations were observed.

In addition to filtering of electrochemical data, in order to search for any kind of correlation between each electrochemical feature, correlation matrix was constructed. Correlation coefficient matrix as dimensionless measure of linear dependence depends on the covariances (which is the joint variability between two random features) between any two features in the data set where covariance is divided by the product of standard deviation of selected two variables. The correlation matrix chart as shown in Figure 5 was constructed in Python 3 environment by importing "pandas" and "matplotlib" packages and using "corr ()" function.

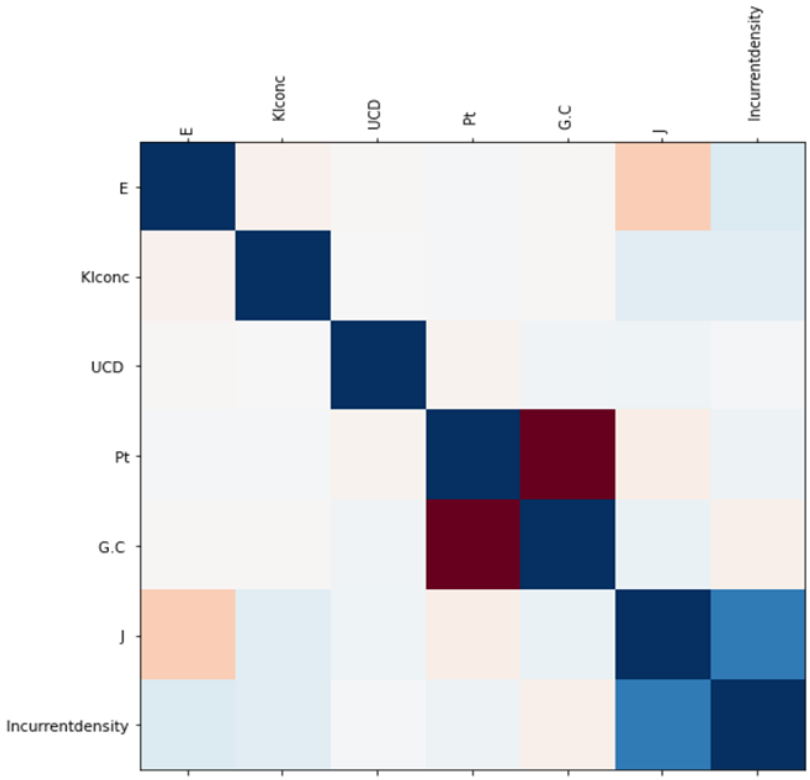

Figure 5. *Correlation Coefficient Matrix Chart between Features in the Electrochemical Data Set (**red box:** negative correlation, **blue box:** positive correlation)*

As seen in Figure 5, there is no strong correlation other than between current density and applied potential and other than a weak positive correlation between current density and KI concentration, there is almost no correlation between UCD values and other features.

3.3. Principal Component Analysis

In order to see the effect of each principal component in total variance (eigen values of covariance matrix) and to decide how many principal components (PC) to keep for explanatory analysis, "explained" together with "pca" was used to determine percent variance of each principal component as seen in Table 1.

Table 1. *Percentage of the Total Variance Explained by Each Principal Component*

Principal Component	Variance
PC1	**82.5**
PC2	**10.1**
PC3	**7.3**
PC4	**0.08**

As can be seen from Table 1, the first two components have 92.6% of the original variance which is enough to retain all the original variance and dimensionality can be reduced to 2 without loss of information. In addition, Table 2 shows that among the coefficients of four input variables (or the weights of input variables) in the first two principal components, current density and type of electrode (1 for Pt electrode, 0 for GC

electrode) are dominant factors in the first principal component; and potential and current density are dominant factors for the second principal component.

Table 2. *Coefficients of First Two Principal Components*

Predictor	**PC 1**	**PC 2**
Potential	-0.03252	-0.6012
ln(1+current density)	-0.1771	0.7895
KI Concentration	0.00364	-0.0142
Pt Electrode (0 or 1)	0.9836	0.1223

In order to understand whether the variation retained in the selected components contains relevant information about the level of output (UCD values), each sample is projected onto these principal components and separate levels of the output (separate clusters of output) were searched on these components as seen in the Figure 6 below:

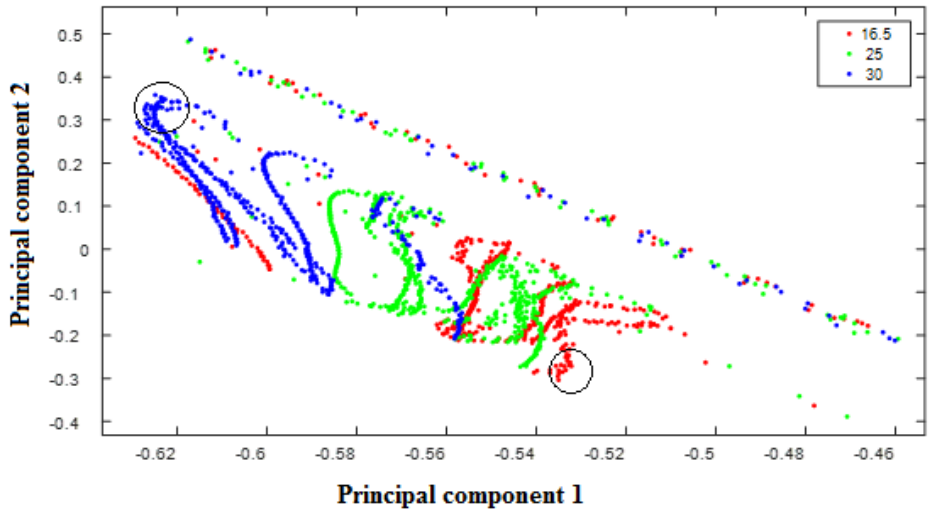

(a)

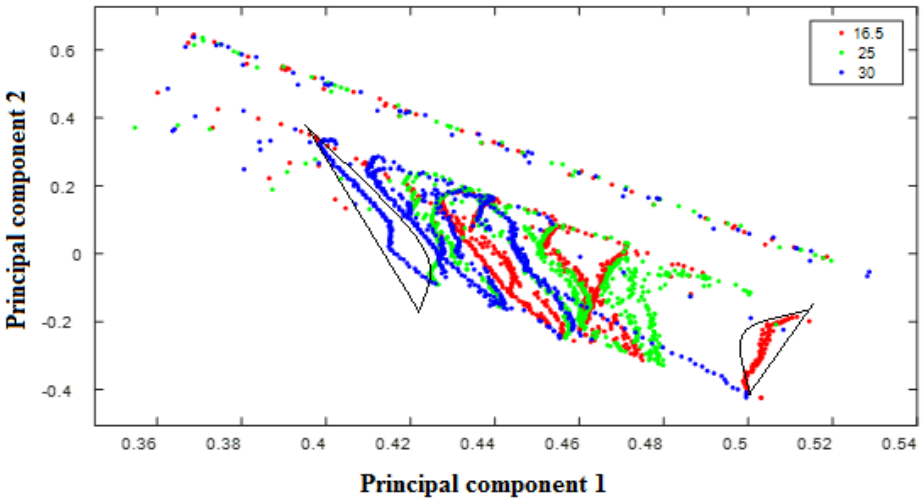

(b)

Figure 6. *Principal Component Analysis of Cyclic Voltammetry Data without Outliers and Distribution of UCD Values with Respect to the First Two Principal Components*
*(**red filled circles:** UCD=16.5; **green filled circles:** UCD=25; **blue filled circles:** UCD=30; pure clusters were surrounded by **black lines**)*
*Range of Principal Component Analysis with PC1 **a)** Between -0.64 and -0.46, **b)** Between 0.34 and 0.54*

In Figure 6, by the representation of UCD values (output levels) with 2 dimensional plots, clusters of UCD values can be visualized. In Figure 6, it was also decided to split the principal component analysis into two regions of first principal component in order to see clearly pure clusters of UCD values. Therefore, from Figure 6a at high current densities (negative PC1), UCD values of 30 and at high potentials and high currents, UCD values of 16.5; and from Figure 6b at high potentials on platinum electrode UCD values of 16.5 could be observed.

3.4. Decision Tree Analysis

For the construction decision tree, in order to see the effect of splitting criterion on the regions of overfit and underfit, initially, testing and training errors which are root mean square error of the difference between class predictions (from decision tree) and observations were compared at different pruning levels. As seen in Figure 7, different splitting criterions (Figure 7a,b,c) exhibit different regions of overfit and underfit; and minimum testing error was achieved at a pruning level of 21 for "deviance" splitting criterion.

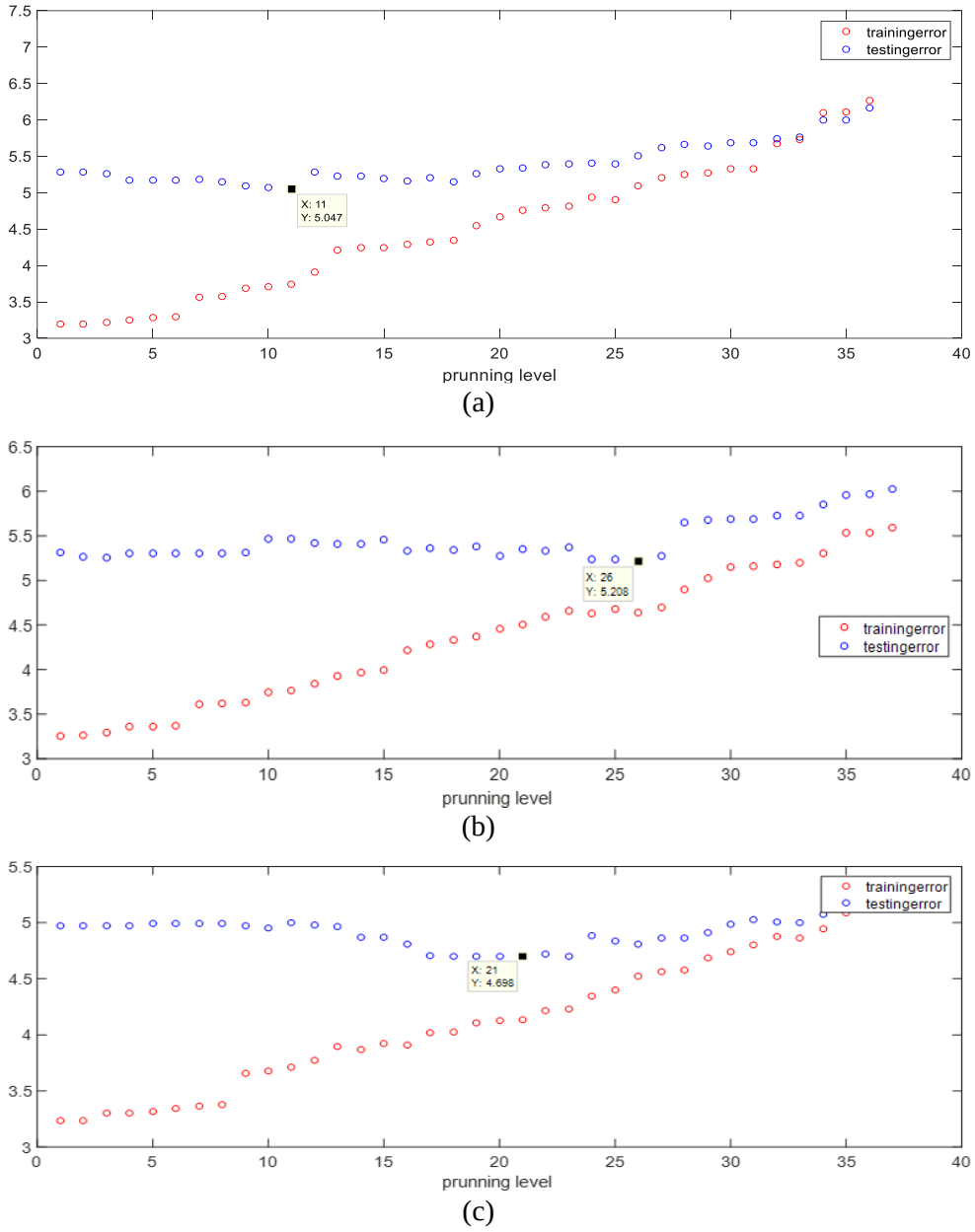

Figure 7. *Testing and Training Errors at Different Pruning Levels for Different Splitting Criterions* ***a)*** *gdi,* ***b)*** *twoing,* ***c)*** *deviance, testing subset:10% of observations*

After determination of training and testing errors for different pruning levels, fraction of misclassified observations were analyzed by determination of confusion matrices with Matlab command "confusionmat" for the three splitting criterion at the optimum pruning level. As seen in Table 3, deviance splitting criterion exhibit lowest number of misclassifications in the confusion matrix.

Table 3. *Confusion Matrix Charts of Testing Data for Different Splitting Criterions* ***a)*** *gdi,* ***b)*** *twoing,* ***c)*** *deviance (**red box:** misclassification, **blue box:** correct classification)*

gdi				
True	**UCD=16.5**	82	21	14
	UCD=25	30	87	12
	UCD=30	11	19	78
		UCD=16.5	**UCD=25**	**UCD=30**
(a)		**Predicted**		
twoing				
True	**UCD=16.5**	73	33	10
	UCD=25	27	92	11
	UCD=30	13	32	63
		UCD=16.5	**UCD=25**	**UCD=30**
(b)		**Predicted**		
deviance				
True	**UCD=16.5**	85	22	9
	UCD=25	20	90	19
	UCD=30	12	19	78
		UCD=16.5	**UCD=25**	**UCD=30**
(c)		**Predicted**		

After construction of binary decision tree with the optimum pruning level ,21, and optimum splitting criterion "deviance" based on minimum testing error and confusion matrix with minimum misclassifications, observations were split with 71 branch and 71 leaf nodes with these hyperparameters (splitting criterion and pruning level) as seen Figure 8.

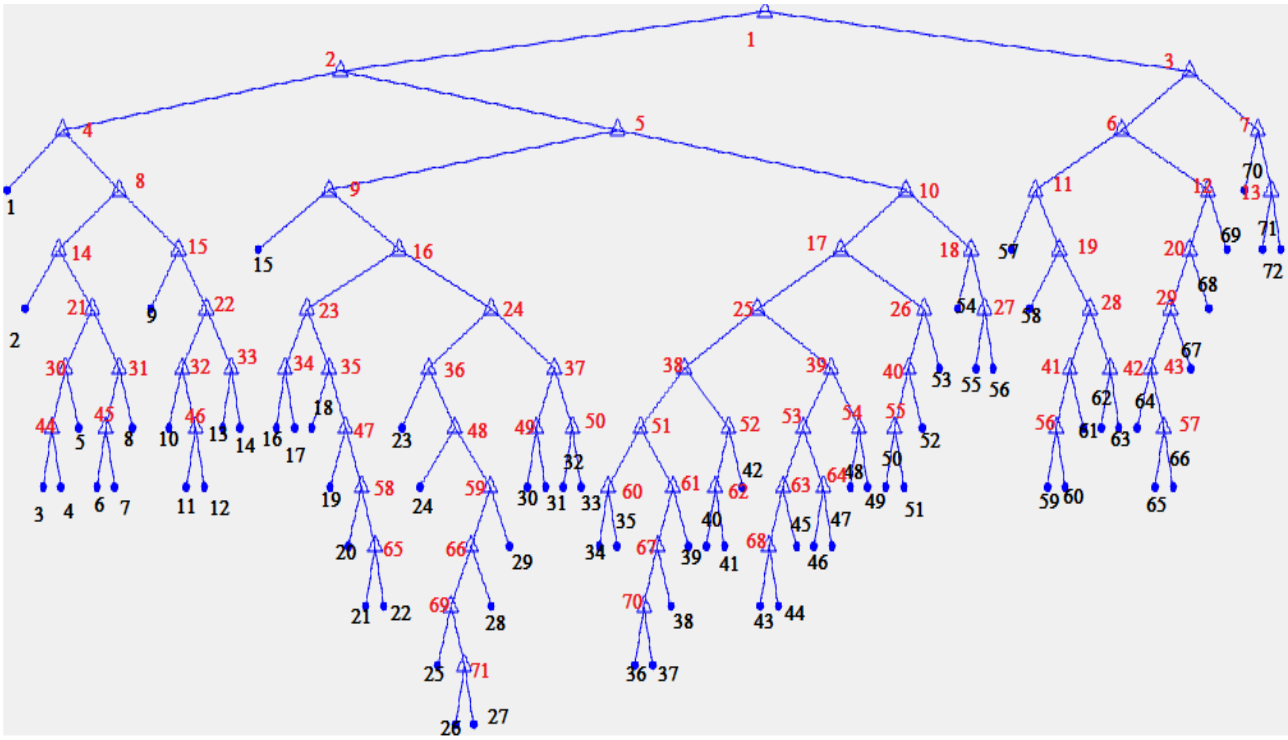

Figure 8. *Binary Classification Tree Constructed by "Deviance" Splitting Criterion*

The rules of branch nodes seen in Figure 8 is also presented in Table 4. As seen in Table 4, the decision tree grows with the root node which uses current density as a rule and the first two main branches are electrode type and current density again. In addition, Table 4 shows that most of the leaf nodes involve "current density" as a rule. It also important to note that branch nodes 7 and 13 are not taken into consideration for further analysis since "electrode type" is not used as a rule in these branch nodes.

Table 4. *Branch Node Rules Based on Binary Decision Tree with "Deviance" Criterion and 21 Pruning Level*

Node#	Rule	Node#	Rule
1	current density (μA/cm^2)<10350.33	36	potential (V) <0.545
2	electrode type (Pt=1,GC=0)=0	37	current density (μA/cm^2)<8392.39
3	current density (μA/cm^2)<12066.73	38	current density (μA/cm^2)<9761.56
4	potential (V) <0.515	39	current density (μA/cm^2)<9735.43
5	current density (μA/cm^2)<9020.36	40	current density (μA/cm^2)<10320.25
6	electrode type (Pt=1,GC=0)=0	41	potential (V) <0.815
7	potential (V) <0.49	42	potential (V) <0.85
8	current density (μA/cm^2)<9794.22	43	potential (V) <0.675
9	current density (μA/cm^2)<6638.42	44	current density (μA/cm^2)<8992.97
10	potential (V) <0.895	45	potential (V) <0.625
11	potential (V) <0.515	46	current density (μA/cm^2)<9817.96
12	current density (μA/cm^2)<11122.55	47	current density (μA/cm^2)<7841.63
13	potential (V) <0.965	48	current density (μA/cm^2)<8439.36
14	current density (μA/cm^2)< 8940.69	49	current density (μA/cm^2)<8189.17
15	potential (V) <0.815	50	potential (V) <0.845
16	current density (μA/cm^2)<8180.00	51	potential (V) <0.615
17	current density (μA/cm^2)<9867.47	52	potential (V) <0.665
18	current density (μA/cm^2)<9842.83	53	potential (V) <0.845
19	KI concentration (M) =0.075	54	potential (V) <0.765
20	potential (V) <0.735	55	potential (V) <0.635
21	current density (μA/cm^2)<9219.37	56	current density (μA/cm^2)<10671.97
22	current density (μA/cm^2)<9846.87	57	current density (μA/cm^2)<10606.54
23	current density (μA/cm^2)<7362.86	58	current density (μA/cm^2)<8139.77
24	potential (V) <0.765	59	potential (V) <0.745
25	potential (V) <0.765	60	current density (μA/cm^2)<9115.58
26	potential (V) <0.735	61	current density (μA/cm^2)<9443.80
27	current density (μA/cm^2)<9995.90	62	current density (μA/cm^2)<9833.28
28	current density (μA/cm^2)<11652.13	63	current density (μA/cm^2)<9167.23
29	current density (μA/cm^2)<10901.09	64	current density (μA/cm^2)<9254.28
30	potential (V) <0.895	65	potential (V) <0.835
31	potential (V) <0.885	66	current density (μA/cm^2)<9009.81
32	potential (V) <0.925	67	current density (μA/cm^2)<9240.23
33	potential (V) <0.925	68	potential (V) <0.785
34	current density (μA/cm^2)<6922.94	69	potential (V) <0.675
35	potential (V) <0.805	70	potential (V) <0.69
		71	current density (μA/cm^2)<8844.20

In order to determine the significance of input variables in the decision tree model, importance of the input variables were also determined by "predictorImportance" function in Matlab environment. In Matlab, predictor importance function sums up changes in the risks of the nodes related to each predictor in the pruned decision tree and divides the sum by the number of branch nodes. The change in the node risk is the difference between the risk for the parent node (related with specific predictor) and sum of risks of child nodes as given in equation 8 where R_p, R_c and N_{branch} is the is parent risk, child node risk and total number of branch nodes. The risk of a node is defined as multiplication of node impurity (equation 3) by the probability of the node which is the ratio of observations that are classified in that node to total number of observations.

$$(R_p - \Sigma R_{ci})/N_{branch} \quad (8)$$

Table 5 shows the importance of the predictors used in the pruned decision tree where current density has the highest impact on UCD. The importance of the predictors can be ordered as current density (J) > potential > electrode type > KI concentration in Table 5.

Table 5. *Importance of Predictors in the Optimum Decision Tree*

Predictor (or Input Variable)	**Importance**
Current Density (J)	$1.03x10^{-3}$
Potential	$7.25x10^{-4}$
Electrode Type (Pt or GC Electrode)	$9.57x10^{-5}$
KI Concentration	$8.78x10^{-5}$

Table 6 shows leaf node number, highest class membership and the leaf node rules for the optimized binary decision tree. High class memberships in the leaf nodes indicate that voltammetric data with different electrode types, damaged starch content flour (UCD values) and electrolyte concentration (KI concentration) can be successfully modeled by classification tree. If the rules in Table 6 are examined based on different UCD values on the same electrode type, it is seen that although rules indicate same potential ranges maximum current density (J) increase with UCD values on the GC electrode and UCD values of 30 give highest current ranges for both GC and platinum electrode. At UCD value of 16.5 and 25, higher currents were seen on GC electrode compared to platinum electrode.

As a final word, although it is difficult to extract physical interpretation from the rules of binary decision tree, performance indicators like confusion matrix and highclass memberships in the leaf nodes demonstrate the high accuracy of predicted UCD values just from voltammetric experiments.

Table 6. *Leaf Node Rules in the Optimum Decision Tree*

Leaf Node #	**Class Membership**	**Branch Nodes**
2	UCD 16.5=93/105	Glassy carbon electrode, potential >0.515V, J(μA/cm^2) <8940.69
10	UCD 16.5=40/43	Glassy carbon electrode, 0.925>potential (V) >0.815, 9794.22<J (μA/cm^2) <9846.87
14	UCD 16.5=14/16	Glassy carbon electrode, potential (V) >0.925, 9846.87<J (μA/cm^2) <10350.33
60	UCD 25=89/121	Glassy carbon electrode, 0.815>potential (V) >0.515, 10671.97<J (μA/cm^2)<11652.13, KI concentration (M) =0.15
61	UCD 25=109/115	Glassy carbon electrode, potential (V) >0.815, 10350.33<J (μA/cm^2)<11652.13, KI concentration (M) =0.15
7	UCD 25=88/90	Glassy carbon electrode,0.625<potential (V) <0.885, 9794.22>J (μA/cm^2)>9219.37
62	UCD 25=39/39	Glassy carbon electrode, 0.515<potential (V) <0.85, 11652.13<J (μA/cm^2)<12066.73, KI concentration (M) =0.15
3	UCD 25=11/14	Glassy carbon electrode, 0.895V>potential >0.515V, 8992.97>J (μA/cm^2)>8940.69
5	UCD 25=13/13	Glassy carbon electrode, 0.895V<potential, 8992.97>J(μA/cm^2) >8940.69
63	UCD 30=25/26	Glassy carbon electrode, potential (V) >0.85, 11652.13<J (μA/cm^2)<12066.73, KI concentration (M) =0.15
58	UCD 30=16/17	Glassy carbon electrode, potential (V) >0.515, 10350.33<J (μA/cm^2)<12066.73,KI concentration (M) =0.075
59	UCD 30=12/13	Glassy carbon electrode, 0.515<potential (V) <0.815, 10350.33<J (μA/cm^2)<10671.97, KI concentration (M) =0.15
15	UCD 16.5=69/80	Platinum electrode, J (μA/cm^2) <6638.42
20	UCD 16.5=43/58	Platinum electrode, potential (V) >0.805, 8139.77> J(μA/cm^2) >7841.63
25	UCD 16.5=43/56	Platinum electrode,0.675>potential (V) >0.545, 9009.81>J (μA/cm^2) >8439.36
24	UCD 16.5=44/51	Platinum electrode,0.545<potential (V) <0.765, 8180.00<J (μA/cm^2) <8439.36
45	UCD 16.5=36/39	Platinum electrode,0.765<potential (V) <0.845, 9167.23<J (μA/cm^2)<9735.43
44	UCD 16.5=15/15	Platinum electrode,0.785<potential (V) <0.845, 9020.36<J (μA/cm^2)<9167.23
30	UCD 16.5=12/14	Platinum electrode, potential (V) >0.765, 8189.17>J (μA/cm^2) >8180.00
18	UCD 25=89/110	Platinum electrode, potential (V) <0.805, 7362.86<J(μA/cm^2)<8180.00
17	UCD 25=25/35	Platinum electrode, 6922.94<J (μA/cm^2)<7362.86
27	UCD 25=16/18	Platinum electrode, 0.675<potential (V) <0.745, 8844.20<J (μA/cm^2) <9009.81
28	UCD 25=12/16	Platinum electrode, 0.545<potential (V) <0.745, 9009.81<J (μA/cm^2) <9020.36
65	UCD 25=13/14	Platinum electrode, 0.675<potential (V) <0.735, 10606.54>J (μA/cm^2) >10350.33
66	UCD 25=13/14	Platinum electrode, 0.675<potential (V) <0.735, 10606.54<J (μA/cm^2) <10901.09
55	UCD 25=12/13	Platinum electrode, potential (V) >0.895, 9842.83<J(μA/cm^2)<9995.90
69	UCD 30=72/92	Platinum electrode, 11122.55<J (μA/cm^2)<12066.73
68	UCD 30=46/47	Platinum electrode, Potential>0.735V, 11122.55<J (μA/cm^2)<12066.73
38	UCD 30=23/24	Platinum electrode, 0.615<potential (V) <0.765, 9240.23<J (μA/cm^2)<9443.80
67	UCD 30=12/14	Platinum electrode, potential (V) <0.735, 10901.09<J (μA/cm^2)<11122.55

4. CONCLUSION

In this study, classification tree was successfully applied on iodine oxidation voltammetric data. High class memberships and testing error in the pruned tree indicate that UCD values (damaged starch ratio) can be predicted from the selected electrochemical variables during voltammetric study. The machine learning strategy can be extended to other electrochemical techniques or with higher number of electrochemical variables for further studies.

ACKNOWLEDGEMENT

We would like to thank Gazi University Scientific Research Projects, BAP #: 06/2018-12 for the financial support.

CONFLICT OF INTEREST

The authors declare no conflict of interest.

REFERENCES

Baysal, M., Günay, M. E., & Yıldırım, R. (2017). Decision tree analysis of past publications on catalytic steam reforming to develop heuristics for performance: A statistical review. *International Journal of Hydrogen Energy*, *42*(1), 243-254. doi:10.1016/j.ijhydene.2016.10.003

Breiman, L., Friedman, J. H., Olshen, R. A., & Stone, C. J. (1984). *Classification and Regression Trees*. Chapman and Hall/CRC. doi:10.1201/9781315139470

Boschloo, G., & Hagfeldt, A. (2009). Characteristics of the Iodide/Triiodide Redox Mediator in Dye-Sensitized Solar Cells. *Accounts of Chemical Research*, *42*(11), 1819-1826. doi:10.1021/ar900138m

Comon, P. (1994). Independent component analysis, A new concept?. *Signal Processing*, *36*(3), 287-314. doi:10.1016/0165-1684(94)90029-9

Dhital, S., Shrestha, A. K., Flanagan, B. M., Hasjim, J., & Gidley, M. J. (2011). Cryo-milling of starch granules leads to differential effects on molecular size and conformation. *Carbohydrate Polymers*, *84*(3), 1133-1140. doi:10.1016/j.carbpol.2011.01.002

Günay, M. E., Türker, L., & Tapan, N. A. (2018). Decision tree analysis for efficient CO_2 utilization in electrochemical systems. *Journal of CO_2 Utilization*, *28*, 83-95. doi:10.1016/j.jcou.2018.09.011

Han, J., Kamber, M., & Pei, J. (2011). *Data Mining: Concepts and Techniques* (3rd ed.). Elsevier.

Jolliffe, I. T., & Cadima, J. (2016). Principal component analysis: a review and recent developments. *Philosophical Transactions of the Royal Society A: Mathematical, Physical and Engineering Sciences*, *374*, 20150202. doi:10.1098/rsta.2015.0202

Larose, D. T., & Larose, C. D. (2014). *Discovering Knowledge in Data: An Introduction to Data Mining* (2nd ed.). John Wiley & Sons.

Li, M., Hasjim, J., Xie, F., Halley, P. J., & Gilbert, R. G. (2014). Shear degradation of molecular, crystalline, and granular structures of starch during extrusion. *Starch-Stärke*, *66*(7-8), 595-605. doi:10.1002/star.201300201

Liu, W-C., Halley, P. J., & Gilbert, R. G. (2010). Mechanism of Degradation of Starch, a Highly Branched Polymer, during Extrusion. *Macromolecules*, *43*(6), 2855-2864. doi:10.1021/ma100067x

Liu, X., Xiao, X., Liu, P., Yu, L., Li, M., Zhou, S., & Xie, F. (2017). Shear degradation of corn starches with different amylose contents. *Food Hydrocolloids*, *66*, 199-205. doi:10.1016/j.foodhyd.2016.11.023

Medcalf, D. G., & Gilles, K. A. (1965). Determination of Starch Damaged by Rate of Iodine Absorption. *Cereal Chemistry*, *42*, 546-557.

Myles, A. J., Feudale, R. N, Liu, Y., Woody, N. A., & Brown, S. D. (2004). An Introduction to Decision Tree Modeling. *Journal of Chemome*trics, *18*(6), 275-285. doi:10.1002/cem.873

Quinlan, J. R. (1986). Induction of Decision Trees. *Machine Learning*, *1*, 81-106. doi:10.1007/BF00116251

Ringnér, M. (2008). What is Principal Component Analysis?. *Nature Biotechnology*, *26*(3), 303-304. doi:10.1038/nbt0308-303

Tapan, N. A., Günay, M. E., & Yildirim, R. (2016). Constructing Global Models from Past Publications to Improve Design and Operating Conditions for Direct Alcohol Fuel Cells. *Chemical Engineering Research and Design*, *105*, 162-170. doi:10.1016/j.cherd.2015.11.018

Walpole, R. E., Myers, R. H., Myers, S. L., & Ye, K. (2012). *Probability & Statistics for Engineers & Scientists* (9th ed.). Prentice Hall, Boston.

Zhu, F. (2016). Buckwheat Starch: Structures, Properties and Applications. *Trends in Food Science & Technology*, *49*, 121-135. doi:10.1016/j.tifs.2015.12.002

Research Article / Araştırma Makalesi GU J Sci, Part A, 8(4): 451-458 (2021) https://doi.org/10.54287/gujsa.1013194

Gazi University
Journal of Science
PART A: ENGINEERING AND INNOVATION
http://dergipark.org.tr/gujsa

On Prime Ideals Related to an Ideal in a Commutative Ring

Ortaç ÖNEŞ[1*]

[1]*Department of Mathematics, Akdeniz University, 07058 Antalya, Turkey*

Keywords

Prime Ideal

Radical Ideal

Localization

Abstract

This article focuses on the notion of prime ideal related to an ideal of a commutative ring. Some of its characteristics are studied and the relations between ideals and prime ideals related to these ideals in a commutative ring are examined. Then some useful connections among them are obtained. Both similarities and differences between prime ideals related to an ideal and prime ideals are pointed out. Moreover a direct connection between prime ideals related to an ideal and radical ideals is obtained.

Cite

Öneş, O. (2021). On Prime Ideals Related to an Ideal in a Commutative Ring. *GU J Sci, Part A*, *8*(4), 451-458.

Author ID (ORCID Number)

O. Öneş, 0000-0001-6777-9192

Article Process

Submission Date 21.10.2021
Revision Date 17.11.2021
Accepted Date 29.11.2021
Published Date 01.12.2021

1. INTRODUCTION

In this article, all rings, which is denoted by R are commutative with identity.

Historically, the discovery of the fact that every positive integer can be uniquely expressed as a product of prime powers arouse an analogous question in the context of ideal theory. Starting from mid 19th century, works of mathematicians such as Kummer, Kronecker and Dedekind did much to shed light on this subject. These studies established a similar decomposability of ideals into prime ideals under certain conditions and as of today constitute a popular topic in algebraic number theory.

The concept of prime ideal is mostly at the center of studies in ring theory and many useful results related to prime ideals have been proved in Kirby (1966; 1969), McConnell & Robson (1987), Jenkins & Smith (1992), Lam (2001), Anderson & Smith (2003), Naghipour (2005), Anderson & Bataineh (2008), Lam & Reyes (2008), Ebrahimpour & Nekooei (2012), Öneş & Alkan (2017; 2018; 2019a,b), Öneş (2020).

This article focuses on the relations between ideals and prime ideals related to these ideals in R.

The ideal $P \neq R$ is prime in R if for any product $ab \in P$ of the elements a, b of R, a or b is in P (Atiyah & MacDonald, 1969).

The notion of primality of an ideal in R was generalized in Öneş (2019) to the case in which R is an ideal in general.

Definition 1.1. (Öneş, 2019) For any ideals P, I in R, P is I -prime if for any product $ab \in P$ of two elements a, b in I, we have that

*Corresponding Author, e-mail: ortacns@akdeniz.edu.tr

$$a \in P \text{ or } b \in P$$

Immediately, it can be seen that R -prime ideals coincides with prime ideals in R. When a specific ideal in R is not mentioned, *-prime ideal is used instead of I -prime ideal.

Example 2.1 includes *-prime ideals in R. The connections between ideals and prime ideals related to them in R are shown in Lemma 2.4 and Corollary 2.5. It is proved that the ideal quotient of P by I is I -prime while P is I -prime ideal, in Lemma 2.6. When P is maximal, its converse is also true. Moreover, in Proposition 2.7, which is stated in Öneş (2019), the proof that any epimorphism respects *-primality under a certain condition is given.

The radical of I, which is an ideal, in R is defined as

$$\{r \in R: \exists n \in \mathbb{Z}^+, r^n \in I\} = \sqrt{I}$$

(Kaplansky, 1974). In Theorem 2.9, a connection between $\sqrt{I}$ -prime and I -prime in R is proved.

In Lemma 2.10, it is proved that in a local ring R, if I is maximal and P is I -prime, then P is prime. A nonempty subset S of R is a multiplicative set if any product ab of two elements $a, b \in S$ is also in S (Matsumura, 1986).

In Theorem 2.11, the proof of *-primality in localization is given.

2. PRIME IDEALS RELATED TO AN IDEAL

Example 2.1.

i) Every prime ideal of $\mathbb{Z}$ is an I -prime in $\mathbb{Z}$ for all ideals I of $\mathbb{Z}$.

ii) $10\mathbb{Z}$ and $15\mathbb{Z}$ are not prime ideals in $\mathbb{Z}$ but $15\mathbb{Z}$ is $10\mathbb{Z}$ -prime in $\mathbb{Z}$ and $10\mathbb{Z}$ is $15\mathbb{Z}$ -prime in $\mathbb{Z}$.

Proof.

i) It is clear with Definition 1.1.

ii) It can be easily proved that $10\mathbb{Z}$ and $15\mathbb{Z}$ are not prime in $\mathbb{Z}$.

We show that $15\mathbb{Z}$ is $10\mathbb{Z}$ -prime in $\mathbb{Z}$ and $10\mathbb{Z}$ is $15\mathbb{Z}$ -prime in $\mathbb{Z}$.

Let $a, b \in 10\mathbb{Z}$ such that $ab \in 15\mathbb{Z}$. Then we have that

$$a = 10x, b = 10y, 15z = 2^2 5^2 xy, \text{ where } x, y, z \in \mathbb{Z}.$$

Hence it follows that $3 | xy$, meaning that $3 | x$ or $3 | y$.

If $3 | x$, then $a \in 30\mathbb{Z} \subseteq 15\mathbb{Z}$, meaning that $a \in 15\mathbb{Z}$.

If $3 | y$, then $b \in 30\mathbb{Z} \subseteq 15\mathbb{Z}$, meaning that $b \in 15\mathbb{Z}$.

Let $a, b \in 15\mathbb{Z}$ such tha t$ab \in 10\mathbb{Z}$. Then we have that

$$a = 15x, b = 15y, 10z = 3^2 5^2 xy, \text{ where } x, y, z \in \mathbb{Z}.$$

Hence it follows that $2|\ xy$, meaning that $2|\ x$ or $2|\ y$.

If $2|\ x$, then $a \in 30\mathbb{Z} \subseteq 10\mathbb{Z}$, meaning that $a \in 10\mathbb{Z}$.

If $2|\ y$, then $b \in 30\mathbb{Z} \subseteq 10\mathbb{Z}$, meaning that $b \in 10\mathbb{Z}$.

Lemma 2.2. (Öneş, 2019) Let I_1, I_2, P be ideals of R, where $I_1 \subseteq I_2$, and let P be I_2 -prime in R. In this case, P is I_1 -prime in R.

Proof. Suppose $a, b \in I_1$ such that $ab \in P$.
Since I_1 is a subset of I_2, it follows that $a, b \in I_2$ with $ab \in P$. Because P is I_2 -prime in R, we have that

$$a \in P \text{ or } b \in P,$$

which is the desired result.

The following corollary is obtained from Lemma 2.2.

Corollary 2.3. Let I_i and P be ideals of R for every $i \in \Lambda$ and let P is I_i -prime in R. Then

i) P is $\bigcap_{i\in\Lambda} I_i$ -prime in R.

ii) P is $\prod_{i\in\Lambda} I_i$ -prime in R, where I_i is a co-maximal ideal of R for every $i \in \Lambda$.

Proof.

i) Let $a, b \in \bigcap_{i\in\Lambda} I_i$ such that $ab \in P$, meaning that $a, b \in I_i$ for every $i \in \Lambda$.

By hypothesis, either $a \in P$ or $b \in P$ holds. Thus P is $\bigcap_{i\in\Lambda} I_i$ -prime in R.

ii) It is clear with **(i)**.

Lemma 2.4. Let P, I and J be ideals of R. If P is I -prime, then $(P:_R J)$ is I -prime.

Proof. Let $a, b \in I$ with $ab \in (P:_R J)$.

Assume that $b \notin (P:_R J)$.

Then we have $bj \notin P$ and $abj \in P$ for an element j in J. Since $a, bj \in I$ and P is I -prime in R, we get that $a \in P$ or $bj \in P$. Because the element bj is not in P, we have that

$$a \in P, \text{ meaning } a \in (P:_R J).$$

Thus $(P:_R J)$ is I -prime in R.

By using Lemma 2.2 and Lemma 2.4, the following result is obtained.

Corollary 2.5. Let P, I and J be ideals of$R$. If P is $(I:_R J)$ -prime, then $(P:_R J)$ is I -prime.

Proof. Let P be $(I:_R J)$ -prime.

Since $I \subseteq (I:_R J)$, then P is I -prime by Lemma 2.2. Thus $(P:_R J)$ is I -prime with Lemma 2.4.

Lemma 2.6. Let I, P be ideals in R, where P is I -prime. Then $(P:_R I)$ is I -prime in R, where $I \neq P$. When P is maximal, its converse is true.

Proof. Let $a, b \in I$ such that $ab \in (P:_R I)$.

Assume that $b \notin (P:_R I)$.

Then we have $bx \notin P$ and $abx \in P$ for an element x in I. Because $a, bx \in I$ and P is I -prime in R, either $a \in P$ or $bx \in P$ holds. Since $bx \notin P$, we have that

$$a \in P, \text{ meaning } a \in (P:_R I).$$

Consequently $(P:_R I)$ is I -prime in$R$.

Suppose that P is maximal in R and $(P:_R I)$ is I -prime in R, where $I \neq P$.

Let $a, b \in I$ with $ab \in P$.

We have $abI \subseteq P$, meaning $ab \in (P:_R I)$. Because $(P:_R I)$ is I -prime in R, it follows that $a \in (P:_R I)$ or $b \in (P:_R I)$. Since $P \subseteq (P:_R I)$, by the assumption it is true that

$$a \in P \text{ or } b \in P.$$

Thus P is I -prime in R.

Here, we prove the following proposition, which is stated in Öneş (2019).

Proposition 2.7. Let S be a commutative ring with identity. Let φ be an epimorphism from R to S, let I and P be ideals in R and $Ker\varphi \subseteq P$. Then

$$P \text{ is } I \text{ -prime iff } \varphi(P) \text{ is } \varphi(I) \text{ -prime.}$$

Proof. $(:\Rightarrow)$ Let a and b be any elements of $\varphi(I)$ such that $ab \in \varphi(P)$.

Then we have $a = \varphi(x)$ and $b = \varphi(y)$ for $x, y \in I$. Then it follows that $ab = \varphi(x)\varphi(y) = \varphi(xy) \in \varphi(P)$. We also have $\varphi(xy) = \varphi(p)$ for $p \in P$. Since $Ker\varphi \subseteq P$, we have $xy \in P$. Because P is I -prime, we get that

$$x \in P \text{ or } y \in P, \text{ meaning that } a \in \varphi(P) \text{ or } b \in \varphi(P).$$

Thus $\varphi(P)$ is $\varphi(I)$ -prime in S.

$(\Leftarrow:)$ Let a and b be any elements of I such that $ab \in P$.

Then we have $\varphi(a)\varphi(b) = \varphi(ab) \in \varphi(P)$ with $\varphi(a), \varphi(b) \in \varphi(I)$. Because $\varphi(P)$ is $\varphi(I)$ -prime in S, either $\varphi(a) \in \varphi(P)$ or $\varphi(b) \in \varphi(P)$ holds. Since $Ker\varphi \subseteq P$, it follows that

$$a \in P \text{ or } b \in P.$$

Thus P is I -prime in R.

Proposition 2.8. Let S be a commutative ring with identity. Let φ be an epimorphism from R to S, let I be an ideal in R and let P be $\varphi(I)$ -prime in S. Then $\varphi^{-1}(P)$ is I -prime in$R$.

Proof. Let a and b be any elements of I such that $ab \in \varphi^{-1}(P)$.

Thus $\varphi(ab) = \varphi(a)\varphi(b)$ is in P, where $\varphi(a)$ and $\varphi(b)$ are in $\varphi(I)$. Because P is $\varphi(I)$ -prime ideal of S, we have that

$$\varphi(a) \in P \text{ or } \varphi(b) \in P \ .$$

It follows that $a \in \varphi^{-1}(P)$ or $b \in \varphi^{-1}(P)$. Thus $\varphi^{-1}(P)$ is I -prime in R.

Theorem 2.9. Let J, I be ideals of R.

i) J is $\sqrt{I}$ -prime in R.

ii) J is I -prime in R.

iii) $\sqrt{J}$ is I -prime in R.

The above statement (i) implies statement (ii), which implies statement (iii). When $J = \sqrt{J}$, all three statements are equivalent.

Proof.

i⇒ii) It is clear with Lemma 2.2.

ii⇒iii) Suppose that J is I -prime in R.

Let $a, b \in I$ such that $ab \in \sqrt{J}$.

Then we have that $(ab)^n = a^n b^n \in J$ for $n \in \mathbb{Z}^+$. We have also $a^n, b^n \in I$. Since J is I -prime in R, either $a^n \in J$ or $b^n \in J$ holds. Thus we have that

$$a \in \sqrt{J} \text{ or } b \in \sqrt{J}.$$

Consequently $\sqrt{J}$ is I -prime in R.

Let $J = \sqrt{J}$.

iii⇒i) Suppose that $\sqrt{J}$ is I -prime in R.

Let $a, b \in \sqrt{I}$ such that $ab \in J$.

There exist positive integers n, m such that $a^n, b^m \in I$. Thus we have that

$$(ab)^{nm} = (a^n)^m (b^m)^n \in J = \sqrt{J}.$$

Because $\sqrt{J}$ is I -prime in R, either $a \in \sqrt{J}$ or $b \in \sqrt{J}$ holds. Since $J = \sqrt{J}$, either $a \in J$or $b \in J$ holds. Consequently J is $\sqrt{I}$ -prime in R.

Lemma 2.10. Let I be a maximal ideal of a local ring R, let P be a proper ideal of R and let P be I -prime in R. Then P is prime in R.

Proof. Let $a, b \in R$ such that $ab \in P$.

We have the following three cases:

i) If a and b are invertible elements in R, then it follows that

$$1_R = a^{-1}abb^{-1} \in P, \text{ meaning} P = R.$$

It is a contradiction.

ii) If a or b is an invertible element in R, then we have that

$$a \in P \text{ or} b \in P.$$

Consequently P is prime in R.

iii) If a and b are not invertible elements in R, then we have that $a, b \in I$. Since P is I -prime, we get that

$$a \in P \text{ or } b \in P.$$

Consequently P is prime in R.

Theorem 2.11. Let S be a multiplicative subset of R and let I, P be ideals of R. If P is an I -prime ideal of R, $I \cap S = \emptyset$ and $P \cap S = \emptyset$, then $S^{-1}P$ is a $S^{-1}I$ -prime ideal of $S^{-1}R$.

Proof. Since $P \cap S = \emptyset$, $S^{-1}P$ is a proper ideal of $S^{-1}R$.

Let $\left(\frac{k}{s_1}\right), \left(\frac{l}{s_2}\right) \in S^{-1}I$ such that $\left(\frac{k}{s_1}\right)\left(\frac{l}{s_2}\right) \in S^{-1}P$.

There exist the elements $s_3, s_4, s_5 \in S$ such that $ks_3, ls_4 \in I$ and $kls_5 \in P$. Then we have that

$$(ks_3s_5)(ls_4) \in P.$$

Since P is I -prime, either $(ks_3s_5) \in P$ or $(ls_4) \in P$ holds.

If $(ks_3s_5) \in P$, then it follows that $\left(\frac{ks_3s_5}{s_1}\right) \in S^{-1}P$. Thus we have that

$$\left(\frac{1}{s_3s_5}\right)\left(\frac{ks_3s_5}{s_1}\right) = \left(\frac{k}{s_1}\right) \in S^{-1}P.$$

If $(ls_4) \in P$, then it follows that $\left(\frac{ls_4}{s_2}\right) \in S^{-1}P$. Thus we have that

$$\left(\frac{1}{s_4}\right)\left(\frac{ls_4}{s_2}\right) = \left(\frac{l}{s_2}\right) \in S^{-1}P.$$

Consequently $S^{-1}P$ is a $S^{-1}I$ -prime ideal of $S^{-1}R$.

ACKNOWLEDGEMENT

This study is supported by the Scientific Research Project Administration of Akdeniz University with the research project number FBA-2019-4969.

The author thanks the referees for their valuable suggestions and comments.

CONFLICT OF INTEREST

The author declares no conflict of interest.

REFERENCES

Anderson, D. D., & Bataineh, M. (2008). Generalizations of prime ideals. *Communications in Algebra*, *36*, 686-696.

Anderson, D. D., & Smith, E. (2003). Weakly prime ideals. *Houston Journal of Mathematics*, 29, 831-840.

Atiyah, M. F., & MacDonald, I. G. (1969). *Introduction to Commutative Algebra*. Addison-Wesley.

Ebrahimpour, M., & Nekooei, R. (2012). On generalizations of prime ideals. *Communications in Algebra*, *40*, 1268-1279.

Jenkins, J., & Smith, P.F. (1992). On the prime radical of a module over a commutative ring. *Communications in Algebra*, *20*, 3593-3602.

Kaplansky, I. (1974). *Commutative Rings*. The University of Chicago.

Kirby, D. (1966). Components of ideals in a commutative ring. *Ann. Mat. Pura Appl.*, *4*, 109-125.

Kirby, D. (1969). Closure operations on ideals and submodules. *J. London. Math. Soc.*, *44*, 283-291.

Lam, T. Y. (2001). *A First Course in Noncommutative rings*. Springer.

Lam, T. Y., & Reyes, M. L. (2008). A prime ideal principle in commutative algebra. *Journal of Algebra*, *319*, 3006-3027.

Matsumura, H. (1986). *Commutative Ring Theory*. Cambridge University Press.

McConnell, J. C., & Robson, J. C. (1987). *Noncommutative Noetherian Rings*. Wiley Chichester.

Naghipour, A. R. (2005). A simple proof of Cohen's theorem. *The American Mathematical Monthly*, *112*, 825-826.

Öneş, O. (2019). A generalization of prime ideals in a commutative ring. In: Proceedings Book of the 2nd Mediterranean International Conference of Pure Applied Mathematics and Related Areas, Paris, France, 28-31 August, 124-126.

Öneş, O. (2020). On radical formula in modules over noncommutative rings. *Filomat*, *34*(2), 443-449.

Öneş, O., & Alkan, M. (2017). On the left O-prime ideals over a noncommutative ring. *Advanced Studies in Contemporary Mathematics*, *27*(1), 107-113.

Öneş, O., & Alkan, M. (2018). A note on graded ring with prime spectrum. *Advanced Studies in Contemporary Mathematics*, *28*(4), 625-634.

Öneş, O., & Alkan, M. (2019a). Multiplication modules with prime spectrum. *Turkish Journal of Mathematics*, *43*(4), 2000-2009.

Öneş, O., & Alkan, M. (2019b). Zariski subspace topologies on ideals. *Hacettepe Journal of Mathematics and Statistics*, *48*(6), 1667-1674.

Research Article / Araştırma Makalesi GU J Sci, Part A, 8(4): 459-481 (2021) https://doi.org/10.54287/gujsa.1005561

Gazi University
Journal of Science
PART A: ENGINEERING AND INNOVATION
http://dergipark.org.tr/gujsa

LPG Stoklama Terminalinde Risk Değerlendirilmesi

Risk Assessment in an LPG Storage Terminal

Baharsu AKDAĞ[1], Saliha ÇETİNYOKUŞ[2*]

[1]*Gazi Üniversitesi, Kazaların Çevresel ve Teknik Araştırması Anabilim Dalı, Ankara*
[2]*Gazi Üniversitesi, Kimya Mühendisliği, Ankara*

Anahtar Kelimeler

Risk Değerlendirmesi
Hata Ağacı Analizi
Olay Ağacı Analizi
HAZOP
Endüstriyel Kazalar

Özet

Çalışmada, gemiyle gelen LPG ürününü depolayıp kara tankerleri ile müşterilere dağıtan bir LPG stoklama terminalinde risk değerlendirmesi amaçlanmıştır. Terminalde depolanan LPG, tehlikeli madde türü ve miktarı yönü ile 2 Mart 2019 tarihli ve 30702 sayılı Resmî Gazete'de yayımlanan Büyük Endüstriyel Kazaların Önlenmesi ve Etkilerinin Azaltılması Hakkında Yönetmelik kapsamına girmektedir. Yürütülen risk değerlendirme çalışmaları bu Yönetmelik kapsamındaki yükümlülükler üzerinden yapılmıştır. Çalışmada nitel ve nicel risk değerlendirme yöntemleri birlikte kullanılmıştır. İlk aşamada, HAZOP (Hazard and Operability) yönetimi ile nitel analiz, sonraki aşamalarda ise Hata Ağacı Analizi (Fault Tree Analysis – FTA) ve Olay Ağacı Analizi (Event Tree Analysis – ETA) yöntemleri ile nicel analizler yürütülmüştür. Bunlara ek olarak, Olay Ağacı Analizinde değerlendirilen alevlenir gazlar ve sıvıların kontrolsüz bir şekilde açığa çıktıklarında tutuşma olasılıklarını tahmin etmek üzere Tutuşma Olasılığı Hesaplama Modülü (CCPS'in Probability of Ignition Calculation Tool) kullanılmıştır. HAZOP çalışmasında, risk matrisine göre kırmızı bölgede ya da şiddetin 2 veya üzerindeki turuncu bölgelerde bulunan olaylar için büyük kaza senaryoları oluşturulmuştur. Hata Ağacı Analizinde, kritik olay olarak tanımlanan hataların kök nedenleri ve bu kök nedenlere bağlı olarak mevcut bariyerlere göre kritik olayın gerçekleşmesine dair frekans değeri bulunmuştur. Hesaplanmış olan bu frekans değeri, terminalde bulunan sınırlayıcı bariyerler ve tutuşma olası çıktıları ile Olay Ağacı Analizi çalışmalarında incelenmiştir. Olay Ağacı Analizinde, yangın, patlama ve yayılım olayları ile ramak kala olaylar kapsamında nihai frekans değerleri bulunmuştur. Yapılan çalışmalar sonucunda oluşturulan senaryolar için belirlenen büyük kaza frekans değerleri, Yönetmelik'teki eşik frekans değeri (≤10-4 /yıl) ile karşılaştırılmıştır. Risk değerlendirmesi sonunda eşik değerden daha düşük belirlenen frekans değerleri, terminalde alınan önlemlerin ve tüm bariyerlerin yeterli olduğunu göstermiş ve herhangi bir iyileştirme yapılmasına ihtiyaç olmadığı belirlenmiştir. Çalışmada sunulan metodolojinin, sanayi kuruluşlarına yol gösterici nitelikte olacağı söylenebilir.

Keywords

Risk Assessment
Fault Tree Analysis
Event Tree Analysis
HAZOP
Industrial Accidents

Abstract

In the study, risk assessment was aimed at an LPG storage terminal that stores the LPG product coming by ship and distributes it to customers by land tankers. The LPG stored in the terminal is within the scope of the Regulation on the Prevention of Major Industrial Accidents and Mitigation of the Effects published in the Official Gazette dated March 2, 2019 and numbered 30702, in terms of the type and amount of dangerous goods. The risk assessment studies performed were carried out over the obligations within the scope of this Regulation. In the study, qualitative and quantitative risk assessment methods were used together. In the first stage, qualitative analysis was carried out with HAZOP (Hazard and Operability), and in the next stages, quantitative analyzes were carried out with Fault Tree Analysis (FTA) and Event Tree Analysis (ETA) methods. Additionally, Ignition Probability Calculation Tool (CCPS's Probability of Ignition Calculation Tool) was used to estimate the ignition probabilities of flammable gases and liquids evaluated in Event Tree Analysis when they were released uncontrollably. In the HAZOP, major accident scenarios were created for events located in the red zone or orange zones of 2 or higher severity, according to the risk matrix. In the Fault Tree Analysis, the root causes of the faults defined as critical events and the frequency value for the realization of the critical event according to the existing barriers were found depending on these root causes. This calculated frequency value was examined in the Event Tree Analysis studies with the limiting barriers in the terminal and possible ignition outputs. In the Event Tree Analysis, final frequency values were found for fire, explosion and propagation events and near miss events. The major accident frequency values determined for the scenarios created as a result of the studies were compared with the threshold frequency value ($\leq 10^{-4}$ /year) in the Regulation. The frequency values determined lower than the threshold value at the end of the risk assessment showed that the precautions taken at the terminal and all barriers were sufficient and it was determined that no improvement was needed. It can be said that the methodology presented in the study will be a guide for industrial organizations.

*Sorumlu Yazar / Corresponding Author, e-mail: salihakilicarslan@gazi.edu.tr

Alıntı / Cite

Akdağ, B., & Çetinyokuş, S. (2021) LPG Stoklama Terminalinde Risk Değerlendirilmesi. *GU J Sci, Part A, 8*(4), 459-481.

Yazar Kimliği / Author ID (ORCID Number)

B. Akdağ, 0000-0002-4883-988X
S. Çetinyokuş, 0000-0001-9955-6428

Makale Süreci / Article Process

Başvuru Tarihi / Submission Date 06.10.2021
Revizyon Tarihi / Revision Date 15.11.2021
Kabul Tarihi / Accepted Date 08.12.2021
Yayım Tarihi / Published Date 10.12.2021

1. GİRİŞ

Son yıllarda endüstriyel üretimlerin artmasına bağlı olarak üretimlerde kullanılan kimyasal maddelerin miktarında da artış görülmektedir. Bu kimyasal maddeler birçok sektörde yer edinmiş olup, sektörlerden başlıcaları maden, enerji, inşaat, tarım olarak belirtilebilir. Kimyasal maddeler sahip oldukları özellikler bakımından bazı proseslerde özel dikkat gerektirmektedir. Bu prosesler, depolama, üretim, bertaraf ve taşıma gibi süreçleri kapsamaktadır. Proseslerde yaşanabilecek hatalar sonuçları ağır olan kazaların meydana gelmesine sebep olabilir. Bu nedenle, bu prosesleri içeren tesislerde/terminallerde bazı özel risk tabanlı çalışmalar yapılması gerekmektedir.

Kimyasalların niteliğine ve miktarına bağlı olarak yaşanabilecek kazalar, endüstriyel kaza sınıfında değerlendirilmekte olup, 2 Mart 2019 tarihli ve 30702 sayılı Resmî Gazete'de yayımlanan "Büyük Endüstriyel Kazaların Önlenmesi ve Etkilerinin Azaltılması Hakkında Yönetmelik" kapsamındadır (Resmî Gazete, 2019). Bu yönetmelikte, büyük endüstriyel kaza, herhangi bir kuruluşun işletilmesi esnasında, kontrolsüz gelişmelerden kaynaklanan ve kuruluş içinde veya dışında insan ve/veya çevre sağlığı için anında veya daha sonra ciddi tehlikeye yol açabilen bir veya birden fazla tehlikeli maddenin sebep olduğu büyük bir yayılım, yangın veya patlama olayını ifade etmektedir. Büyük endüstriyel kazaların önlenmesi ve etkilerinin azaltılmasına dair yapılan çalışmalar proses güvenliği çalışmaları olarak adlandırılmakta olup, bu çalışmalar tehlikeli madde içeren tesisler/terminaller için büyük önem arz etmektedir. Proses güvenliği, insana, çevreye ve ekipmana olan hasarın ileri seviye analizini gerektirmektedir. Bu analizler, nitel ve nicel analizler olmak üzere risk değerlendirme çalışmalarını oluşturmaktadır. Risk değerlendirme çalışmaları sonucunda elde edilen bulgulara göre prosesin durumu göz önüne alınarak herhangi bir iyileştirmenin ihtiyaç olup olmadığına karar verilebilmektedir.

Literatürde oldukça tehlikeli LPG (Liquefied Petroleum Gas/Sıvılaştırılmış Petrol Gazı) kimyasalını içeren tank ve boru hattı etrafında risk değerlendirme çalışmalarının yapıldığı görülmektedir. Sarvestani vd. (2021) tarafından LPG tankı geçmiş kazaları araştırılmış ve kazaları önlemek ve kontrol altına almak için çözümler sunulmuştur. Kazalar 23 hata ağacı analizi ile incelenmiştir. Kazaların %67'sinin en az bir kazazedeye sahip olduğu, kazaların %70'inde domino etkisi meydana geldiği belirtilmiştir. Riad vd. (2020) tarafından Cezayir'in en önemli rafinerisi olarak kabul edilen SKIKDA rafinerisinde LPG depolama tankları için D-HIGRAPH ve HAZOP (Hazard and Operability-Tehlike ve İşletilebilirlik) yöntemlerine dayalı bir çalışma yürütülmüştür. Özellikle eski olan bu tesiste güvenliği artırmak için çeşitli öneriler sunulmuş, tankın bir patlama senaryosunun termal etkisine ilişkin bazı sonuçlar paylaşılmıştır. Hosseini vd. (2020) tarafından bir gaz işleme tesisinde yangın riskini değerlendirmek için hata ağacı analizi (FTA-Fault Tree Analysis) ve olay ağacı analizi (ETA-Event Tree Analysis) geliştirilmiştir. Bulanık mantık ise uzmanların belirsiz görüşlerinden FTA'daki temel olayların olasılığını türetmek için kullanılmıştır. Önerilen metodolojide hesaplanan risk, karar vericilerin güvenlik önlemleri ve risk azaltma konusundaki yatırımlarının maliyetine yönelik de fayda sağlamıştır. Martins & Vianna (2020) tarafından, bir LPG küresel depolama tankı için vaka çalışması yapılmıştır. Termal radyasyonun etki yarıçapının belirlenmesi ve soğutulacak kürelerin seçiminde ALOHA (Areal Locations of Hazardous Atmospheres) yazılımı kullanılmıştır. Brezilya'da kabul edilen standartlar uluslararası standartlarla karşılaştırarak, Brezilya standartlarının yangın mühendisliğindeki ilerlemeleri değerlendirilmiştir. Akbar vd. (2019) tarafından hem kalitatif hem de kantitatif yöntemler bir arada kullanarak bir LPG terminali için risk değerlendirmesi yapılmıştır. İlk aşamada, HAZOP ile tehlikeler belirlenmiş, sonraki aşamada FTA ve ETA kullanarak riskin olasılığı hesaplanmıştır. Şiddet seviyesi ise amaçlanan senaryoların yangın modellemesi ile elde edilmiştir. Boult (2000) tarafından, Hong Kong'daki ulaşım faaliyetlerinde LPG'nin risk yönetimi gerçekleştirilmiş, riskleri en aza indirmek için öneriler sunulmuştur. Renjith vd. (2017) tarafından Hindistan'ın

güney kesiminde yer alan 238 km'lik LPG boru hattı için bulanık hata ağacı analizi (TDFFTA) yürütülmüştür. 36 temel olay tanımlanmış ve bu temel olayların hata frekansları, uzaman görüşü üzerinden bulanık mantık ile oluşturulmuştur. Akyuz & Çelik (2015) tarafından belirlenmiş görevler için insan hatası potansiyellerini sistematik olarak tahmin etmek ve LPG tanker gemilerinde gerekli güvenlik kontrol seviyelerini belirlemek için çalışmalar yürütülmüştür. LPG tanker gemilerinde kargo yükleme süreci ile birlikte insan güvenilirliğini değerlendirmek için CREAM (Bilişsel güvenilirlik ve hata analizi yöntemi) benimsemiştir. Sachan & Premi (2015) tarafından yürütülen çalışmada, LPG'nin depolanması ve taşınması sırasında tüm süreçler analiz edilmiş, çeşitli risk değerlendirme metodolojileri kullanılmıştır. Tüm bu analizler temelinde güvenlik önerilerinde bulunulmuştur. Spoelstra vd. (2015) tarafından LPG ve propan depolama alanları için güvenlik mesafelerinin nasıl elde edilebileceği açıklanmıştır. Güvenlik mesafeleri iki ulusal standart (PGS18 ve 19) üzerinden bir BLEVE (Boiling liquid expanding vapor explosion/kaynayan sıvı genleşen buhar bulutu patlaması) olasılığını azaltacak şekilde tanımlanmıştır. Güvenliği tanımlamak için kullanılan varsayımlar tartışılmış, ulusal standartların domino etkisi olasılığını kabul edilebilir bir düzeye indirebileceği belirtilmiştir. Tauseef vd. (2010) tarafından, LPG ve diğer basınçla sıvılaştırılmış gazlarla uğraşan büyük tesislerde BLEVE'nin tehlikelerine odaklanılmış ve BLEVE'lerin yapısı, mekanizması ve kontrol araçları tartışılmıştır. Shebeko vd. (2007) tarafından yürütülen çalışmada, büyük ölçekli petrol ihracat terminali için yangın ve patlama risk değerlendirmesi yapılmıştır. Potansiyel bireysel ve sosyal riskler hesaplanmıştır. Bireysel risk, belirli bir kişinin yangın ve patlama gibi tehlikeli faktörler tarafından yaralanma sıklığı olarak tanımlanmış, sosyal risk genellikle en az 10 kişinin yaralanması durumunda belirlenmiştir.

Farklı kimyasallar üzerinde risk değerlendirmesi yapılan çalışmalar da literatürde mevcuttur. Dinariyana vd. (2021) tarafından Doğu Java'daki petrol şirketlerinden birinde petrol rafinerisinin sosyal risk değerlendirmesi yapılmıştır. 200 mm delik çapı bulunan besleme stoku tankında jet yangını için kabul edilemez risk belirlenmiş, LOPA ile sistem arızası sıklığını 1.44E-03'ten 2.88E-06'ya değiştiren bir gaz dedektörü eklenerek risk kabul edilebilir bölgeye getirilmiştir. James & Renjith (2021) tarafından sıvılaştırılmış doğal gazın çevreye salınmasıyla sonuçlanabilecek arızaları belirlemek ve sıralamak için risk değerlendirmesi yapılmıştır. Sıvılaştırılmış doğal gaz depolama tesisinin yedi senaryosunun her bir Bağımsız Koruma Katmanının (IPL) güvenlik bütünlüğü seviye değerini bulmak için, bulanık risk matrisi ve koruma katmanı analizi (LOPA) entegresyonu yapılmıştır. HAZOP kullanılarak yedi senaryo belirlenmiş, güvenlik bütünlüğü seviyesi değeri Field Device Tool (FDT) yöntemiyle karşılaştırılmış ve risk azaltma faktörünü bulmak için risk grafiğinden yararlanılmıştır. Török vd. (2020) tarafından, bir kimya tesisi için Romanya arazi kullanım planlaması (LUP) kriterlerinin ve riske dayalı nicel yaklaşımın uygulandığı karşılaştırmalı bir vaka çalışması yapılmıştır. Klor ve propilen içeren kaza senaryoları, sonuç ve risk modelleme yazılımı ve CBS tekniği kullanılarak kapsamlı bir şekilde analiz edilmiştir. Çalışmanın karar vericiler için sahada daha sürdürülebilir ve güncel risk değerlendirme uygulamalarına yönelik bir referans çerçevesi olacağı belirtilmiştir.

Bu çalışmada, bir LPG stoklama terminaline dair gemiden ürün alım sırasında açığa çıkabilecek risklerin analizi yapılmış, operasyon esnasında oluşabilecek tüm tehlikeler nitel ve nicel olarak belirlenmiştir.

2. MATERYAL VE METOT

LPG tehlikeli kimyasalının depolandığı ve transferlerinin yapıldığı bir stoklama terminali için risk değerlendirme çalışması yürütülmüştür. LPG'nin bulunduğu sektör ve stoklama terminali enerji sektörü kapsamına girmektedir. Depolanan LPG kimyasalı ise ısınma, tüp dolumu ve araçlarda yakıt olarak kullanılmaktadır. LPG, sıvı halde, basınç altında ve ortam sıcaklığında depolanmaktadır. Yanıcı ve parlayıcı özelliğe sahiptir ve sudaki çözünürlüğü azdır. Renksiz ve kokusuz olan LPG, herhangi bir gaz kaçağının anlaşılabilmesi için merkaptanlar ve kükürt bileşenleriyle kokulandırılmaktadır. Ürünlerin tanka transferi esnasında boru hattına enjeksiyon yapılarak bu işlem yürütülmektedir. LPG ülkemizde, karışım LPG (%30 propan ve %70 bütan) ve propan (%95 ve üzeri saflıkta) olarak piyasaya sürülmektedir.

TOBB'un yayınlamış olduğu Türkiye Sıvılaştırılmış Petrol Gazı Meclisi Sektör Raporunda yer alan ifadeye göre (TOBB, 2012); 2010 yılında Avrupa Komisyonu, düşük karbonlu ve karbonsuz alternatif yakıt türlerinin kısa, orta ve uzun vadede daha fazla kullanılması için inisiyatif alınması çağrısında bulunmuştur. LPG karayolu yolcu ve yük taşımacılığı ile kısa mesafeli deniz taşımacılığında etkili bir alternatif yakıt olarak tanımlanmaktadır. Hali hazırda dünyada en fazla kullanılan alternatif yakıt olan LPG'nin, geleceğin ulaşım

yakıtları arasında, iklim değişikliği ile mücadele de dahil olmak üzere pek çok avantaj sunduğu dile getirilmiştir. Avrupa Komisyonu'nun hazırlattığı bu rapor, elektrik, hidrojen, metan, bio ve sentetik yakıtlar gibi LPG'nin de geleceğin yakıt alternatifleri içinde giderek daha önem kazanacağını vurgulamaktadır. Diğer alternatif yakıtların yüksek yatırım maliyetlerine kıyasla LPG'nin oto gaz olarak kullanımının, yeni ve büyük yatırımlar gerektirmemekte olduğu görülmektedir.

Analiz edilen LPG stoklama terminali, gemiden terminalde yer alan depolama tanklarına ürün alarak, depolama sonrası müşteri taleplerine göre kara tankerleri ile dağıtım yapmaktadır. Terminalde depolanan LPG kimyasalının endüstriyel kaza potansiyeli bulunmaktadır. Endüstriyel kaza riskleri, jet yangını, buhar bulutu patlaması, parlama yangını ve yayılım şeklinde sonuçlanabilmektedir. Tüm bu riskler dikkate alınarak terminal için herhangi bir kazaya sebep olabilecek durumlar belirlenmiş ve analiz edilmiş, çevreye, insana ve ekipmana zararı önlemek için risk değerlendirme çalışmaları yapılmıştır.

2.1. Risk Değerlendirmesi

2.1.1. Ön Hazırlık

Varsayımlar

Nitel ve nicel risk değerlendirmesi çalışmaları, Büyük Endüstriyel Kazaların Önlenmesi ve Etkilerinin Azaltılması Hakkında Yönetmelik (Resmî Gazete, 2019) kapsamında gerçekleştirilmiştir. Yönetmelik Madde 8'de yer alan "Büyük Kaza Senaryo Dokümanı" ve buna dair yayınlanmış olan Büyük Endüstriyel Kazalarla İlgili Hazırlanacak Büyük Kaza Senaryo Dokümanı Tebliği (Resmî Gazete, 2020) dikkate alınarak çalışmalar yapılmıştır. Çalışmaların yapıldığı yer örnek bir LPG stoklama terminalidir. Terminalde sadece mix (LPG) depolaması yapıldığı göz önünde bulundurulmuştur.

Sınırlar

Terminalde gemi ile LPG ürünü alınıp daha sonra kara tankerleriyle dağıtımı yapılmaktadır. Çalışmada, terminaldeki operasyonlar içerisinden gemiden T-001 nolu küre tanka mix (LPG) transferi değerlendirilmiştir. Tank ve boru hatları tehlikeli ekipmandır. Yalnızca operasyonel çalışmalar değerlendirilmiş olup harici tehlikeler (sel, deprem, toprak kayması, yıldırım, komşu kuruluştan kaynaklanabilecek tehlikeler) ve sabotaj bu çalışmanın kapsamına dahil edilmemiştir.

İş Yerinin Tanıtımı

Terminalin ana faaliyet konusu, LPG'nin gemilerden elleçlenerek depolama tanklarına alınması ve kara tankerlerine dolumunun yapılması olup tankerler aracılığı ile müşterilere gönderimi sağlanmaktadır. Terminalde her biri 3000 m^3 olan 4 adet LPG tankı bulunmaktadır. Tesise ait iş akış şeması Şekil 1'de sunulmuştur.

Tesiste gerçekleşen operasyonlar aşağıdaki gibidir:

Gemiden T-001 Nolu Küre Tanka Mix (LPG) Transferi,

Tanktan Tankere Mix (LPG) Transferi,

Küre Tanktan Küre Tanka Mix (LPG) Transferi

Tankerden T-001 Nolu Tanka Mix (LPG) Transferi (Kompresör ile)

Daha sonra tankerler aracılığı ile müşterilere ikmal yapılmaktadır.

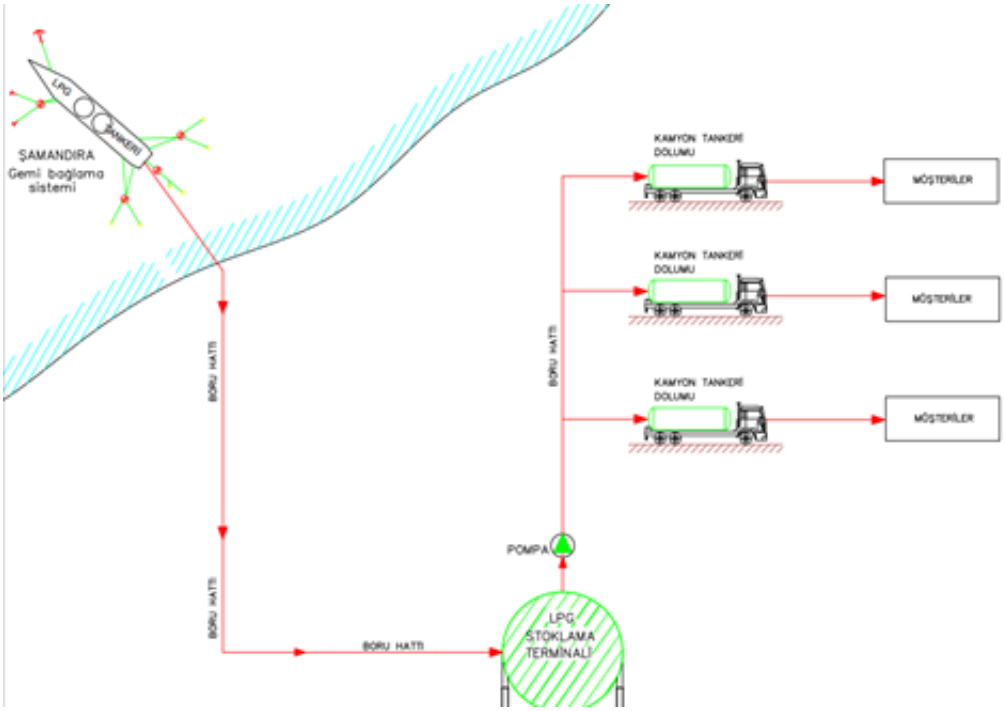

Şekil 1*. LPG Stoklama Terminali İş Akış Şeması*

Kullanılan İş Ekipmanları

Terminalde 4 adet her biri 3000 m^3 olan LPG depolama tankları bulunmaktadır. Buna ek olarak operasyonlar sırasında kullanılan iş ekipmanları aşağıda listelenmiştir:

- Transfer hatları (boru hatları)
- Ürün aktarımının sağlanması için 150 m^3/saat debiye sahip 3 adet pompa
- Transfer hatları üzerinde herhangi bir basıncın yaşanmasına bağlı olarak operasyonu güvenli hale getirmek amacıyla hatta biriken basıncı dışarı veren basınç tahliye vanaları
- Tanklardaki seviyeyi ölçmek için kullanılan her bir tanka sabitlenen seviye transmitteri
- Tanklardaki basıncı ölçmek için kullanılan her bir tanka sabitlenen basınç transmitteri
- Ürün transfer esnasında hatlarda yer alan motorlu ve manuel vanalar
- Operasyonların takip edilmesini sağlayan kontrol lojik ünite (PLC)

Kullanılan Kimyasallar

Terminalde yalnızca LPG depolaması yapılmakta olup acil durumlarda kullanılmak amacı ile terminalde bulunan jeneratörün çalıştırılması için az miktarda dizel yakıt da bulunmaktadır. LPG, Büyük Endüstriyel Kazaların Önlenmesi ve Etkilerinin Azaltılması Hakkında Yönetmelik Ek-1, Tablo 2/18'de yer almaktadır (Resmî Gazete, 2019).

Risk Değerlendirmesinin Amacı

Terminal için yapılan risk değerlendirmesi çalışmalarının amacı; Büyük Endüstriyel Kazaların Önlenmesi ve Etkilerinin Azaltılması Hakkında Yönetmelik (Resmî Gazete, 2019), Madde 9'da verilen büyük kaza frekans değerinin ($\leq 10^{-4}$/yıl) sağlanıp sağlanmadığının tespitidir. Risk değerlendirme çalışmaları sonucunda belirtilen frekans değeri, ilgili eşik değer ile karşılaştırılarak terminalde endüstriyel kazalara yönelik iyileştirme ihtiyacının olup olmadığına karar verilebilecek ve terminal güvenli hale getirilebilecektir.

Seçilen Risk Değerlendirme Yöntemleri

Çalışmada uygulanan risk değerlendirme yöntemleri sırasıyla aşağıda verilmiştir:

Belirlenen tehlikeli ekipmanlar için operasyon esnasında ortaya çıkabilecek dahili tehlikelere yönelik önce nitel çalışmalar yürütülmüş, HAZOP (Hazard and Operability) analizinden yararlanılmıştır.

Ardından Hata Ağacı Analizi (Fault Tree Analysis – FTA) ve Olay Ağacı Analizi (Event Tree Analysis – ETA) kullanılarak nicel analiz çalışmaları yapılmıştır.

Hata Ağacı Analizi'nin çözümlenmesinde "TOP Event FTA" yazılımı kullanılmıştır. Bu yazılımın kullanım amacı, karmaşık senaryolarda Minimal Kesit Seti ve İkili Karar Diyagramı kullanılarak ağacın çözümlenmesidir. Yazılımda tanımlanan hata ağacındaki tüm kök nedenlerin hata frekansı veya hata olasılığı verileri bulunarak kritik olayın frekansı hesaplanmıştır. Kritik olayı takip eden farklı büyük kaza senaryolarının frekans değerini hesaplamak için Olay Ağacı Analizi kullanılmıştır. Olay Ağacı Analizi'nin çözümlenmesinde ise "LOGAN" yazılımından yararlanılmıştır.

Kullanılan Veriler

HAZOP çalışması kapsamında; operasyon sırasında pompanın debisi, operasyon basıncı, tankın maksimum olabileceği kapasite ve basınç tahliye vanalarının açıldığı basınç gibi veriler terminalden sağlanmıştır. Ayrıca, CCPS (Center for Chemical Process Safety – AIChE) tarafından oluşturulan Tutuşma Olasılığı Hesaplama Modülü kullanılarak operasyon sırasında kullanılan kimyasalın tutuşma olasılıkları hesaplanmıştır (CCPS, 2014). Elde edilen değerler, Olay Ağacı Analizinde kullanılmıştır. Buna ek olarak, ekipmanların hatalarına dair olasılık ve frekans değerleri terminalden temin edilmiş, Hata Ağacı Analizi çalışmaları sırasında kullanılmıştır. Tesisteki ekipmanların bakım sıklığı yılda 1 olarak değerlendirilmiştir.

2.1.2. Uygulama

HAZOP Analizi

HAZOP, tesiste bulunan tehlikeli ekipmanlar üzerinden yapılmıştır. HAZOP, kalitatif bir teknik olup, tasarım, proses, prosedür veya sistemin her aşamasında, tasarım amacının veya işletme koşullarının nasıl sağlanamayacağını sorgulayan rehber kelimeleri temel alır (TSE, 2016). HAZOP, "tasarım" ve incelenecek proses, sistem veya prosedür özelliklerini ele alıp bunların her parçasını gözden geçirerek, ne tür performans sapmaları ve muhtemel sonuçları olabileceğini bulmaya çalışır. Bu da sistemin, prosesin veya prosedürün her bir parçasının proses parametrelerindeki değişime nasıl tepki vereceği, uygun rehber / yardımcı kelimelerin uygulanması ve sistematik olarak incelenmesi ile elde edilir. Yardımcı kelimeler belirli bir sistem, proses veya prosedüre uyarlanabilir ya da her türlü farklılaşmayı içerecek genel kelimeler kullanılabilir (TSE, 2010). HAZOP çalışması içerisinde her bir sapma için BS ISO/IEC 27005:2008 standardındaki matris (Tablo 1), kullanılarak nitel risk değerlendirme çalışması yapılmıştır. Matriste "F" harfi frekans kodlarını, "S" harfi ise şiddet kodlarını temsil etmektedir. Bu risk matrisi, 3 gruba ayrılmış tehlike kategorileri için (insana olan zarar, çevreye verilen zarar ve mala olan hasar) ayrı ayrı uygulanmıştır. Risk skoru belirlenirken frekans değeri ile şiddet değerinin kesişimleri kullanılmıştır. Risk matrisine göre kırmızı bölgede ya da şiddetin 2 veya üzerindeki turuncu bölgelerde bulunan olaylar için bir sonraki adım olan büyük kaza senaryolarının oluşturulması, analizi ve değerlendirilmesine geçilmiştir.

Tablo 1. *Risk Matrisi*

F4	**4**	**5**	**6**	**7**	**8**
F3	**3**	**4**	**5**	**6**	**7**
F2	**2**	**3**	**4**	**5**	**6**
F1	**1**	**2**	**3**	**4**	**5**
F0	**0**	**1**	**2**	**3**	**4**
	S0	**S1**	**S2**	**S3**	**S4**

F = Frekans Kodu S = Şiddet Kodu

Tablo 1'de yer alan frekans kodları, tehlike kategori kodları ve şiddet kodları aşağıda sunulmuştur.

Frekans Kodları:

[0] Olasılık o kadar düşük ki, ortaya çıkmayacağı varsayılabilir.

[1] Olasılık düşük olmasına rağmen sistemin hayatı boyunca ortaya çıkabilir.

[2] Sistemin hayatı boyunca birkaç kez ortaya çıkabilir.

[3] Sistemin hayatı boyunca defalarca ortaya çıkabilir.

[4] Sık sık meydana gelebilir.

Tehlike Kategori Kodları:

[1] Çalışanlara Olan Zarar

[2] Çevreye Verilen Zarar

[3] Ekipmana/Mala Olan Hasar

Şiddet Kodları:

[0] Önemsiz

[1] Küçük

[2] Ciddi

[3] Büyük

[4] Katastrofik

İlgili matris ve kodlar ile oluşturulan şiddet/tehlike kategorisi matrisi Tablo 2'de sunulmuştur.

Tablo 2. *Şiddet / Tehlike Kategori Matrisi*

	0 Önemsiz	**1 Küçük**	**2 Ciddi**	**3 Büyük**	**4 Katastrofik**
1 İnsana Olan Zarar	İnsana zarar vermez	Tesis içerisinde 1 kişinin hafif yaralanmasına sebep olur	Tesis içerisindeki 1 kişinin ölümü veya 6 kişinin yaralanması / Tesis dışındaki 1 kişinin yaralanması	Tesis içerisindeki tüm popülasyon kaybedilir	Bölgesel popülasyonu etkiler ve toplu ölümlere sebep olur
2 Çevreye Verilen Zarar	Çevreye zarar vermez	Karasal ve su habitata geçici ve geri dönülebilir etki	Tesis sınırları içerisinde karasal ve su habitata uzun süreli hasar	Tesis sınırları içerisinde karasal ve su habitata kalıcı hasar	Tesis sınırları dışına taşan karasal ve su habitata kalıcı hasar
3 Mala Olan Hasar	Mala hasar vermez	Tesisteki 5M TL / Tesis dışı 2M TL'den az hasar	Tesisteki 5M TL / Tesis dışı 2M TL hasar	Tesisteki 5M TL'den fazla hasar	Tesis dışı 2M TL'den fazla hasar

Tablo 2, Büyük Endüstriyel Kazaların Önlenmesi ve Etkilerinin Azaltılması Hakkında Yönetmelik Ek-6 Büyük Endüstriyel Kaza Bildirim Kriterleri'ne göre hazırlanmıştır (Resmî Gazete, 2019).

HAZOP analizinde kullanılan varsayımlar aşağıda sıralanmıştır:

- Proses ekipmanı, enstrümantasyon ve emniyet cihazlarındaki arızalar rastgele meydana gelir.
- Emniyet cihazlarının arıza oranları ve talep oranları düşük kabul edilir.
- Ekipmanı tamir etme veya bakım yapma süresi ihmal edilebilir olarak kabul edilir.
- Tesis, emniyetle ilgili iyi yönetim sistemi ve mühendislik standartlarına göre tasarlanmış, çalıştırılmış ve bakımı yapılmıştır.
- Bir arızayı tehlikeli yapan en önemli faktör, o arızanın farkında olunmamasıdır. Yani arızanın gizli olmasıdır.
- Bir alarma insan tepki süresi en az 2 dakika olarak kabul edilir. Bu nedenle operatöre 2 dakikadan daha az süre veren alarmlar etkin bariyer olarak dikkate alınmaz.
- Paralel işletilen özdeş sistemler için tek bir sistem analiz edilip bulgular diğer sistemlere de uygulanır.

Hata Ağacı Analizi

Hata ağacı analizi, belirli bir istenmeyen olaya ("kritik olay" olarak adlandırılır.) neden olan faktörleri tanımlamak ve analiz etmek için kullanılan bir tekniktir. Nedensel faktörler tümden gelimli olarak tanımlanır, mantıksal biçimde organize edilir ve mantıksal faktörler ve bunların kritik olayla mantıksal ilişkisi şekilsel olarak bir ağaç diyagramında sunulur. Hata ağacında tanımlanan faktörler; istenmeyen olaylara sebebiyet veren donanım bileşen hatası, insan hatası veya diğer alakalı olaylar ile ilişkilendirilmiş olaylar olabilir (TSE, 2016). Yönetmeliğin 9 uncu maddesinde yer alan büyük endüstriyel kaza frekansının sınır değeri ile karşılaştırma yapmaya elverişli sonuçlar üretilebilmesi için hata ağacındaki tüm kök nedenlerin hata frekansları veya hata olasılığı verileri bulunmuştur.

Olay Ağacı Analizi

Olay ağacı analizi, kritik olayı takip eden farklı kaza senaryolarının frekans değerini hesaplamak için kullanılmıştır. Hata ağacı analizinden farklı olarak olay ağacı analizinde tümevarım mantığı vardır. Bu analiz, nitel veya nicel olarak uygulanabilir, çalışmada nicel uygulama gerçekleştirilmiştir. Olay ağacı bir kritik olayın seçilmesi ile başlar. Daha sonra sonuçları en aza indirmek için mevcut bulunan fonksiyonlar ve sistemler sıra ile listelenir. Olay ağacı analizi, ikili sistem üzerinden yürümektedir. Her bir fonksiyon veya sistem için, bu fonksiyon veya sistemlerin başarısını ya da hatasını gösteren bir çizgi çizilir. Her çizgiye hatanın olasılığı atanır bu yolla kritik olaydan çıkan farklı sonuçlar değerlendirilebilir (TSE, 2010).

3. BULGULAR VE TARTIŞMA

3.1. HAZOP Analizi

Şiddet / Tehlike Kategori Matrisi ile Risk Matrisi temel alınarak LPG stoklama terminalinde yapılan HAZOP çalışması Tablo 3'te sunulmuştur.

HAZOP çalışma sonucu kırmızı bölgede ya da şiddetin 2 veya üzerindeki turuncu bölgelerde bulunan olaylar için büyük kaza senaryoları oluşturulmuştur. LPG stoklama terminali için oluşturulan senaryo listesi Tablo 4'te verilmiştir.

Tablo 3. *Terminal için Yapılan HAZOP Analizi*

NOD: 1

İNCELENEN TARİH: 21.12.2020

PARÇA: Gemiden T-001 Nolu Küre Tanka LPG Transferi

LPG; gemiden T-001 nolu tanka, gemi pompası kullanılarak T-001 nolu tankın seviyesi %85'e ulaşana dek 200 ton/saat akış hızında, 8 barg basınçta ve ortam sıcaklığında transfer edilmektedir.

ÇİZİMLER VE DOKÜMANLAR

LPG STOKLAMA TERMİNALİ P&ID 202301-1

LPG STOKLAMA TERMİNALİ P&ID 202301-2

LPG STOKLAMA TERMİNALİ P&ID 202301-3

LPG STOKLAMA TERMİNALİ P&ID 202301-4

NO	SAPMA	NEDEN	SONUÇ	BARİYER	EYLEMLER
1	BASINÇ FAZLA	Hidrolik güç ünitesi (HGÜ) sisteminde yer alan hatlarda kaçak olması	Hidrolik vananın kapanması sonucu hatta basıncın artması ile hat üzerinde bulunan basınç tahliye vanalarından atmosfere LPG salınımı ve tutuşturucu kaynak varlığında parlama / patlama meydana gelmesi Frek: [4] Ktgr: [1] [2] [3] Şiddt: [2] [1] [2] Risk: [6] [5] [6]	1- Hidrolik güç ünitesinde yer alan basınç transmitterinden alınan düşük basınç verisi ile operatör sisteminin kontrolünü yapar ve gerekli durumda gemiye haber vererek operasyonun durmasını sağlar. 2- Hidrolik güç ünitesinde yer alan manuel pompa basınç sivicinden alınan veri ile operatör tarafından devreye alınır.	Nicel risk analizi çalışmalarında değerlendirilmiş olup detaylar FTA 01 / ETA 01'de yer almaktadır.
2	BASINÇ FAZLA	Motorlu kelebek vananın talep anında açılmaması	Motorlu kelebek vananın kapalı kalması sonucu hatta basıncın artması ile hat üzerinde bulunan basınç tahliye vanalarından atmosfere LPG salınımı ve tutuşturucu kaynak varlığında parlama / patlama meydana gelmesi Frek: [4] Ktgr: [1] [2] [3] Şiddt: [2] [1] [2] Risk: [6] [5] [6]	Seviye transmitteri verisi ile seviyenin artmadığı sistemden (kontrol lojik ünite) operatör tarafından gözlemlenir, gemi ile iletişime geçilerek operasyon durdurulur.	Nicel risk analizi çalışmalarında değerlendirilmiş olup detaylar FTA 01 / ETA 01'de yer almaktadır.
3	BASINÇ FAZLA	Frekans konventörü hatası sonucu gemi pompasının yüksek debide çalışması	Hatta basınç artışı yaşanması Frek: [4] Ktgr: [1] [2] [3] Şiddt: [0] [0] [0] Risk: [4] [4] [4]	Sayaç sisteminde yer akış transmitteri verisi ile akış hızı kontrol edilir. Gerekli durumda operatör gemi ile iletişime geçerek operasyonu durdurur.	Risk skoru göz önüne alındığında kabul edilebilir seviyede olması nedeniyle nicel risk değerlendirme çalışmalarında değerlendirilmemiştir.
4	BASINÇ FAZLA	Operatör hatası nedeniyle hat üzerinde bulunan manuel vananın kapalı olması	Hatta basıncın artması ile hat üzerinde bulunan basınç tahliye vanalarından atmosfere LPG salınımı ve tutuşturucu kaynak varlığında parlama / patlama meydana gelmesi Frek: [4] Ktgr: [1] [2] [3] Şiddt: [2] [1] [2] Risk: [6] [5] [6]		Nicel risk analizi çalışmalarında değerlendirilmiş olup detaylar FTA 01 / ETA 01'de yer almaktadır.
5	BASINÇ FAZLA	Deniz altındaki boru hattının dış kaynaklı sebeplerle ezilerek boru çapında daralma meydana gelmesi	Ezilme öncesi hatta basıncın artması ile boru hattının zayıf noktasından denize LPG sızıntısı ve tutuşturucu kaynak varlığında parlama / patlama meydana gelmesi Frek: [4] Ktgr: [1] [2] [3] Şiddt: [2] [1] [2] Risk: [6] [5] [6]	1- Seviye transmitteri verisi ile seviyenin artmadığı sistemden (kontrol lojik ünite) operatör tarafından gözlemlenir, gemi ile iletişime geçilerek operasyon durdurulur. 2- Sayaç sisteminde yer akış transmitteri verisi ile akış hızı kontrol edilir. Gerekli durumda operatör gemi ile iletişime geçerek operasyonu durdurur.	Nicel risk analizi çalışmalarında değerlendirilmiş olup detaylar FTA 02 / ETA 02'de yer almaktadır.
6	BASINÇ FAZLA	Bakım / test esnasında boru hattında yabancı bir parçanın unutulması veya gemi kaynaklı yabancı maddenin hatta girmesi	Hatta basınç artışı yaşanması Frek: [4] Ktgr: [1] [2] [3] Şiddt: [0] [0] [0] Risk: [4] [4] [4]		Risk skoru göz önüne alındığında kabul edilebilir seviyede olması nedeniyle nicel risk değerlendirme çalışmalarında değerlendirilmemiştir.

Tablo 3. *(Devam ediyor)*

7	BASINÇ FAZLA	Operatör hatası nedeniyle gemi pompasının çıkışında yer alan by-pass vanasının yanlış ayarlanması ile yüksek debide hatta ürün verilmesi	Hatta basınç artışı yaşanması Frek: [4] Ktgr: [1] [2] [3] Şiddt: [0] [0] [0] Risk: [4] [4] [4]	Sayaç sisteminde yer akış transmitteri verisi ile akış hızı kontrol edilir. Gerekli durumda operatör gemi ile iletişime geçerek operasyonu durdurur.	Risk skoru göz önüne alındığında kabul edilebilir seviyede olması nedeniyle nicel risk değerlendirme çalışmalarında değerlendirilmemiştir.
8	BASINÇ AZ	Gemi pompasının düşük debide çalışması	İşletilebilirlik problemi yaratması Frek: [4] Ktgr: [1] [2] [3] Şiddt: [0] [0] [0] Risk: [4] [4] [4]		Risk skoru göz önüne alındığında kabul edilebilir seviyede olması nedeniyle nicel risk değerlendirme çalışmalarında değerlendirilmemiştir.
9	BASINÇ AZ	Deniz altındaki boru hattının dış kaynaklı sebeplerle ezilerek boru çapında daralma olması	Operasyon süresinin uzaması ile işletilebilirlik problemi yaratması Frek: [4] Ktgr: [1] [2] [3] Şiddt: [0] [0] [0] Risk: [4] [4] [4]	Sayaç sisteminde yer akış transmitteri verisi ile akış hızı kontrol edilir. Gerekli durumda operatör gemi ile iletişime geçerek operasyonu durdurur.	Risk skoru göz önüne alındığında kabul edilebilir seviyede olması nedeniyle nicel risk değerlendirme çalışmalarında değerlendirilmemiştir.
10	SEVİYE FAZLA	İnsan hatası sonucu yanlış hesaplama yapılması ve LPG tankına fazla ürün transferi	Tank seviyesinin yükselmesi ile tankta yer alan basınç tahliye vanalarından atmosfere gaz fazda LPG'nin salınımı ve tutuşturucu kaynak varlığında parlama / patlama meydana gelmesi Frek: [3] Ktgr: [1] [2] [3] Şiddt: [2] [1] [2] Risk: [5] [4] [5]	1-Gemi manifold basıncının yükselmesi sebebiyle operatör müdahalede bulunur. 2- Seviye transmitteri verisi ile seviyenin yükseldiği sisteminden (kontrol lojik ünite) operatör tarafından gözlemlenir, gemi ile iletişime geçilerek operasyon durdurulur. 3- Seviye transmitteri verisi ile seviyenin yükseldiği sisteminden (kontrol lojik ünite) gemi operatör tarafından gözlemlenir, operasyon durdurulur. 4- Seviye transmitteri verisi ile seviyenin yükseldiği sisteminden (kontrol lojik ünite) güvenlik tarafından gözlemlenir, gemi ile iletişime geçilerek operasyon durdurulur. 5- Seviye transmitteri verisi ile dolum yapılan tankın motorlu vanası kapanır ve diğer tankın motorlu vanasını açılır.	Nicel risk analizi çalışmalarında değerlendirilmiş olup detaylar FTA 03 / ETA 03'te yer almaktadır.
11	SEVİYE AZ	İnsan hatası sonucu yanlış hesaplama yapılması ve LPG tankına az ürün transferi	İşletilebilirlik problemi yaratması Frek: [4] Ktgr: [1] [2] [3] Şiddt: [0] [0] [0] Risk: [4] [4] [4]		Risk skoru göz önüne alındığında kabul edilebilir seviyede olması nedeniyle nicel risk değerlendirme çalışmalarında değerlendirilmemiştir.
12	AKIŞ YOK	Gemi pompasının çalışmaması	İşletilebilirlik problemi yaratması Frek: [4] Ktgr: [1] [2] [3] Şiddt: [0] [0] [0] Risk: [4] [4] [4]		Risk skoru göz önüne alındığında kabul edilebilir seviyede olması nedeniyle nicel risk değerlendirme çalışmalarında değerlendirilmemiştir.
13	AKIŞ YOK	Operatör hatası nedeniyle hat üzerinde bulunan manuel vananın kapalı olması	Hatta basıncın artması ile hat üzerinde bulunan basınç tahliye vanalarından atmosfere LPG salınımı ve tutuşturucu kaynak varlığında parlama / patlama meydana gelmesi Frek: [4] Ktgr: [1] [2] [3] Şiddt: [2] [1] [2] Risk: [6] [5] [6]		Nicel risk analizi çalışmalarında değerlendirilmiş olup detaylar FTA 01 / ETA 01'de yer almaktadır.
14	AKIŞ YOK	Bakım / test esnasında boru hattında yabancı bir parçanın unutulması veya gemi kaynaklı yabancı maddenin hatta girmesi	Hatta basınç artışı yaşanması Frek: [4] Ktgr: [1] [2] [3] Şiddt: [0] [0] [0] Risk: [4] [4] [4]		Risk skoru göz önüne alındığında kabul edilebilir seviyede olması nedeniyle nicel risk değerlendirme çalışmalarında değerlendirilmemiştir.

Tablo 3. *(Devam ediyor)*

15	AKIŞ YOK	Motorlu kelebek vananın talep anında açılmaması	Motorlu kelebek vananın kapalı kalması sonucu hatta basıncın artması ile hat üzerinde bulunan basınç tahliye vanalarından atmosfere LPG salınımı ve tutuşturucu kaynak varlığında parlama / patlama meydana gelmesi	Seviye transmitteri verisi ile seviyenin artmadığı sistemden (kontrol lojik ünite) operatör tarafından gözlemlenir, gemi ile iletişime geçilerek operasyon durdurulur.	Nicel risk analizi çalışmalarında değerlendirilmiş olup detaylar FTA 01 / ETA 01'de yer almaktadır.
16	AKIŞ FAZLA	Frekans konventörü hatası sonucu gemi pompasının yüksek debide çalışması	Hatta basınç artışı yaşanması Frek: [4] Ktgr: [1] [2] [3] Şiddt: [0] [0] [0] Risk: [4] [4] [4]	Sayaç sisteminde yer akış transmitteri verisi ile akış hızı kontrol edilir. Gerekli durumda operatör gemi ile iletişime geçerek operasyonu durdurur.	

Tablo 4. *LPG Stoklama Terminali Senaryo Listesi*

Senaryo Kodu	**Kritik Olay**
FTA-ETA 01	Gemiden Tanka Transferde Hat Üzerinde Bulunan Basınç Tahliye Vanalarından LPG Salınımı
FTA-ETA 02	Deniz Altındaki Borunun Dış Kaynaklı Sebeplerle Ezilmesi Nedeniyle Boru Çapında Daralma Olması Sonucu Boru Hattının Zayıf Noktasından LPG Salınımı
FTA-ETA 03	İnsan Hatası Sonucu Yanlış Hesaplama Yapılması ve LPG Tankına Fazla Ürün Transferi Sonucu Tank Seviyesinin Yükselmesi ile Tankta Yer Alan Basınç Tahliye Vanalarından Atmosfere Gaz Fazda LPG Salınımı
Sınırlayıcı Bariyer (ETA'da SB olarak gösterilmiştir.)	Gaz dedektörünün devreye girmesi ile operatörün operasyonu durdurması

Terminal için toplam 4 kritik olay tanımlanmıştır.

3.2. Hata Ağacı Analizi

Hata ağacı analizinde kullanılmak üzere terminaldeki ekipmanların hata frekansları ve yılda yapılan bakım sıklığı değerleri Tablo 5'te sunulmuştur.

Tablo 5. *Ekipmanlara ait Hata Frekansları ve Bakım Sıklıkları*

Senaryo Kodu	**Ekipman Adı**	**Hata Frekansı (/Saat)**	**Hata Frekansı (/Yıl)**	**Yılda Yapılan Bakım Sıklığı (/Yıl)**
FTA-01	Hidrolik Güç Ünitesinde Yer Alan Basınç Transmitteri	3.000E-07	2.628E-03	1
	Analog Giriş Modül (Hatası)	2.500E-07	2.190E-03	1
	Analog Giriş Kanal (Hatası)	4.000E-08	3.504E-04	1
	Ana İşlemci (Hatası)	2.000E-06	1.752E-02	1
	HGÜ'de Yer Alan Basınç Anahtarı / Switch	2.000E-06	1.752E-02	1
	Röle	2.000E-07	1.752E-03	1
	HGÜ'de Yer Alan Pompa (Akım Kesici Hatası)	3.000E-07	2.628E-03	1
	Motorlu Kelebek Vana (Açılmaması)	1.000E-07	8.760E-04	1
	Seviye Transmitteri	6.000E-07	5.256E-03	1

Tablo 5. *(Devam ediyor)*

Senaryo Kodu	Ekipman Adı	Hata Frekansı (/Saat)	Hata Frekansı (/Yıl)	Yılda Yapılan Bakım Sıklığı (/Yıl)
FTA-02	Seviye Transmitteri	6.000E-07	5.256E-03	1
	Analog Giriş Modül (Hatası)	2.500E-07	2.190E-03	1
	Analog Giriş Kanal (Hatası)	4.000E-08	3.504E-04	1
	Ana İşlemci (Hatası)	2.000E-06	1.752E-02	1
	Akış Transmitteri (Hatası)	6.000E-07	5.256E-03	1
FTA-03	Seviye Transmitteri	6.000E-07	5.256E-03	1
	Analog Giriş Modül (Hatası)	2.500E-07	2.190E-03	1
	Analog Giriş Kanal (Hatası)	4.000E-08	3.504E-04	1
	Ana İşlemci (Hatası)	2.000E-06	1.752E-02	1
	Motorlu Vana (Kapanmaması)	5.000E-07	4.380E-03	1
	Motorlu Vana (Açılmaması)	1.000E-07	8.760E-04	1
Sınırlayıcı Bariyer (Gaz Dedektörü)	Gaz Dedektörü Hatası	2.200E-06	1.927E-02	12
	Analog Giriş Modül (Hatası)	2.500E-07	2.190E-03	12
	Analog Giriş Kanal (Hatası)	4.000E-08	3.504E-04	12
	Ana İşlemci (Hatası)	2.000E-06	1.752E-02	12

Sınırlayıcı bariyer dışında bakım sıklığını terminalde yılda 1 olduğu görülmektedir. Her bir senaryo özelinde gerçekleştirilen hata ağacı analizi sırasıyla Şekil 2-5'te verilmiştir.

Şekil 5'ten en yüksek frekans değeri tankta yer alan basınç tahliye vanalarından LPG'nin gaz fazında salınımı kritik olayı için belirlenmiştir.

3.3. Olay Ağacı Analizi

Terminal için oluşturulan senaryolar için Olay Ağacı Analizleri ise Şekil 6-8'de sunulmuştur.

Şekil 7'den boru hattının zayıf noktasından LPG salınımı kritik olayı (ETA/02) ile başlayıp, toksik yayılım ile sonuçlanan senaryo en yüksek frekans değerinde bulunmuştur. Herhangi bir yangın, patlama veya toksik yayılım sonucu vermeyen ramak kala olayların frekans değeri dikkat çekicidir.

Olay ağacı analizinde değerlendirilen alevlenir gazlar ve sıvıların kontrolsüz bir şekilde açığa çıktıklarında tutuşma olasılıklarını tahmin etmek üzere ileri analiz teknikleri kullanılarak hesaplamalar yapılır. Bu hesaplamalar yapılırken Tutuşma Olasılığı Hesaplama Modülü (CCPS'in Probabability of Ignition Calculation Tool) kullanılır. Olay Ağacı Analizi'nde kullanılan olasılıklar aşağıdaki şekilde tanımlanır:

- Ani Tutuşma Olasılığı (Probability of Immediate Ignition – POII),
- Gecikmeli Tutuşma Olasılığı (Probability of Delayed Ignition – PODI),
- Gecikmeli Tutuşma Sırasında Patlama Olasılığı (Probability of Explosion Given Delayed İgnition – POEGDI)

Tutuşma olasılıklarını tahmin etmek için modül içerisindeki ayrıntılı sonuç veren Seviye 3 (İleri) Analiz algoritması kullanılmıştır. Analizde öncelikle, değerlendirilecek olan alevlenir sıvı ya da gaz hesaplama modülünün kütüphanesinde yer almıyor ise bu maddelere ait kimyasal özellikler (kaynama noktası, parlama

noktası, minimum tutuşma enerjisi, kendiliğinden tutuşma sıcaklığı ve reaktivite) modül kütüphanesine eklenmiştir. Sonraki adımda senaryo ile ilişkili sızıntı koşullarına dair proses sıcaklığı, proses basıncı, sızıntı çapı ve sızıntı süresi bilgileri modüle girilmiştir. Bu verilerin girilmesi ile sızıntı ile ilgili veriler oluşturulmuştur. Bir sonraki adımda, tutuşturucu kaynak verileri modül içerisine girilmiştir. Açığa çıkan kimyasalın oluşturacağı olay ortamda bulunan tutuşturucu kaynak varlığına göre belirlenmiştir. Ortamda bulunan tutuşturucu kaynaklar; noktasal, hatsal ya da alansal kaynak olarak modülde tanımlıdır. Bu kaynak tiplerinden ortamda mevcut olanlar modül içerisine girilmiştir. Açık ortamlarda son olarak tutuşturucu kaynak kontrolüne ilişkin, kuruluşun aldığı önlemlere (kıvılcım çıkarmayan ekipman, anti statik kıyafet gibi) göre modül içerisinde tanımlanan tutuşturucu kaynak kontrolü (zayıf, orta, iyi) verisi girilmiştir. Kapalı ortamlarda ise havalandırma sistemine dair veriler modül içerisine eklenmiştir. Tüm verilerin girilmesi ile sonuç olasılıkları modül tarafından hesaplanmıştır. ETA-01 için POII-PODI hesaplamaları ekran görüntüleri Şekil 9'da sunulmuştur.

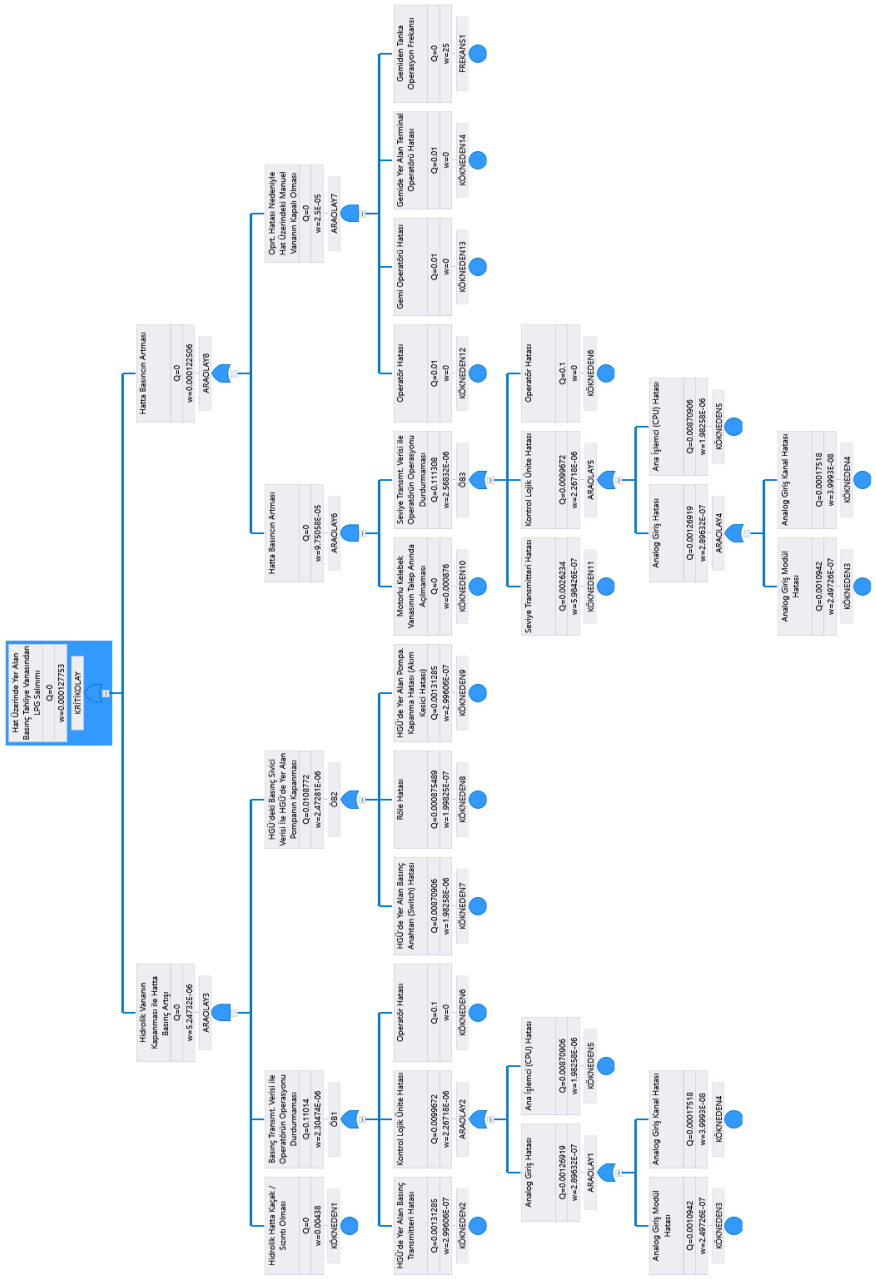

Q: olasılık, w: frekans

Şekil 2. *FTA-01 Hata Ağacı Analizi*

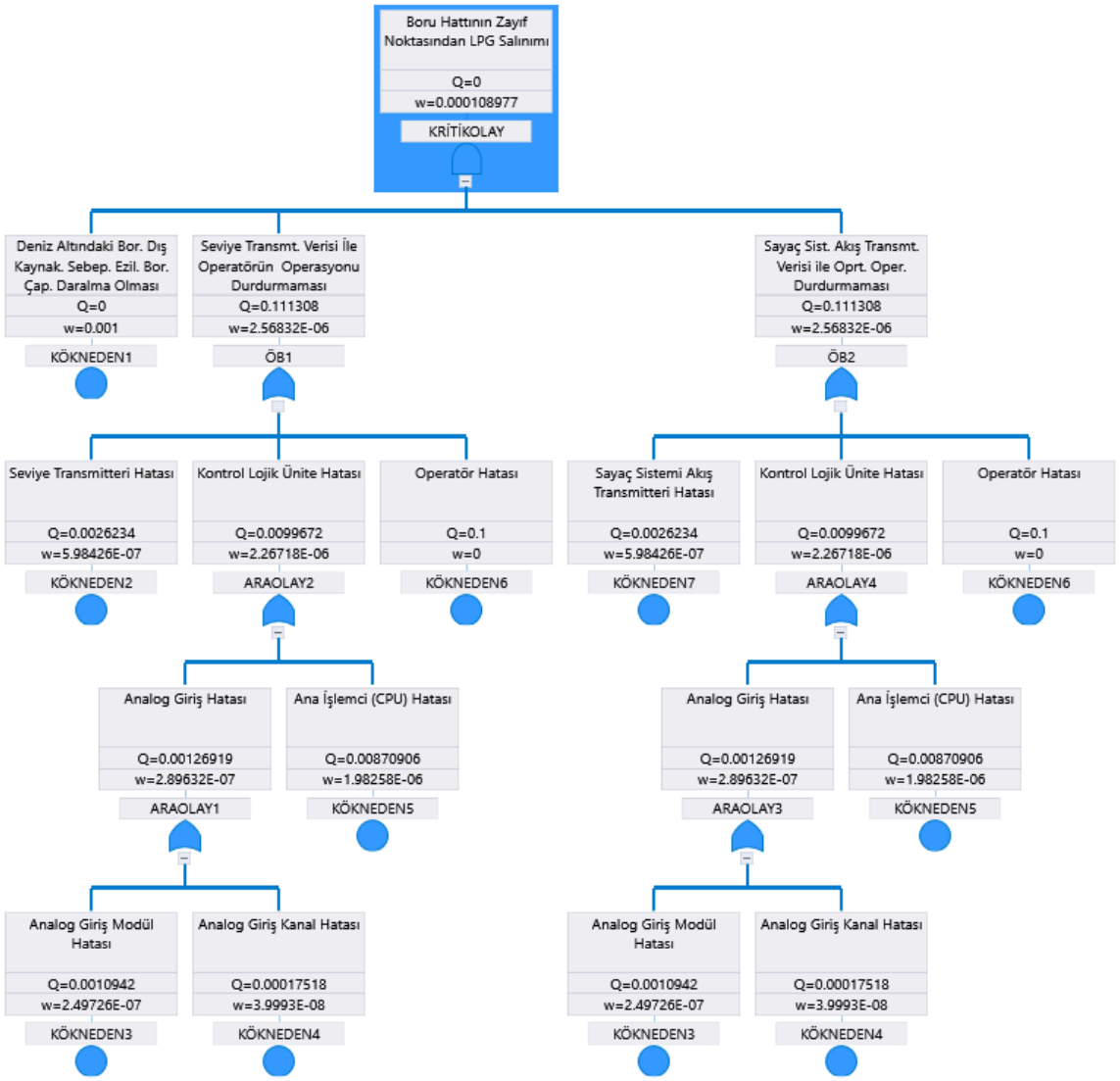

Q: olasılık, w: frekans

Şekil 3. *FTA-02 Hata Ağacı Analizi*

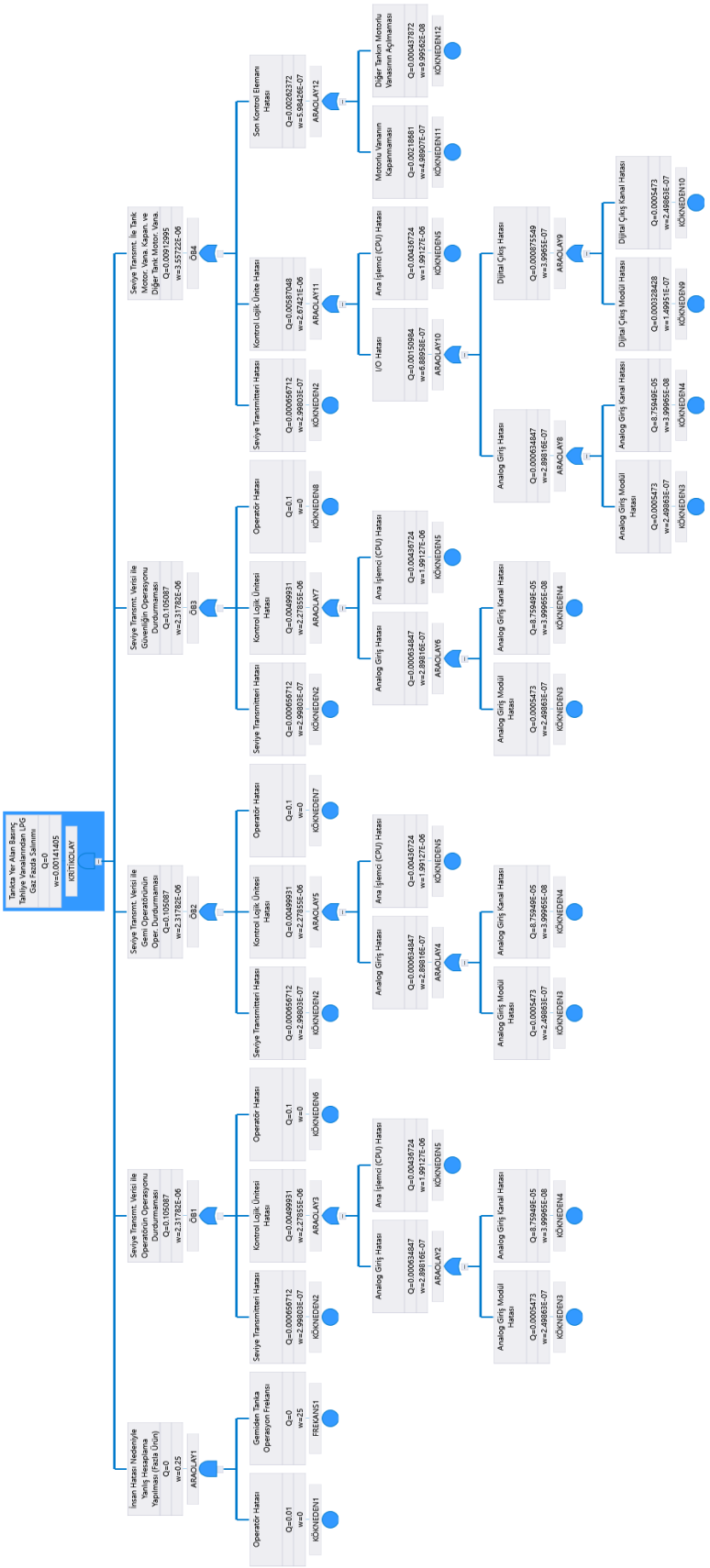

Q: olasılık, w: frekans

Şekil 4. *FTA-03 Hata Ağacı Analizi*

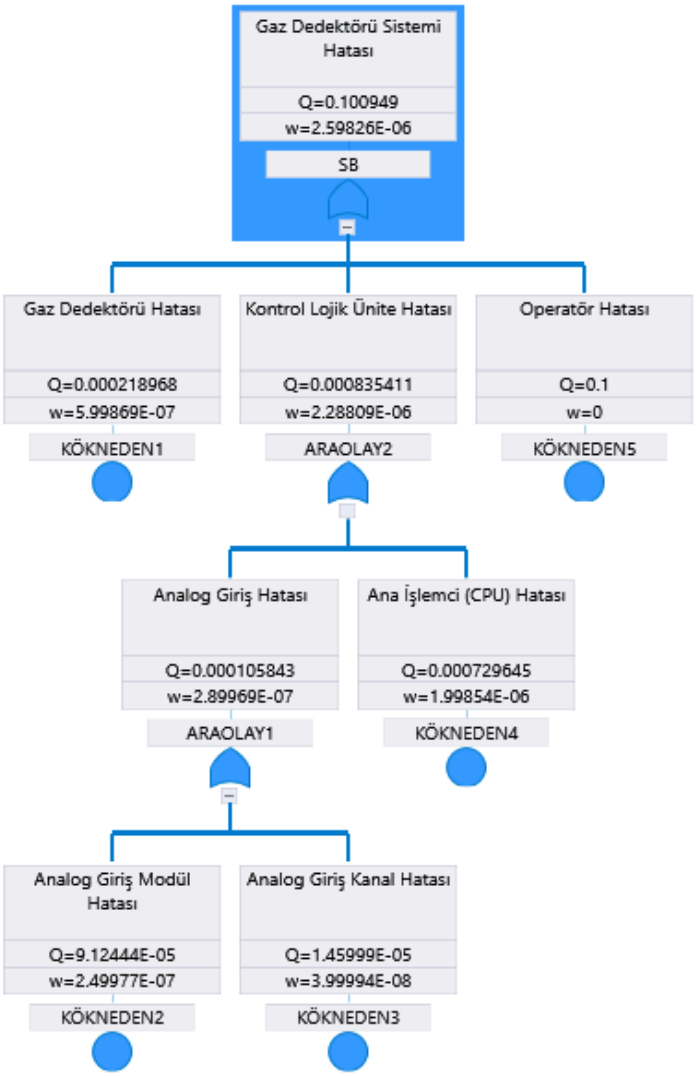

Q: olasılık, w: frekans

Şekil 5. *FTA-04 Hata Ağacı Analizi*

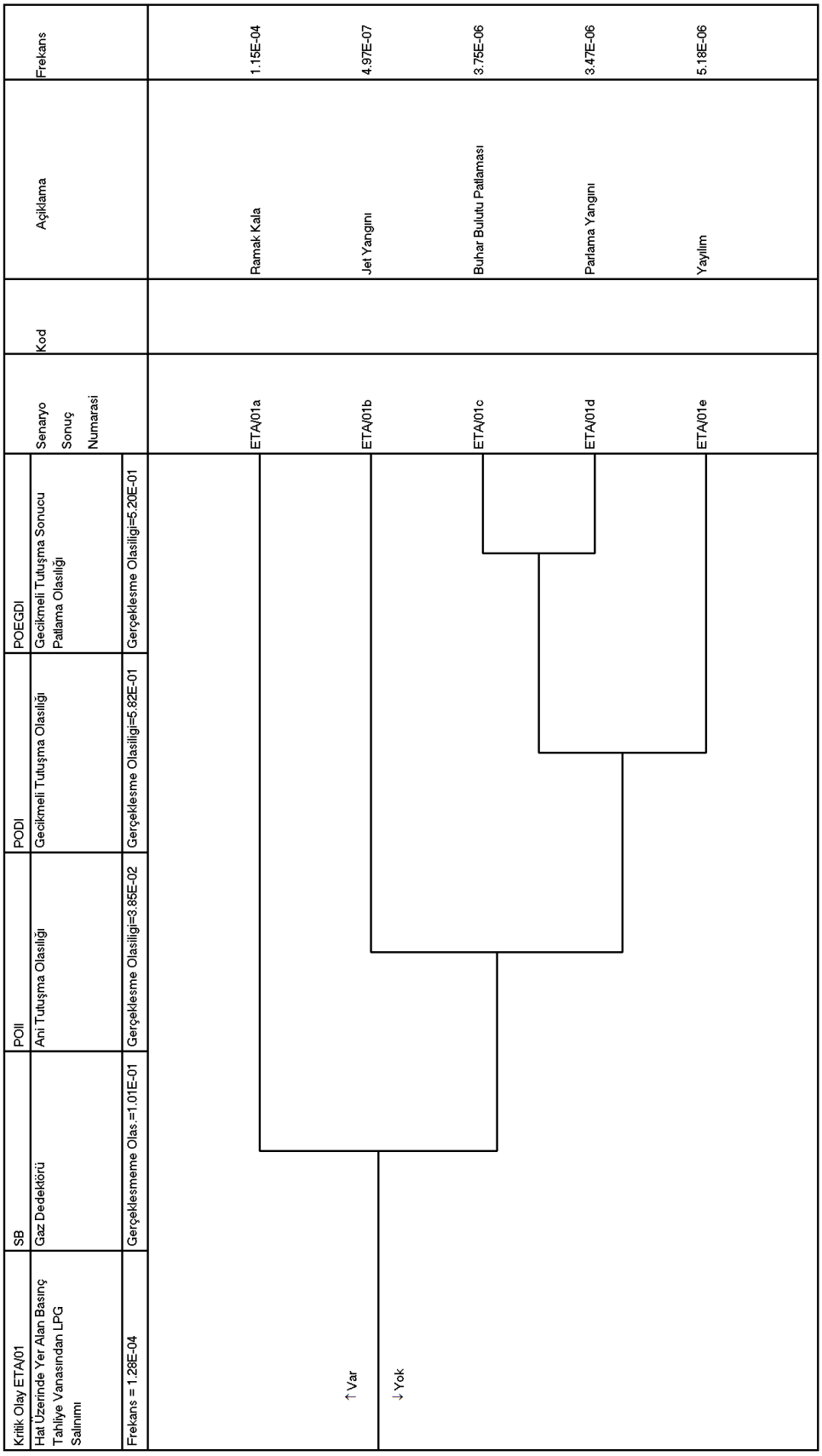

Şekil 6. *ETA-01 Olay Ağacı Analizi*

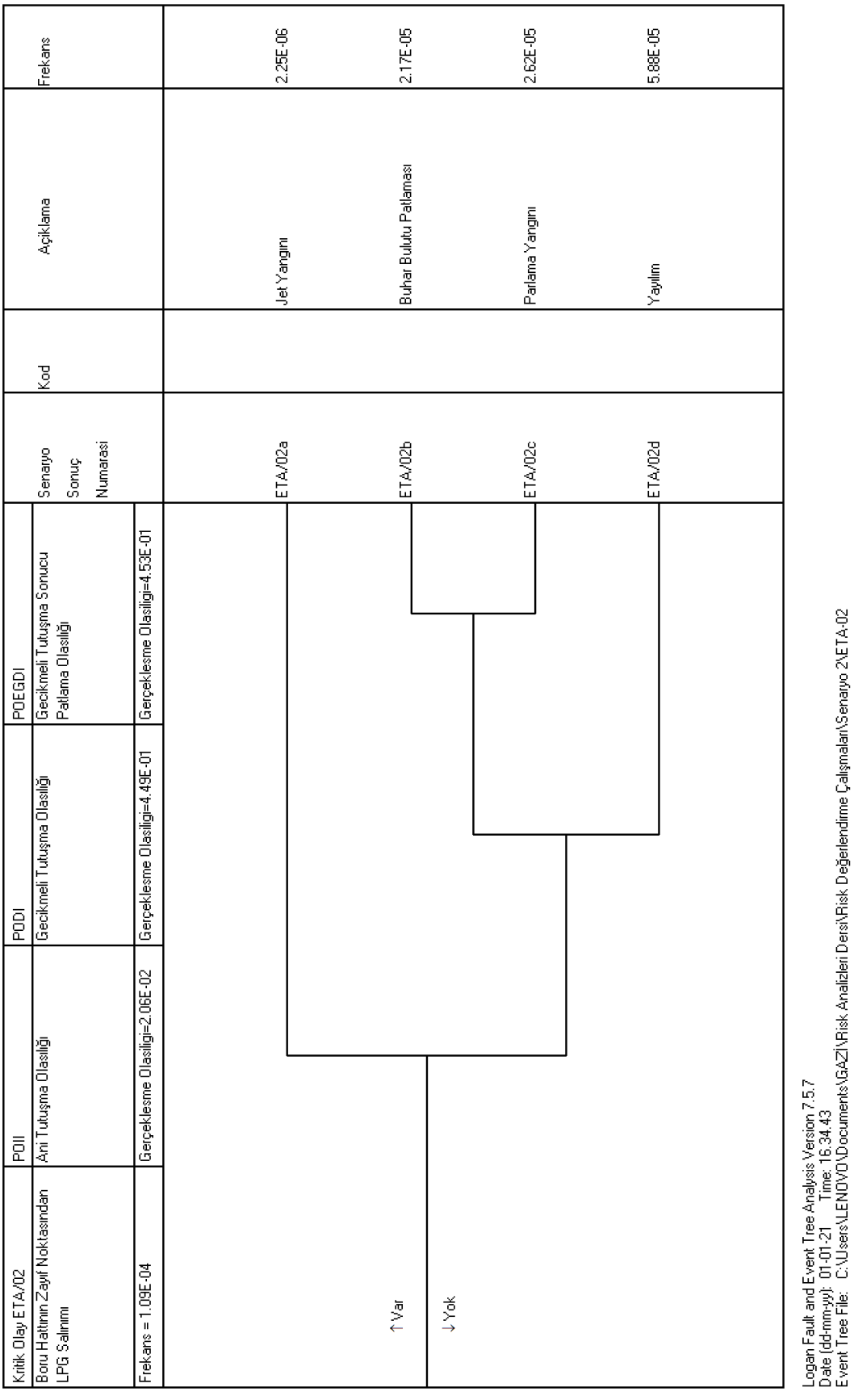

Şekil 7. *ETA-02 Olay Ağacı Analizi*

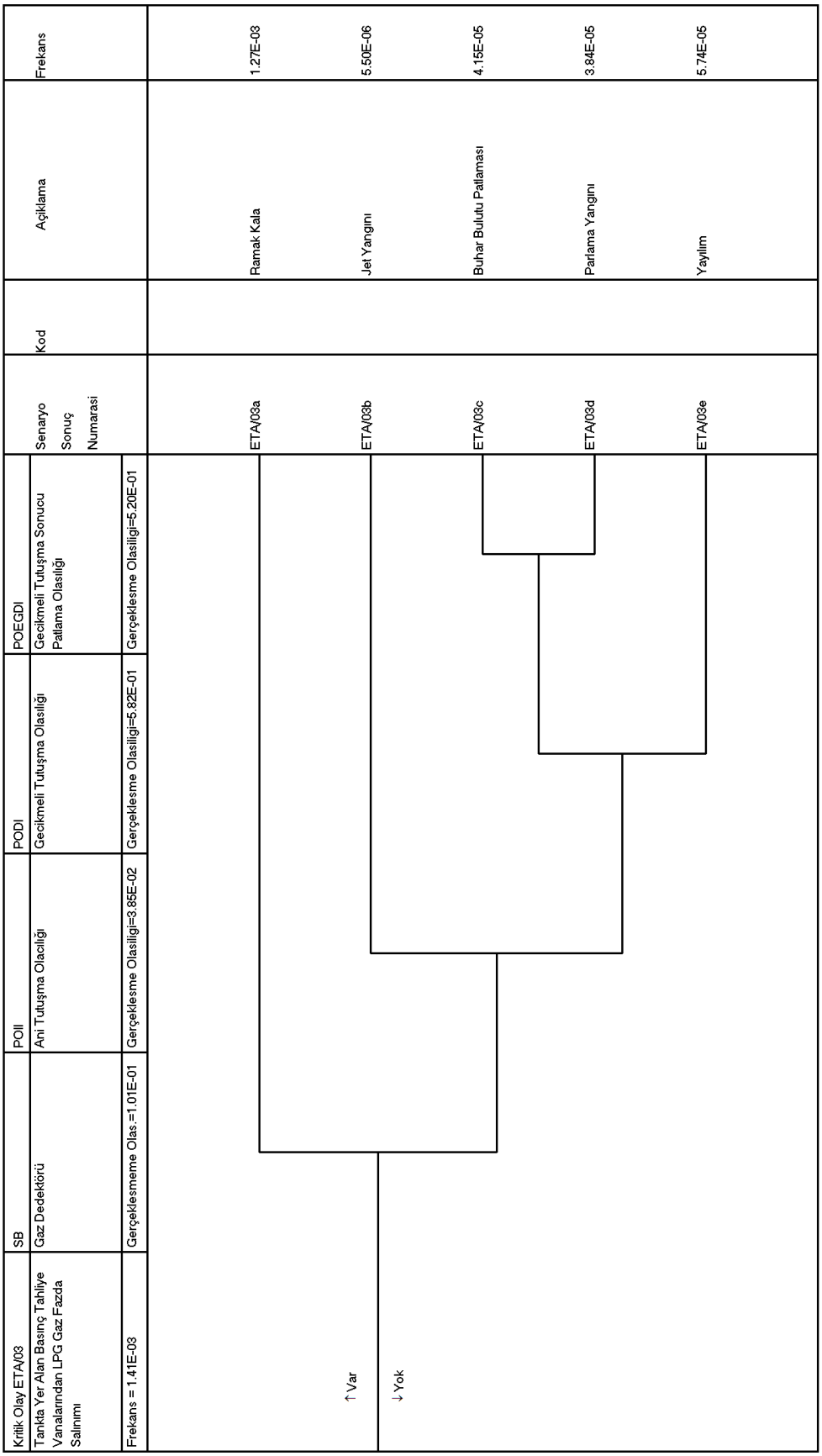

Şekil 8. *ETA-03 Olay Ağacı Analizi*

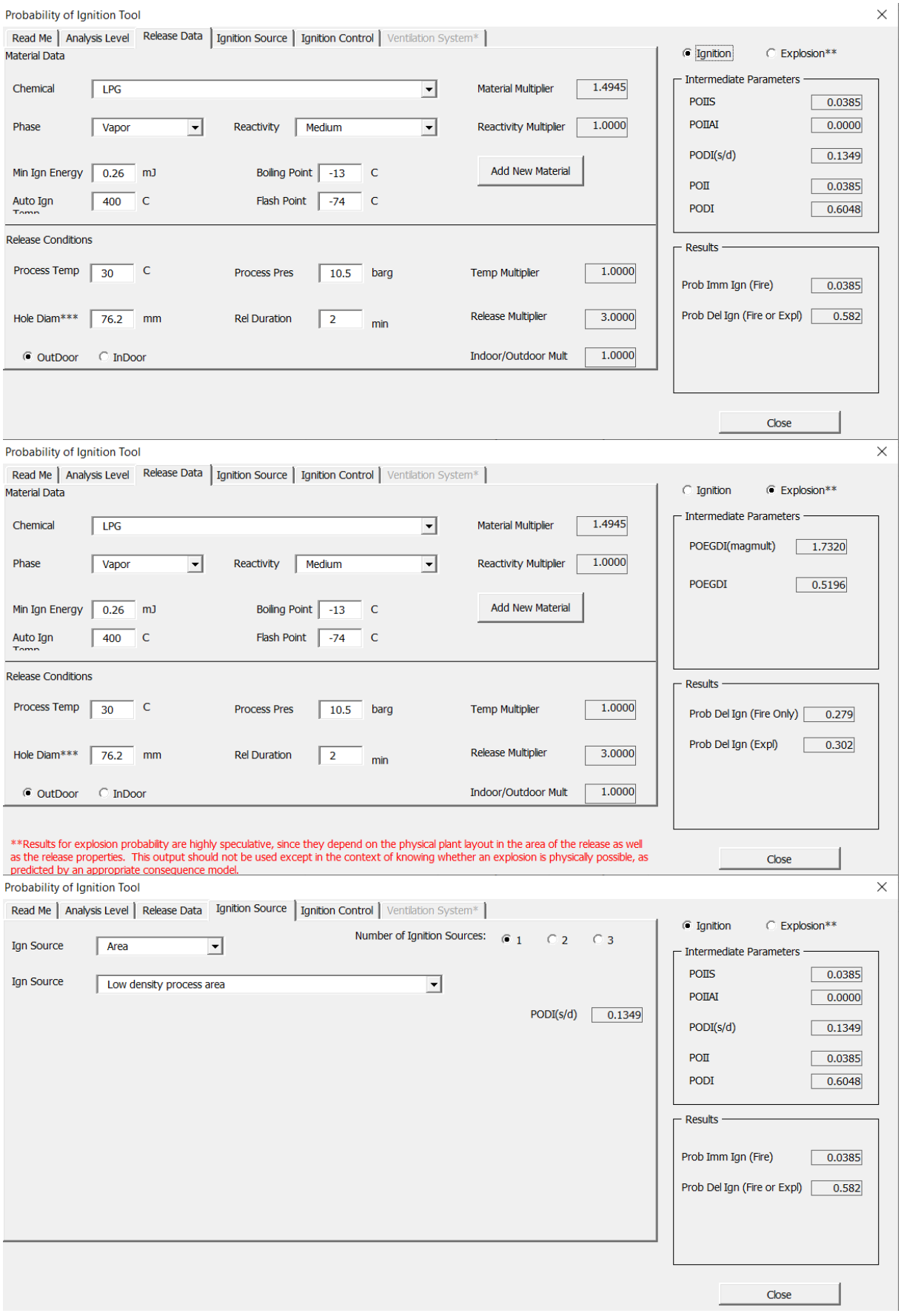

Şekil 9. *ETA-01 için POII-PODI Hesaplamaları Ekran Görüntüleri*

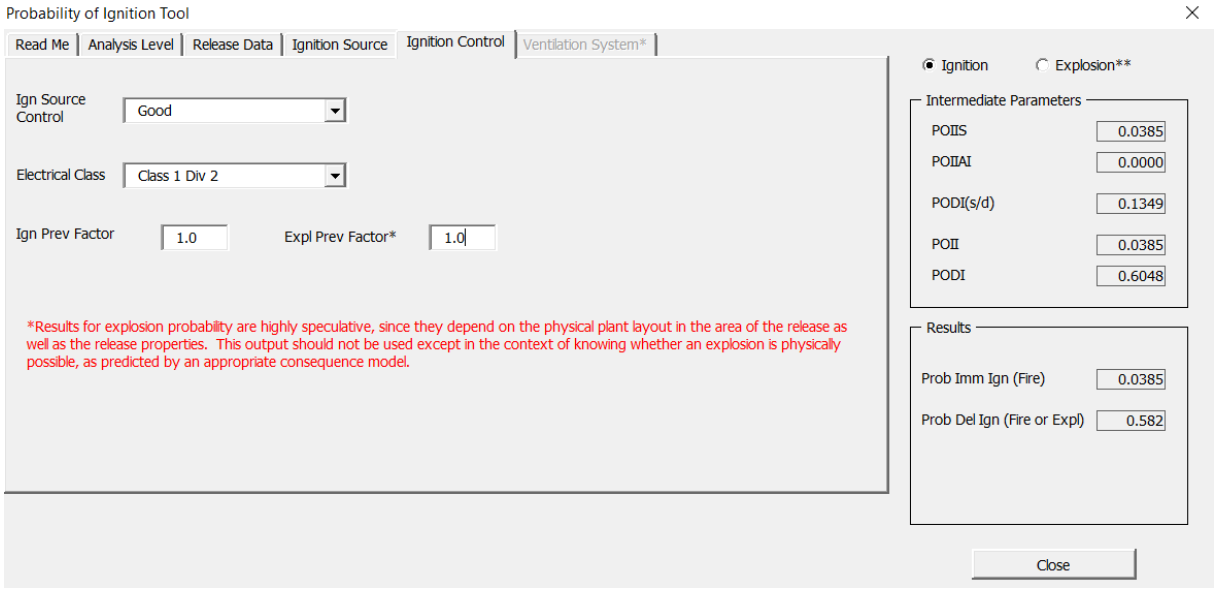

Şekil 9. *(Devam Ediyor)*

İlgili yazılımda, tutuşma veya patlama durumları için ilgili parametre hesaplaması elde edilmektedir. Kimyasal seçimi, buna ait faz seçimi, salınım koşulları ile ortam özelliklerinin tanımlanması gerekmektedir.

Yapılan risk değerlendirme çalışmaları ile büyük endüstriyel kazaya neden olabilecek senaryolar için hesaplanan frekans değerler Tablo 6'da verilmiştir.

Tablo 6. *Senaryolara ait Hesaplanan Frekans Değerleri*

Senaryo Numarası	**Senaryo Adı**	**Büyük Kaza Senaryo Sonucu Frekansı**
FTA-ETA 01	Gemiden Tanka Transferde Hat Üzerinde Bulunan Basınç Tahliye Vanalarından LPG Salınımı	Ramak Kala: 1.15E-04
		Jet Yangını: 4.97E-07
		Buhar Bulutu Patlaması: 8.75E-06
		Parlama Yangını: 3.47E-06
		Yayılım: 5.18E-06
FTA-ETA 02	Deniz Altındaki Borunun Dış Kaynaklı Sebeplerle Ezilmesi Nedeniyle Boru Çapında Daralma Olması Sonucu Boru Hattının Zayıf Noktasından LPG Salınımı	Jet Yangını: 2.25E-06
		Buhar Bulutu Patlaması: 2.17E-05
		Parlama Yangını: 2.62E-05
		Yayılım: 5.88E-05
FTA-ETA 03	İnsan Hatası Sonucu Yanlış Hesaplama Yapılması ve LPG Tankına Fazla Ürün Transferi Sonucu Tank Seviyesinin Yükselmesi ile Tankta Yer Alan Basınç Tahliye Vanalarından Atmosfere Gaz Fazda LPG Salınımı	Ramak Kala: 1.27E-03
		Jet Yangını: 5.50E-06
		Buhar Bulutu Patlaması: 4.15E-05
		Parlama Yangını: 3.84E-05
		Yayılım: 5.74E-05

Tablo 6'daki frekans değerleri, FTA-ETA 03 senaryosu/ramak kala dışında mevzuatta belirtilen 10^{-4} /yıl eşit frekans değerini karşılar niteliktedir. Ramak kala olayların büyük endüstriyel kaza yaratmayacağı düşünülerek eşik frekans değerini sağlama şartı aranmamaktadır.

4. SONUÇLAR

Çalışmada, LPG stoklama terminalinde gerçekleşen gemiden tanka operasyon için risk analizi çalışmaları yapılmış ve sonuçlar değerlendirilmiştir. Yapılan risk çalışmaları nitel ve nicel olmak üzere iki aşamada gerçekleştirilmiş ve bir metodoloji oluşturulmuştur. Nitel olarak HAZOP, nicel olarak Hata ve Olay Ağacı Analizlerinden yararlanılmıştır. Çalışmada elde edilen her bir büyük kaza senaryo frekans değeri, Yönetmelik Madde 9'da yer alan 10^{-4} /yıl eşik frekans değeri ile karşılaştırılmıştır. Eşik frekans değerinden daha düşük belirlenen frekans değerleri, terminalde önlemlerin yeterli ve mevcut önlemlerin kabul edilebilir seviyede olduğunu göstermiştir. Terminalde risk değerlendirmesi sonucu bir yatırım gerekmediği ortaya çıkmıştır. Ancak sistemin devamlılığı önem arz etmektedir. Bu devamlılığı da sağlamanın yolu test, bakım, periyodik kontrol gibi unsurların her bir ekipman için aksatılmadan gerçekleştirilmesi ile mümkündür. Bu sorumluluk terminale ait olup söz konusu unsurlar gerçekleşmediği takdirde yapılan çalışmaların gerçek hayatta bir karşılığı olmayacaktır.

LPG doğası gereği son derece tehlikelidir ve gerçekleşebilecek kazaların şiddeti de daha büyüktür. Bu büyük endüstriyel kazalar çevreye, insana ve ekipmanlarda ciddi zararlara ve kayıplara neden olmaktadır. Bu kapsamda LPG stoklama terminalleri için proses güvenliği büyük önem arz etmekte olup risk değerlendirme çalışmaları şeffaflıkla yürütülmelidir. Tüm bu çalışmalar esnasında kullanılan veriler gerçek durumu yansıtmalı ve prosese hâkim olan uzman kişilerce gerçekleştirilmelidir.

ÇIKAR ÇATIŞMASI

Yazarlar çıkar çatışması beyan etmemektedir.

KAYNAKLAR

Akbar, T. A., Dinariyana, A. A. B., Baheramsyah, A., Prastyasari, F. I., & Setyorini, P. D. (2019). Risk Assessment on Liquefied Petroleum Gas (LPG) Handling Facility, Case Study: Terminal LPG Semarang. *IOP Conference Series: Materials Science and Engineering*, *588*, 012007.

Akyuz, E., & Celik, M. (2015). Application of CREAM human reliability model to cargo loading process of LPG tankers. *Journal of Loss Prevention in the Process Industries*, *34*, 39-48. doi:10.1016/j.jlp.2015.01.019

Boult, M. (2000). Risk management of LPG transport activities in Hong Kong. J*ournal of Hazardous Materials*, *71*, 85-100. doi:10.1016/S0304-3894(99)00073-4

CCPS, Center for Chemical Process Safety. (2014). *Guidelines for Determining the Probability of Ignition of a Released Flammable Mass*. John Wiley & Sons, Inc.

Dinariyana, A. A. B, Artana, K. B., Handani, D. W., Sarasvati, F. I., & Aprilia, P. W. (2021). Societal risk assessment of terminal and oil refinery unit. *IOP Conference Series: Materials Science and Engineering*, *1052*, 012025.

Hosseini, N., Givehchi, S., & Maknoon, R. (2020). Cost-based fire risk assessment in natural gas industry by means of fuzzy FTA and ETA. *Journal of Loss Prevention in the Process Industries*, *63*, 104025. doi:10.1016/j.jlp.2019.104025

James, S., & Renjith, V. R. (2021) Risk Assessment and Vulnerability Analysis of Liquefied Natural Gas (LNG) Regasification Terminal. *Process Integration and Optimization for Sustainability*, *5*, 99-121. doi:10.1007/s41660-020-00138-3

Martins, R. M. S. T., & Vianna, R. F. (2020). Calculation of Thermal Radiation for the Design of Protection and Fire Fighting Systems for LPG Storage Parks. *Brazilian Journal of Petroleum and Gas*, *14*(1), 33-44. doi:10.5419/bjpg2020-0004

Renjith, V. R., Vijayan, V., & Soman, S. (2017). Fuzzy Fault Tree Analysis of LPG Cross Country Pipelines -A Case Study. *International Journal of Current Trends in Engineering & Technology*, *03*(05), 221-227.

Resmî Gazete (2019, 2 Mart). Büyük Endüstriyel Kazaların Önlenmesi ve Etkilerinin Azaltılması Hakkında Yönetmelik (Sayı: 30702).

Resmî Gazete (2020, 30 Haziran). Büyük Endüstriyel Kazalarla İlgili Hazırlanacak Büyük Kaza Senaryo Dokümanı Tebliği (Sayı: 31171).

Riad, B., Elarkam, M., Ilhem, B., & Hayett, A. (2020). Risk Asseessment For LPG Storage Tanks Area In Skikda Refinery-ALGERIA Using D-Higraph And Hazop Methods & Simulation of Dangerous Scenarios Using ALOHA Software. In: 2020 International Conference on Electrical Engineering (ICEE), September 25-27, Istanbul, Turkey. doi:10.1109/ICEE49691.2020.9249952

Sachan, S. S., & Premi, R. (2015). Hazard Identification and Risk Assessment in LPG Bottling Plant. *IJSTE - International Journal of Science Technology & Engineering*, *1*(12), 19-22.

Sarvestani, K., Ahmadi, O., & Alenjareghi, M. J. (2021). LPG Storage Tank Accidents: Initiating Events, Causes, Scenarios, and Consequences. *Journal of Failure Analysis and Prevention*, *21*, 1305-1314. doi:10.1007/s11668-021-01174-y

Shebeko, Y. N., Bolodian, I. A., Molchanov, V. P., Deshevih, Y. I., Gordienko, D. M., Smolin, I. M., & Kirillov, D. S. (2007). Fire and explosion risk assessment for large-scale oil export terminal. *Journal of Loss Prevention in the Process Industries*, *20*, 651-658. doi:10.1016/j.jlp.2007.04.008

Spoelstra, M., Mahesh, S., Kooi, E., & Heezen, P. (2015). Domino effects at LPG and propane storage sites in the Netherlands. *Reliability Engineering & System Safety*, *143*, 85-90. doi:10.1016/j.ress.2015.06.018

Tauseef, S. M., Abbasi, T., & Abbasi, S. A. (2010). Risks of Fire and Explosion Associated With the Increasing Use of Liquefied Petroleum Gas. *Journal of Failure Analysis and Prevention*, *10*, 322-333. doi:10.1007/s11668-010-9360-9

TOBB, Türkiye Odalar ve Borsalar Birliği. (2012). Türkiye Sıvılaştırılmış Petrol Gazı Meclisi Sektör Raporu, Ankara, TOBB Yayın Sıra No: 2012/174.

Török, Z., Petrescu-Mag, R-M., Mereuță, A., Maloș, C. V., Arghiuș, V-I., & Ozunu, A. (2020). Analysis of territorial compatibility for Seveso-type sites using different risk assessment methods and GIS technique. *Land Use Policy*, *95*, 103878. doi:10.1016/j.landusepol.2019.02.037

TSE, Türk Standartları Enstitüsü. (2010). Risk Yönetimi - Risk Değerlendirme Teknikleri (IEC / ISO 31010:2009), Ankara.

TSE, Türk Standartları Enstitüsü. (2016) Tehlike ve İşlerliği Çalışmaları (HAZOP Çalışmaları) - Uygulama Kılavuzu (IEC 61882:2016), Ankara.

Research Article / Araştırma Makalesi GU J Sci, Part A, 8(4): 482-493 (2021) https://doi.org/10.54287/gujsa.1008633

Gazi University
Journal of Science
PART A: ENGINEERING AND INNOVATION
http://dergipark.org.tr/gujsa

Thermal and Computational Fluid Dynamics (CFD) Analysis of a Modified Two Stroke Spark Ignition Engine Block

Sunday BAKO[1*], Jacob Nonom DOGO[1], Muhammed Bello UMAR[1], Ige BORI[2]

[1]*Department of Mechanical, Engineering, Nuhu Bamalli Polytechnic, Zaria, NIGERIA*
[2]*Department of Mechanical, Engineering, Federal University of Technology, Minna, NIGERIA*

Keywords

Conceptulization
Solidworks Simulation
Steady State Analysis
Transient State Analysis
CFD Analysis

Abstract

An engine block is the main supporting structure for other components of the engine. Poor heat dissipation of the engine block causes excessive thermal expansion and frictional wearing of the engine components and makes engine oil to lose its lubricating power. Therefore, there is a need to modify the design of the engine block in order to improve its effectiveness. In this analysis, a two stroke spark ignition engine block was initially used as a reference model for the development of the modified model. Solidworks (2013) simulation software was used to model and conduct a thermal and computational fluid dynamics (CFD) analysis on the two models. The thermal analysis results shows that, the maximum temperature gradient and heat flux obtained during the steady state and transient thermal analysis were, $2.237 \times 10^7 K/m$, $3.6817 \times 10^4 K/m$, and $1.066 \times 10^7 W/m^2$, $1.661 \times 10^6 W/m^2$ for the reference model, while $1.771 \times 10^6 K/m$, $4.913 \times 10^4 K/m$, and $7.970 \times 10^7 W/m^2$, $2.211 \times 10^6 W/m^2$ for the modified model respectively. The results shows that the modified model has an improved heat dissipation rate than the reference model. The CFD analysis shows that, the reference model is subjected to high pressure and air resistance than the modified model. This increases the drag force acting on the reference model. While the modified model has high air flow velocity round the engine block, than the reference model. This is due to fins modification of the modified model. This makes the engine block model to have low air restriction. It is hereby recommended that further validation should be carried out to ascertain the effectiveness of the modified model. The performance of the modified model can also be improved by converting its fins into triangular fins geometry.

Cite

Bako, S., Dogo, J. N., Umar, M. B., & Bori, I. (2021). Thermal and Computational Fluid Dynamics Analysis of a Modified Two Stroke Spark Ignition Engine Block. *GU J Sci*, *8*(4), 482-493.

Author ID (ORCID Number)

S. Bako, 0000-0003-2348-1217
J. N. Dogo, 0000-0001-5791-870X
M. B. Umar, 0000-0001-6679-1835
I. Bori, 0000-0001-7001-094X

Article Process

Submission Date 12.10.2021
Revision Date 07.12.2021
Accepted Date 28.12.2021
Published Date 29.12.2021

1. INTRODUCTION

Unlike the earlier work done by Bako et al. (2021), on development and structural analysis of a modified two stroke spark ignition engine; this paper presents the thermal and computation fluid dynamics analysis of the modified two stroke spark ignition engine block. The paper tends to ascertain the thermal and the fluid dynamic behavior of the engine blocks. The engine block is the solid foundation for housing and supporting of other components of the engine. It is subjected to high structural and thermal stress during the compression and the expansion stroke of the engine. Approximately 30% of the heat energy released in the engine is converted into mechanical energy, while the remaining energy is lost in the form of heat and friction (Ansari et al., 2020). Therefore the cooling of the engine block needs to be improve because this high temperature can cause damage to engine components and lubricants. This heat is conducted to engine components, thereby causing high frictional wear and looses. Due to this effect, the engine efficiency is reduced (Subramanian et al., 2019). Uncontrolled heating of the engine causes expansion of the piston and piston rings, which will also increase frictional losses. The viscosity of the lubricating oil used in the engine,

*Corresponding Author e-mail: s2bako@yahoo.com

and the cooling system requirements are greatly affected by the engine heat dissipation rate. The two stroke engine blocks wear much faster than four stroke engines block (Jiang, 2015). Unlike the Gas Turbine (GT) engine that uses Brayton's Cycle, and the Steam Turbine (ST) engine that uses Rankine's Cycle (Bakare et al., 2016); the two stroke engine uses Otto's Cycle and it produces power during every crankshaft rotation. The heat released inside the engine increases frictional wear and affects the engine cycle efficiency (Thomas, 2009). Therefore, there is a need to come up with measures to improve the heat dissipation rate of the engine in order to improve its efficiency. This leads to the concept of the research.

Due to high demand for two stroke spark ignition engine in the global market and the need to improve the engine performance; some researchers (Thomas, 2009; Khan & Shaikh, 2016; Schneider et al., 2016; Subramanian et al., 2019; Ansari et al., 2020) have carried out research works to analyze and to improve the engine efficiency. These engines are air cooled engines. The temperature of the engines is convectively cooled with the help of the cooling fins. In order to enhance the engine cooling, Jain et al. (2016) optimized the cooling system dimension of a two stroke air cooled internal combustion engine by reducing the total volume occupied by the engine. It was noted that, modifying cooling system and the entire engine design would reduce emission and improve engine efficiency. Babu & Lavakumar (2013) and Rao & Vardhan, (2013) analyzed the thermal properties of the engine by altering the fins geometry, material and thickness on the engine cylinder. While Yeh et al. (1997) and Dempsey (2010) recommended the addition and modification of fins on an engine cylinder, in order to increase its surface area for heat dissipation. Therefore, design modification of the engine cylinder is highly needed, in order to make the pressure and temperature distribution to be uniformly distributed on the engine block. This will reduce the waste of un-burnt charges and decrease environmental pollution (Babu et al., 2013).

Most researchers primarily focused on design modification of the two stroke engine for alternative fuel usage and power density, as well as to achieve higher efficiency through more complex porting systems (Borman & Nishiwaki, 1987; Blarigan & Keller, 1998; Bernard & Baranescu, 1999). Therefore the concept of this paper came up as a measure to improve the engine performance through fins modification. The first series of this research work presents the modeling and structural analysis of a modified two stroke spark ignition engine block. The work shows that, the modified model is more rigid and has more strength than the reference model. Therefore this paper as continuation, presents the thermal and computational fluid dynamics analysis of the modified two stroke spark ignition engine block. The paper aimed at conducting and comparing the thermal and aerodynamics performance of the two respective models, and to ascertain the model with improved heat dissipation, and aerodynamics behaviors. Figure 1 illustrates the working principle of the two stroke spark ignition engine.

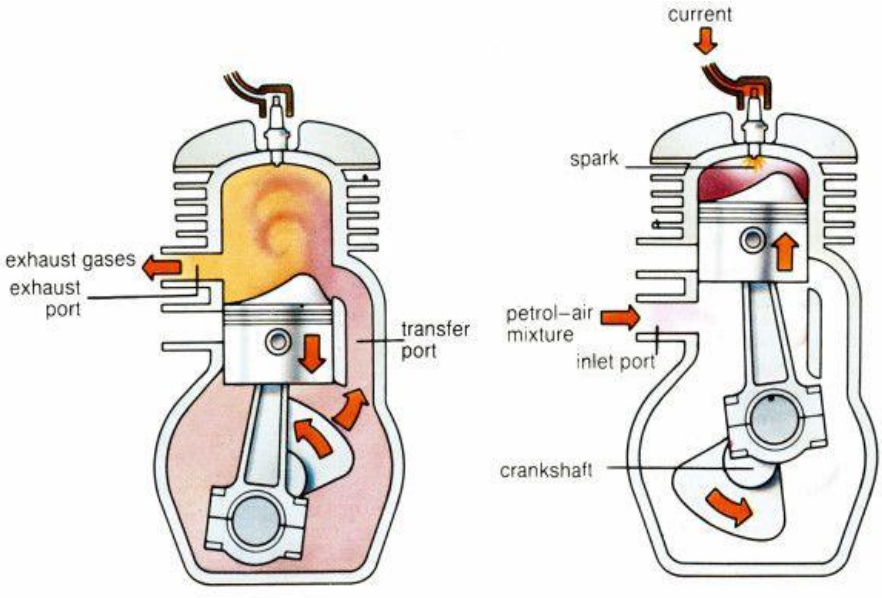

Figure 1. *Shematic Diagram of a Two Stroke Engine (Cameron, 2015)*

2. MATERIALS AND METHOD

The key materials used in the analysis are, AutoCAD 2018 for the conceptual presentation, and Solidworks 2013 for modeling and simulation. An engine block model was used as a reference model. Calculations were done to calculate the various fins parameters for the development of the modified model. A solid model of the engine blocks were developed and simulated using the solidworks 2013 simulation software. A steady state and transient state thermal analysis were carried out on the two models to ascertain their thermal performance. Also a computational fluid dynamics analysis were also carried on the two models to investigate the aerodynamics behavior of the engine block models. The simulation results for the two models were compared to ascertain their thermal and aerodynamics behaviours.

2.1. Conceptualization and Analysis

The wet and dry cylinders liners of a four stroke engines are circular and cylindrical in shape. This makes the cylinder to have uniform thermal and structure stress distribution. Therefore the engine block of the two stroke engine should also be made circular in design in order to enhance its heat dissipation, aerodynamics and uniform stress distribution. For this reason, the modified model of the two stroke spark ignition engine block was made be circular in design. Figure 2 shows the conceptual development.

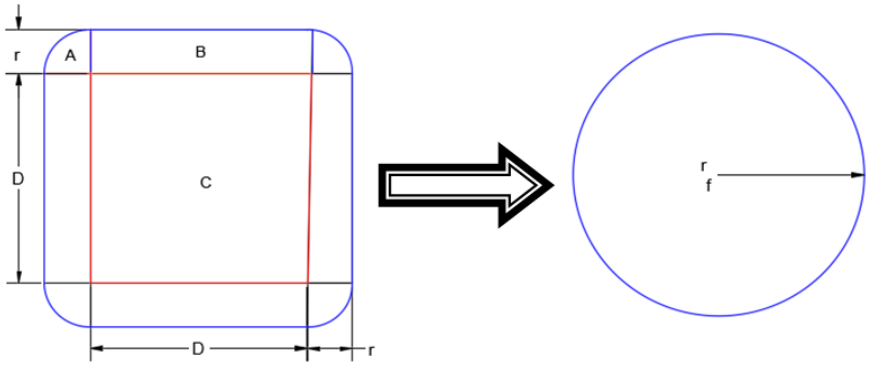

Figure 2. *Conceptual Development*

2.1.1. Fins Outer Radius

The cross sectional area of the reference model is equal to the cross sectional area of the modified model as illustrated in Figure 2.

$$4A + 4B + C = \pi r_f \tag{1}$$

r_f : Fin Radius (outer radius of the engine block)

A : Sector

B : Rectangle

C : Square

$$\frac{4\emptyset\pi r^2}{360} + 4rb + b^2 = \pi r_f^2 \tag{2}$$

$\emptyset = 90^{\circ}$ (Angle of sector A in Figure 1)

$$r_f = \sqrt{\frac{r(\pi r + 4b) + b^2}{\pi}} \tag{3}$$

2.1.2. Fins Length

Unlike the reference model, the length of the fin of the modified is uniformly equal all round the engine cylinder. This would ensure uniform stress distribution round the engine cylinder The length of the fins is given by;

$$L_f = r_f - r_b \tag{4}$$

2.1.3. Normalized Fins Radius

The Normalize fins radii is given by Acosta-Iborra & Campo (2013) as;

$$R_f = \frac{r_f}{r_b} \tag{5}$$

While the normalize radii ratio should be within the range of;

$$1 \leq \frac{r_f}{r_b} \leq 5 \tag{6}$$

2.1.4. Convective Heat Transfer

Annand's Correlation is used for calculating the Convective heat transfer h_g (Lounici et al., 2010),

$$h_g = a.\frac{k_g}{B}.Re^{0.7} + b.\frac{(T_g^4 - T_w^4)}{(T_g - T_w)} \tag{7}$$

$a = 0.35 - 0.8$, and $b = 4.3 \times 10^{-9} W/m^2K^{-4}$

$$Re = \frac{\rho \cdot V \cdot L}{\mu} \tag{8}$$

2.1.5. Heat Flux

Gangwar et al. (2017) noted that Woschni, Equation 9 calculates heat flux as a function of the cylinder bore, the characteristic velocity, the cylinder pressure and temperature as,

$$q = a.D^{-0.2}.p^{0.8}.V^{0.8}.T^{-0,53}.\left(T_g - T_w\right) \tag{9}$$

D : Cylinder Bore (m)

L : Characteristic Length (m)

P : Pressure (pa)

q : Heat Flux (W/m^2)

T : Temperature (K)

V : Characteristic Velocity (m/s)

μ : Dynamic Viscosity ($N.s/m^2$)

ρ : Density (kg/m)

2.2. Finite Element Formulation for the Thermal Analysis

Figure 3 illustrate the temperature distribution on the cylinder wall. By using finite element method and assuming a linear variation of temperature. The resulting stiffness matrix is given by Lewis et al. (2004) as;

$$[K] = \frac{2\pi k}{l}\frac{(r_i + r_j)}{2}\begin{bmatrix} 1 & -1 \\ -1 & 1 \end{bmatrix} + 2\pi r_o h \begin{Bmatrix} 0 & 0 \\ 0 & 1 \end{Bmatrix} \quad (10)$$

$$Q^e = hT_\infty 2\pi r_o \begin{bmatrix} 0 \\ 1 \end{bmatrix} \quad (11)$$

It is also noted in Hutton (2004), that the Finite Element Equation with conduction and convection can be expressed as

$$([K_T^e] + [K_C^e])[T] = [Q^e] + [q^e] \quad (12)$$

$$\left(\frac{2\pi k}{l}\frac{(r_i + r_j)}{2}\begin{bmatrix} 1 & -1 \\ -1 & 1 \end{bmatrix} + 2\pi r_o h \begin{Bmatrix} 0 & 0 \\ 0 & 1 \end{Bmatrix}\right)\begin{bmatrix} T_i \\ T_j \end{bmatrix} = \begin{bmatrix} Q_i^e & q_i^e \\ Q_j^e & q_j^e \end{bmatrix} \quad (13)$$

e : Element, i, j : Nodes, l : Length (m)

Q^e : Thermal load corresponding to the heat source (W/m^3)

q : Vector of nodal heat flows across the cross-section (W/m^3)

T_∞ : The ambient temperature of the brake drum (K)

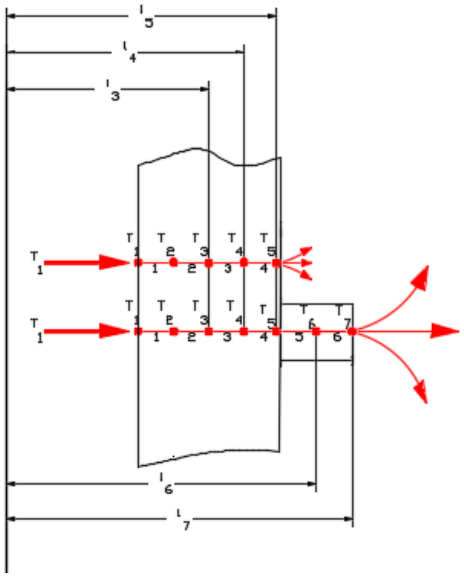

Figure 3. *Sectional of the Engine Cylinder with Nodal Points*

In situation where the Prandtl number differ from unity, the Nuseelt number can be express as (Broekaert et al., 2016),

$$Nu = 0.332 \cdot Re^{1/2} \cdot Pr^{1/3} \quad (14)$$

The Reynold (*Re*) was expressed in Equation 8, while the Prandtl Number (*Pr*) is expressed as;

$$Pr = \frac{\mu \cdot C_p}{k} \quad (15)$$

In fluid mechanics, mach number (M) is define as the ratio of the inertia force (F_i) to the elastic force (F_e). It is expressed as;

$$M = \sqrt{\frac{Inertia\ Force}{Elastic\ Force}} = \sqrt{\frac{\rho A V^2}{KL^2}}$$

$$M = \frac{V}{\sqrt{K/\rho}} \tag{16}$$

While the square of the mach number is called Cauchy Number (C) (Al-Shemmeri, 2012).

The coefficient of drag C_D is expressed as:

$$C_D = \frac{Drag\ Force\ (F_D)}{Kinetic\ Pressure\ (K_P) \cdot Frontal\ Area\ (A_f)}$$

$$C_D = \frac{F_D}{\rho V^2/_2 \cdot A_f} = \frac{2F_D}{\rho V^2 \cdot A_f} \tag{17}$$

$$F_D = \frac{C_D \cdot \rho V^2 \cdot A_f}{2} \tag{18}$$

When a given body is moving through a fluid, it does work on the fluid to overcome the drag force. This rate of work done is given by the power equation:

$$P = F_D \cdot V_b \tag{19}$$

Where, P is the power needed to overcome the drag force (F_D) and (V_b) is the speed of the body (Elger et al., 2016).

2.3. Modelling and Simulation

During the simulation process, the engine block models were treated under the same boundary conditions to ascertain the model with an improved heat dissipation and aerodynamics performance. Most engine blocks are made of cast iron material. They are designed to withstand high temperature of more than 2000℃ (Babu et al, 2013; Ansari et al., 2020). Therefore, a cast iron material was selected during the simulation analysis. Just as Ansari et al. (2020), a steady state and transient thermal analysis were performed on the two models at the temperature of 1000℃ and ambient temperature 20℃. While during the computational fluid dynamics analysis, the models were subjected to air stream at the velocity of 60m/s.

2.3.1. Model Assumption

In order to unify the analysis, the two models were treated under the same boundary conditions. While in order to simplify the analysis, It was assumed that, after the expansion stroke of the engine, the heat dissipation needs to be carried out at a fast rate to prevent unusual heating of the combustion chamber and the entire engine. Therefore the heat dissipation of the engine was assumed to take place through the entire wall of the engine cylinder. It was also assumed that, the arrangements of the fins can affect the aerodynamic behavior of the engine block. Therefore the two models were subjected under the same air velocity. Figure 4 shows the solid and the meshed model of the reference and the modified model of the engine block respectively.

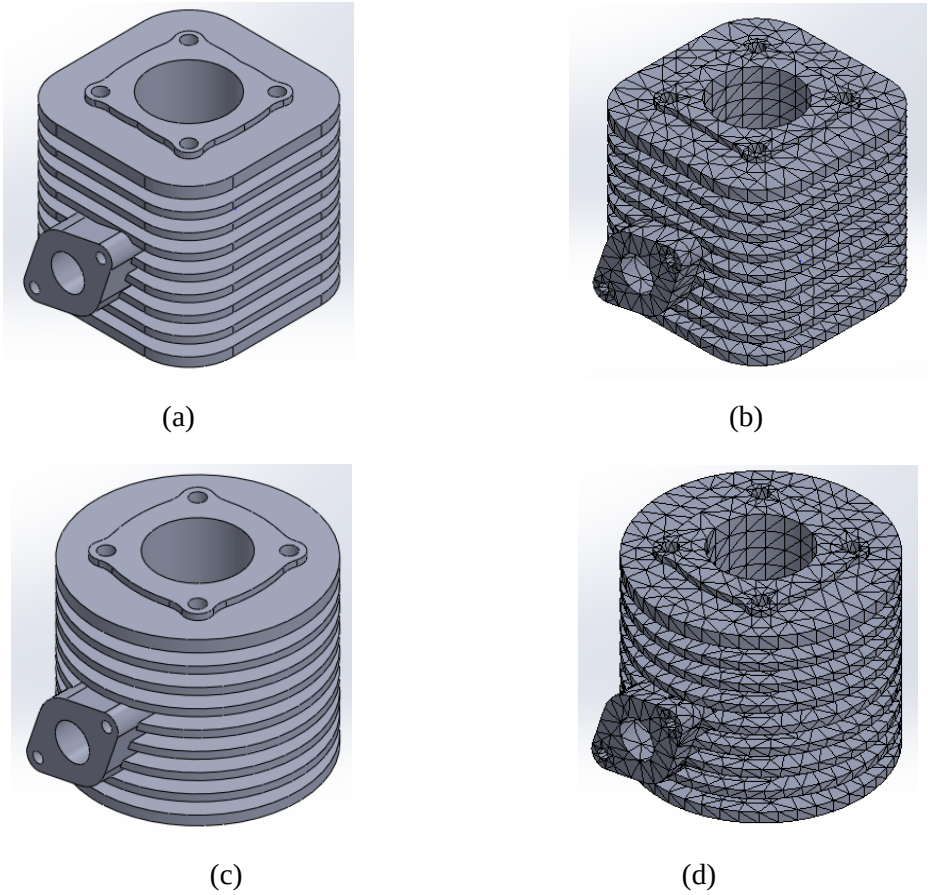

(a) (b)

(c) (d)

Figure 4. *Engine Block Models,* ***a)*** *and* ***b)*** *Solid and Meshed Model of the Reference Model,* ***c)*** *and* ***d)*** *Solid and Meshed Model of the Modified Model*

3. RESULTS AND DISCUSSION

The simulation result shows that, no element of the two models was damaged as the result of distortion; as this could affect the simulation results. The result also shows that, the two models have the same Jocobian point (4), % distortion (0), element size (0.0160m), and element tolerance (00080). This justified that, the two models were treated under the same boundary condition. Meanwhile, the modified model shows high number of elements (13758) and nodal points (23949) than the reference model (13285 and 23290). This shows that, the surface area of the modified model has been extended in order to enhance its heat dissipation.

A steady state thermal analysis was carried out on both models under the same boundary conditions. The analysis was to investigate and compare the thermal performance of the models under the same boundary conditions. The rate of heat transfers between the combustion chamber and the surrounding are not uniform and unsteady, and difficult to evaluate. The steady state analysis showed that, the maximum and minimum temperature distribution of the refrence model (Figure 5a), are greater than that of the modified model (Figure 6a). The low temperature distribution shown by the modified model implied that the model has high rate of heat dissipation than the reference model.

Temperature gradient is the change in temperature over a given length of material or component. The two models where investigated under the same temperature condition. However, the refrence model (Figure 5b) shows a higher value of temperature gradient than the modified model (Figure 6b). This showed that, the temperature changes through a longer distance from the inner wall of the engine cylinder to the tip of the fins of the modified model than that of the reference model. This increase in distance is as the result of the geometric modification of the fins on the surface of the modified engine block.

The modified model has high value of heat flux than the reference model. The heat flux or thermal flux, sometimes referred to as heat flux density or heat flux density, is the flow of energy per unit of area per unit

of time. The simulation results showed that, the rate of heat transfer of the reference model (Figure 5c) is less than that of the modified model (Figure 6c). This implied that more heat was dissipated from the fins of the modified model compare to the reference model.

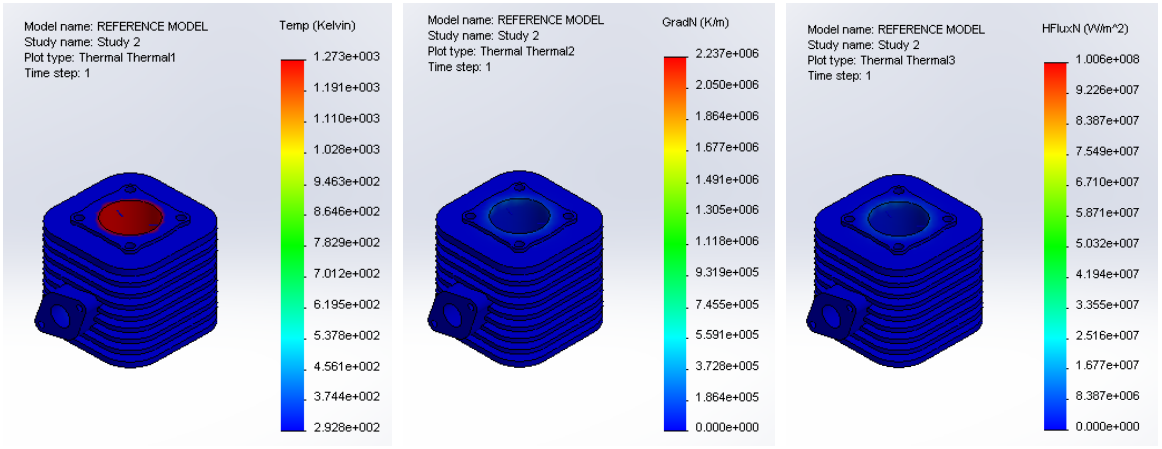

(a) (b) (c)

Figure 5. *Steady State Thermal Analysis for Reference Model,*
a) *Temperature Distribution,* ***b)*** *Thermal Gradient,* ***c)*** *Heat Flux*

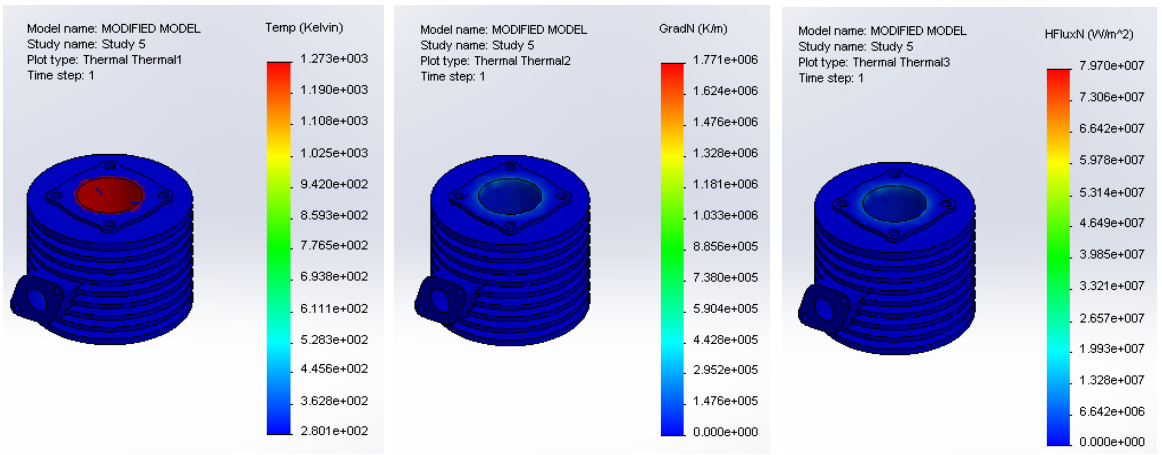

(a) (b) (c)

Figure 6. *Steady State Thermal Analysis for Modified Model*
a) *Temperature Distribution,* ***b)*** *Thermal Gradient,* ***c)*** *Heat Flux*

The transient thermal analysis evaluates temperature and heat flux of the model over a assigned period of time. The transient thermal analysis for this analysis was carried out over a period of 300 seconds, and time increments of 10 seconds. Therefore the simulation calculated the results 30 times. The results showed that, the reference model (Figure 7a) has higher temperature over this given period of time, than that of the modified model (Figure 8a). This also implied that more amount of heat energy has been dissipated from the modified model, than that of the reference model. Meanwhile the temperature gradient and the heat flux of the reference model (Figure 7b and 7c) are less than that of the modified model (Figure 8b and 8c), which implied that more heat were dissipated at a fast rate and within a shorter period of time compare to that of the reference model. The analysis showed that, the fins has improved the thermal performance of the modified engine block. The high temperature shown by the reference model implies that, the model retained more amount of heat energy. This retained amount of heat energy in a given component is the major cause of thermal problems associated with some mechanical systems (Bako et al., 2020). Therefore, this retained heat energy in the engine block is the major causes of the thermal problems associated with the two stroke spark ignition engine as earlier mentioned in the paper.

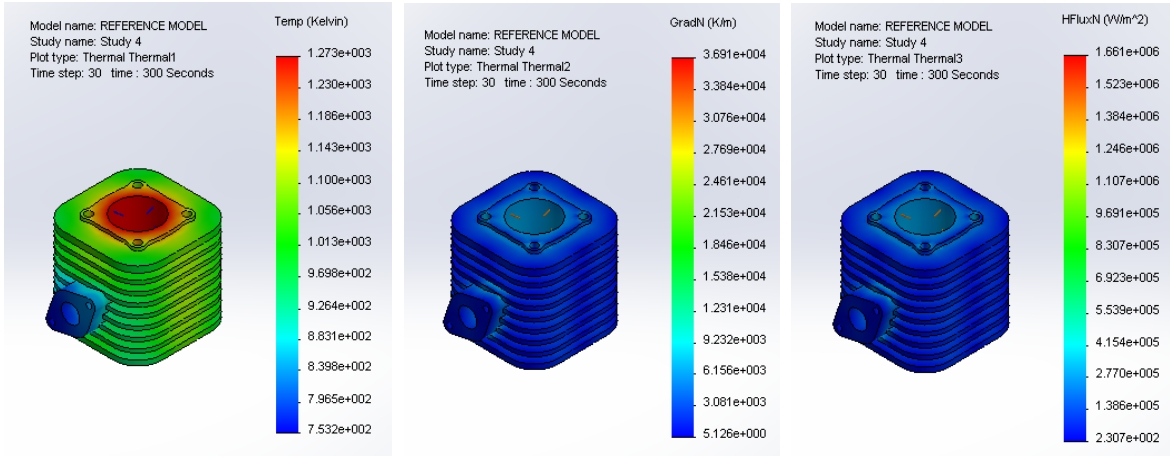

(a) (b) (b)

Figure 7. *Transient Thermal Analysis for Reference Model,*
a) *Temperature Distribution,* ***b)*** *Thermal Gradient,* ***c)*** *Heat Flux*

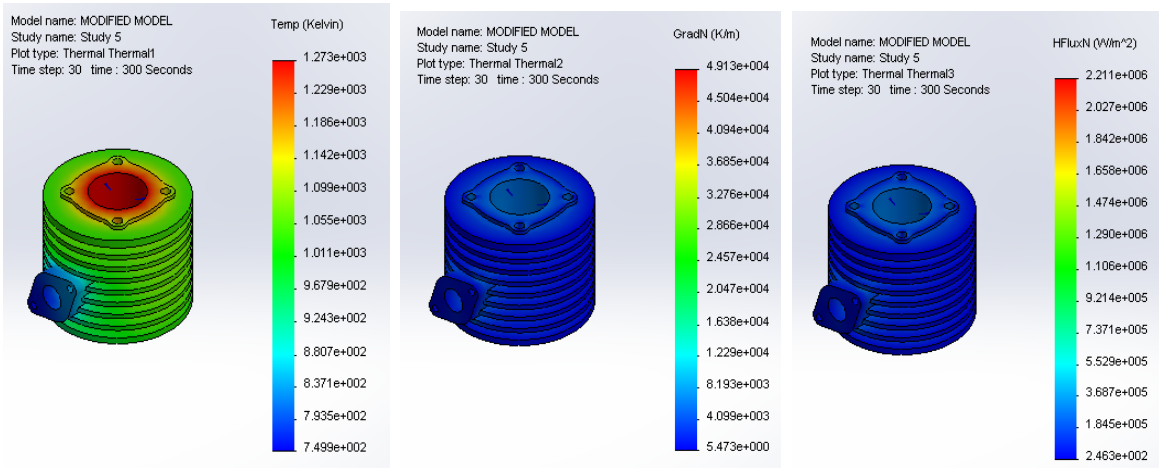

(a) (b) (c)

Figure 8. *Transient Thermal Analysis for Modified Model,*
a) *Temperature Distribution,* ***b)*** *Thermal Gradient,* ***c)*** *Heat Flux*

The computation fluid dynamics analysis of the engine block models analyzed the impact of air flow on the models. During the computational fluid dynamics analysis, it takes 221 iterations at 42 minutes 53 seconds on the modified model, and 226 iterations at 8 hours, 05 minutes, 24 seconds for reference model respectively, both to complete the simulations. The higher iteration taken by the reference model is as the result of the geometry complicity of the model fins arrangemnet of the model. The complicity of the fins arrangement of the reference model would affect its air resistance, air flow round the engine block, and its heat dissipation (Table 1).

The results (Table 1) shows that, the reference model has high total pressure and dynamic pressure than the modified model. This increase in pressure, increases the drag force acting on the engine. This shows the modified model has high air flow velocity than the reference model. This is due to the fins modification round the engine block. This makes the engine block model to have low air restriction on the surface of the engine block. In line with Equation 17 and 19 above, the high velocity shown by the modified model would reduce the drag coefficient and reduce the power required to overcome the drag force.

The CFD results (Table 1) shows that the reference model has high temperature than the modified model. This agreed with the results obtained earlier during the thermal analysis of the engine blocks. Meanwhile,

heat is transferred from a region of higher temperature to a region of lower temperature. During the simulation, the surrounding air of the modified model has low fluid thermal conductivity, specific heat, and fluid density. This is as the result of the heat transfer enhancement by the fins in the modified model. While the high fluid thermal conductivity, specific heat, and fluid density shown by the reference model, implies that the some amount heat are retained in the engine block. This retained heat energy contributes to thermal problems earlier mentioned.

Table 1. *Computational Fluid Dynamics Analysis Results*

Parameter	Reference Model			Modified Model		
	Minimum	**Maximum**	**Average**	**Minimum**	**Maximum**	**Average**
Pressure (Pa)	15.755641	1.01604E+14	6.4888E+11	149.497139	1.03599E+14	3.04532E+11
Total Pressure (Pa)	161.965128	5.77247E+43	1.79168E+37	281.215975	5.42705E+36	3.69148E+32
Dynamic Pressure (Pa)	17.216195	3.37613E+13	15634822500	61.1102775	3.56193E+13	5521918770
Density (Fluid) (kg/m^3)	0.497496662	1158911190	3392130.97	0.033950154	1142510500	1269771.46
Velocity (m/s)	1.00878893	8350.57759	77.0553136	3.76379057	774.338598	84.8789113
Velocity (X) (m/s)	-1867.81072	8350.33827	-1.47732447	-772.930548	765.738329	2.7958421
Velocity (Y) (m/s)	-2517.73893	1743.85097	33.179026	-773.183945	773.20881	25.963943
Velocity (Z) (m/s)	-947.911654	1023.53305	1.56786409	-768.297218	701.44137	-6.16695285
Mach Number [ ]	0.002930754	1414601.35	2.1356413	0.010934759	128163.333	10.7358892
Turbulent Viscosity (Pa s)	1.63819E-07	30784.4769	175.563996	4.62505E-07	1879665.02	163.09085
Turbulent Time [s]	1.35451E-07	0.157767018	0.151551284	7.83279E-06	0.157767018	0.143583217
Turbulence Length (m)	6.57869E-09	0.001905	0.001836869	4.97949E-07	0.001905	0.001755192
Turbulence Intensity (%)	0.001141236	446.495556	0.545262818	0.007851275	73.049692	0.65393956
Turbulent Energy (J/kg)	0.004163308	98371.0652	87.2651398	0.005394532	52080.3403	73.8013881
Turbulent Dissipation (W/kg)	0.034227686	30915523800	6551457.21	0.034227686	3396071120	2513835.55
Specific Heat (Cp) (J/(kg K))	1006.0876	2860.8392	1007.16168	1006.0876	1029.115	1006.96882
Dynamic Viscosity (Pa s)	0.00000604	0.0000955	1.81376E-05	0.00000604	1.8239E-05	1.77864E-05
Prandtl Number ( )	0.53679653	0.797692716	0.707883917	0.707362959	0.797692716	0.709424297
Temperature /Fluid (K)	6.8792E-10	3051.16637	293.768406	9.14212E-08	294.981023	286.170573
Total Temperature (K)	238.8894	33879.6667	303.242027	213.475494	295.035451	294.75345
Stagnation Density (kg/m^3)	3.19316023	2.06696E+36	4.63867E+29	0.034471458	3.87034E+28	2.61904E+24
Total Enthalpy (J/kg)	245844.725	34866073	308678.489	243360.145	304628.393	299752.863
Fluid Thermal Conductivity W/(m K)	0.007792292	0.486	0.026339827	0.007792292	0.025963111	0.024459105

4. CONCLUSION

This study presents thermal and aerodynamics analysis of a two stroke spark ignition engine block. The modified model shows uniform fins arrangement round the engine cylinder in order to enhance its strength and its heat dissipation. The low temperature shown by the modified model with high temperature gradient and heat flux, indicates that, the modified model has high heat dissipation rate than the reference model, which will subsequently improve the engine efficiency.

The CFD analysis shows that, the reference model has high total pressure and dynamic pressure than the modified model. This increase in pressure, increases the drag force acting on the model. While the modified model has high air flow velocity than the reference model; due to its fins modification. This made the

modified model to have low air restriction. The CFD results also shows that the reference model has higher temperature than the modified model. This agreed with the results obtained earlier during the thermal analysis of the engine blocks. This analyis also shows that the modified engine block model would have the following advantages over the reference model;

1. High heat dissipatio rate which would minimise the thermal problem associated with the two stroke spark ignition engines.
2. Low aerodynamic resistance, which would also lead to low fuel consumption and easy circulation of air round the engine block.
3. Improved engine block strength, which would also reduce engine vibration.
4. Low wearing of engine components as a result of friction; this would be as the result of the high heat dissipation rate and improved engine block strength.
5. The engine oil of the modified engine block would have long service life due to its low temperature which would prolong the engine oil lubricating power.

This paper has provided a method of developing a modified model of a two stroke spark ignition engine. It is hereby recommended that, physical validation should be carried out to ascertain the effectiveness of the modified model. The strength and heat dissipation rate of the engine block can also be improve by, converting the fins of the modified model into a triangular fins of equal length, and fins base; and also by adding the remaining part of the fin to the engine cylinder.

CONFLICT OF INTEREST

The authors of this manuscript have hereby declared that, there is no conflict of interest associated with the publication of this paper.

REFERENCES

Acosta-Iborra, A., & Campo, A. (2013). Approximate Analytic Analysis of Annular Fins with Uniform Thickness by way of the Mean Value Theorem for Integration that Avoids Modified Bessel Functions. *Latin American and Caribbean Journal of Engineering Education*, *7*(1), 1-23.

Al-Shemmeri, T. (2012). *Engineering Fluid Mechanics*. Bookboon Learning.

Ansari, M. B., Haque, M. F. U., & Joshi, P. S. (2020). Design and Analysis of Engine Block. *International Research Journal of Engineering and Technology*, *7*(5), 3514-3520.

Babu, G., & Lavakumar, M. (2013). Heat Transfer Analysis and Optimization of Engine Cylinder Fins of Varying Geometry and Material. *IOSR Journal of Mechanical and Civil Engineering*, *7*(4), 24-29.

Babu, G. S., Jagadeesh, S. D. V. S., Saicharan, U. B., & Praneeth, P. R. S. (2013). Analysis of a Single Cylinder Combustion Engine using CFD. *International Journal of Innovative Technology & Exploring Engineering*, *2*(5), 164-167.

Bakare, A. O., Nasir, A., Abiodun, O. R., & Bako, S. (2016). Combined Cycle Gas Turbine: Operation and Performance Analysis. In: Proceedings of the 1st AGM and Conference of the Nigerian Institution of Mechanical Engineers (pp. 57-68), Minna, Nigeria.

Bako, S., Nasir, A., Ige, B., & Musa, N. (2020). Cavitational deterioration of diesel power plant cylinder liner. *Journal of Mechanical and Energy Engineering*, *4*(3), 239-246. doi:10.30464/jmee.2020.4.3.239

Bako, S., Dogo, J. N., Umar, M. B., & Jesuloluwa, S. I. (2021). Development and Structural Analysis of a Modified Two Stroke Spark Ignition Engine Block. In: Proceedings of the 5th AGM and Annual National Conference of the Nigerian Institution of Mechanical Engineers (pp 57-68), Minna, Nigeria.

Bernard, C., & Baranescu, R. (1999). *Diesel Engine Reference Book*. England: Butterworth-Heinemann.

Blarigan, P. V., & Keller, J. O. (1998). A hydrogen fuelled internal combustion engine designed for single speed/power operation. *International Journal of Hydrogen Energy*, *23*(7), 603-609. doi:10.1016/S0360-3199(97)00100-6

Borman, G., & Nishiwaki, K. (1987). Internal-combustion engine heat transfer. *Progress in Energy and Combustion Science*, *13*(1), 1-46. doi:10.1016/0360-1285(87)90005-0

Broekaert, S., Demuynck, J., De Cuyper, T., De Paepe, M., & Verhelst, S. (2016). Heat transfer in premixed spark ignition engines part I: Identification of the factors influencing heat transfer. *Energy*, *116*(1), 80-391. doi:10.1016/j.energy.2016.08.065

Cameron, K. (2015). Two Stroke Engines: Defining Their Purpose. (Accessed:03/12/2021) www.cycleworld.com/2015/04/06/two-stroke-motorcycle-engines-explained-tech-talk-by-kevin-cameron/

Dempsey, P. (2010). *Two-Stroke Engine Repair & Maintenance*. New York: McGraw-Hill Companies.

Elger, D. F., LeBret, B. A., Crowe, C. T., & Robertson, J. A. (2016). *Engineering Fluid Mechanics* (11th ed.). Hoboken: John Wiley & Sons, Inc.

Gangwar, A., Singh, A., & Pratap, A. (2017). Performance and Analysis of Two Stroke Dual and Triple Spark plug Single Cylinder SI Engine with Gasoline fuel. *International Journal of Thermal Technologies*, *7*(4), 204-206.

Hutton, D. V. (2004). *Fundamental of Finite Element Analysis*. New York: Mcgraw-Hill Companies.

Jain, A., Saraswat, A. A., & Shukla, O. P. (2016). A Survey on Heat Transfer of Air Cooled Internal Combustion Engine Various Fin Cutting Shape. *International Research Journal of Engineering and Technology*, *3*(2), 1413-1418.

Jiang, S. (2015). Numerical Analysis of Two-Stroke Engine with Direct Injection and Jet Ignition. BSc Thesis, School of Aerospace Mechanical and Manufacturing Engineering, College of Science Engineering and Health, RMIT University, Melbourne.

Khan, T. A., & Shaikh, R. (2016). Performance and Emission Analysis of Two Stroke Dual Sparkplug SI Engine. *IOSR Journal of Mechanical & Civil Engineering*, (Special Issue: 5th National Conference on RDME) *2*, 50-53. doi:10.9790/1684-1500850-53

Lewis, R. W., Nithiarasu, P., & Seetharamu, K. N. (2004). *Fundamentals of Finite Element Method for Heat and Fluid Flow*. Hoboken: John Wiley and Sons Ltd. doi:10.1002/0470014164

Lounici, M. S., Loubar, K., Balistrou, M., & Tazerout, M. (2010). Investigation on heat transfer evaluation for a more efficient two-zone combustion model in the case of natural gas SI engines. *Applied Thermal Engineering*, *31*(2-3), 319-328. doi:10.1016/j.applthermaleng.2010.09.012

Rao, M. N. P. R., & Vardhan, T. V. (2013). Thermal Analysis of Engine Cylinder Fins By Varying Its Geometry and Material. *International Journal of Engineering Research & Technology*, *2*(8), 404-412.

Schneider, S., Chiodi, M., Friedrich, H., & Bargende, M. (2016). Development and Experimental Investigation of a Two-Stroke Opposed-Piston Free-Piston Engine. SAE Technical Paper 2016-32-0046. doi:10.4271/2016-32-0046

Subramanian, T. S., Murali, B. S., Vairamuthu, M., Saravanan, M. V., & Kumar, M. M. (2019). Design and Analysis of Cylinder and Cylinder Head of 6-Stroke SI Engine for Weight Reduction. *International Journal of Innovative Research in Science, Engineering & Technology*, *8*(3), 3276-3288.

Thomas, G. (2009). Computational Fluid Dynamics Modelling and Analysis of an Opposed Piston Internal Combustion Engine. MSc Thesis, School of Mechanical, Materials and Mechatronics Engineering, University of Wollongong, Wollongong.

Yeh, R-H., Liaw, S-P., & Chang, M. (1997). Optimum Spacings of Longitudinal Convective Fin Arrays. *Journal of Marine Science and Technology*, 5(1), 6. doi:10.51400/2709-6998.2537

Research Article / Araştırma Makalesi GU J Sci, Part A, 8(4): 494-504 (2021) https://doi.org/10.54287/gujsa.972137

Gazi University
Journal of Science
PART A: ENGINEERING AND INNOVATION
http://dergipark.org.tr/gujsa

Artificial Neural Network Predictive Modelling of *luffa cylindrica* Seed Oil Antioxidant Yield

Kenechi NWOSU-OBIEOGU[1*]

[1]*Chemical Engineering Department, College of Engineering and Engineering Technology, Michael Okpara University, Umudike, Nigeria*

Keywords

ANN
Terpineol
Polyphenol
Antioxidant

Abstract

This study applied artificial neural network (ANN) in evaluating the models for terpineol and polyphenol yield from *luffa cylindrica* seed oil. The experiment was carried out at a temperature (60-80^{o}C), time (4-6 hours), and solvent/seed ratio (8-12 ml/g) with response as antioxidant yield. FTIR (Fourier Transform Infra-red Spectroscopy) revealed the presence of terpineol and polyphenol at peaks of 1461.1cm^{-1} and 3008.0cm^{-1} respectively. The ANN prediction indices are thus; terpineol (R^2= 9.9999E-1, MSE=2.25766E-9) and polyphenol (R^2=9.9999E-1, MSE=4.42588E-10). This study reveals that the ANN technique can successfully predict antioxidants from *luffa cylindrica* seed oil.

Cite

Nwosu-Obieogu, K. (2021). Artificial neural network predictive modelling of luffa cylindrica seed oil antioxidant yield. *GU J Sci, 8*(4), 494-504.

Author ID (ORCID Number)

K. Nwosu-Obieogu, 0000-0002-4920-8676

Article Process

Submission Date 15.07.2021
Revision Date 08.12.2021
Accepted Date 28.12.2021
Published Date 30.12.2021

1. INTRODUCTION

Antioxidants occur naturally in vegetables and fruits, prevents free radical attack and reduce carcinogenic disease risk (Karadžić Banjac et al., 2018). In addition, studies have revealed that food rich in antioxidants (flavonoids, polyphenols, vitamins and minerals) has positive health impacts. Hence, their regular consumption reduces cardiovascular diseases, vision problems, high blood cholesterol and cancer. (Ohlsson & Bengtsson, 2002; Liyana-Pathirana et al., 2006; Gonçalves et al., 2012).

Luffa cylindrica is a non-edible fibrous vegetable with fruits containing black seeds found in the tropics, a *Cucurbitaceae*, intensifying considerable attention from researchers to harness its potentials (Oboh &Aluyor, 2009). However, antioxidants in leaves and fruits of *luffa cylindrica* have been revealed to offer interesting economic values. (Oyetayo & Ojo, 2012).

Reports have shown that *luffa*-based derivatives constitute antioxidants such as terpineol, polyphenol present in our food, applied in the treatment of various ailments, and cosmetics production. (Vladimir-Knežević et al. 2011; Park et al., 2012; Zengin & Baysal, 2014; Akinsanmi et al., 2015; Shendge & Belemkar, 2018; Yu et al., 2018; Okla et al., 2019). (Vladimir-Knežević et al. (2011), Zengin & Baysal (2014), and Campone et al. (2020) have researched extensively on terpineol and polyphenol extraction from plants. However, the relationship between factors that affect the extraction process and its response (polyphenol/terpineol yield)) is uncertain and complex from earlier reports (Khaleel et al., 2018; Molina et al., 2019; Sales et al., 2020).

ANN has shown its capability of controlling imprecise relationships among variables (Maosudi et al., 2018); ANN comprises mathematical models that apply biological neurons in solving intricate and uncertain processes, hence can be relied upon than linear and multivariate statistical procedures that have shown their

*Corresponding Author e-mail: kenenwosuobie@mouau.edu.ng

inefficiency in handling nonlinear trends in data. (Almeida, 2002; Soto et al., 2019; Ojediran et al., 2020; Oke et al., 2020; 2021).

ANN modeling approach has been proven as a reliable technique in antioxidant yield estimation of plants, thus, the antioxidant properties of bananas (Guiné et al., 2015), beet-root (Kovacević et al., 2015), tea (Cimpoiu et al., 2011), polyphenols from green tea (Xi et al., 2013), essential oils (Cabrera & Prieto, 2010), polyphenols from pine fallen foliage (Vats & Negi, 2013), blueberries (Guiné et al., 2018) and lettuce (Karadžić Banjac et al., 2018) have been predicted successfully by ANN. However, there is sparse literature on antioxidant yield from vegetable seed oil. Thus, this study predicts polyphenol and terpineol yield from *luffa cylindrica* seed oil using the ANN model.

2. MATERIAL AND METHOD

2.1. Sample Preparation

Luffa cylindrica fruits were procured from nearby bushes at Amawom, Umuahia, Nigeria. The seed was winnowed, husks and dirt removed, after which it was sun-dried for easy removal of the shell and was also oven-dried at 60^{o}C to constant weight before grinding to increase the surface area for oil extraction.

The experimental matrix was designed using Design-Expert version 10, where Box-Behnken implementing response surface methodology on a three factors and three-level basis was employed to generate seventeen runs. The factors include time, temperature, and seed/solvent ratio, and the response is polyphenol/terpineol yield. The summary is shown in Table 1.

Table 1. *Design of Experiment*

Factors	**Units**	**Level**		
		-1	**0**	**1**
Temperature	^{o}C	60	70	80
Time	Hour	4	5	6
Solvent/seed	ml/g	8	10	12

2.2. Experimental Procedure

Luffa oil extraction process was carried out at Chemical Engineering Department laboratory, Michael Okpara University of Agriculture Umudike, Abia State, Nigeria, using the method described by (Afolabi et al., 2014). 40 g of grounded *luffa* seed was utilized for each experimental run. 250 cm^3 capacity Soxhlet apparatus and *n*-hexane of analytical grade was employed for the process. The solvent was recovered at every interval and the obtained oil was weighed, the oil yield was calculated using the equation below.

$$Y = \frac{M_o}{M_s} \times 100 \quad (1)$$

Where: Y : oil yield (%)

M_o : mass of oil extracted (g)

M_s : mass of *luffa* seed (g)

2.2.1. Terpineol Concentration Determination

The terpineol concentration was determined using a method modified by Ghorai et al. (2017). 0.1g of the *luffa* oil was introduced into a test tube, 1 ml methanol was added, placed in a water bath, it was stirred for 30minutes at a temperature of 100°C, 1 ml sulphuric acid was introduced, the colour turned to reddish-brown, it was allowed to stand for 30minutes then the absorbance was taken in a UV spectrophotometer, the standard curve was generated by treating the linalool as the sample with serial dilution.

2.2.2. Polyphenol Yield Determination

The total polyphenol content was determined using the Folin Ciocalteu method by Singleton & Rossi (1965). About 0.1g of the oil extract was weighed in a test tube, 1ml of methanol was introduced into a water bath and shaker, where it was allowed to shake for 30minutes at 40^0C. Next, the sample was removed, and 1ml of Folin-Ciocalteu and 2ml of 20% Na_2CO_3 were introduced; the mixture was allowed to stand for 10 minutes before it was stirred in a centrifuge for 20minutes at 400rpm; the absorbance was taken using a UV spectrophotometer at 625nm. The standard curve was generated by preparing different concentrations ranging from 10mg/l of Gallic acid.

2.2.3. FT-IR Analysis

Fourier transform infrared (FTIR) analysis was carried out to determine the functional groups present on *luffa oil* using the FTIR spectroscope (PerkinElmer Spectrum one v3.02 Spectrometer, India).

2.3. ANN Model Development

ANN modeling of the extraction process was developed using the neural fitting toolbox of MATLAB R2014b. The architecture consists of 3 input layers (temperature, time and solute/solvent ratio), two output layers (polyphenol and terpineol yield) and a hidden layer. The dataset obtained from the extraction process was split into (training, validation and testing) with 70%, 15%, and 15%. The ANN structure is presented in Figure 1. To determine the best algorithm for the prediction, MSE and R^2 were used as the statistical criteria to assess the algorithm's performance. (Uzuner & Cekmecelioglu, 2016; Masoudi et al., 2018; Nwosu-Obieogu et al., 2020).

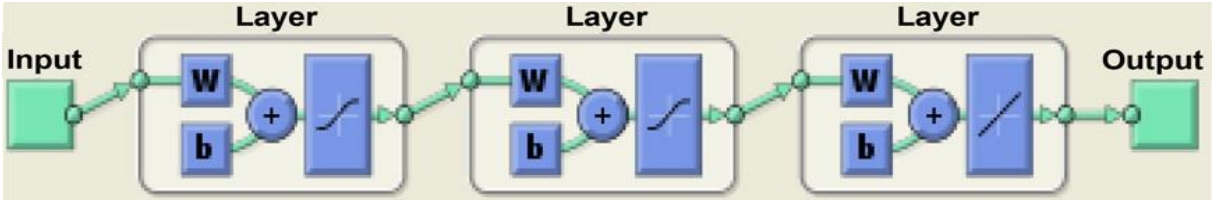

Figure. 1. *ANN Structure*

3. RESULTS AND DISCUSSION

3.1. Antioxidant Yields from *luffa* oil

The maximum terpineol yield of 2657 ml/g was obtained at a solvent/ solute concentration of 12mol/g, temperature of 80ºC, and a time of 5hours, while polyphenol yield of 609.37 ml/g was obtained at a solvent/solute ratio concentration of 10mol/g, the temperature of 80ºC and time of 6 hours as shown in Table 2, increase in process parameters led to an increase in terpineol and polyphenol yield, indicating that the factors had a significant effect on the antioxidant product (Afolabi et al.,2014; Oniya et al., 2017; Yu et al., 2018). The data were utilised in ANN prediction of terpineol and polyphenol yield (Nwosu-Obieogu et al., 2020).

The ANN-based model was developed based on the feed-forward, backpropagation (BP) algorithms. The hidden layer comprises ten neurons; the coefficient of determination (R^2) value at training, validation and testing is 1 for terpineol yield, while the polyphenol yield prediction gave 1 for training and testing, and 0.99996 for confirmation, as shown in Figure 2 and 3; these indicate the level of variability of the experimental results captured by the predicted. As shown in Table 3 and 4, the Bayesian regularization was the best of the algorithms for terpineol and polyphenol yield, having the smallest MSE of 2.25766E-9 and 4.42588E-10, respectively; the optimal results were obtained at epoch 901 and 701 for terpineol and polyphenol yield as shown in Figure 4 and 5, these comparisons indicate that the model predicted antioxidants yield from *luffa oil* appropriately; The effectiveness of the expected ANN model results is in agreement with reports from (Uzuner & Cekmecelioglu, 2016; Karadžić Banjac et al., 2018; Oke et al., 2020; Adeniyi et al., 2021).

***Table 2**. Experimental Values for the Total Terpineol/Polyphenol Yield*

Runs	Time (hours)	Temperature (ºC)	Solvent/seed ratio (ml/g)	Terpineol yield (g/ml)	Polyphenol yield (g/ml)
1	5	70	10	1613	258.43
2	5	70	10	1613	258.43
3	4	80	10	1091	266.67
4	4	70	12	1109	183.82
5	4	60	10	713	107.43
6	5	70	10	1613	258.43
7	6	80	10	1724	609.37
8	5	60	8	978	340.1
9	6	60	10	1858	228.35
10	5	80	8	1639	128.57
11	5	80	12	2657	393.16
12	5	70	10	1613	258.43
13	5	60	12	1700	156.86
14	5	70	10	1613	258.43
15	4	70	8	668	151.72
16	6	70	8	1534	145.35
17	6	70	12	2172	126.92

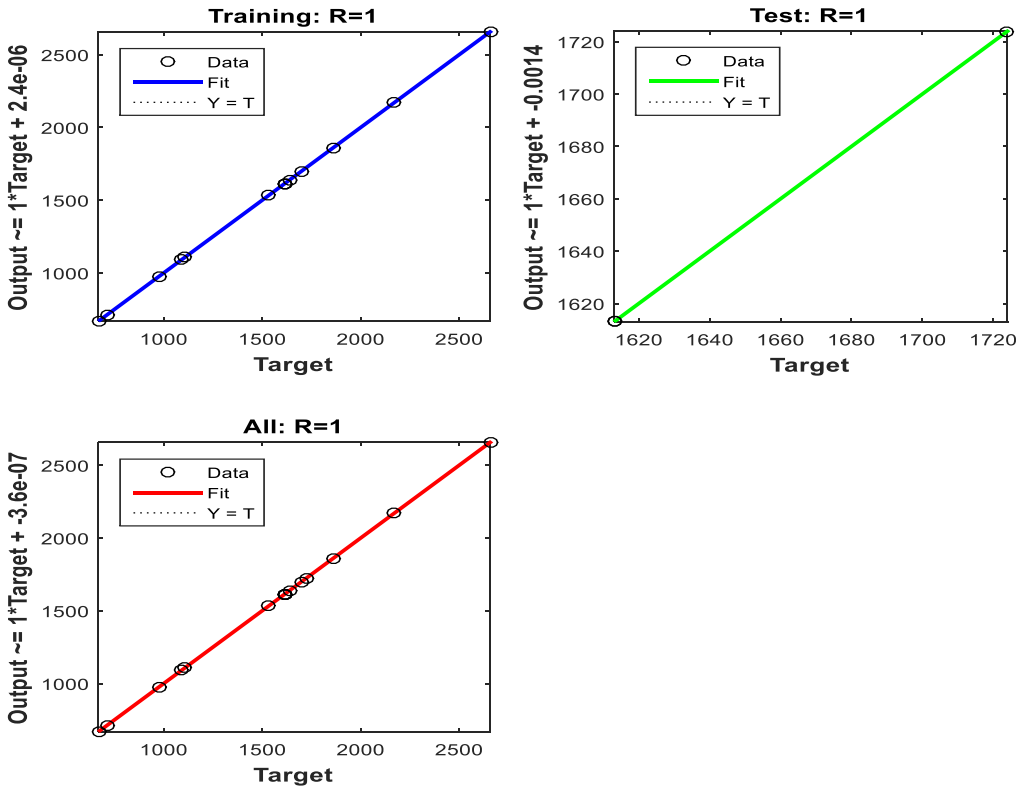

***Figure 2**. ANN Regression Graph for Terpineol Yield Prediction*

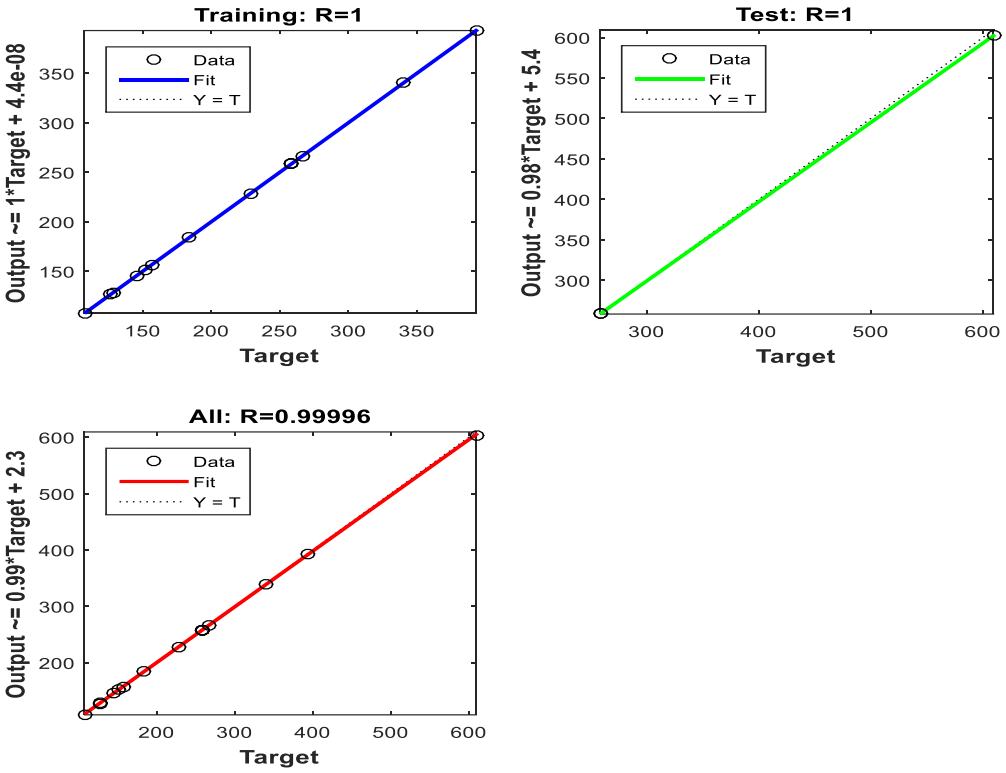

Figure 3. *ANN Regression Graph for Polyphenol Yield Prediction*

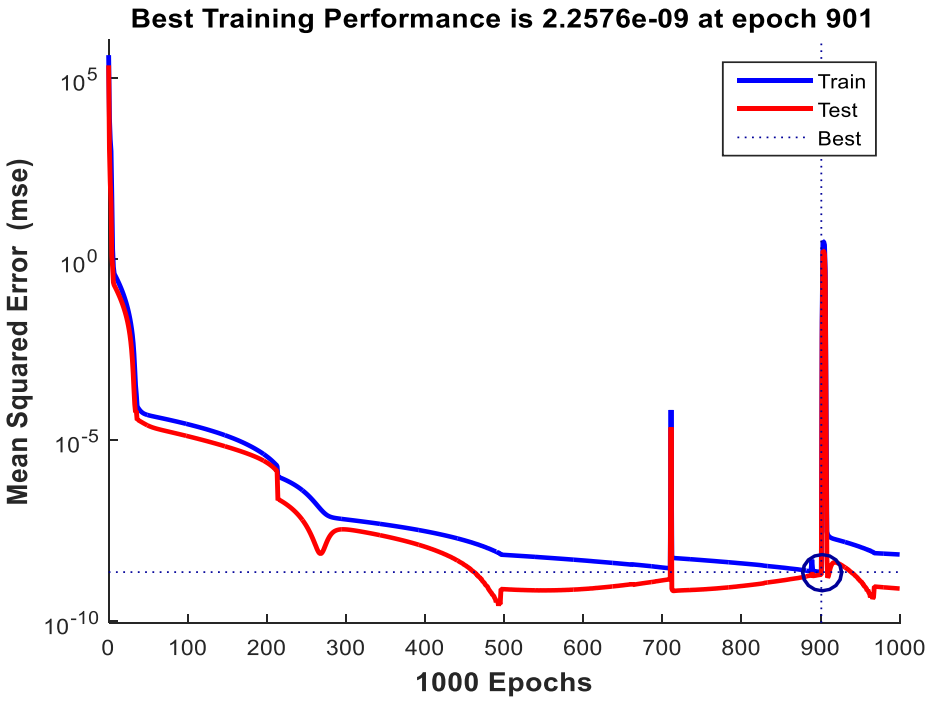

Figure 4. *Training Error (mean squared error, MSE) Curve for Terpineol Yield Prediction*

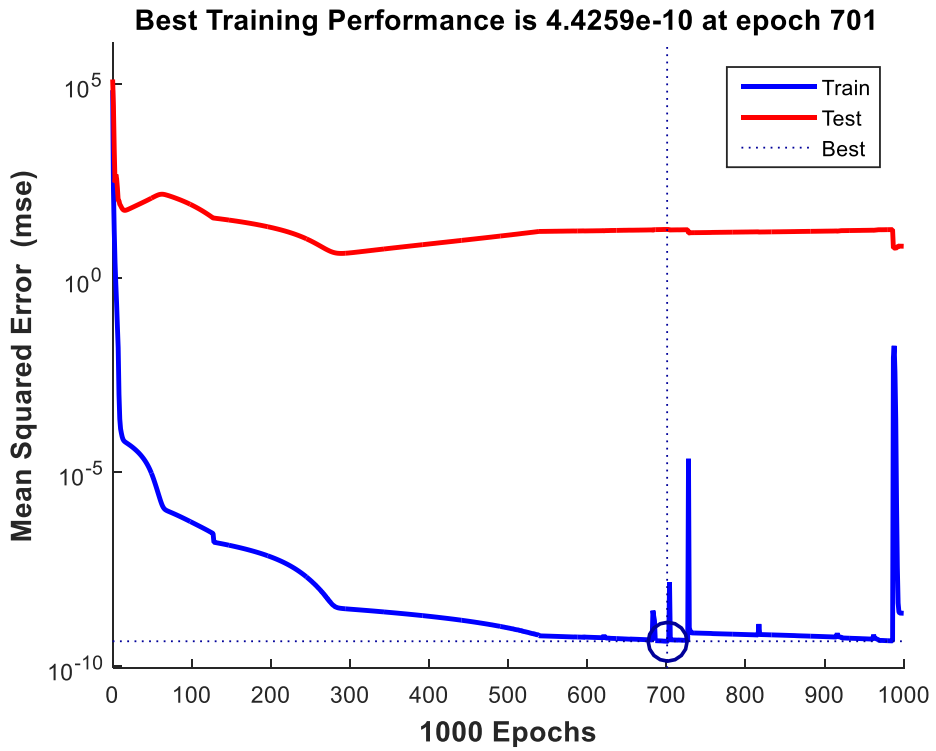

Figure 5. *Training Error (mean squared error, MSE) Curve for Polyphenol Yield Prediction*

Table 3. *Comparison of the ANN Algorithm for Terpineol Yield*

S/N	Algorithm	MSE	R^2
1	Levenberg-Marquardt	4523.36933E-0	0.9935
2	**Bayesian Regularization**	**2.25766E-9**	**0.9999**
3	Scaled Conjugate Gradient	401381.42860E-0	0.0011
4	*trainrp*	5.0602E4	0.9436
5	*traincgf*	1.1738E05	0.9998
6	*traincgp*	1.4700E05	0.9732
7	*traincgb*	1.2690E04	0.9889
8	*trainbfg*	1.3758E05	0.9829
9	*trainoss*	1.5833E04	0.9971
10	*traingd*	1.5693E06	0.3644
11	*traingdx*	2.0683E05	0.9433
12	*traingdm*	2.6889E06	0.8609

Table 5 shows the antioxidant yield of *luffa* oil compared to guava plant, lemon plant, Sorghum Moench and apple pomace; the yield of 2657mg/l for terpineol compared to the result of 348ml/g and 97ml/g for guava and lemon plant respectively and, 609.37ml/g of polyphenol compared to 313ml/g and 775 ml/g for sorghum Moench and apple pomace, respectively, indicates that *luffa* oil contains plenty of antioxidants that can be harnessed to proper use.

Table 4. *Comparison of the ANN Algorithm for Polyphenol Yield*

S/N	Algorithm	MSE	R^2
1	Levenberg-Marquardt	4.75287E-1	0.9998
2	**Bayesian Regularization**	**4.42588E-10**	**0.9999**
2	Scaled Conjugate Gradient	4220.33975E-0	0.8912
3	*trainrp*	1.2821E04	0.9315
4	*traincgf*	400.1718	0.9980
5	*traincgp*	3.2516E03	0.9998
6	*traincgb*	9.4288E03	0.9921
7	*trainbfg*	1.7404E04	0.5519
8	*trainoss*	648.1305	0.9924
9	*traingd*	2.7824E05	0.8954
10	*traingdx*	2.4738E03	0.8351
11	*traingdm*	1.4876E05	0.9994

Table 5*. Comparison of Terpineol and Polyphenol Present in Some Seed Oils with Luffa Seed Oil*

Oils	Terpineol yield (g/ml)	Polyphenol yield (g/ml)
Luffa seed oil (present study)		
Guava plant	348 (de Lima et al., 2010)	-
Lemon plant	97 (Ferhat et al., 2007)	
Sorghum Moench	-	313 (Liu et al., 2018)
Apple pomace		775 (Skrypnik &Novikova, 2020)

3.2. FTIR Result

The FT-IR results of the oil yield from *luffa cylindrica* is shown in Figure 6, the peak at 3008.0cm^{-1} can be ascribed to –OH stretching, which indicates the presence of polyphenol, two sharp-pointed peaks at 2922.2 cm^{-1} and 2855.1cm^{-1} indicated alkane group, another sharply pointed peak with value 1744 cm^{-1} indicates the presence of esters (6-membered lactone) with the structure C=O, hence the oil has high saponification value

and could be recommended for soap production. The shorter, smaller pointed peak with a vibrational mode at 1461.1 cm^{-1} indicates the presence of terpineol (Agatonovic-Kustrin et al., 2020), while a medium sharp peak was observed with a value of 1379 cm^{-1}, indicating an alkane of gem dimethyl group. The peak at 1237.5cm^{-1} indicates an alkyl aryl ether with structure C – O – C, while 987.7cm^{-1} and 723.1cm^{-1} peaks indicated alkene compounds. The presence of unsaturated hydrocarbons makes oil suitable for plastic and paint industries, as a drying agent in the production of cosmetics, and may be edible for animal feed (Oli et al., 2014).

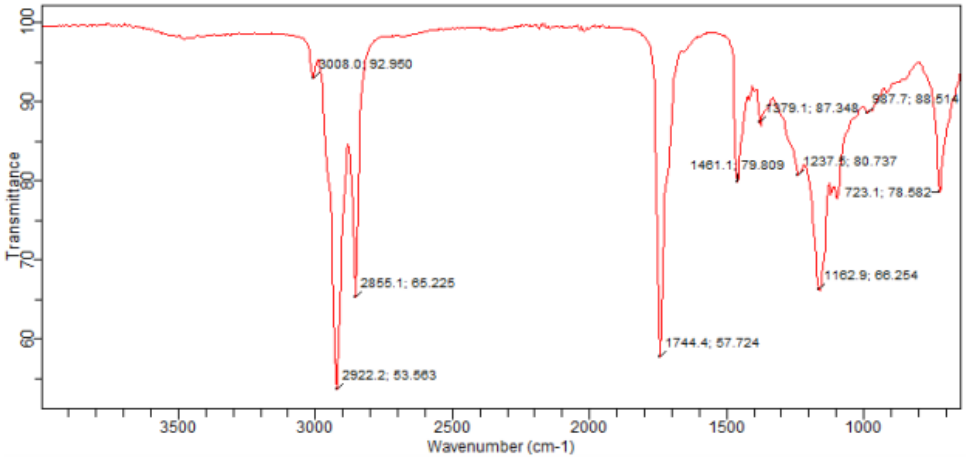

Figure 6 *FT-IR Result of the Oil Yield*

4. CONCLUSION

In this study, ANN has been applied to model antioxidant yields from *luffa* oil. Various conclusions were drawn from the findings. The coefficient of determination (R^2) value at validation was 1 for terpineol yield with optimal results obtained at epoch 901 and 0.99996 for polyphenol yield with optimal results obtained at epoch 701, the accuracy of the model was validated with experimental results. The study's findings are relevant in designing and developing a dynamic neural network controller for antioxidant production from vegetable seed oils.

ACKNOWLEDGEMENT

The author acknowledges the staff working in the unit operation laboratory, chemical engineering department, Michael Okpara University of Agriculture, Umudike, that assisted us with the necessary apparatus and reagents needed for the extraction process.

CONFLICT OF INTEREST

The author declares no conflict of interest.

REFERENCES

Adeniyi, A. G., Igwegbe, C. A. & Ighalo, J. O. (2021) ANN modelling of the adsorption of herbicides and pesticides based on sorbate-sorbent interphase. *Chemistry Africa*, *4*, 443-449. doi:10.1007/s42250-020-00220-w

Afolabi, T. J., Onifade, K. R., Akindipe, V. O. & Odetoye, T. E. (2014). Optimization of Solvent Extraction of *Parinari polyandra* Benth Seed Oil Using Response Surface Methodology. *British Journal of Applied Science & Technology*, *5*(5), 436-446.

Agatonovic-Kustrin, S., Ristivojevic, P., Gegechkori, V., Litvinova, T. M., Morton, D. W. (2020). Essential oil quality and purity evaluation via FT-IR spectroscopy and pattern recognition techniques. *Applied sciences*, *10*(20), 1-12. doi:10.3390/app10207294

Akinsanmi, A. O., Oboh, G., Akinyemi, J. A., & Adefagha, A. S. (2015). Assessment of the nutritional, antinutritional, and antioxidant capacity of unripe, ripe, and overripe plantain (*Musa paradisiaca*) peels. *International Journal of Advanced Research*, *3*(2), 63-72.

Almeida, J. S. (2002) Predictive Non-linear Modelling of Complex Data by Artificial Neural Networks. *Current Opinion in Biotechnology*, 13(1), 72-76. doi:10.1016/s0958-1669(02)00288-4

Cabrera, A. C. & Prieto, J. M. (2010) Application of artificial neural networks to the prediction of the antioxidant activity of essential oils in two experimental *in vitro* models. *Food Chemistry*, *118*(1), 141-146. doi:10.1016/j.foodchem.2009.04.070

Campone, L., Celano, R., Rizzo, S., Piccinelli, A. L., Rastrelli, L., & Russo, M. (2020). Development of an Enriched Polyphenol (Natural Antioxidant) Extracts from Orange Juice (*Citrus sinensis)* by Adsorption on Macroporous Resins. *Journal of Food Quality*, 1251957, 1-9. doi:10.1155/2020/1251957

Cimpoiu, C., Cristea, V-M., Hosu, A., Sandru, M., & Seserman, L. (2011) Antioxidant activity prediction and classification of some teas using artificial neural networks. *Food Chemistry*, *127*(3), 1323-1328. doi:10.1016/j.foodchem.2011.01.091

de Lima, R. K., Cardoso, M. das G., Andrade, M. A., Nascimento, E. A., de Morais, S. A. L., & Nelson, D. L. (2010). Composition of the essential oil from the leaves of tree domestic varieties and one wild variety of the guava plant (Psidium guajava L., Myrtaceae). *Revista Brasileira de Farmacognosia*, *20*(1), 41-44. doi:10.1590/S0102-695X2010000100009

Ferhat, M. A., Meklati, B. Y., & Chemat, F. (2007). Comparison of different isolation methods of essential oil from *Citrus* fruits: cold pressing, hydrodistillation and microwave 'dry' distillation. *Flavour and Fragrance Journal*, *22*(6), 494-504. https://doi.org/10.1002/ffj.1829

Ghorai, N., Chakraborty, S., Gucchait, S., Saha, S. K., & Biswas, S. (2012). Estimation of total terpenoids concentration in plant tissues using a monoterpene, linalool as the standard reagent. *Protocol Exchange*. doi:10.1038/PROTEX.2012.055

Gonçalves, F. J., Rocha, S. M., & Coimbra, M. A. (2012) Study of the retention capacity of anthocyanins by wine polymeric material. *Food Chemistry*, *134*(2), 957-963. doi:10.1016/j.foodchem.2012.02.214

Guiné, R. P. F., Barroca, M. J., Gonçalves, F. J., Alves, M., Oliveira, S., & Mendes, M. (2015) Artificial neural network modelling of the antioxidant activity and phenolic compounds of bananas submitted to drying treatments. *Food Chemistry, 168*, 454-459. doi:10.1016/j.foodchem.2014.07.094

Guiné, R. P. F, Matos, S., Goncalves, F. J., Costa, D. & Mendes M. (2018) Evaluation of phenolic compounds and antioxidant activity of blueberries and modelization by artificial neural networks. *International Journal of Fruit Science*, *18*(2), 199-214. doi:10.1080/15538362.2018.1425653

Karadžić Banjac, M. Ž., Kovačević, S. Z., Jevrić, L. R., Podunavac-Kuzmanović, S. O., Tepić Horecki, A. N., Vidović, S. S., Šumić, Z. M., Ilin, Ž. M., Adamović, B. D., & Kuljanin, T. A. (2018). Artificial neural network modelling of the antioxidant activity of lettuce submitted to different postharvest conditions. *Journal of Food Processing and Preservation*, *43*(3), e13878. doi:10.1111/jfpp.13878

Khaleel, C., Tabanca, N., & Buchbauer, G., (2018). α-Terpineol, a natural monoterpene: A review of its biological properties. *Open Chemistry*, *16*(1), 349-361. doi:10.1515/chem-2018-0040

Kovacević, S. Z., Jevrić, L. R., Podunavac-Kuzmanović, S. O., Kalaidiziia, N. D., & Loncar, E. S. (2015) Quantitative structure-retention relationship analysis of some xylofuranose derivatives by linear multivariate method. *Acta Chimica Slovenica*, *60*(2), 420-428. doi:10.17344/acsi.2014.888

Liu, L., Chen, L., Abbasi, A. M., Wang, Z., Li, D., & Shen, Y. (2018) Optimization of extraction of polyphenols from Sorghum Moench using response surface methodology, and determination of their antioxidant activities. *Tropical Journal of Pharmaceutical Research*, *17*(4), 619-626. doi:10.4314/tjpr.v17i4.8

Liyana-Pathirana, C. M., Shahidi, F., & Alasalvar, C. (2006). Antioxidant activity of cherry laurel fruit (*Laurocerasus officinalis Roem*.) and its concentrated juice. *Food Chemistry*, *99*(1), 121-128. doi:10.1016/j.foodchem.2005.06.046

Maosudi, S., Sima, M., & Tolouei-Rad, M. (2018). Comparative study of ANN and ANFIS models for predicting temperature in machining. *Journal of Engineering Science and Technology*, *13*(1), 211-225.

Molina, G., Pessôa, M. G., Bicas, J. L., Fontanille, P., Larroche, C., & Pastore, G. M. (2019). Optimization of limonene biotransformation for the production of bulk amounts of α-terpineol. *Bioresource Technology*, *294*, 122180. doi:10.1016/j.biortech.2019.122180

Nwosu-Obieogu, K., Aguele, F. & Chiemenem, L. I. (2020) Soft computing prediction of oil extraction from huracrepitan seeds. *Kem. Ind.*, *69*(12), 653-658. doi:10.15255/KUI.2020.006

Oboh, I. O. & Aluyor, E. O. (2009). *Luffa cylindrica*-an emerging cash crop. *African Journal of Agricultural Research*, *4*(8), 684-688. doi:10.5897/AJAR.9000476

Ohlsson, T. & Bengtsson, N. (2002). *Minimal processing technologies in the food industry*. Woodhead Publishing.

Ojediran, J. O., Okonkwo, C. E., Adeyi, A. J., Adeyi, O., Olaniran, A. F., George, N. E., & Olayanju, A. T. (2020) Drying characteristics of yam slices (*Dioscorea rotundata*) in a convective hot air dryer: application of ANFIS in the prediction of drying kinetics. *Heliyon*, *6*(3), e03555. doi:10.1016/j.heliyon.2020.e03555

Oke, E. O., Nwosu-Obieogu, K., & Ude, J. C. (2020) Experimental Study and Exergy Efficiency Prediction of Three-Leaved Yam (*Dioscorea Dumetorum*) Starch Drying. *International Journal of Exergy*, *33*(4), 427-443. doi:10.1504/IJEX.2020.111690

Oke, E. O., Nwosu-Obieogu, K., Okolo, B., I., Adeyi, O., Omotoso, A. O., & Ude, C. U. (2021) *Hevea brasiliensis* oil epoxidation: hybrid genetic algorithm–neural fuzzy–Box–Behnken (GA–ANFIS–BB) modelling with sensitivity and uncertainty analyses. *Multiscale and Multidisciplinary Modelling, Experiments and Design*, 4, 131-144. doi:10.1007/s41939-020-00086-y

Okla, M. K., Alamri, S. A., Salem, M. Z. M., Ali, H. M., Behiry, S. I., Nasser, R. A., Alaraidh, I. A., Al-Ghtani, S. M., & Soufan, W. (2019). Yield, Phytochemical Constituents, and Antibacterial Activity of Essential Oils from the Leaves/Twigs, Branches, Branch Wood, and Branch Bark of Sour Orange (*Citrus aurantium L.*). *Processes*, *7*(6), 363. doi:10.3390/pr7060363

Oli, C. C., Onuegbu, T. U., & Ezeudu. E. C. (2014). Proximate composition, characterization, and spectroscopic analysis of luffa aegyptiaca seed. *International Journal of Life Sciences Biotechnology and pharma Research*, *3*(4), 194-200.

Oniya, O. O., Oyelade, J. O., Ogunkunle, O., & Idowu, D. O. (2017) Optimization of Solvent extraction of Oil from Sandbox Kernels (*Hura crepitans L.*) by a Response Surface Method. *Energy and Policy Research*, *4*(1), 36-43. doi:10.1080/23815639.2017.1324332

Oyetayo, F. L., & Ojo, B. A., (2012). Food value and phytochemical composition of *Luffa cylindrica* seed flour. *American Journal of Biochemistry*, *2*(6), 98-103. doi:10.5923/j.ajb.20120206.02

Park, S-N., Lim, Y. K., Friere, M. O., Cho, E., Jin, D., & Kook, J-K. (2012). Antimicrobial effect of linalool and α-terpineol against periodontopathic and cariogenic bacteria. *Anaerobe*, *18*(3) 369-372. doi:10.1016/j.anaerobe.2012.04.001

Sales, A., Felipe, L. de O., & Bicas, J. L. (2020). Production, Properties, and Applications of α-Terpineol. *Food and Bioprocess Technology*, *13*, 1261-1279. doi:10.1007/s11947-020-02461-6

Shendge, P. N., & Belemkar, S., (2018). Therapeutic Potential of *Luffa acutangula*: A Review on Its Traditional Uses, Phytochemistry, Pharmacology and Toxicological Aspects. *Frontiers in Pharmacology*, *9*. doi:10.3389/fphar.2018.01177

Singleton, V. L., & Rossi, J. A., (1965). Colorimetry of total phenolics with phosphomolybdic-phosphotungstic acid reagents. *Am J Enol Vitic*, *16*(3), 144-158.

Skrypnik, L., & Novikova, A. (2020) Response Surface Modeling and Optimization of Polyphenols Extraction from Apple Pomace Based on Nonionic Emulsifiers. *Agronomy*, *10*(1), 92. doi:10.3390/agronomy10010092

Soto, J., Castilo, O., Melin, P., & Pedrycz, W. (2019) A new approach to multiple time series predictions using MIMO fuzzy aggregation models with modular neural networks. *International Journal of Fuzzy Systems*, *21*, 1629-1648. doi:10.1007/s40815-019-00642-w

Uzuner, S., & Cekmecelioglu, D. (2016). Comparison of Artificial neural networks (ANN) and Adaptive Neuro-fuzzy inference system (ANFIS) models in simulating polygalacturonase production. *Bioresources*, *11*(4), 8676-8685. doi:10.15376/biores.11.4.8676-8685

Vats, S. & Negi, S. (2013) Use of artificial neural network (ANN) for the development of bioprocess using *Pinus roxburghii* fallen foliages for the release of polyphenols and reducing sugars. *Bioresource Technology*, *140*, 392-398. doi:10.1016/j.biortech.2013.04.106

Vladimir-Knežević, S., Blaženković, B., Štefan, M. B. & Babac, M. (2011). Plant polyphenols as antioxidants influencing the human health. In: V. Rao (Eds.), *Phytochemicals as Nutraceuticals - Global Approaches to Their Role in Nutrition and Health* (pp. 155-180), IntechOpen. doi:10.5772/27843

Xi, J., Xue, Y., Xu, Y. & Shen, Y. (2013) Artificial neural network modelling and optimization of ultrahigh-pressure extraction of green tea polyphenols. *Food Chemistry*, *141*(1), 320-326. doi:10.1016/j.foodchem.2013.02.084

Yu, L., Jin, W., Li, X., & Zhang, Y. (2018). Optimization of bioactive ingredient extraction from Chinese herbal medicine *Glycyrrhiza glabra*: a comparative study of three optimization models. *Evidence-Based Complementary and Alternative Medicine*, 6391414. doi:10.1155/2018/6391414

Zengin, H., & Baysal, A. H. (2014). Antibacterial and antioxidant activity of essential oil terpenes against pathogenic and spoilage-forming bacteria and cell structure-activity relationships evaluated by SEM microscopy. *Molecules*, *19*(11), 17773-17798. doi:10.3390/molecules191117773

Research Article / Araştırma Makalesi GU J Sci, Part A, 8(4): 505-514 (2021) https://doi.org/10.54287/gujsa.1009605

Gazi University
Journal of Science
PART A: ENGINEERING AND INNOVATION
http://dergipark.org.tr/gujsa

Rh_2CoX (X=Al, Ga ve In) Bileşiklerinin Yapısal, Elastik, Elektronik ve Manyetik Özellikleri

Rh_2CoX (X=Al, Ga and In) Compounds Structural, Elastic, Electronic and Magnetic Properties

Ziya MERDAN[1*], Fadime I. BALMUMCU[1]

[1]*Gazi University, Sciences Faculty, Department of Physics, 06500, Ankara, Turkey*

Anahtar Kelimeler

Elektronik Yapı
Full Heusler Bileşikleri
DFT
Elastik Özellik
GGA-PBE

Özet

Bu çalışmada full Heusler tipi Rh_2CoX (X=Al, Ga ve In) bileşiklerinin yapısal özellikleri yoğunluk fonksiyonel teorisi kullanılarak incelenmiştir. Rh_2CoX (X=Al, Ga ve In) bileşikleri için hesaplanan örgü sabiti ve magnetizasyon değerleri literatür sonuçları ile uyumludur. Literatürde mevcut olan bulgulara ilaveten ab-initio toplam enerji hesaplamaları yapan VASP programı ile yeni veriler eklenmiş ve bileşiklerin bant, DOS yapıları ve elektronik özellikleri üzerine yoğunlaşılmıştır. Ayrıca bileşikler için elastik sabitler hesaplanmıştır ve elde edilen elastik sabitler bu bileşiklerin mekanik kararlı yapıda olduklarını göstermektedir.

Keywords

Electronic Structure
Full Heusler Compunds
DFT
Elastic Property
GGA-PBE

Abstract

Density functional theory was used to investigate the structural properties of full Heusler type Rh_2CoX (X=Al, Ga ve In) compounds in the present study. When the calculated lattice constant and magnetization values for Rh_2CoX (X=Al, Ga ve In) compounds are consistent with the literature results. In addition to the previously published findings, new data were added using the VASP program, which performs ab-initio total energy calculations and focuses on the band, DOS structures and electronic properties of the compounds. Furthermore, elastic constants for the compounds were calculated, and it was showed that these compounds were mechanically stable using the elastic constants obtained.

Alıntı / Cite

Merdan, Z., Balmumcu, F.I. (2021). Rh_2CoX (X=Al, Ga ve In) bileşiklerinin yapısal, elastik, elektronik ve manyetik özellikleri, *GU J Sci, Part A, 8*(4), 505-514.

Yazar Kimliği / Author ID (ORCID Number)

Z. Merdan, 0000-0001-8708-8583
F. I. Balmumcu, 0000-0001-7011-110X

Makale Süreci / Article Process

Başvuru Tarihi / Submission Date 22.10.2021
Revizyon Tarihi / Revision Date 20.12.2021
Kabul Tarihi / Accepted Date 29.12.2021
Yayım Tarihi / Published Date 30.12.2021

1. GİRİŞ

Heusler tipi bileşikler 1903 yılında Friedrich Heusler tarafından CuMn bileşiklerine 3. grup eklenmesi ile bulunmuştur ve bu bileşiklerin ferromanyetik bir malzemeye dönüştüğü keşfedilmiştir (Heusler, 1903). Heusler bileşikleri yarı Heusler, tam Heusler ve dörtlü Heusler olmak üzere üçe ayrılmakadır. $C1_b$ (No:216) kristal yapısında olan yarı Heusler bileşikler XYZ kimyasal formülüne sahiptir (Otto vd., 1987; 1989; Offernes vd., 2008). $L2_1$ (No:225) kristal yapısında olan tam Heusler bileşikler X_2YZ kimyasal formülüne sahiptir (Villars & Calvert, 1991). LiMgPdSn-tipi kristal yapısında olan dörtlü Heusler bileşikler ise XX'YZ kimyasal formülüne sahiptir.

XYZ kimyasal formülüne sahip yarı-Heusler bileşikleri F-43m uzay grubundadır, stokiyometrik kompozisyonu 1:1:1 şeklinde olup üç tane iç içe girmiş fcc alt örgüsünden oluşmaktadır. X_2YZ kimyasal

*Sorumlu Yazar / Corresponding Author, e-mail: ziyamerdan@gazi.edu.tr

formülüne sahip tam Heusler bileşikleri Fm-3m uzay grubundadır ve stokiyometrik kompozisyonu 2:1:1 şeklinde verilmektedir (Xing vd., 2009). XX'YZ kimyasal formülüne sahip olan dörtlü Heusler bileşikleri ise F-43m uzay grubunda yer almaktadır ve stokiyometrik kompozisyonu 1:1:1:1 şeklindedir (Xu vd., 2013). Tam Heusler bileşiklerinde, X ve Y genellikle iki farklı geçiş metali iken Z manyetik olmayan III-VI A grubu yani sp grubu elementidir. Dörtlü Heusler bileşiklerinde X, X' ve Y elementleri periyodik tablonun geçiş metali grubunda olup Z elementleri ise periyodik tablonun ana grup elementidir ve dörtlü Heusler bileşikleri için LiMgPdSn yapısı örnek olarak gösterilebilir (Eberz vd., 1980; Xu vd., 2013).

Heusler tipi bileşiklerin en önemli özelliği, bileşikleri oluşturan elementlerin bir araya geldiklerinde ferromanyetik özelliklerinin değişebilmesidir. Ferromanyetik özellik gösteren bu bileşikler, metal ya da yarı metalik özellik göstermektedirler. Spintronik (Žutić vd., 2004) ve termodinamik uygulamalarda önemli bir yere sahip olan tam Heusler bileşikleri ferromanyetik yarı metal davranışlarının yanı sıra şekil hatırlatma özelliği ve manyetik özellikleri nedeniyle önemli ölçüde dikkat çekmektedir. Heusler bileşiklerinin başlıca uygulama alanları; manyetik sensörler, manyetik hafızalar, spintronik sistemleridir. Ayrıca tünelleme manyetik direnç, spin enjeksiyon cihazlarının ve polarize ışık yayan LED üretiminde de kullanılmaktadır.

Heusler bileşikleri sahip oldukları bu özelliklerinden dolayı son yıllarda bir çok araştırmaya konu olmuştur. Ancak Rh_2CoX (X=Al, Ga ve In) bileşiklerinin elektronik ve manyetik özellikleri ile ilgili bugüne kadar kapsamlı bir çalışma yapılmamıştır. Sadece M. Gillben'in (Gilleßen, 2009) yapmış olduğu doktora tez çalışmasında Rh_2CoX (X=Al, Ga ve In) bileşikleri için örgü sabiti ve toplam manyetik değerleri incelenmiştir. Bu çalışmada ise, Vienna Ab initio Simulation Package (VASP) programı kullanılarak Rh_2CoX (X=Al, Ga ve In) bileşikleri için örgü sabitleri, manyetik moment değerleri ve elastik özellikler incelenmiştir. Elde edilen sonuçlar literatürde mevcut veriler ile karşılaştırılmıştır.

2. MATERYAL VE METOT

Değiş-tokuş ve korelasyon etkileri standart Yoğunluk Fonksiyon Teorisi'nde (DFT) Yerel Yoğunluk Yaklaşımı (LDA) veya Genelleştirilmiş Gradyant Yaklaşımı (GGA) ile ele alınmaktadır. Bu çalışmada değiş-tokuş kolerasyon enerjisi için Perdew-Burke-Ernzerhof (PBE), GGA Yaklaşımı kullanılmıştır (Kresse & Hafner, 1993; 1994; Kresse & Furthmüller, 1996a, b; Perdew vd., 1996). Rh tabanlı Rh_2CoX (X=Al, Ga ve In) bileşiklerin yapısal ve manyetik özellikleri VASP programı kullanılarak incelenmiştir. Dalga fonksiyonlarının açılımında kullanılan düzlem dalga taban kümesi için kesme kinetik enerji değeri 500 eV olarak belirlenmiştir. Tüm grafikler Orijin Pro 8.0 programı ile çizilmiştir ve tüm parametrelerin sabit tutulması ile VASP Mede-A paket programı yardımıyla Rh_2CoX (X=Al, Ga ve In) bileşikleri için elastik sabitler elde edilmiştir.

Vienna Ab initio Simulation Package (VASP) (Kresse & Joubert, 1999) programının temeli Mike Payne (Chadi & Cohen, 1973) tarafından oluşturulmuş olan bir programa dayanmaktadır ve yoğunluk fonksiyonel teorisi içinde düzlem dalga setleri, pseudo potansiyeller, PAW metodu ve iz düşümsel birleştirilmiş dalga yapılarını kullanarak ab initio moleküler dinamik ve kuantum mekaniksel simülasyonları yapabilmektedir. Ayrıca VASP programı aracılığı ile termodinamik ve manyetik özellikler, dinamik özellikler, mekanik özellikler, yapısal özellikler, optik özellikler, atomik kuvvetler, durgun dielektrik tensörü gibi temel fiziksel özellikler başarılı bir şekilde hesaplanabilmektedir.

3. BULGULAR VE TARTIŞMA

3.1. Yapısal ve Elastik Özellikler

Atomların kristal sistemlerindeki diziliş biçimi örgü yapıyı oluşturmaktadır. Atomik pozisyonlar kristal yapıyı ve malzemenin özelliklerini anlamak için büyük önem taşımaktadır. Rh_2CoX (X=Al, Ga ve In) bileşiklerinin kristal yapıları Şekil 1'de gösterilmiştir.

Tam Heusler bileşikleri $L2_1$ formunda Fm-3m uzay gruplu ve yüzey merkezli kübik yapıda kristalleşmektedir. Rh_2CoX (X=Al, Ga ve In) bileşikleri için örgü sabitleri ve manyetik moment değerleri elde edilerek bu değerler Tablo 1'de sunulmaktadır. Rh_2CoX (X=Al, Ga ve In) bileşikleri için hesaplanan değerlerin literatür ile uyumlu olduğu görülmektedir.

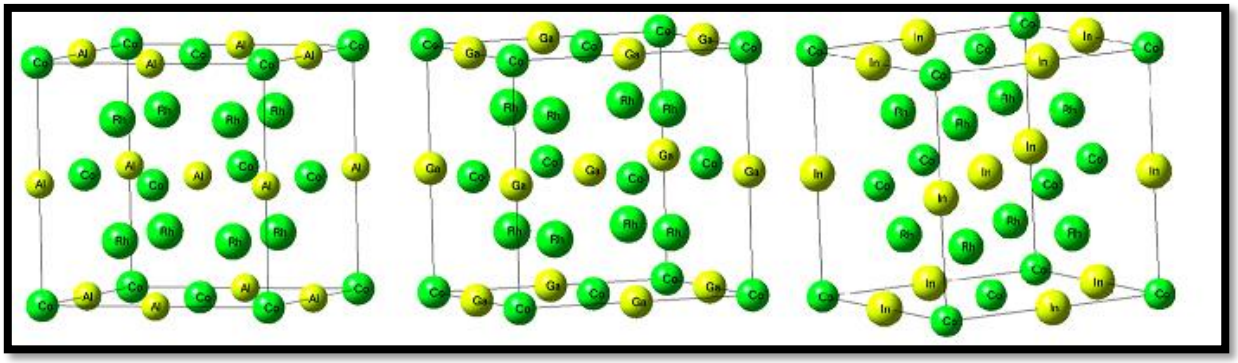

Şekil 1. *Rh_2CoX (X=Al, Ga ve In) Full Heusler Bileşiklerinin Kristal Yapıları*

Tablo 1*. Örgü Sabitleri (A^0) ve Manyetik Moment Değerleri (μ_B/f.u)*

Bileşik	a_0 (Å) (Bu çalışma)	a_0 (Å) Teori (Gilleßen, 2009)	M (μ_b/f.u.) (Bu çalışma)	M (μ_b/f.u.) Teori (Gilleßen, 2009)
Rh_2CoAl	5.9359	5.979	3.2730	3.02
Rh_2CoGa	5.9605	5.998	3.2763	3.00
Rh_2CoIn	6.1859	6.222	3.2636	3.00

Bir katının elastik sabitleri o kristal için dinamiksel ve mekaniksel özellikleri arasında bağlantı kurmaktadır. Elastik sabitleri, kristalin sertlik ve kararlılığı hakkında önemli bilgiler vermektedir ve elastik sabitlerinin doğru bir şekilde hesaplanmasından elde edilen bilgiler sayesinde, sert malzeme tasarımında ve katının makroskopik mekaniksel özelliklerinin araştırılmasında önemli bir yere sahiptir. Ayrıca bir dış zorlanmaya karşı kristalin gösterdiği tepkiler ve en yakın komşu atomlar arasındaki bağ şiddetleri elastik sabitlerden yararlanılarak elde edilebilmektedir.

Elastik sabitleri hesaplamak amacıyla temelde iki yöntem mevcuttur. Bunlardan birincisi, kristalin birim hücresinin hacmini koruyacak şekilde belirli ve küçük bir deformasyon uygulamaktır. Diğeri ise, zor-zorlanma ilişkisinin orantı katsayısı olarak alınmasıdır. Bir kübik kristal C_{11}, C_{12} ve C_{44} olmak üzere üç tane bağımsız ikinci mertebeden elastik sabitine sahiptir (Rassoulinejad-Mousavi vd., 2016; Luan vd., 2018). Elastik sabitleri C_{ij} şeklinde gösterilmektedir ve Rh_2CoX (X=Al, Ga ve In) bileşikleri için elde edilen değerler Tablo 2'de verilmiştir. Kübik kristallerin mekanik kararlı olabilmeleri için Born kararlılık kriterlerini sağlaması gerekmektedir ve bu koşullar aşağıda verilmiştir (Wu vd., 2007; Mogulkoc, vd., 2013; Mouhat & Coudert, 2014);

$$C_{11} > 0, C_{44} > 0, C_{11} > |C_{12}|, (C_{11} + 2C_{12}) > 0 \quad (1)$$

Buna göre Rh_2CoX (X=Al, Ga ve In) bileşiklerinin Born Kararlılık kriterlerini sağladığı ve mekaniksel kararlı oldukları sonuçlarına varılmıştır.

Tablo 2. *Rh_2CoX (X=Al, Ga ve In) Bileşikleri için Hesaplanan Elastik Sabitleri C_{ij} (C_{11}, C_{12} ve C_{44})*

Bileşik	C_{11} (Gpa)	C_{12} (Gpa)	C_{44} (Gpa)
Rh_2CoAl	279.881	182.560	116.428
Rh_2CoGa	270.706	182.929	111.689
Rh_2CoIn	216.149	169.165	84.528

Elastik sabitleri aracılığıyla, Bulk modülü (B), İzotropik kayma (Shear) modülü, Poisson oranı, Young modülü (E), Debye sıcaklığı ve Ortalama ses hızları hesaplanabilmektedir. Hesaplamalar için kullanılan formüller aşağıda verilmiştir;

$$B = \frac{1}{3}(C_{11} + 2C_{12}) \tag{2}$$

$$G = \frac{1}{5}(C_{11} - C_{12} + 3C_{44}) \tag{3}$$

$$C' = \frac{1}{2}(C_{11} - C_{12}) \tag{4}$$

$$C'' = (C_{11} - C_{44}) \tag{5}$$

$$E = \frac{9BG}{3B + G} \tag{6}$$

Kristalin birim hücresi denge durumunda iken küçük zorlamalar uygulanmış ve enerjideki değişimden yararlanılarak Bulk modülü (B) hesaplamaların gerçekleştirilmiş olduğu VASP (Mede-A) programı aracılığı ile elde edilmiştir. Ayrıca, Rh_2CoX (X=Al, Ga ve In) bileşikleri için Shear modülü (G), B/G oranı, Young Modülü (E) ve Poisson oranları (ν) hesaplanmıştır ve Rh_2CoX (X=Al, Ga ve In) bileşikleri için yapılan hesaplama sonuçları Tablo 3'te yer almaktadır.

Tablo 3. *Rh_2CoX (X=Al, Ga ve In) Bileşikleri için Hesaplanan Bulk Modülü (B), Shear Modülü (G), B/G Oranı, Young Modülü (E) ve Poisson Oranı (ν)*

Bileşik	B	G	B/G	E	ν
Rh_2CoAl	215.000	82.048	2.620	218.365	0.331
Rh_2CoGa	212.188	76.800	2.763	205.596	0.339
Rh_2CoIn	184.826	50.782	3.640	139.564	0.374

Shear modülü ve Bulk modülü katıların sertliğinin bir ölçüsüdür. Farklı bileşikler kıyaslandığında bulk modülü en büyük olan bileşik en az sıkışabilirlik değerine sahip olduğu yorumunu yapılabilmektedir. Young modülü, gerilme zoruna karşılık gelen gerilme zorlanmasının oranı olarak ifade edilmektedir ve malzeme sert ise Young modülü yüksektir. Dışarıdan gelen bir kuvvetten dolayı katı cismin çapının ne kadar büyüyüp küçüleceğini Poisson oranı vermektedir. Kovalent materyallar için poisson oranı 0,1'dir ve iyonik materyaller için 0,25'tir. Eğer poisson oranı 0.5'e yaklaşırsa bulk modülü kayma modülünden daha büyük hale gelir ve malzeme sıkıştırılamaz. Poisson oranı 1'e yaklaştığında malzeme son derece sıkıştırılabilir olurken, kesme gerilimleri altında şekil değişikliğine karşı direnci artmaktadır. Pugh'a (Pugh, 1954) göre B/G oranı 1.75'ten büyükse malzeme sünek davranış gösterirken, B/G oranı 1.75'ten küçük ise malzeme kırılgan davranış göstermektedir (Perdew vd., 1993; Mouhat & Coudert, 2014). Tablo 3'te verilen değerlere göre Rh_2CoX (Al, Ga ve In) bileşikleri için hesaplanan B/G oranı kritik değer olan 1.75 ten büyük olduğu için Rh_2CoX (X=Al, Ga ve In) bileşiklerinin sünek yapıda oldukları gözlemlenmiştir.

Elde edilen örgü sabit değerleri literatür ile karşılaştırıldığında Michael Gilleßen (Gilleßen, 2009) tarafından 2009 yılında yapılan tez çalışmasına göre Rh_2CoAl için örgü sabit değeri yaklaşık % -0.72, Rh_2CoGa için örgü sabit değeri yaklaşık % -0.63 farkla ve Rh_2CoIn için örgü sabit değeri yaklaşık % -0.58 farkla elde edilmiştir. Dolayısı ile örgü sabiti için elde edilen hesaplama sonuçlarının, literatürde mevcut çalışma ile uyumlu olduğu görülmektedir.

Bir kristalin bant yapısının bilinmesi o malzemenin; mekanik özellikleri, manyetik özellikleri, optik özellikleri, elektronik özelliklerinden kaynaklanan yapısal bozulmalar ve elektronik iletkenliği gibi birçok özelliğinin belirlenmesinde önemli rol oynamaktadır (Galanakis vd., 2006; Gilleßen & Dronskowski, 2009; 2010). Denge durumundaki örgü sabitleri kullanılarak $L2_1$ kristal yapısındaki Rh_2CoX (X=Al, Ga ve In) bileşiklerinin yüksek simetri yönleri boyunca elektronik bant yapısı Şekil 2'de gösterilmiştir.

Rh_2CoX (X=Al, Ga ve In) bileşiklerinin elektronik bant yapısı eğrileri temel simetri yönleri boyunca hem spin aşağı hem de spin yukarı durumları için çizdirilmiştir. Fermi seviyeleri sıfır olarak alınmıştır ve Fermi seviyesindeki yoğunluk azaldıkça yapı daha kararlı (stable) olmaktadır. Şekil 2'de görüldüğü üzere Rh_2CoX (X=Al, Ga ve In) bileşikleri için Fermi seviyesinde herhangi bir yasak enerji aralığı yoktur. Diğer ifade ile, valans ve iletkenlik bantları Fermi seviyesinde büyük oranda çakışmaktadır. Bu yüzden Rh_2CoX (X=Al, Ga ve In) bileşiklerinin metalik karakter gösterdiği sonucuna varılabilir. Bu özellik spin kutuplu taşıma için çok aranan bir özelliktir. Spin kutuplu sistemler manyetik alana çok duyarlıdır. Çünkü bu sistemlerde özdirenç manyetik alanla değişmektedir. Özdirencin manyetik alanla değişmesi esasına dayanan manyetik sensörler ve manyetik hafızalar yapılmaktadır. Ayrıca tünelleme manyetik direnç (TMR), polorize ışık yayan LED'ler spin–spin enjeksiyon cihazlarının üretilmesinde de Heusler bileşikleri kullanılmaktadır. Sonuç olarak Rh_2CoX (X=Al, Ga ve In) bileşiklerinin spintronik aygıtlar için kullanılmaya aday malzemeler olduğu söylenebilir.

Rh_2CoX (Al, Ga ve In) bileşiklerinin elektronik band yapılarının grafiklerinin daha iyi analiz edilebilmesi için toplam ve kısmi durum yoğunlukları hesaplanarak çizdirilmiştir.

Fermi enerji seviyesi sıfır noktasında sabitlenmiştir ve Fermi enerji seviyesinde elektron yoğunluğunun bulunmasından dolayı Rh_2CoX (Al, Ga ve In) bileşikleri metalik özellik göstermektedir. Şekil 3'te Rh_2CoX (Al, Ga ve In) bileşikleri için spin yönelimlerine göre hesaplanan durum yoğunluk (DOS) eğrileri verilmiştir. Durum yoğunluk eğrileri, bandların yoğun olduğu noktalarda maksimum pik değerlerine ulaşmıştır. -5 ve 0 eV aralığında toplam durum yoğunluk eğrilerine (DOS) ana katkılar geçiş metali olan Co'dan gelmektedir. Yani Rh_2CoX (Al, Ga ve In) bileşikleri için fermi seviyesinin etrafındaki maksimum pikler geçiş metallerine aittir.

Elektron dizilimine göre, d yörüngesi elektron dağılımının en dış yörüngesidir. Atomik durum yoğunluğu eğrileri incelendiğinde durum yoğunluk eğrilerine en çok katkının d orbitallerinden gelmesi beklenmektedir. Rh_2CoX (Al, Ga ve In) tam Heusler bileşikleri için s, p ve d orbitallerinin katkıları Şekil 4'te verilmektedir. -5 ve 0 eV aralığında maksimum piklerin Co atomunun d orbitallerinden geldiği görülmektedir.

Şekil 5 incelendiğinde Rh_2CoX (Al, Ga ve In) bileşikleri için toplam manyetik moment değerleri -0.5 μ_B/f.u. ve 3.5 μ_B/f.u. değerleri arasında yer almaktadır. Rh_2CoAl bileşiği için toplam manyetik moment değeri 3.2730

μ_B/f.u., Rh_2CoGa bileşiği için toplam manyetik moment değeri 3.2763 μ_B/f.u. ve Rh_2CoIn bileşiği için ise toplam manyetik moment değeri 3.2636 μ_B/f.u. şeklindedir.

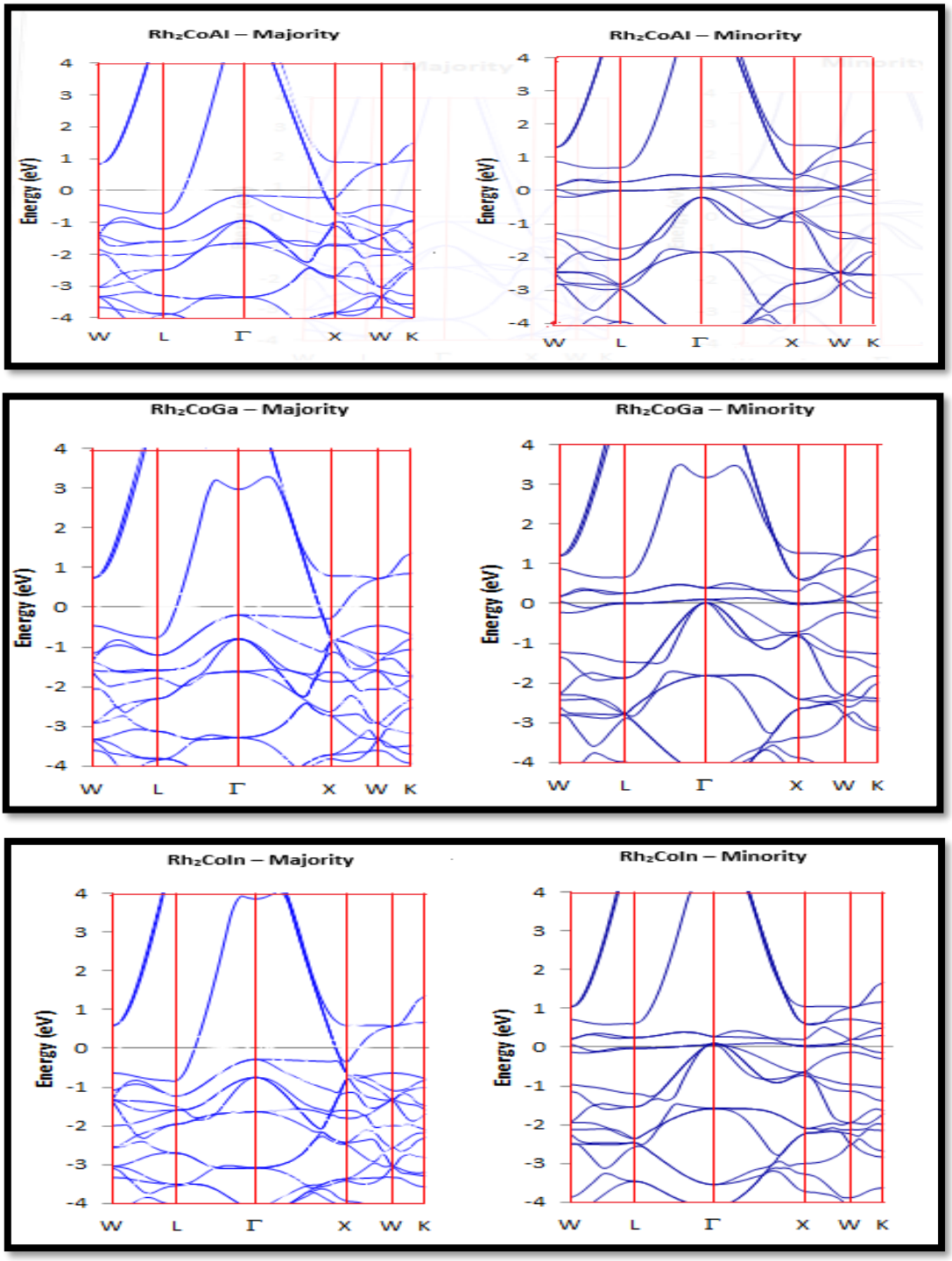

Şekil 2. *Rh_2CoX (X=Al, Ga ve In) Heusler Bileşikleri için Simetri Yönleri Boyunca Hesaplanan Elektronik Bant Yapıları*

Tablo 4'te görüldüğü üzere Rh_2CoAl bileşiği için toplam manyetik moment değeri 3.2730 μ_B/f.u. dir. Manyetik moment değerleri Rh için 0.555 μ_B/f.u , Co için 1.933 μ_B/f.u ve Al için -0.012 μ_B/f.u'dur ve en büyük katkı Co atomundan gelmektedir. Rh_2CoGa bileşiği için toplam manyetik moment değeri 3.2763 μ_B/f.u. olmak üzere manyetik moment değerleri Rh için 0.553 μ_B/f.u , Co için 1.917 μ_B/f.u ve Ga için -0.015 μ_B/f.u'dur ve en büyük katkı Co atomundan gelmektedir. Rh_2CoIn bileşiği için toplam manyetik moment değeri 3.2636 μ_B/f.u. dir ve manyetik moment değerleri Rh için 0.537 μ_B/f.u , Co için 1.972 μ_B/f.u, In için -0.020 μ_B/f.u'dur ve en büyük

katkı Co atomundan gelmektedir. Ayrıca Rh_2CoX (Al, Ga ve In) bileşikleri için elde edilen kısmi manyetik moment değerleri Tablo 5'te yer almaktadır.

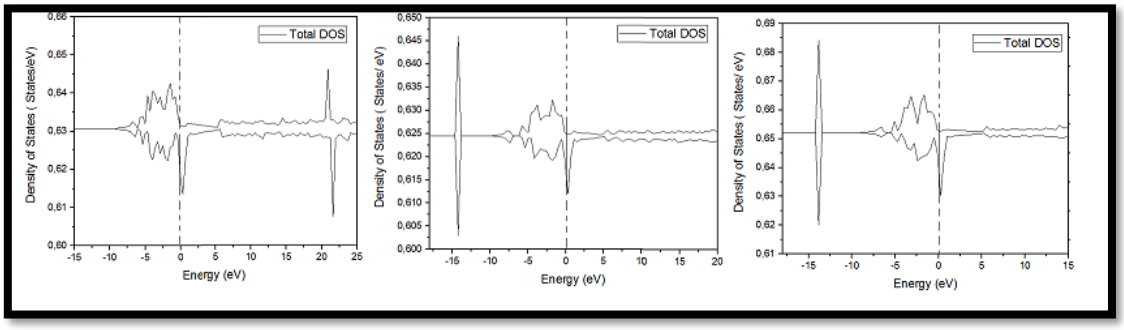

Şekil 3. *Rh_2CoX (X=Al, Ga ve In) Heusler Bileşikleri için Spin Yönelimlerine Göre Hesaplanan Toplam Durum Yoğunluk Eğrileri (DOS)*

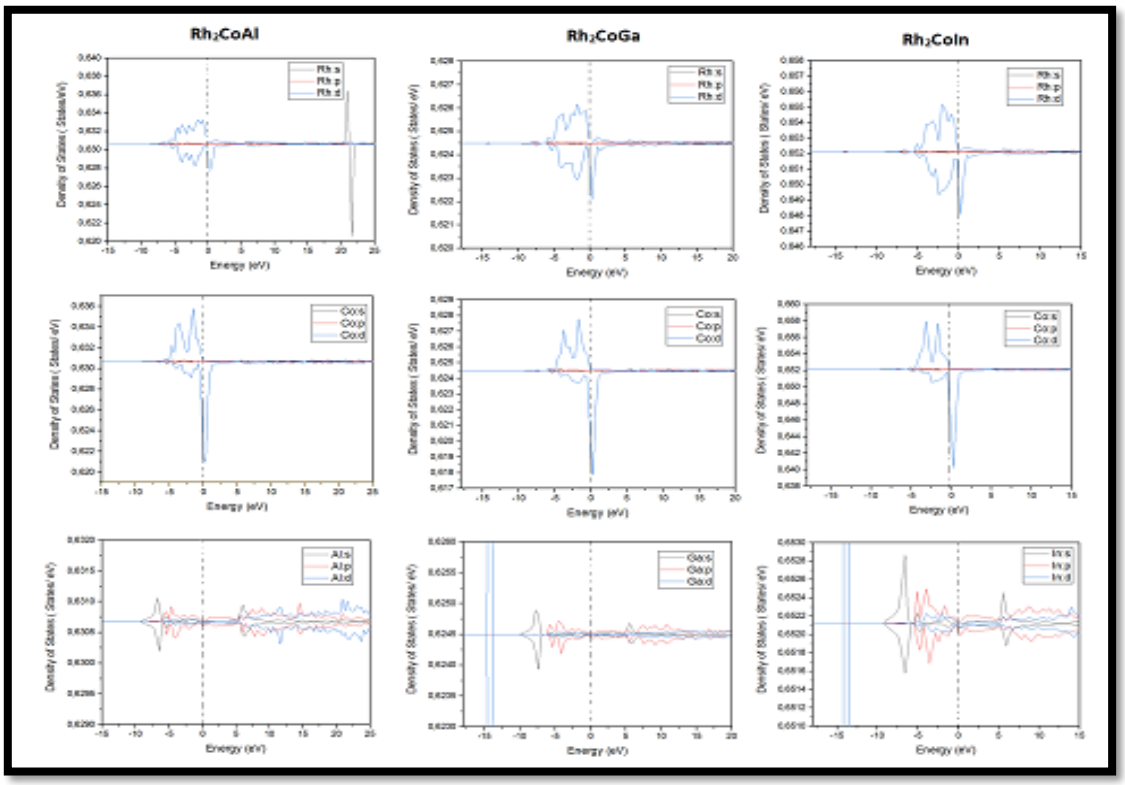

Şekil 4. *Rh_2CoX (X=Al, Ga ve In) Heusler Bileşiklerinin Parçalı Durum Yoğunluğu Eğrileri*

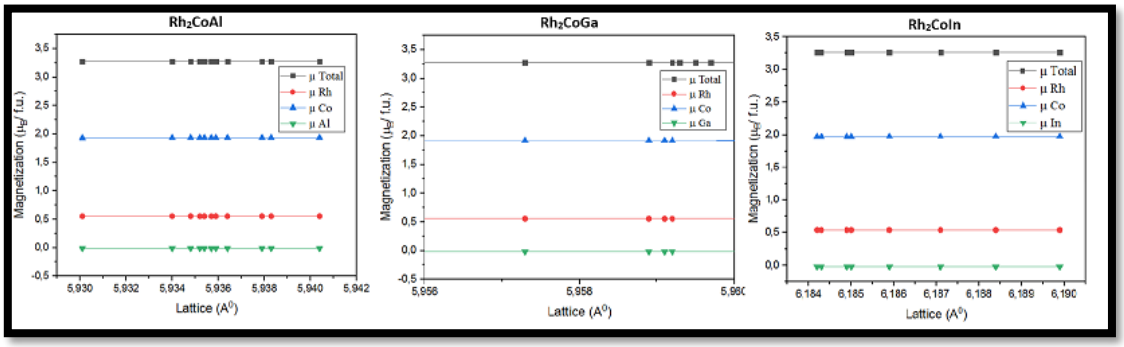

Şekil 5. *Rh_2CoX (X=Al, Ga ve In) Heusler Bileşiklerinin Magnetizasyon Eğrileri*

Tablo 4. *Rh_2CoX (X=Al, Ga ve In) Heusler Bileşikleri için Hesaplanan Toplam ve Atomik Manyetik Moment Değerleri*

Bileşik	**Rh_2CoAl**	**Rh_2CoGa**	**Rh_2CoIn**
μ_{Tot} (μ_B/f.u.)	3.2730	3.2763	3.2636
μ_{Rh} (μ_B/f.u.)	0.555	0.553	0.537
μ_{Co} (μ_B/f.u.)	1.933	1.917	1.972
μ_{Al} (μ_B/f.u.)	-0.012	-	-
μ_{Ga}(μ_B/f.u.)	-	-0.015	-
μ_{In} (μ_B/f.u.)	-	-	-0.020

Tablo 5. *Rh_2CoX (X=Al, Ga ve In) Heusler Bileşikleri için Kısmi Manyetik Moment Değerleri*

Bileşik	**Atom**	**s**	**p**	**d**
Rh_2CoAl	Rh	-0.004	-0.007	0.565
	Co	0.008	-0.002	1.927
	Al	-0.001	-0.009	-0.002
Rh_2CoGa	Rh	-0.004	-0.007	0.563
	Co	0.007	-0.002	1.911
	Ga	-0.003	-0.011	-0.001
Rh_2CoIn	Rh	-0.004	-0.006	0.548
	Co	0.008	-0.002	1.965
	In	0.003	-0.016	-0.002

4. SONUÇLAR

Bu çalışmada uzay grubu Fm-3m olan Rh_2CoX (X=Al, Ga ve In) bileşiklerinin yapısal ve manyetik özellikleri Yoğunluk Fonksiyonel Teorisi ile incelenmiştir. Elde edilen örgü sabit değerleri literatür ile karşılaştırıldığında Michael Gilleßen (Gilleßen, 2009) tarafından 2009 yılında yapılan tez çalışmasına göre Rh_2CoAl için örgü sabit değeri yaklaşık % -0.72, Rh_2CoGa için örgü sabit değeri yaklaşık % -0.63 farkla ve Rh_2CoIn için örgü sabit değeri yaklaşık % -0.58 farkla elde edilmiştir.

Manyetik moment değerleri ise, Michael Gilleßen (Gilleßen, 2009) tarafından 2009 yılında yapılan tez çalışması ile karşılaştırıldığında Rh_2CoAl için manyetik moment değeri yaklaşık % +8.37 , Rh_2CoGa için manyetik moment değeri yaklaşık % +9.21 farkla ve Rh_2CoIn için manyetik moment değeri yaklaşık % +8.78

farkla elde edilmiştir. Bu bileşikler için örgü parametreleri manyetik moment değerleri hesaplanmıştır ve çıkan sonuçların literatür ile oldukça uyumlu olduğu gözlemlenmiştir. Tablolarda verilen diğer değerler ile ilgili olarak daha önce bu veriler ile ilgili deneysel veya teorik bir çalışma yapılmadığı için herhangi bir kıyaslama yapılamamıştır.

Rh_2CoX (X=Al, Ga ve In) bileşikleri için elastik sabitler hesaplanmıştır ve Born Kararlılık kriterlerini sağlamaktadırlar. Bu durumda Rh_2CoX (X=Al, Ga ve In) bileşiklerinin mekanik kararlı oldukları söylenebilir. Rh_2CoX (X=Al, Ga ve In) için Poisson oranları 1,75 kritik değerinden yüksek olduğu için bileşiklerin sünek yapıda olduğu gözlemlenmiştir. Rh_2CoX (X=Al, Ga ve In) bileşikleri için bant yapıları ve durum yoğunluk grafikleri elde edilmiştir ve elde edilen grafiklere göre bu bileşikler metalik özellik sergilemektedir. Sonuç olarak Rh_2CoX (X=Al, Ga ve In) bileşikleri göstermiş olduğu özelliklerden dolayı spintronik ve magneto-elektronik cihazlarda kullanılmak üzere yeni aday malzemeler olabileceği söylenebilir.

ÇIKAR ÇATIŞMASI

Yazar çıkar çatışması beyan etmemektedir.

KAYNAKLAR

Chadi, D. J., & Cohen, M. L. (1973). Special Points in the Brillouin Zone. *Phys. Rev. B*, *8*(12), 5747-5753. doi:10.1103/PhysRevB.8.5747

Eberz, U., Seelentag, W., & Schuster, H. U. (1980). Coloured Ternary and Quaternary Zintl-Phase. *Zeitschrift für Naturforschung B*, *35*(11), 1341-1343. doi:10.1515/znb-1980-1103

Galanakis, I., Mavropoulos, P., & Dederichs, P. H. (2006). Electronic structure and Slater‐Pauling behaviour in half-metallic Heusler alloys calculated from first principles. *Journal of Physics D: Applied Physics*, *39*(5), 765-775. doi:10.1088/0022-3727/39/5/S01

Gilleßen, M., & Dronskowski, R. (2010). A combinatorial study of inverse Heusler alloys by first-principles computational methods. *Journal of Computational Chemistry*, *31*(3), 612-619. doi:10.1002/jcc.21358

Gilleßen, M., & Dronskowski, R. (2009). A combinatorial study of full Heusler alloys by first-principles computational methods. *Journal of Computational Chemistry*, *30*(8), 1290-1299 doi:10.1002/jcc.21152

Gilleßen, M. (2009). Über die quantenchemischen Untersuchungen einiger ternarer intermetallischer Verbindungen, PhD Thesis, Aachen University. zur Erlangung des akademischen Grades eines.

Heusler, F. (1903). Übermagnetischemanganlegierungen Verhandlugen der Deutschen Physikalischen Gesellschaft, sec. 5, pp. 219.

Kresse, G., & Hafner, J. (1993). Ab initio molecular dynamics for liquid metals. *Phys. Rev. B*, *47*(1), 558-561. doi:10.1103/PhysRevB.47.558

Kresse, G., & Hafner, J. (1994). Ab initio molecular-dynamics simulation of the liquid-metalamorphous-semiconductor transition in germanium. *Phys. Rev. B*, *49*(20), 14251-14269. doi:10.1103/PhysRevB.49.14251

Kresse, G., & Furthmüller, J. (1996a). Efficiency of ab-initio total energy calculations for metals and semiconductors using a plane-wave basis set. *Computational Materials Science*, *6*(1), 15-50. doi:10.1016/0927-0256(96)00008-0

Kresse, G., & Furthmüller, J. (1996b). Efficient iterative schemes for ab initio total-energy calculations using a plane-wave basis set. *Phys. Rev. B*, *54*(16), 11169-11186. doi:10.1103/PhysRevB.54.11169

Kresse, G. & Joubert, D. (1999). From ultrasoft pseudopotentials to the projector augmented-wave method. *Phys. Rev. B*, *59*(3), 1758-1775.doi:10.1103/PhysRevB.59.1758

Luan, X., Qin, H., Liu, F., Dai, Z., Yi, Y., & Li, Q. (2018). The mechanical properties and elastic anisotropies of cubic Ni_3Al from first principles calculations. *Crystals*, *8*(8), 307. doi:10.3390/cryst8080307

Mogulkoc, Y., Ciftci, Y.O., Kabak, M., & Colakoglu, K. (2013) First-principles study of structural, elastic and electronic properties of $NdTe_2$ and $TlNdTe_2$. *Cumhuriyet Science Journal*, *34*(3), 12-28.

Mouhat, F., & Coudert, F-X. (2014). Necessary and sufficient elastic stability conditions in various crystal systems. *Phys. Rev. B*, *90*, 224104. doi:10.1103/PhysRevB.90.224104

Offernes, L., Ravindran, P., Seim, C. W., & Kjekshus, A. (2008). Prediction of composition for stable half-heusler phases from electronicband-structure analyses. *Journal of Alloys and Compounds*, *458*(1-2), 47-60. doi:10.1016/j.jallcom.2007.04.038

Otto, M. J., Feil, H., van Woerden, R. A. M, Wijngaard, J., van der Valk, P. J., van Bruggen, C. F., & Haas, C. (1987). Electronic structure and magnetic, electrical and optical properties of ferromagnetic heusler alloys. *Journal of Magnetism and Magnetic Materials*, *70*(1-3), 33-38. doi:10.1016/0304-8853(87)90354-4

Otto, M. J., van Woerden, R. A. M., van der Valk, P. J., Wijngaard, J., van Bruggen, C. F., Haas, C., & Buschow, K. H. J (1989). Half-metallic ferromagnets. ı. structure and magnetic properties of NiMnSb and related ıntermetallic compounds. *Journal of Physics: Condensed Matter*, *1*(13), 2341. doi:10.1088/0953-8984/1/13/007

Perdew, J. P., Chevary, J. A., Vosko, S. H., Jackson, K. A., Pederson, M. R., Singh, D. J., & Fiolhais, C. (1993). Atoms, molecules, solids, and surfaces: Applications of the generalized gradient approximation for exchange and correlation. *Phys. Rev. B*, *46*(11), 6671-6687. doi:10.1103/PhysRevB.46.6671

Perdew, J. P., Burke, K., & Ernzerhof, M. (1996). Generalized gradient approximation made simple. *Phys. Rev. Lett.*, *77*(18), 3865-3868. doi:10.1103/PhysRevLett.77.3865

Pugh, S. F. (1954). XCII. Relations between the elastic moduli and the plastic properties of polycrystalline pure metals. *The London, Edinburgh, and Dublin Philosophical Magazine and Journal of Science*, *45*(367), 823-843. doi:10.1080/14786440808520496

Rassoulinejad-Mousavi, S. M., Mao, Y., & Zhang, Y. (2016). Evaluation of copper, aluminum, and nickel interatomic potentials on predicting the elastic properties. *Journal of Applied Physics*, *119*, 244304 doi:www.doi.org/10.1063/1.4953676

Villars, P., & Calvert, L. D. (1991). *Pearson's handbook of crystallographic data for intermetallic phases* (2nd ed.), ASM International, Materials Park, OH.

Wu, Z-J., Zhao, E-J., Xiang, H-P., Hao, X-F., Liu, X-J., & Meng, J. (2007). Crystal structures and elastic properties of superhard Ir N_2 and Ir N_3 from first principles. *Phys. Rev. B*, 76, 054115. doi:10.1103/PhysRevB.76.054115

Xing, N., Gong, Y., Zhang, W., Dong, J., & Li, H. (2009). First-principle prediction of half-metallic properties for the Heusler alloys V2YSb (Y=Cr, Mn, Fe, Co). *Computational Materials Science*, *45*(2), 489-493. doi:10.1016/j.commatsci.2008.11.008

Xu, G. Z., Liu, E. K., Du, Y., Li, G. J., Liu, G. D., Wang, W. H., & Wu, G. H. (2013). A New Spin Gapless Semiconductors Family: Quaternary Heusler Compounds. *EPL: A Letters Journal Exploring the Frontiers of Physics*, *102*, 17707.

Žutić, I., Fabian, J. & Das Sarma, S. (2004). Spintronics: Fundamentals and applications. *Reviews of Modern Physics*, *76*, 323-410. doi:10.1103/RevModPhys.76.323

Research Article / Araştırma Makalesi GU J Sci, Part A, 8(4): 515-528 (2021) https://doi.org/10.54287/gujsa.1025050

Gazi University
Journal of Science
PART A: ENGINEERING AND INNOVATION
http://dergipark.org.tr/gujsa

Evaluation of Student Attitudes Using Multivariate Statistical Analysis

Nurfer CIZMECI[1*], Fusun YALCIN[2]

[1]*Ministry of Education, Antalya Turkey*
[2]*Akdeniz University, Faculty of Science, Department of Mathematics, Antalya, Turkey*

Keywords

Multivariate Statistical Analysis
Factor Analysis
Cluster Analysis
Applied Mathematics

Abstract

This study aims to classify the high school students' attitudes towards Mathematics and Geometry courses with exploratory factor analysis and cluster analysis and to determine whether there is a difference between several variables determined using t-test. For this purpose, 1265 students were selected from 8 schools in Antalya province using by random sampling method and they were asked to respond to the survey form given to them. The collected data are classified using Factor Analysis and Cluster Analysis which are among the multivariate statistical methods. According to the factor analysis results, 4 factors were determined using the Geometry Attitude Scale, and two factors were determined by evaluating the Mathematics attitude scale. It was also investigated whether there was a difference between the attitudes of the students towards mathematics and geometry courses based on the averages of the responses provided by the students according to the variables of gender, grade level, and parents' education level. The results of the analyses revealed that there was a significant difference according to the grade level, while it did not differ according to gender and education level of the parents. It was observed that the average increased as the grade level increased.

Cite

Cizmeci, N., & Yalcin, F. (2021). Evaluation of Student Attitudes Using Multivariate Statistical Analysis. *GU J Sci, Part A, 8*(4), 515-528.

Author ID (ORCID Number)

N. Cizmeci, 0000-0002-5275-6120
F. Yalcin, 0000-0002-2669-1044

Article Process

Submission Date 17.11.2021
Revision Date 15.12.2021
Accepted Date 29.12.2021
Published Date 30.12.2021

1. INTRODUCTION

Mathematics and geometry courses are the courses that the students most concerned about at every stage of their education, and their average points are relatively lower. The student's attitude towards a course must be positive to be successful in that course. For this reason, the studies on how to increase the interest of students towards mathematics and geometry courses have been increasing and gaining prominence day by day. The authors applied a t-test in their study to determine the effects of cooperative learning on students' achievement in mathematics and their attitudes towards mathematics courses (Bramlett & Herron, 2007; Zakaria et al., 2010; Akay, 2011; Avcu & Avcu, 2015; Moloi, 2019; Berger et al., 2020; Celik, 2020; Ibáñez et al., 2020; Kolaczyk et al., 2020; Moreno-Guerrero et al., 2020). They concluded that cooperative learning methods positively affect the students' achievement in mathematics and their attitudes towards mathematics courses. In his study, the author examined the effect of parent-teacher cooperation on students' achievement in mathematics by using a t-test to analyze the data (Sirvani, 2007). At the end of the study, he concluded that parent-teacher cooperation had a positive effect on students' achievement in mathematics. The authors aimed to examine students' attitudes towards geometry courses according to some variables and they analyzed the data by using ANOVA and t-test methods (Avci et al., 2014). The researchers concluded their study by stating that there was no significant difference between students' attitudes towards geometry course and gender and grade level variables, however, they reported that there was a significant difference between the variables of the students' education field and their school type. In their study carried out at a science high school, the authors aimed to examine students' attitudes towards mathematics course and their academic self-

*Corresponding Author, e-mail: ncizmeci17@gmail.com

designs according to some variables (Pehlivan & Koseoglu, 2010). They used a t-test, one-way variance analysis, and Scheffe test to analyze the data. At the end of their study, the researchers stated that students' attitudes towards mathematics courses show a significant difference in terms of the variable of gender in favor of the male students and the variable of grade level. However, they concluded that there was no significant difference in terms of the university faculty that the students planned to study. In a study conducted across Turkey, the authors aimed to investigate the students 'attitudes towards mathematics courses and the factors influencing the students 'attitudes towards mathematics courses according to some variables (Yasar et al., 2014). They used One-way Analysis of Variance (One-way ANOVA), Least Significant Difference (LSD) tests and Factor Analysis methods to analyze the data in their study. The researchers concluded their study by reporting that the students' attitudes towards mathematics courses were moderate and the differences between students' attitudes towards mathematics courses by their gender varied according to the region. However, they concluded that students' attitudes towards mathematics courses differ significantly in each region according to the variables of the students' school type and the university entrance exam score type they wanted.

This study is original because it is the first study conducted in Antalya, where students' attitudes towards mathematics and geometry lessons were examined together. In this study, the data obtained from the master's thesis study were used; factor analysis, cluster analysis and t-test were performed and interpreted on these data. The aim of the study was to examine these factors in terms of some variables (gender, class level, education level of parents). In addition, it was aimed to make suggestions to teachers and students based on the findings of the research.

2. MATERIAL AND METHOD

The population of this study is composed of the students at the high schools, to which the students were placed by the address-based system, in the central districts of Antalya province in the 2018-2019 academic year. The sample of the study consists of 1320 students at the 10th, 11th, and 12th grades, who were selected using an appropriate sampling method. The study was carried out in the Muratpaşa, Kepez, Konyaaltı, Aksu, Döşemealtı, and Korkuteli districts. A school was selected from each district, but two schools were selected from Muratpaşa and Kepez districts since they were central districts. Exploratory Factor Analysis and Cluster Analysis were applied to determine high school students' attitudes towards Mathematics and geometry courses. For this purpose, a total of 44 items were included in these analyses.

In the study, the students were asked to respond to the scales consisting of three parts. In the first part of the scale, there were questions the about several demographic information. In the second part, the "Attitude Scale towards Geometry Course" developed by Cansiz et al. were used to measure students' attitudes towards geometry course (Aktas & Aktas, 2013). In the third part, the "Attitude Scale towards Mathematics Course" developed by Askar (1986) was used to measure students' attitudes towards mathematics courses.

After the students were provided with the required information about the study which data collection tools were distributed based on volunteering. The response rate for the survey was found to be 100%. 1265 survey forms that were filled without any mistakes were imported to SPSS 23 software package in the computer environment. Cronbach's Alpha Reliability Coefficients were calculated to test the reliability of the scales. Exploratory factor analysis and cluster analysis were performed to observe, analyze, classify, and compare students' attitudes towards geometry and mathematics courses. Independent sample t-test, one-way analysis of variance, and Kruskal-Wallis (KW) test were conducted to examine whether gender, number of siblings, grade level, and education level of the parents affected students' attitudes towards geometry and mathematics courses.

2.1. Reliability Analysis

Reliability analysis is one of the methods to test the power and sufficiency of scales to measure the intended feature. One of the most common methods to test the reliability of a scale is to examine the Cronbach's Alpha Coefficient, which is a measure of the internal consistency of the items (Yildiz & Uzunsakal, 2018). Cronbach's alpha coefficient of the scale having k items can be calculated using the following equation 1:

$$\alpha = \frac{k}{k-1}\left(1 - \frac{\sum_{i=1}^{k} s_i^2}{s_k^2}\right) \quad (1)$$

where s_i^2 stands for variance and s_k^2 stands for the general variance (Ozdamar, 2017). The following assumptions can be made based on the value of the reliability coefficient of α. If α < 0.5,the scale is considered to be unreliable (unacceptable); if it is in the range between 0.5 < α < 0.6 the reliability of the scale is considered to be poor; if it is in the range between 0.6 < α < 0.7,the reliability of the scale is questionable; if it is in the range between 0.7 < α < 0.8, the reliability of the scale is acceptable; if it is in the range between 0.8 < α < 0.9, the reliability of the scale is good; it is 0.90 < α,the scale is considered to be highly reliable (Cronbach, 1951).

2.2. Exploratory Factor Analysis

Factor analysis is a multivariate statistical method that derives a few uncorrelated variables that are conceptually meaningful from many correlated variables and classifies these variables (Buyukozturk, 2002). In factor analysis, variables with significant correlations between themselves are classified and a few uncorrelated factors are obtained (Mert, 2016).The main purpose of this analysis is to reduce the number of variables and to classify them by obtaining a few significant factors independent of each other from many correlated variables (Kalayci, 2010).Exploratory factor analysis is a method that aims to derive fewer factors by making use of the correlation between the variables in a data matrix (Ozdamar, 2004).If the variance values of the variables are quite different from each other, the correlation matrix is used in the exploratory factor analysis. If data has a homogeneous structure, the covariance matrix is used. The correlation matrix is tested as a whole in the Bartlett's Test of Sphericity, thus, the suitability of the data set for factor analysis is examined Bartlett Sphericity Test requires rejecting the H_0 hypothesis which is established as "the correlation matrix is a unit matrix (Bramlett & Herron, 2007).In other words, it is interpreted that the correlationmatrix is suitable for factoring (Bartlett, 1950; Albayrak, 2006).The hypothesis for Bartlett's Test of Sphericity is as following equation 2 where I denotes the unit matrix and R denotes correlation matrix (Fisher, 1925):

$$\begin{aligned} H_0&: R = I \\ H_a&: R \neq I \end{aligned} \quad (2)$$

To determine whether the correlation matrix with *p* variables of N units is a unit matrix or not, the χ^2 value for the Bartlett's Test of Sphericity statistics is calculated as following equation 3:

$$\chi^2 = -\left[n - 1 - \left(\frac{1}{6}\right)(2p+5)\right]\ln|R| \quad (3)$$

where $|R|$ value stands for the natural algorithm of the correlation matrix (Albayrak, 2006). The determinant |R| of a correlation matrix can be calculated by multiplying all of the eigenvalues showing the contribution rate of factors to the variance (Albayrak, 2006).

Kaiser Meyer Olkin (KMO) Test measures the correlations between variables as a whole and also tests the adequacy of the sample. The KMO value ranges between 0 and 1. In case a variable in the data set is accurately predicted by other variables, the KMO value is found to be 1. KMO value is obtained by proportioning the simple correlation coefficient to the partial correlation coefficient (Kalayci, 2010; Alpar, 2017; URL1, 2020)

Kaiser Mayer Olkin sample adequacy measure is calculated as following equation 4 (Cureton & D'Agostino, 1993; URL1, 2020):

$$KMO = \frac{\sum_{i \neq j} \sum r_{ij}^2}{\sum_{i \neq j} \sum r_{ij}^2 + \sum_{i \neq j} \sum a_{ij}^2} \quad (4)$$

where r_{ij} denotes a simple correlation coefficient between ith and jth variables, and a_{ij} denotes partial correlation coefficient between ith and jth variables (Cureton & D'Agostino, 1993; Albayrak, 2006; URL1, 2020). Principal component analysis (PCA) is the most used factor derivation method. The principal component analysis model is established using m common factors where k stands for the number of variables and m stands for the number of factors (m ≤ k). The factor model for the jth variable is established as following equation 5:

$$x_j = l_{j1}F_1 + l_{j2}F_2 + l_{j3}F_3 + \cdots + l_{jk}F_k \quad (5)$$

where x_j denotes jth variable, F denotes common factors, and l denotes the factor loads (Cureton & D'Agostino, 1993; Albayrak, 2006).

The principal component analysis method initially assumes that the number of variables is equal to the number of factors. It assumes that several of these common factors will explain a significant part of the total variance and the remaining factors will explain specific variances (Albayrak, 2006).

Various approaches such as criteria, graphs, and tests have been developed to determine the number of factors. The most commonly used of these approaches are the variance contribution criterion and the scree test criterion.

2.3. Cluster Analysis

As a multivariate statistical method, cluster analysis classifies individuals or objects that are similar by considering variables (Islamoglu, 2009). The groups formed by the cluster analysis are homogeneous among themselves and heterogeneous among other groups. The groups are geometrically distant to each other. The grouping is performed based on the difference in the data, ie. the variance-covariance in factor analysis, and clustering analysis, while the grouping is performed based on the proximity-distance relationship (Hair et al., 2006).The cluster analysis method has four stages: obtaining the data matrix, obtaining and calculating the distance (similarity/difference) matrix, determining the clustering method and creating clusters, and interpreting the results (Alpar, 2017; Ozdamar, 2017).There are a great number of methods to calculate distances between units in cluster analysis. The most commonly used of these methods is the Euclidean distance measure. If the number of units is more than 100, Euclidean distance measurement is recommended to use (Cokluk et al., 2018). In a structure with k variables, the Euclidean distance measure used to determine the distance between ith and jth units is calculated as following equation 6:

$$d_{ij} = \sqrt{\sum_{n=1}^{k} \left(x_{in} - x_{jn}\right)^2} \quad (6)$$

where d_{ij}denotes the distance between the ith and jth observations, x_{in}in denotes the value of the nth variable of the ith observation, x_{jn}denotes the value of the nth variable of the jth observation (Anderberg, 1973; Alpar, 2017).

2.4. t-Test

t-Test, which is a parametric test, is used when comparing the average of a population with any value. Whether the population meets the assumption of normality should be examined at first as it is a parametric test. However, if the sample is larger than 30 (n > 30) this assumption may not be required (Box, 1987; Mert, 2016). The averages of the data from a sample group or sample groups are compared and analyzed using a t-test. If the data are obtained from two sample groups, the homogeneity of the variances of the means of the sample groups is examined. In case the variances are homogeneous, several types of t-tests can test whether there is a significant difference between the two means. The equality of the sample numbers is important in selecting the relevant test. If the sample numbers are not equal, the total number is important (Box, 1987;

Cepni, 2010). The t-test statistics are calculated as following equation 7,8,9 based on sample numbers (Box, 1987; Cepni, 2010).

1) t-test to be used when $n_1 = n_2 = n$:

$$t = \frac{\overline{X_1} - \overline{X_2}}{\sqrt{\frac{s_1^2 + s_2^2}{n}}} \tag{7}$$

2) t-test to be used when $n_1 \neq n_2 \; ve \; n_1 + n_2 < 200$:

$$t = \frac{\overline{X_1} - \overline{X_2}}{\sqrt{\left[\frac{(n_1 - 1)s_1^2 + (n_2 - 1)s_2^2}{n_1 + n_2 - 2}\right]\left(\frac{1}{n_1} + \frac{1}{n_2}\right)}} \tag{8}$$

3) t-test to be used when $n_1 \neq n_2 \; ve \; n_1 + n_2 \geq 200$

$$t = \frac{\overline{X_1} - \overline{X_2}}{\sqrt{\frac{s_1^2}{n_1} + \frac{s_2^2}{n_2}}} \tag{9}$$

3. RESULTS AND DISCUSSION

Descriptive statistics obtained from the scale applied to determine high school students' attitudes towards mathematics and geometry courses are given in Table 1. According to this table, 56% of the students participating in this study are female, 53% of them have one or two siblings, the mothers of 40.4% of them have a high school or university degree, and the fathers of 54.4% of them have a high school or university degree. Also, Muratpaşa ranks first with the participation rate of 27.3% among the districts where the study was conducted. Then Kepez district ranks second with the percentage of 23.9%. The district with the lowest participation rate is Korkuteli with 9.6%. Considering the participation in the study in terms of grade level, it is seen that there is an almost equal number of 1 participants from the three grade levels involved in the study.

The results of the Keiser-Meyer-Olkin (KMO) test were examined for evaluating the suitability of the sample size to factor analysis. The KMO value was found to be 0.973 (97.3%) for the mathematics attitude scale, and 0.944 (94.4%) for the geometry attitude scale. Moreover, Bartlett's Test of Sphericity was applied to both scales. The results of the test revealed the following values for the mathematics attitude scale: $X^2 = 17800{,}958$; $p = 0.00 < 0.01$. For the geometry attitude scale, the following results were obtained: $X^2 = 9213.16$; $p = 0.00 < 0.01$. These results showed that both scales were suitable for factor analysis. Principal Component Analysis was used as the factor deriving method and Varimax Rotation Method was used as the rotation method for both scales. Also, the Cronbach's Alpha Coefficient of the mathematics attitude scale was found to be 0.995 while it was determined to be 0.95 for the geometry attitude scale.

The factors related to high school students' attitudes towards geometry course have the following names: Factor 1: "Self Confidence", Factor 2: "Anxiety", Factor 3: "Usability", and Factor 4: "Significance". The names of the factors related to high school students' attitudes towards mathematics courses are as follows: Factor 1: "Interest", Factor 2: "Anxiety". It was observed that the structures and numbers of the factors obtained by exploratory factor analysis and cluster analysis were the same. Determined by exploratory factor analysis, the factor load values of geometry and mathematics attitude scales are given in Table 2 and Table 3.

Table 1. *Descriptive Statistics*

Gender	**n**	**%**
Female	708	56
Male	557	44
Grade Level		
10 th Grade	441	34.9
11th Grade	436	34.5
12th Grade	388	30.7
School Name/District		
Hacı Şerife Ethem Kavukçu Anatolian High School/Korkuteli	122	9.6
Kepez Anatolian High School/Kepez	158	12.5
Aldemir Atilla Konuk Anatolian High School/Muratpaşa	180	14.2
Halil Akyüz Anatolian High School/Döşemealtı	152	12
Akdeniz Anatolian High School/Konyaaltı	183	14.5
Metin Nuran Çakallıklı Anatolian High School/Muratpaşa	166	13.1
Aksu Anatolian High School/Aksu	160	12.6
Atatürk Anatolian High School/Kepez	144	11.4
Number of Siblings		
1-2	671	53
3-4	513	40.6
5 and above	81	6.4
Education Level of the Mother		
University	165	13
High School	347	27.4
Secondary School	286	22.6
Primary School	422	33.6
Uneducated	45	3.6
Education Level of the Father		
University	284	22.5
High School	403	31.9
Secondary School	289	22.8
Primary School	282	22.3
Uneducated	7	0.6
Total	1265	100

The clusters of the items belonging to the geometry and mathematics attitude scales are given in Table 4. The items covered by the factors at the end of the exploratory factor analysis and clustering analysis are the same in the mathematics attitude scale, however, there are minor differences in the geometry attitude scale.

The results of sub-factors determined by factor analysis of the scale of high school students' attitudes towards geometry and mathematics course based on several variables are given in Table 5, 6, 7, 8. The significance of the difference between the mean values of the scores of high school students' attitudes towards geometry and mathematics courses by the gender variable has been evaluated using independent samples t-test. As can be seen in Table 5, there is not a significant difference between the students' attitudes towards geometry and mathematics course by gender.

Table 2. *Factor Load Values of Mathematics Attitude Scale*

Items	Factor 1	Factor 2
M14	0,784	0,383
M13	0,747	
M11	0,731	0,415
M20	0,726	
M17	0,699	0,464
M18	0,695	0,419
M8	0,668	0,508
M4	0,666	0,366
M5	0,659	0,307
M1	0,646	0,492
M16	0,302	0,769
M12		0,762
M15	0,417	0,745
M2	0,349	0,695
M19	0,346	0,647
M7	0,333	0,636
M9	0,485	0,604
M10		0,602
M3	0,470	0,582
M6	0,512	0,551
* Load values below 0.30 are not given.		

Table 3. *Factor Load Values of Geometry Attitude Scale*

Items	Factor 1	Factor 2	Factor 3	Factor 4
G22	0,644			
G10	0,633			
G19	0,588	0,372		
G13	0,586			
G1	0,558			
G7	0,515			
G11	0,485			0,349
G16				
G14		0,667		
G24		0,640		
G18		0,539	0,324	0,378
G12	0,318	0,525		
G20	0,302	0,516		
G4	0,344	0,516		
G15	0,313	0,512		
G8			0,699	
G5	0,349	0,366	0,664	
G9	0,378		0,636	
G3			0,608	
G2			0,595	
G23			0,508	
G17		0,363	0,461	0,679
G21	0,393			0,664
G6				0,623
* Load values below 0.30 are not given.				

Table 4. *Clusters of Items Belonging to Mathematics and Geometry Attitude Scale*

MAS Items	**Clusters**	**Items**	**Clusters**
M1	1	M11	1
M2	2	M12	2
M3	2	M13	1
M4	1	M14	1
M5	1	M15	2
M6	2	M16	2
M7	2	M17	1
M8	1	M18	1
M9	2	M19	2
M10	2	M20	1
GAS Items			
G1	1	G13	1
G2	4	G14	2
G3	3	G15	3
G4	2	G16	2
G5	3	G17	4
G6	4	G18	2
G7	1	G19	1
G8	3	G20	2
G9	3	G21	4
G10	1	G22	1
G11	1	G23	2
G12	2	G24	2

To compare high school students' attitudes towards geometry and mathematics courses by the variable of grade level, one-way analysis of variance was applied where the assumption of homogeneity was provided. Table 6 reveals that the difference by the grade level is not statistically significant in Factor 2 for geometry course.

Table 5. *Relationship of Geometry Attitude Scale (GAS) and Mathematics Attitude Scale (MAS) Sub-Factors with the Variable of Gender*

GAS Factors	**Gender**	**Mean ± SD**	**t**	**p**
Factor 1	Male	3.26 ± 0.80	1.90	0.057
	Female	3.17 ± 0.79		
Factor 2	Male	3.28 ± 0.77	1.61	0.106
	Female	3.21 ± 0.78		
Factor 3	Male	3.39 ± 0.85	1.28	0.200
	Female	3.32 ± 0.82		
Factor 4	Male	3.30 ± 1.02	-0.44	0.654
	Female	3.33 ± 1.01		
MAS Factors				
Factor 1	Male	3.38 ± 1.08	-0.53	0.593
	Female	3.41 ± 1.04		
Factor 2	Male	3.53 ± 1.03	-1.93	0.053
	Female	3.64 ± 0.98		

Table 6. *Relationship of Geometry Attitude Scale and Mathematics Attitude Scale Sub-Factors with the Variable of Grade Level*

GAS Factors	Grade Level	Mean ± SD	F/KW	p
Factor 1	12th Grade	3.29 ± 0.75	KW:13.55	0.001
	11th Grade	3.24 ± 0.87		
	10th Grade	3.11 ± 0.75		
Factor 2	12th Grade	3.25 ± 0.75	F:2.42	0.089
	11th Grade	3.30 ± 0.80		
	10th Grade	3.18 ± 0.78		
Factor 3	12th Grade	3.45 ± 0.78	KW:8.39	0.015
	11th Grade	3.36 ± 0.89		
	10th Grade	3.26 ± 0.82		
Factor 4	12th Grade	3.54 ± 0.91	KW:8.39	0.015
	11th Grade	3.41 ± 1.01		
	10th Grade	3.03 ± 1.04		
MAS Factors				
Factor 1	12th Grade	3.64 ± 0.92	KW:27.60	0.000
	11th Grade	3.31 ± 1.13		
	10th Grade	3.26 ± 1.05		
Factor 2	12th Grade	3.80 ± 0.89	KW:21.25	0.000
	11th Grade	3.53 ± 1.09		
	10th Grade	3.47 ± 0.99		

In cases where the homogeneity assumption was not provided, the Kruskal-Wallis (KW) test, one of the non-parametric tests, was applied. Table 6 also reveals that the difference between the grade level is statistically significant for Factor 1, Factor 3, and Factor 4 for geometry course and Factor 1 and Factor 2 for mathematics course ($p<0.05$). These differences are in favor of 12th graders for all factors. Also, it is in favor of the 11th graders compared to the 10th graders. In this case, it was observed that the average score increases as the grade level increases.

To compare high school students' attitudes towards geometry and mathematics courses by the variable of the education level of parents, one-way analysis of variance were applied since the data provided the assumption of homogeneity. Considering Table 7 and Table 8 at the end of this evaluation, it is seen that there is no significant difference in the students' attitudes towards geometry and mathematics by the education level of parents.

It is observed that there is no significant difference between high school students' attitudes towards mathematics and geometry courses by the variables of gender and education level of parents. However, there is a significant difference between all the geometry attitude scale factors, except for the "anxiety" factor, by the variable of grade level. There are similar studies in the literature (Bindak, 2004; Caglayan, 2010; Pehlivan & Koseoglu, 2010; Yaratan & Kasapoglu, 2012; Avci et al., 2014; Yasar et al., 2014). In the study conducted by Bindak (2004), the geometry attitude scale was applied to 773 students and the geometry attitude scores of the females were found higher than the scores of the males according to the data. However, it was found that this difference was not statistically significant. Considering the relationship between students' attitudes towards geometry course and the program they wanted to study at the university, it was found that the geometry attitude scores of the students who wanted to study science and medicine were higher than those of the students who wanted to study social sciences, arts, law, and politics. Also, the geometry attitude scores of the students who wanted to study a program that would require geometry found to be higher than those of the students who wanted to study a program that would not require geometry. The study was also concluded that there was no relationship between the socioeconomic levels of families and the students' attitudes towards the geometry course. In the study counducted by collecting data from 553

students, it was concluded that self-efficacy perception and attitude predicted academic achievement in the geometry course (Caglayan, 2010). When examined in terms of gender, the self-efficacy perceptions and attitudes of female students were found to predict the academic achievement in geometry. While male students' self-efficacy perceptions for geometry courses were found to predict academic achievement in the geometry course, their attitude towards geometry course was found not to predict academic achievement. The study was concluded that the students' self-confidence and motivation towards geometry courses predicted their academic achievement in geometry courses. It was also concluded that the students' self-efficacy perceptions predicted their academic achievement in geometry. However, their perceptions of using geometry knowledge did not predict academic achievement in geometry courses. According to the results of the study conducted by the participation of 345 students by Pehlivan & Koseoglu, the students' attitudes towards mathematics courses differ by the variable of the gender; it was also concluded that this difference was in favor of male students (Pehlivan & Koseoglu, 2010).

Table 7. *Relationship of Geometry Attitude Scale and Mathematics Attitude Scale Sub-Factors with the Variable of Education Level of Mother*

GAS Factors	**Education Level of Mother**	**Mean ± SD**	**F/KW**	**p**
Factor 1	University	3.28 ± 0.81	F:1.42	0.225
	High School	3.25 ± 0.76		
	Secondary School	3.12 ± 0.80		
	Primary School	3.21 ± 0.81		
	Uneducated	3.21 ± 0.88		
Factor 2	University	3.25 ± 0.77	F:0.46	0.762
	High School	3.27 ± 0.77		
	Secondary School	3.19 ± 0.80		
	Primary School	3.24 ± 0.77		
	Uneducated	3.28 ± 0.79		
Factor 3	University	3.30 ± 0.86	F:0.67	0.611
	High School	3.39 ± 0.87		
	Secondary School	3.31 ± 0.79		
	Primary School	3.37 ± 0.82		
	Uneducated	3.28 ± 0.90		
Factor 4	University	3.41 ± 1.01	F:1.12	0.342
	High School	3.34 ± 1.04		
	Secondary School	3.22 ± 1.04		
	Primary School	3.34 ± 1.00		
	Uneducated	3.21 ± 0.86		
MAS Factors				
Factor 1	University	3.29 ± 1.04	F:0.93	0.446
	High School	3.39 ± 1.01		
	Secondary School	3.35 ± 1.09		
	Primary School	3.46 ± 1.06		
	Uneducated	3.46 ± 1.14		
Factor 2	University	3.49 ± 0.99	F:0.96	0.427
	High School	3.60 ± 1.00		
	Secondary School	3.55 ± 0.99		
	Primary School	3.64 ± 1.02		
	Uneducated	3.73 ± 0.95		

Moreover, a significant difference was found between the students' grade level and their academic achievement in the mathematics course. However, they concluded that there was no significant difference between their achievements by the variable of the university faculty they planned to study.

Table 8. *Relationship of Geometry Attitude Scale and Mathematics Attitude Scale Sub-Factors with the Variable of Education Level of Father*

GAS Factors	**Education Level of Father**	**Mean ± SD**	F/KW	p
Factor 1	University	3.26 ± 0.81	F:1.03	0.389
	High School	3.23 ± 0.77		
	Secondary School	3.11 ± 0.79		
	Primary School	3.19 ± 0.81		
	Uneducated	2.83 ± 1.02		
Factor 2	University	3.28 ± 0.80	F:0.42	0.792
	High School	3.25 ± 0.77		
	Secondary School	3.25 ± 0.78		
	Primary School	3.19 ± 0.76		
	Uneducated	3.24 ± 0.63		
Factor 3	University	3.34 ± 0.85	F:0.25	0.906
	High School	3.34 ± 0.84		
	Secondary School	3.35 ± 0.84		
	Primary School	3.39 ± 0.81		
	Uneducated	3.24 ± 0.75		
Factor 4	University	3.38 ± 1.04	F:1.37	0.242
	High School	3.38 ± 1.04		
	Secondary School	3.30 ± 1.01		
	Primary School	3.34 ± 0.97		
	Uneducated	2.57 ± 1.19		
MAS Factors				
Factor 1	University	3.29 ± 1.04	F:1.06	0.373
	High School	3.39 ± 1.01		
	Secondary School	3.35 ± 1.09		
	Primary School	3.46 ± 1.06		
	Uneducated	3.46 ± 1.14		
Factor 2	University	3.49 ± 0.99	F:0.697	0.594
	High School	3.60 ± 1.00		
	Secondary School	3.55 ± 0.99		
	Primary School	3.64 ± 1.02		
	Uneducated	3.73 ± 0.95		

4. CONCLUSION

At the end of this study, Cronbach's Alpha Coefficients for the mathematics attitude scale and geometry attitude scale was obtained to be 0.959 and 0.905 respectively. Total variances explained by the mathematics and geometry attitude scales were found to be 61.715% and 48.866% respectively. These results are consistent with the results obtained by the other studies in the literature (Askar, 1986; Peker & Mirasyedioglu, 2003; Kurbanoglu & Takunyaci, 2012; Aktas & Aktas, 2013).

Our teachers should play an active role in changing students' attitudes towards courses through education and training. In this context, the scales developed for the courses are of great prominence. Our students' attitudes towards the course should be determined using the developed attitude scales, thus, required arrangements should be introduced for the improvement of education and training activities. In this study, according to results of the factor analysis and cluster analysis obtained from the attitude scale towards mathematics course, two factors, namely interest, and anxiety were determined related to mathematics course, and four factors, namely self-confidence, anxiety, usefulness, and significance, were obtained regarding the geometry attitude scale. These results coincide with similar studies. According to these results, it is thought that the Ministry of National Education (MoNE) and Mathematics teachers should make extra

efforts to increase the interest in Mathematics and Geometry courses and to relieve the students' anxiety. In this context, the Ministry of National Education is suggested to support and review the studies that investigate students' attitudes towards the course. Mathematics teachers should endeavor to increase the interest in these courses and to relieve the anxiety of the students.

The teachers can begin the lesson with a material that will attract the students' attention. It is recommended that the lessons should be student-centered not teacher-centered. In-class competitions can be organized on the subject of the lesson to make students more active in mathematics lessons.

Course flow programs offered in the Education Information Network of MoNE can be used. Since it is the technology age, the students' interest in the course can be achieved by offering technology in the lesson. Another factor was found to be anxiety. Mathematics course is one of the most challenging courses for the students. This anxiety gradually increases with high school entrance and university entrance exams. Seminars on the subject can be given to the students by the school's counselor to reduce students' anxiety for mathematics and geometry courses. The teachers are recommended to make the students solve a few easy questions on the board in the lesson or to make them participate in the lessons by in-class activities to ensure students' self-confidence against mathematics courses.

ACKNOWLEDGEMENT

This work was supported by the Akdeniz University Scientific Research Projects (BAP) Coordination Unit with the project number FYL-2019-4384.

CONFLICT OF INTEREST

No conflict of interest was declared by the authors.

REFERENCES

Akay, G. (2011). The effect of peer instruction method on the 8th grade students' mathematics achievement in transformation geometry and attitudes towards mathematics. MSc Thesis, Middle East Technical University.

Aktaş, M. C., & Aktaş, D. Y. (2013). Geometriye yönelik güncel bir tutum ölçeğinin geliştirilmesi. *Necatibey Eğitim Fakültesi Elektronik Fen ve Matematik Eğitimi Dergisi*, *7*(2), 225-247. doi:10.12973/nefmed208

Albayrak, A. S. (2006). *Uygulamalı Çok Değişkenli İstatistik Teknikleri*. Ankara: Asil Yayın Dağıtım Ltd. Şti.

Alpar, R., (2017). *Applied Multivariate Statistical Techniques*. Ankara: Detay Yayincilik.

Anderberg, M R. (1973). *Cluster Analysis for Applications*. Elsevier. doi:10.1016/C2013-0-06161-0

Askar, P. (1986). Developing Attitude Mathematics Scala. *Education and Science, 8,* 31-36.

Avci, E., Özenir, Ö. S., Coşkuntuncel, O., Özcihan, H. G., & Su, G. (2014). Ortaöğretim Öğrencilerinin Geometri Dersine Yönelik Tutumları. *Turkish Journal of Computer and Mathematics Education*, *5*(3), 304-317.

Avcu, R., & Avcu, S. (2015). Turkish adaptation of Utley geometry attitude scale: A validity and reliability study. *Eurasian Journal of Educational Research, 58*, 1-23. doi:10.14689/ejer.2015.58.1

Bartlett, M. S. (1950). Tests of significance in factor analysis. *British Journal of Statistical Psychology*, *3*(2), 77-85. doi:10.1111/j.2044-8317.1950.tb00285.x

Berger, N., Mackenzie, E., & Holmes, K. (2020). Positive attitudes towards mathematics and science are mutually beneficial for student achievement: a latent profile analysis of TIMSS 2015. *The Australian Educational Researcher*, *47*, 409-444. doi:10.1007/s13384-020-00379-8

Bindak, R. (2004). Geometri tutum ölçeği güvenirlik geçerlik çalışması ve bir uygulama. PhD Thesis. Dicle University, Diyarbakır.

Box, J. F. (1987). Guinness, Gosset, Fisher, and small samples. *Statistical science*, *2*(1), 45-52.

Bramlett, D. C. & Herron, S. (2007) A study of African-American college students' attitudes towards mathematics. *Journal of Mathematical Sciences and Mathematics Education*, *3*(2), 43-51.

Buyukozturk, Ş. (2002). Faktör Analizi: Temel Kavramlar ve Ölçek Geliştirmede Kullanımı. Kuram ve Uygulamada Eğitim Yönetimi, *32*, 470-483.

Caglayan, O. S. (2010), The capability of high school 1st-grade students' self-efficacy perception and attitude towards geometry course to predict their academic success in the geometry course. MSc. Thesis, Yildiz Technical University, Istanbul.

Celik, H. C. (2020). The effect of modelling, collaborative and game-based learning on the geometry success of third-grade students. *Education and Information Technologies*, *25*(1), 449-469. doi:10.1007/s10639-019-09983-3

Cepni, S. (2010). *Introduction to research and project*. Trabzon: Celepler Publishing.

Cokluk, Ö., Şekercioğlu, G., & Buyukozturk, Ş. (2018). *Sosyal bilimler için çok değişkenli istatistik: SPSS ve LISREL uygulamaları* (5. Baskı). Pegem.

Cronbach, L. J. (1951). Coefficient alpha and the internal structure of tests. *Psychometrika*, *16*(3), 297-334. doi:10.1007/BF02310555

Cureton, E. E., & D'Agostino, R. B. (1993). *Factor analysis: An applied approach*. Psychology press.

Fisher, R. A. (1925). *Statistical methods for research workers*. Edinburg: Oliver and Boyd.

Hair, J. F., Black, W. C., Babin, B. J., Anderson, R. E., & Tatham, R. (2006). *Multivariate data analysis*. Uppersaddle River.

Ibáñez, M. B., Portillo, A. U., Cabada, R. Z., & Barrón, M. L. (2020). Impact of augmented reality technology on academic achievement and motivation of students from public and private Mexican schools. A case study in a middle-school geometry course. *Computers & Education*, *145*, 103734. doi:10.1016/j.compedu.2019.103734

Islamoglu A. H. (2009). *Research Methods in Social Sciences: (with SPSS applications)*. Beta Basim Yayim Dagitim A.S.

Kalayci, S. (2010). *Multivariate Statistics Techniques with SPSS Applications*. Ankara: Dinamik Akademi Yayin Dagitim.

Kolaczyk, E. D., Lin, L., Rosenberg, S., Walters, J., & Xu, J. (2020). Averages of unlabeled networks: Geometric characterization and asymptotic behavior. *The Annals of Statistics*, *48*(1), 514-538. doi:10.1214/19-AOS1820

Kurbanoglu, N. I., & Takunyaci, M. (2012). An investigation of the attitudes, anxieties and self-efficacy beliefs towards mathematics lessons high school students' in terms of gender, types of school, and students' grades. *Journal of Human Sciences*, *9*(1), 110-130.

Mert, M. (2016) *Cross-Sectional Data Analysis Computer Applications*. Ankara: Detay Yayincilik.

Moloi, K. (2019). Learners and educators as agents of social transformation in dysfunctional South African schools. *South African Journal of Education*, *39*(1), 1-8. doi:10.15700/saje.v39ns1a1800

Moreno-Guerrero, A. J., Rondon Garcia, M., Martinez Heredia, N., & Rodriguez-Garcia, A. M. (2020). Collaborative learning based on harry potter for learning geometric figures in the subject of mathematics. *Mathematics*, *8*(3), 369. doi:10.3390/math8030369

Ozdamar, K. (2004). *Statistical Data Analysis Using Software Packages (Multivariate Analysis)*. Eskişehir: Kaan Kitapevi.

Ozdamar, K. (2017). *Structural Equation Modeling for Scale and Test Development*. Eskisehir: Nisan Kitabevi.

Pehlivan, H., & Köseoğlu, P. (2010). Attitudes towards biology course and the academic self concept of the students attending at Ankara science high school. *Hacettepe University Journal of Education*, *38*, 225-235.

Peker, M., & Mirasyedioglu, S. (2003) The relationship between attudesand successes of high school students for mathematics course, 14(2)157-166.

Sirvani, H. (2007). The effect of teacher communication with parents on students' mathematics achievement. *American Secondary Education*, *36*(1), 31-46.

Yaratan, H., & Kasapoglu, L. (2012). Eighth grade students' attitude, anxiety, and achievement pertaining to mathematics lessons. *Procedia - Social and Behavioral Sciences, 46,* 162-171. doi:10.1016/j.sbspro.2012.05.087

Yasar, M., Çermik, H., & Güner, N. (2014). Türkiye'deki Lise Öğrencilerinin Matematik Dersine İlişkin Tutumları ve Bu Tutumlarını Etkileyen Faktörler. *Ankara University Journal of Faculty of Educational Sciences (JFES), 47*(2), 41-64. doi:10.1501/Egifak_0000001337

Yildiz, D., & Uzunsakal, E. (2018). A comparison of reliability tests in field researches and an application on agricultural data. *Journal of Business Administration and Social Studies*, *2*(1), 14-28.

Zakaria, E., Chin, L. C., & Daud, M. Y. (2010). The effects of cooperative learning on students' mathematics achievement and attitude towards mathematics. *Journal of Social Sciences, 6*(2), 272-275. doi:10.3844/jssp.2010.272.275

URL1: (2020, February 25) https://de.wikipedia.org/wiki/Kaiser-Meyer-Olkin-Kriterium#Kaiser-Meyer-Olkin-Kriterium

Research Article / Araştırma Makalesi GU J Sci, Part A, 8(4): 529-536 (2021) https://doi.org/10.54287/gujsa.1026957

Gazi University
Journal of Science
PART A: ENGINEERING AND INNOVATION
http://dergipark.org.tr/gujsa

Synthesis, Spectroscopic and Thermal Characterization of a New Sustainable Polymer

Nevin ÇANKAYA[1], & Nevin TURAN[2*]

[1]*Usak University, Department of Chemistry, 64100 Uşak, Turkey*
[2]*Muş Alparslan University, Department of Chemistry, Faculty of Arts and Sciences, 49250 Muş, Turkey*

Keywords

D-limonene
Sustainable Polymer
Copolymer
Synthesis and Characterization
Thermal Stability

Abstract

Copolymerization is a very important method in the synthesis of products having the physical and chemical properties sought in industrial sense. In this paper, the copolymerization of N-(4-nitrophenyl) acrylamide monomer with D-limonene was carried out and LIM-*co*-NPA copolymer was synthesized by free radical chain polymerization reaction. The structure of sustainable copolymer of limonene was chemically characterized by FT-IR, ^{1}H-NMR spectroscopic techniques. In addition, thermal stability of copolymer investigated by TGA/DTG/DTA simultaneous thermal analysis methods. The spectroscopic results are compatible with the amide or limonene polymers synthesized in the literature. From the important thermal results of the sustainable copolymer, it has been found that the initial decomposition temperature is 226°C, and the maximum decomposition temperatures is 329°C, glass transition temperature at 261°C and crystallization temperature at 340°C. It can be said that this promising sustainable copolymer is suitable for other mechanical, physical and biological study and research fields.

Cite

Çankaya, N., & Turan, N. (20**). Synthesis, Spectroscopic and Thermal Characterization of a New Sustainable Polymer *GU J Sci, Part A, 8*(4), 529-536.

Author ID (ORCID Number)

N. Çankaya, 0000-0002-6079-4987
N. Turan, 0000-0001-6740-6812

Article Process

Submission Date 22.11.2021
Revision Date 17.12.2021
Accepted Date 29.12.2021
Published Date 30.12.2021

1. INTRODUCTION

Polymeric materials take part in our daily lives, because they are cheap, easy to produce and chemical resistance. However, owing to the petroleum-based resources of polymer raw materials, the restricted resources of natural monomeric give rise to difficulties about expense and sustainability in the manufacture of these materials. Limonene is a significant workspace for natural polymer resources (Sharma & Srivastava, 2004; 2006). Limonene is a vigorous, naturally being formed, antinociceptive and antitumor compound present in citrus fruits, such as lemon, grapefruit, oranges, and also in the seeds of caraway and dill (Sun, 2007; Sharma & Srivastava, 2003). The main component of the bark essence is limonene, constituting about 95% of it. D-limonene (1-methyl-4-(1-methylethenyl)cyclohexane), a cyclic monoterpene in lemon flavor, is the main component of citrus peel essential oils (Farhat et al., 2011). The researches have been reported being one of the most plentiful terpenes in cannabis, has 16% of the essential oil fraction (Sharma & Srivastava, 2003; Hartsel et al., 2016). D-Limonene, which is used in the food, cosmetics, perfumery, gum, beverage and soap industries, is one of the additives that are generally accepted as safe. D-limonene is used in humans to dissolve cholesterol-containing gallstones and as a chemical preservative in many types of cancer. In addition, it is most commonly used in the treatment of gastric reflux or heartburn due to its gastric acid regulating and normal peristalsis-providing effects (Sun, 2007). In addition, limonene is used in the cosmetic area for aromatic property, in dermatology for percutaneous transfer of drugs, and in food as sweetening (Bacanlı et al., 2018). Many previous studies reported that it has anti-inflammatory and antioxidant features and treatment of many types of cancer such as lung, gastric, hepatocellular carcinoma (Guyton & Kensler, 2002; Lu et al., 2003; Yu

*Corresponding Author, e-mail: nevintrn@hotmail.com

et al., 2018; Hajizadeh et al., 2019; Souto et al., 2020). However, low solubility of limonene is a major problem in biological fluids and leads to limited treatment options in cancer therapy (Murali et al., 2013; Hajizadeh et al., 2019).

Due to the limited fossil resources and the worrying plastic accumulation, the development of biobased and sustainable polymers and composites has been a highly studied research topic in recent years (Zhang et al., 2018). Many scientists have stepped up their efforts to design and implement more sustainable approaches for polymer synthesis (Monica & Kleij, 2020). Various bio-based synthetic polymers can be synthesized from naturally derived monomers and exhibit biodegradability (Neumann et al., 2021).

In this study, copolymer of limonene, a natural monomer, and N-(4-nitrophenyl)acrylamide (NPA), an amide derivative, was synthesized and the characterization results were proven to be compatible with the literature. From the spectroscopic and thermal results, it is thought that this newly synthesized sustainable polymer can find applications in different fields of study.

2. MATERIAL AND METHOD

2.1. Materials

2,2'-Azobis(isobutyronitrile) (AIBN) as an initiator, chloroform, tetrahydrofuran and N, N-dimethylformamide as a solvent, and also D-limonene (Merck), p-amino nitrobenzene (Across), acryloyl chloride (Merck), triethylamine, were purchased from Aldrich.

2.2. Synthesis of LIM-co-NPA

In the presence of *p*-amino nitrobenzene (1.0 mole), acryloyl chloride (1.2 mole) and trimethylamine (1.0 mole), N-(4-nitrophenyl)acrylamide (NPA) monomer was synthesized (Figure 1). Acrylic chloride was diluted with tetrahydrofuran solvent and added dropwise to the solution at 0-5°C with continuous stirring. When the exothermic reaction was finished, the solution was filtered, excess solvent was removed and precipitated in ice water. Then, monomer was synthesized by crystallization in chloroform with 65% yield (Çankaya & Temüz, 2012; Tanış et al., 2019). Two suitable monomers that D-limonene (1 mole) and NPA (1 mole) with the radical initiator AIBN in *N*,*N*-dimethylformamide were added the into polymerization flask. The system was kept in inert gas at 65°C for 24 h. The synthesized polymer was crystallized several times in ethyl alcohol (Figure 2). (Çankaya & Temüz, 2012; Çankaya et al., 2019; 2021) and the copolymer was characterized by spectroscopic methods FT-IR and ^{1}H-NMR (Figure 3 and Figure 4).

2.3. Instrumental Measurements

Studies on FT-IR were performed using the Perkin-Elmer Two (UATR) spectrometer. The scanned wavenumbers between 400-4000 cm^{-1}. ^{1}H-NMR spectrum was conducted on BrukerTopSpinUltraShilt 400 MHz in DMSO-d_6. Thermal analyze of the copolymer was made with a Hitachi 7000 TGA/DTG/DTA (Thermal Gravimetric Analysis/Differential Thermogravimetric Analysis/Differential Thermal Analysis). Measurement was carried out from room temperature to 600°C, at a heating rate of 10°C min^{-1} and in a nitrogen atmosphere.

3. RESULTS AND DISCUSSION

3.1. Spectroscopic Characterization of LIM-co-NPA Copolymer

The copolymer was synthesized by the free radical polymerization method, using AIBN as the initiator (Figure 2). The spectroscopic structure of the LIM-co-NPA was approved by FT-IR and ^{1}H-NMR.

The FT-IR spectrum of the copolymer LIM-co-NPA is indicated in Figure 3. FT-IR (cm^{-1}, the most characteristic bands): 1673 (C=O amide stretch), 3311 stretch and 1595 bending vibration (N–H), 2980 and 2950 (C–Ar–H), 1504 asymmetric and 1330 symmetric stretch (NO_2) (Sharma & Srivastava, 2003; 2004; 2006; Çankaya & Temüz, 2012; Singh & Kamal, 2012; Brum et al., 2013; Ren et al., 2015; Zhang & Dubé, 2015; Çankaya et al., 2019; 2021; Tanış et al., 2019; Zhang & Dubé, 2014). The clear observability of

characteristic bands in the amide monomer and the absence of alkene bands in the monomers show that our newly synthesized polymer has formed and the literature also support this allegation (Coşkun et al., 2002; Kurt et al., 2019a). Actually, the FT-IR spectrum is the first spectroscopic measurement method that shows us whether newly synthesized materials are formed or not, and has been used in the literature for many years (Turan & Şekerci, 2009; Temüz, 2017; Coşkun et al., 2019; Kurt et al., 2020).

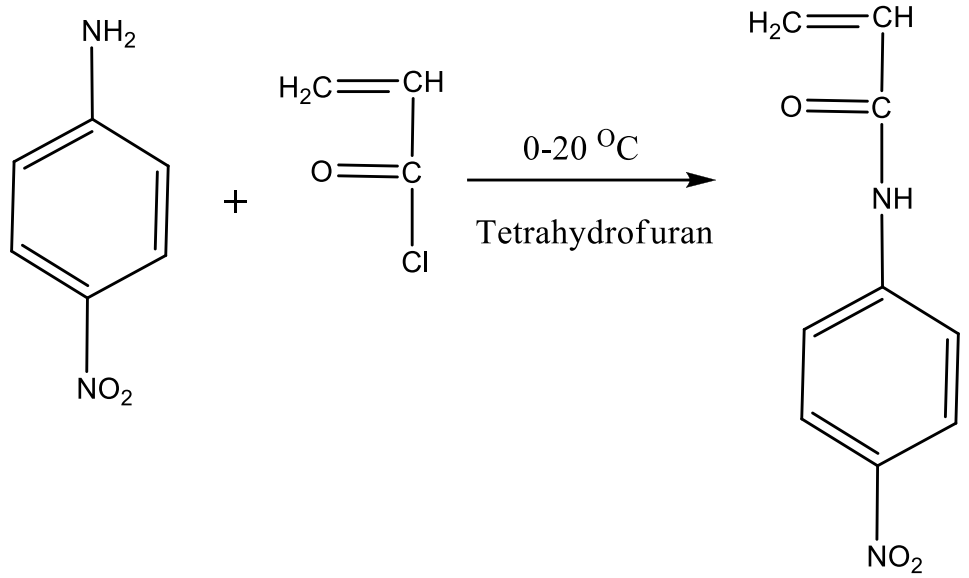

Figure 1. *Synthesis of the N-(4-nitrophenyl)acrylamide (NPA) Monomer*

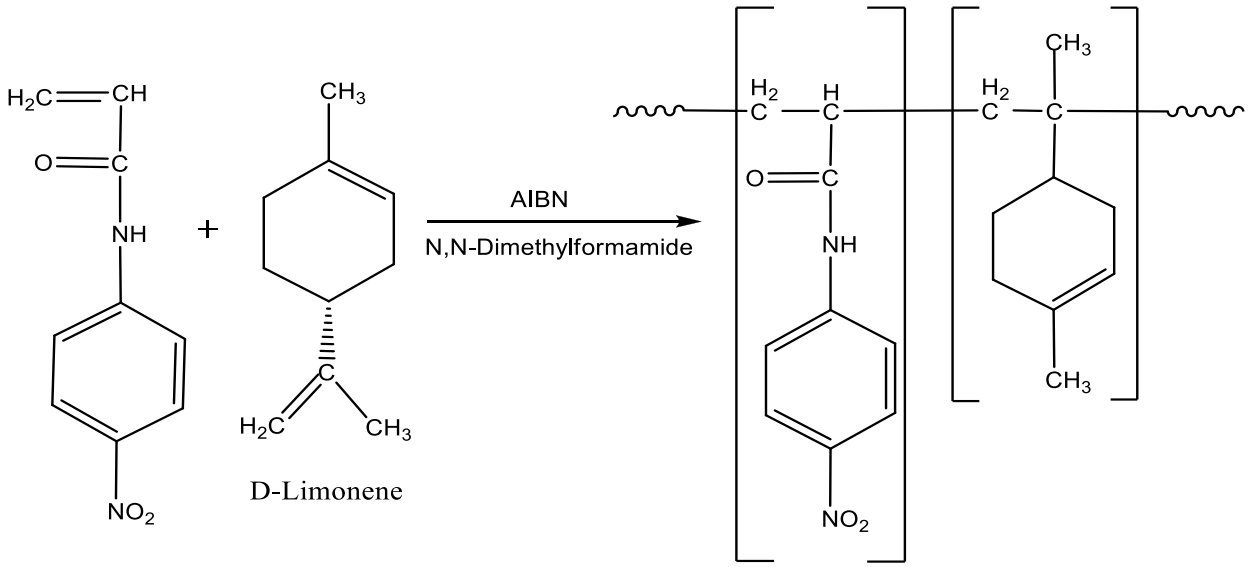

Figure 2. *Synthesis of the LIM-co-NPA Copolymer*

The ^{1}H-NMR spectrum of LIM-co-NPA is indicated in Figure 4. In the ^{1}H-NMR spectrum of the copolymer, the subsequent peaks were seen δ (ppm): N–H structure at 9.4 ppm, ring protons at 8.2 and 7.9 ppm, endocyclic and exocyclic –CH cyclohexene protons at 5.9 and 5.3 ppm, limonene CH_3 and its cyclohexane CH_2 at 2.4 ppm, protons which exist along the polymer chains at 1.4 ppm (Ren et al., 2015; Tanış et al., 2019; Çankaya et al., 2019; 2021). Limonene contains unsaturated endocyclic and exocyclic double bonds. Since endocyclic in double bonds in the limonene ring is more reactive and stable than exocyclic, endo peaks were observed in lower area in NMR results (Brum et al., 2013; Ren et al., 2015; Çankaya et al., 2019; 2021). The data obtained from the ^{1}H-NMR spectrum were found to be in agreement with the polymers synthesized with limonene in the literature (Sharma & Srivastava, 2003; 2004; 2006; Singh & Kamal, 2012; Ren et al., 2015; Zhang & Dubé 2015; Çankaya et al., 2019; 2021).

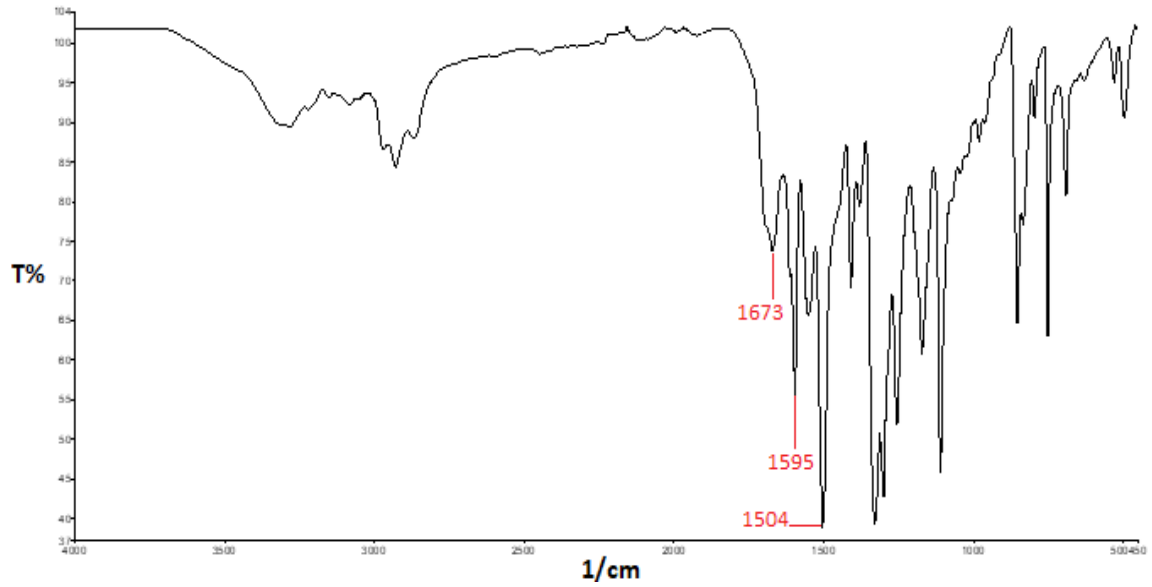

Figure 3. *The FT-IR Spectrum of LIM-co-NPA*

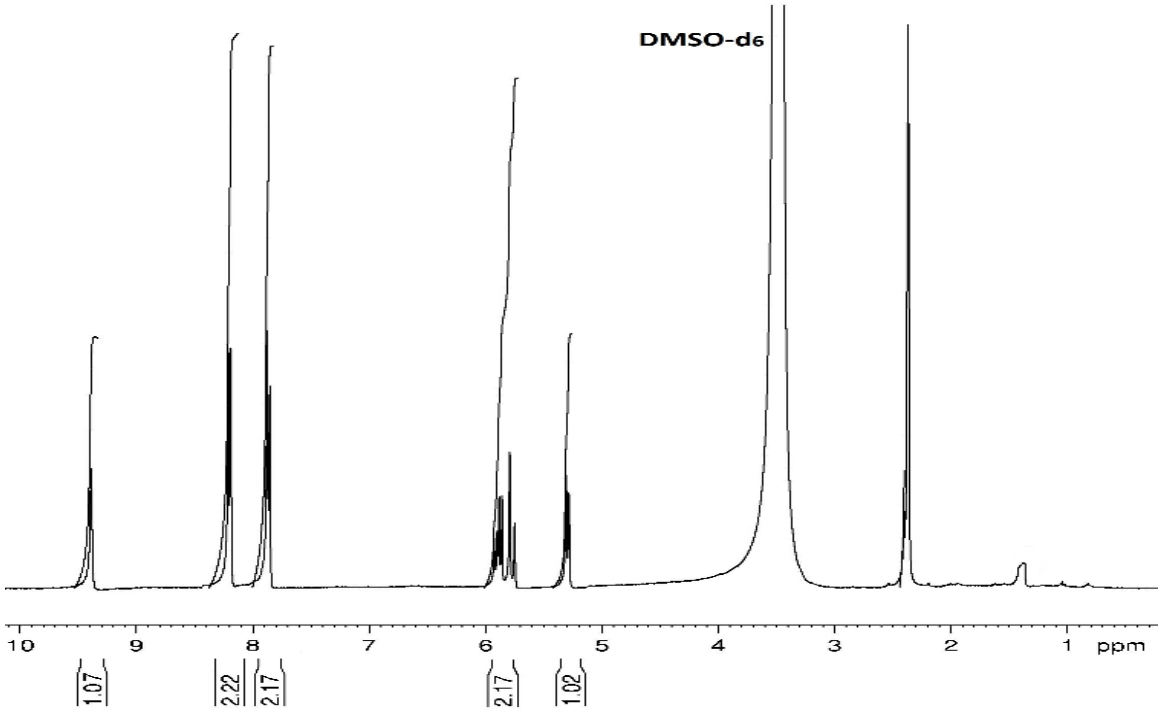

Figure 4. *The ^{1}H-NMR Spectrum of LIM-co-NPA*

3.2. Thermal Characterization of LIM-co-NPA Copolymer

The thermal features of copolymer were performed by TGA/DTG/DTA simultaneous system, a heating rate of 10°C min^{-1} in nitrogen atmosphere, from room temperature to 600°C temperatures. The decomposition temperature and the temperature at weight loss are taken as a measure of thermal stability. Some thermal data such as degradation temperatures at various temperature intervals and mass loss percentages are presented in Table 1. Important thermal results for copolymer; first decomposition temperature was 226°C, decomposition temperatures were 269°C, 281°C, and 367°C for 20%, 25% and 50%, respectively; weight loss at 400°C, 450°C, and 500°C were 53%, 56%, and 60% respectively; residue at 500°C, 550°C and 600°C were 40%, 37% and 35%, respectively. The first and second maximum decomposition temperatures were 261°C and 329°C, respectively. In addition, from the DTA curve, it was seen that Tg (Glass transition temperature) was 261°C and Tc (Crystallization temperature) was 340°C. The thermal curves of copolymer are given in Figure 5

(Coşkun et al., 2002; Turan & Şekerci, 2009; Adiguzel et al., 2011; Arrieta et al., 2013; Brum et al., 2013; Temüz, 2017; Çankaya et al., 2019; 2021; Kurt et al., 2019b; 2020; Bingöl & Turan, 2020).

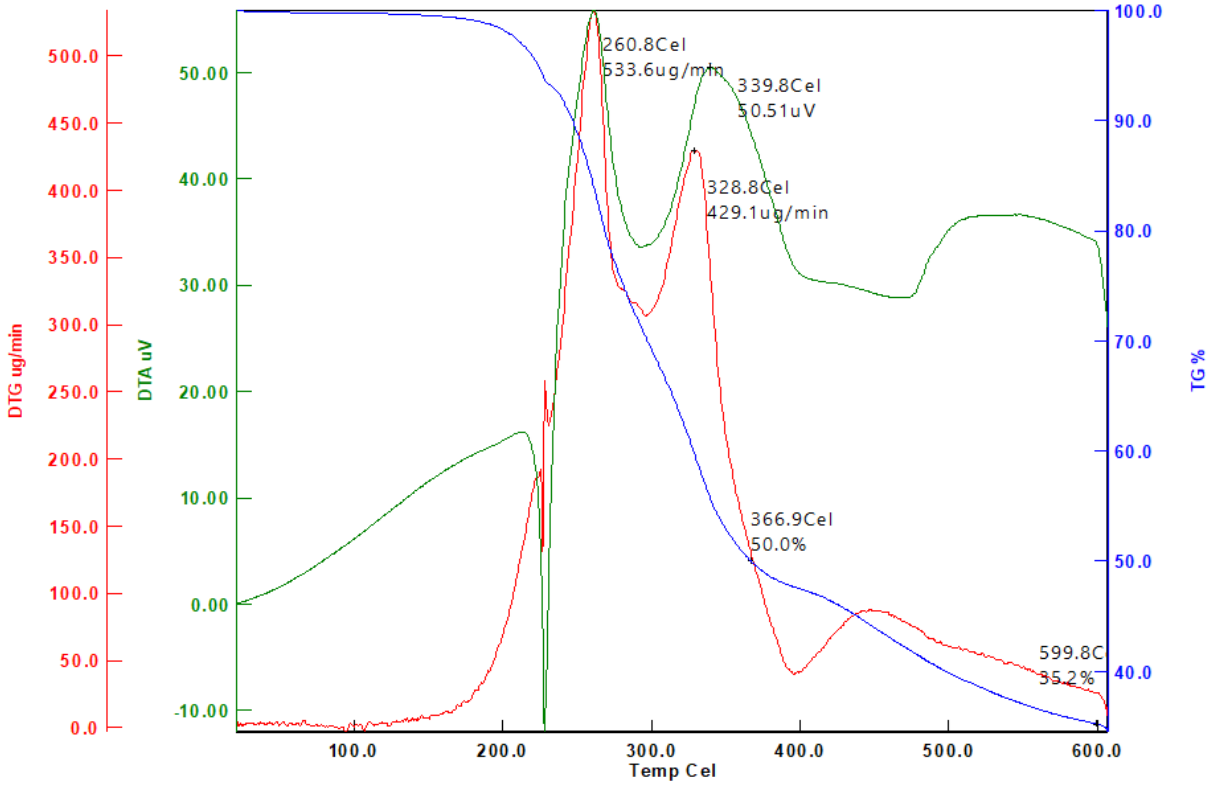

Figure 5. *The TGA/DTG/DTA Curves of the LIM-co-NPA Copolymer*

Table 1. *Some Thermal Data of the LIM-co-NPA Copolymer*

Sample	Maximum decomposition temperature	Decomposition temperature at 20, 25, and 50%	% Weight loss 400, 450, and 500 °C	% Residue 500, 550, 600 °C
Copolymer	261°C and 329°C	269°C, 281°C, and 367°C	53%, 56%, and 60%	40%, 37%, and 35%

4. CONCLUSION

In this study, sustainable poly(D-limonene-co-N-(4-nitrophenyl)acrylamide) (LIM-co-NPA) has been synthesized via free-radical polymerization. The copolymer was characterized by FT-IR and ^{1}H-NMR spectroscopy techniques. Thermal behavior of copolymer was investigated by the TGA/DTG/DTA simultaneous system. The results obtained from spectroscopic techniques were in agreement with the literature. The thermal stability of the sustainable copolymer was also good. It is hoped that this newly synthesized copolymer will find application in different fields of study in the future.

ACKNOWLEDGEMENT

The authors thank the Uşak University Research Fund (2014/ÖAP002) for their support for the thermal analyzes of this study.

CONFLICT OF INTEREST

The authors declare no conflict of interest.

REFERENCES

Adiguzel, R., Ergin, Z., Sekerci, M., & Tascioglu, S. (2011). Synthesis and structural characterization of bis(2-amino-1,3,4-thiadiazolyl)methane complexes. *Journal of the Chemical Society of Pakistan*, *33*(2), 238-244.

Arrieta, M. P., López, J., Ferrándiz, S., & Peltzer, M. A. (2013). Characterization of PLA-limonene blends for food packaging applications. *Polymer Testing*, *32*(4), 760-768. doi:10.1016/j.polymertesting.2013.03.016

acanlı, M., Başaran, A. A., & Başaran, N. (2018). Effects and Usage of a Citrus Compound, Limonene. In: R. R. Watson, V. R. Preedy, & S. Zibadi (Eds.) *Polyphenols: Prevention and Treatment of Human Disease* (Second Ed.) (pp. 419-424). Cambridge: Academic Press. doi:10.1016/B978-0-12-813008-7.00032-1

Bingöl, M., & Turan, N. (2020). Schiff base and metal(II) complexes containing thiophene-3-carboxylate: Synthesis, characterization and antioxidant activities. *Journal of Molecular Structure*, *1205*, 127542. doi:10.1016/j.molstruc.2019.127542

Brum, F. J. B., Laux, F. N., & Forte, M. M. C. (2013). Synthesis of hydrocarbon polymers by cationic polymerization and their thermal properties. *Designed Monomers and Polymers*, *16*(3), 291-301. doi:10.1080/15685551.2012.747145

Coşkun, D., Gündüz, B., & Coşkun, M. F. (2019). Synthesis, characterization and significant optoelectronic parameters of 1-(7-methoxy-1-benzofuran-2-yl) substituted chalcone derivatives. *Journal of Molecular Structure*, *1178*, 261-267. doi:10.1016/j.molstruc.2018.10.043

Coşkun, M., Erol, İ., Coşkun, M. F., & Demirelli, K. (2002). Thermal degradation behavior of two methacrylate polymers with side chain amide groups. *Polymer Degradation and Stability*, *78*(1), 49-55. doi:10.1016/S0141-3910(02)00118-0

Çankaya, N., & Temüz, M. M. (2012). Characterization and monomer reactivity ratios of grafted cellulose with N-(4-nitrophenyl)acrylamide and methyl methacrylate by atom transfer radical polymerization. *Cellulose Chemistry and Technology*, *46*(9-10), 551-558.

Çankaya, N., Tanış, E., Elmalı, H. G., & Bulut, N. (2019). A new synthesize of limonene copolymer: Experimental and theoretical analysis. *Polymer Bulletin*, *76*(7), 3297-3327. doi:10.1007/s00289-018-2543-3

Çankaya, N., Tanış, E., & Sapan, P. G. (2021). New synthesis of homopolymer and limonene copolymer: Experimental analysis and density functional theory study. *Russian Journal of Physical Chemistry A*, *95*(1), 139-153. doi:10.1134/S0036024421010052

Farhat, A., Fabiano-Tixier, A-S., Maataoui, M. E., Maingonnat, J-F., Romdhane, M., & Chemat, F. (2011). Microwave steam diffusion for extraction of essential oil from orange peel: Kinetic data, extract's global yield and mechanism. *Food Chemistry*, *125*(1), 255-261. doi:10.1016/j.foodchem.2010.07.110

Guyton, K. Z., & Kensler, T. W. (2002). Prevention of liver cancer. *Current Oncology Reports*, *4*(1), 464-470. doi:10.1007/s11912-002-0057-4

Hajizadeh, M. R., Maleki, H., Barani, M., Fahmidehkar, M. A., Mahmoodi, M., & Torkzadeh-Mahani, M. (2019). In vitro cytotoxicity assay of D-limonene niosomes: an efficient nano-carrier for enhancing solubility of plant-extracted agents. *Research in Pharmaceutical Sciences*, *14*(5), 448-458. doi:10.4103/1735-5362.268206

Hartsel, J. A., Eades, J., Hickory, B., & Makriyannis, A. (2016). *Cannabis Sativa* and Hemp. In: R. C. Gupta (Eds.) *Nutraceuticals*: *Efficacy, Safety and Toxicity* (pp. 735-754). Elsevier Inc: London. doi:10.1016/B978-0-12-802147-7.00053-X

Kurt, A., Gündüz, B., İlter, Z., & Koca M. (2019a). Optoelectronic properties of 3-acetyl-6-bromocoumarin compound in various solvents and concentrations. *Kuwait Journal of Science*, *46*(3), 60-70.

Kurt, A., Gündüz, B., & Koca, M. (2019b). A detailed study on the optical properties of 3-benzoyl-7-hydroxy coumarin compound in different solvents and concentrations. *Macedonian Journal of Chemistry and Chemical Engineering*, *38*(2), 227-236. doi:10.20450/mjcce.2019.1403

Kurt, A., Andan, H., & Koca, M. (2020). Synthesis and characterization of a new bithiazole-containing conjugated polymer and its thermal decomposition kinetics. *Macedonian Journal of Chemistry and Chemical Engineering*, *39*(2), 227-237. doi:10.20450/mjcce.2020.2025

Lu, X-g., Feng, B-a., Zhan, L-b., & Yu, Z-h. (2003). D-limonene induces apoptosis of gastric cancer cells. *Chinese Journal of Oncology*, *25*(4), 325-327.

Monica, F. D., & Kleij A. W. (2020). From terpenes to sustainable and functional polymers. *Francesco Polymer Chemistry*, 11(32), 5109-5127. doi:10.1039/D0PY00817F

Murali, R., Karthikeyan, A., & Saravanan, R. (2013). Protective effects of D-limonene on lipid peroxidation and antioxidant enzymes in streptozotocin-induced diabetic rats. *Basic & Clinical Pharmacology &Toxicology*, *112*(3), 175-181. doi:10.1111/bcpt.12010

Neumann, S., Hu, P., Bretschneider, F., Schmalz, H., & Greiner A. (2021). Blends of bio-based poly(limonene carbonate) with commodity polymers. *Macromolecular Materials and Engineering*, *306*(7), 2100090. doi:10.1002/mame.202100090

Ren, S., Trevino, E., & Dube, M. A. (2015). Copolymerization of limonene with n-butyl acrylate. *Macromolecular Reaction Engineering*, 9(4), 339-349. doi:10.1002/mren.201400068

Sharma, S., & Srivastava, A. K. (2003). Alternating copolymers of limonene with methyl methacrylate: kinetics and mechanism. *Journal of Macromolecular Science Part A Pure and Applied Chemistry*, *40*(6), 593-603. doi:10.1081/MA-120020867

Sharma. S., & Srivastava, A. K. (2004). Synthesis and characterization of copolymers of limonene with styrene initiated by azobisisobutyronitrile. *European Polymer Journal*, *40*(9), 2235-2240. doi:10.1016/j.eurpolymj.2004.02.028

Sharma, S., & Srivastava, A. K. (2006). Radical co-polymerization of limonene with N-vinyl pyrrolidone: Synthesis and characterization. *Designed Monomers and Polymers*, *9*(5), 503-516. doi:10.1163/156855506778538001

Singh, A., & Kamal, M. (2012). Synthesis and characterization of polylimonene: Polymer of an optically active terpene. *Journal of Applied Polymer Science*, *125*(2), 1456-1459. doi:10.1002/app.36250

Souto, E. B., Zielinska, A., Souto, S. B., Durazzo, A., Lucarini, M., Santini, A., Silva, A. M., Atanasov, A. G., Marques, C., Andrade, L. N., & Severino, P. (2020). (+)-Limonene 1,2-epoxide-loaded SLNs: Evaluation of drug release, antioxidant activity, and cytotoxicity in an HaCaT cell line. *International Journal of Molecular Sciences*, *21*(4), 1449. doi:10.3390/ijms21041449

Sun, J. (2007). D-limonene: Safety and clinical applications. *Alternative Medicine Review-A Journal of Clinical Therapeutics*, *12*(3), 259-264. PubMed:18072821

Tanış, E., Çankaya, N., & Yalçın, S. (2019). Synthesis, characterization, computation of global reactivity descriptors and antiproliferative activity of N-(4-nitrophenyl)acrylamide. *Russian Journal of Physical Chemistry B*, *13*(1), 49-61. doi:10.1134/S1990793119010147

Temüz, M. M. (2017). Radical copolymerization of acrloylmorpholine with 2-hydroxyethyl methacrylate: Monomer reactivity ratios and thermal properties. *Anadolu University Journal of Science and Technology A-Applied Sciences and Engineering*, *18*(5), 929-938. doi:10.18038/aubtda.306626

Turan, N., & Şekerci, M. (2009). Metal complexes of Schiff base derived from terephthalaldehyde and 2-amino-5-ethyl-1,3,4-thiadiazole synthesis, spectral and thermal characterization. *Synthesis and Reactivity in Inorganic Metal-Organic and Nano-Metal Chemistry*, *39*(10), 651-657. doi:10.1080/15533170903433162

Yu, X., Lin, H., Wang, Y., Lv, W., Zhang, S., Qian, Y., Deng, X., Feng, N., Yu, H., & Qian, B. (2018). D-limonene exhibits antitumor activity by inducing autophagy and apoptosis in lung cancer. *OncoTargets and Therapy*, *11*, 1833-1847. doi:10.2147/OTT.S155716

Zhang, X., Fevre, M., Jones, G. O., & Waymouth, R. M. (2018). Catalysis as an enabling science for sustainable polymers. *Chemical Reviews*, *118*(2), 839-885. doi:10.1021/acs.chemrev.7b00329

Zhang, Y., & Dubé, M. A. (2014). Copolymerization of *N*-butyl methacrylate and D-limonene. *Macromolecular Reaction Engineering*, *8*(12), 805-812. doi:10.1002/mren.201400023

Zhang, Y., & Dubé, M. A. (2015). Copolymerization of 2-ethylhexyl acrylate and D-limonene, copolymerization of 2-ethylhexyl acrylate and D-limonene. *Polymer-Plastics Technology and Engineering*, *54*(5), 499-505. doi:10.1080/03602559.2014.961080

Research Article / Araştırma Makalesi GU J Sci, Part A, 8(4): 537-550 (2021) https://doi.org/10.54287/gujsa.1032149

Gazi University
Journal of Science
PART A: ENGINEERING AND INNOVATION
http://dergipark.org.tr/gujsa

Chromitite Ore Types and Geochemical Investigation of Pozantı-Karsantı Ophiolite in Mazmılı Region (Turkey)

Ali TÜMÜKLÜ[1*]

[1]*Nigde Omer Halisdemir University, Engineering Faculty, Geological Engineering Department, 51240, Nigde, Turkey*

Keywords

Ophiolite
Chromitite
Geochemistry
Pozanti-Karsanti

Abstract

The Pozantı-Karsantı Ophiolite located in the middle Taurus has significant chromitite reserves in Turkey. The chromitite ore bodies belong to concordant and subconcordant form and are located within mantle harzburgite surrounded by bodies of dunite. Chromitite ore types are small or medium bodies of massive, disseminated, banded and nodular, also the result of a combination of at least two of these types of ores consist of mixed-type ore. Chromite ores bear traces of plastic deformation under the influence of lateral forces developing in the lateral direction. Plastic deformation is also observed at the micro scale. This study presents the concentrations of a complete suite of major (SiO_2, Cr_2O_3, MgO, Al_2O_3, and FeO(t)) and trace elements (Ni, Ti, Co, V, Zn, S, Ca, Ga and Cl) in podiform chromitites of the Pozantı-Karsantı Ophiolite. According to the chromite ore whole-rock geochemical analysis, there was a positive relationship between the amount of Cr_2O_3 and Zn, V, Ti, and Co, while a negative relationship was found between Ni, S and Ca. This situation is opposite with the dunites in which the chromite ore is located.

Cite

Tumuklu, A. (2021). Chromitite Ore Types and Geochemical Investigation of Pozantı-Karsanti Ophiolite in Mazmılı Region (Turkey). *GU J Sci, Part A, 8*(4), 537-550.

Author ID (ORCID Number)

A. Tumuklu, 0000-0003-1215-8748

Article Process

Submission Date 03.12.2021
Revision Date 15.12.2021
Accepted Date 29.12.2021
Published Date 30.12.2021

1. INTRODUCTION

The characteristics of the rock groups belonging to the ophiolites, the geochemical and mineralogical-petrographical data obtained from the peridotites are important for the production of information about the upper mantle. Some studies on this subject; Niu et al., 1997; Takazawa et al., 2000; Choi et al., 2008; Dilek & Morishita, 2009; Uysal et al., 2012. During the last decades, improvements in analytical techniques have allowed detailed geochemical studies of well-selected ophiolites and podiform chromitites on worldwide. One of the important topics for ore geology is ore type and major-trace element geochemistry. The only known economic mineral of the chromium element is the chromite mineral of spinel group and its ore chromitite. Therefore, the geochemistry and macro properties of the chromite ore are important in terms of Cr mining. In the current study, we present new ore chemistry of chromitite, mineralogy and macro-ore properties from Pozanti-Karsanti Ophiolite (PKO) (Southern-Turkey) in order to contribute to the understanding of podiform chromitite.

2. GEOLOGICAL BACKGROUND AND DESCRIPTION OF THE POZANTI-KARSANTI OPHIOLITE

Pozantı-Karsantı Ophiolite forms the subject of this study is included Dilek & Robinson (2003) group Tethyan-Carribbean Ophiolite and Bouider & Nicolas (1985) harzbugite subtypes in Eastern Tauride belt in southern Turkey (Figure 1). In Southern Turkey, there are two main units, the ophiolitic and carbonate platform, within the Taurus belt. Overlying ophiolites are mid-late Cretaceous and carbonates are in the late

*Corresponding Author, e-mail: alitum@ohu.edu.tr

Devonian to early Cretaceous age range (Blumenthal, 1946; Tekeli, 1981; Tekeli et al., 1984; Polat & Casey, 1995). PKO is represent one of the largest fragments of oceanic in southern Turkey lies in the Eastern Tauride Belt (Aladağ region), offset from the Mersin ophiolite by the sinistral Ecemis fault (Çakır, 1978; Yetiş, 1984; Parlak et al., 2002). In upward succession, the rock groups belonging to the PKO are fragments of the neotethys ocean and consist of peridotites, mafic-ultramafic cumulates and gabbros belonging to tectonites. Cumulate gabbros and peridotites are cut by dolerite-diabase dykes (Figure 2) (Anıl, 1990). Geochemical data of ultramafic and mafic groups of ophiolitic rocks show that this group is derived from tholeiitic material with island arc characteristic occurring in subduction zones (Parlak et al., 2002).

Chromitite ore production proceed continuously in about 50-60 area in PKO by open pit or underground mining methods since 1940. While raw material having high degree (35 and up % Cr2O3) is evaluated without progress, low degree (min 5-7 and up % Cr2O3) ore is evaluated domestic and export markets mining stocks after concentrated in plant.

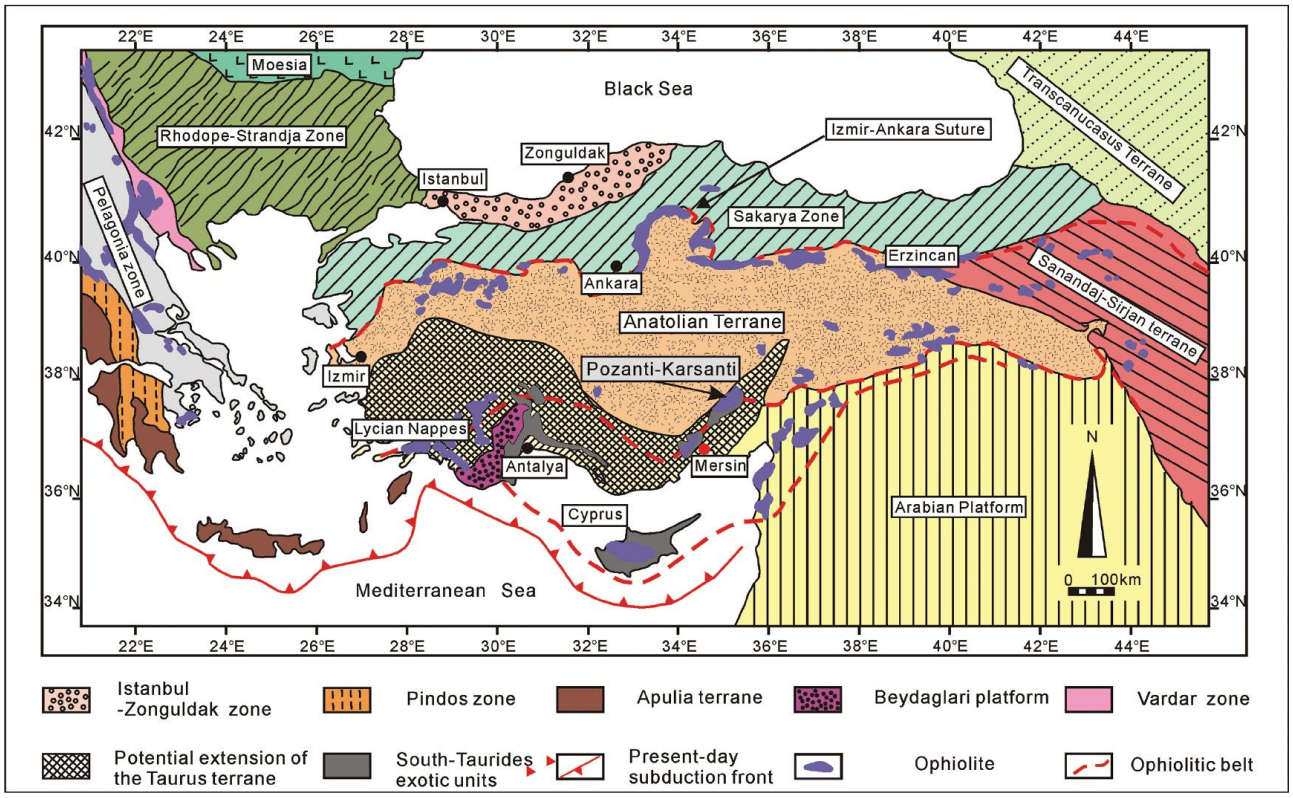

Figure 1. *Distribution of Ophiolites and Surrounding Regions of Turkey (from Lian et al., 2017)*

3. SAMPLES AND ANALYTICAL METHODS

Chromitite and peridotite samples used for this study are collected from the outcrop and mining area in the western part of the PKO in Mazmılı area. A total of 25 samples were collected from slickensides, ores and host rocks in chromitite outcrops and the mining areas in Mazmlı region. Thin sections were made from the rock samples and polished sections were made from the ore samples. Microscopic structures and textures and ore paragenesis were determined by examining the sections in N. Ömer Halisdemir University, Engineering Faculty, Geological Engineering Department, mineralogy-petrography laboratory. As a result of the microscope studies, 10 samples representing the mineralization were determined for geochemical analysis. The ore samples were grinded with a pulverizer at 80 mesh (177 μ) size in N. Ömer Halisdemir University Engineering Faculty Geological Engineering laboratories. The non-homogeneously grinded samples were homogenized using agate mortar and placed in 15 grams locked plastic bags and made ready for analysis. Geochemical analyses were carried out at TUBİTAK-MAM Center with the wavelength dispersed X-Ray Fluorescence Spectrometer (WD-XRF) method, and the amounts of major oxides and trace elements were determined.

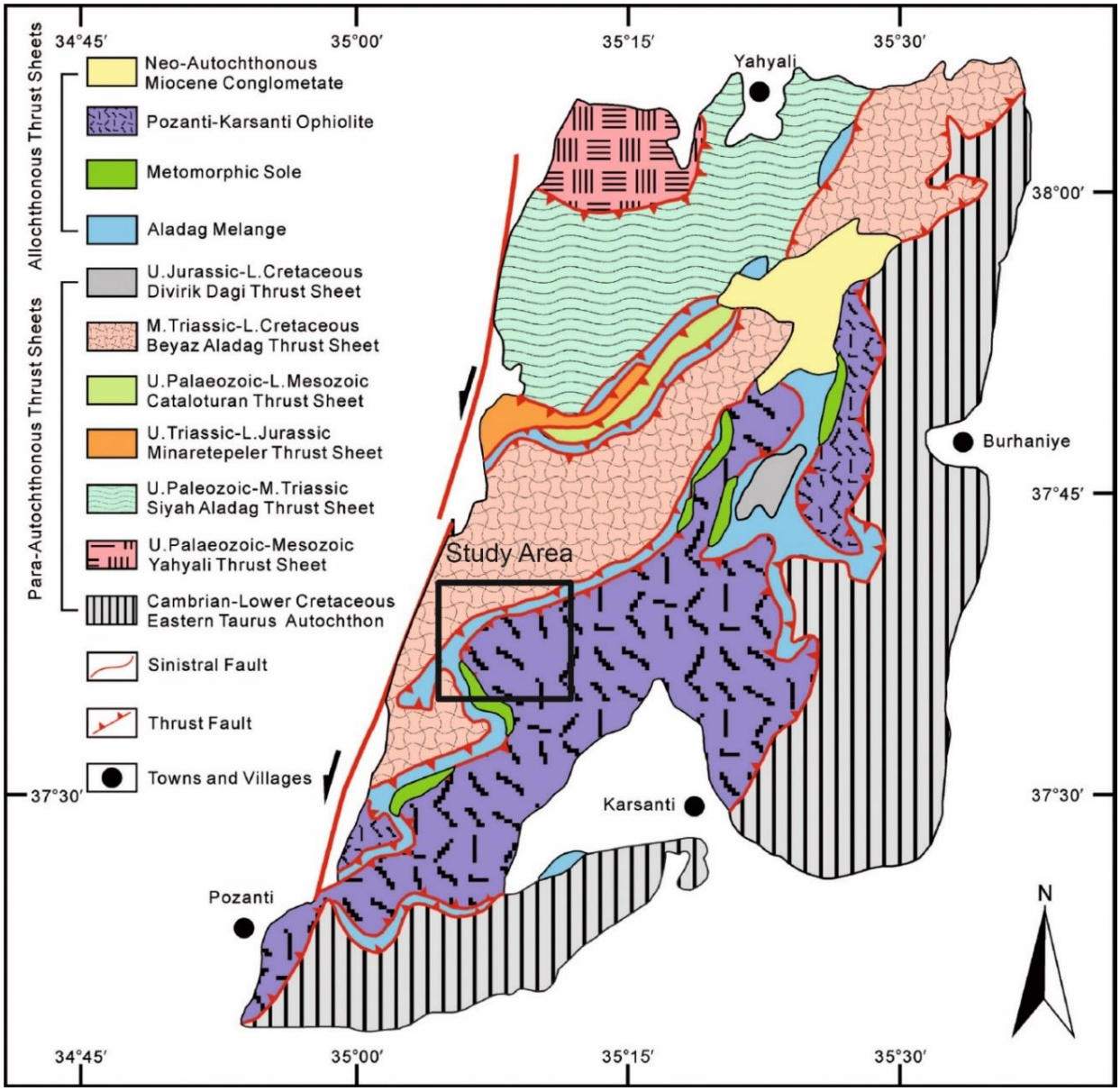

Figure 2. *Geological map of the study area and its surroundings (from Bingöl, 1978).*

4. RESULTS

4.1. Chromitite Ore Types

The chromitite ore bodies of Mazmılı field at Pozantı-Karsantı Ophiolite belong to concordant and subconcordant form and are located within mantle harzburgite surrounded by bodies of dunite. Chromitite ore types are small or medium bodies of massive, disseminated, banded and nodular, also the result of a combination of at least two of these types of ores consist of mixed-type ore.

Massive ore bodies consisting of more than 90 vol. % Cr-spinel are lens, pipe or tabular shapes of highly variable size, lens bodies dominate. The size of individual massive ore bodies ranges from 2-3 cm to 14-15 m thickness and 5-6 cm up to 60-70 m in length. The boundaries of the ore bodies with enclosing dunite are either well defined or gradual to disseminated (Figure 3a-d). Plastic deformation signature has been detected in 4-5 cm long massive type ore. Forces acting along the long axis direction of massive ore were effective on the area of incoming force direction (Figure 3a). However, the forces acting along the short axis of other massive ore were also effective on the symmetry of incoming force side at one body (Figure 3b). In the massive ore, this detail was observed as macro (Figure 3d).

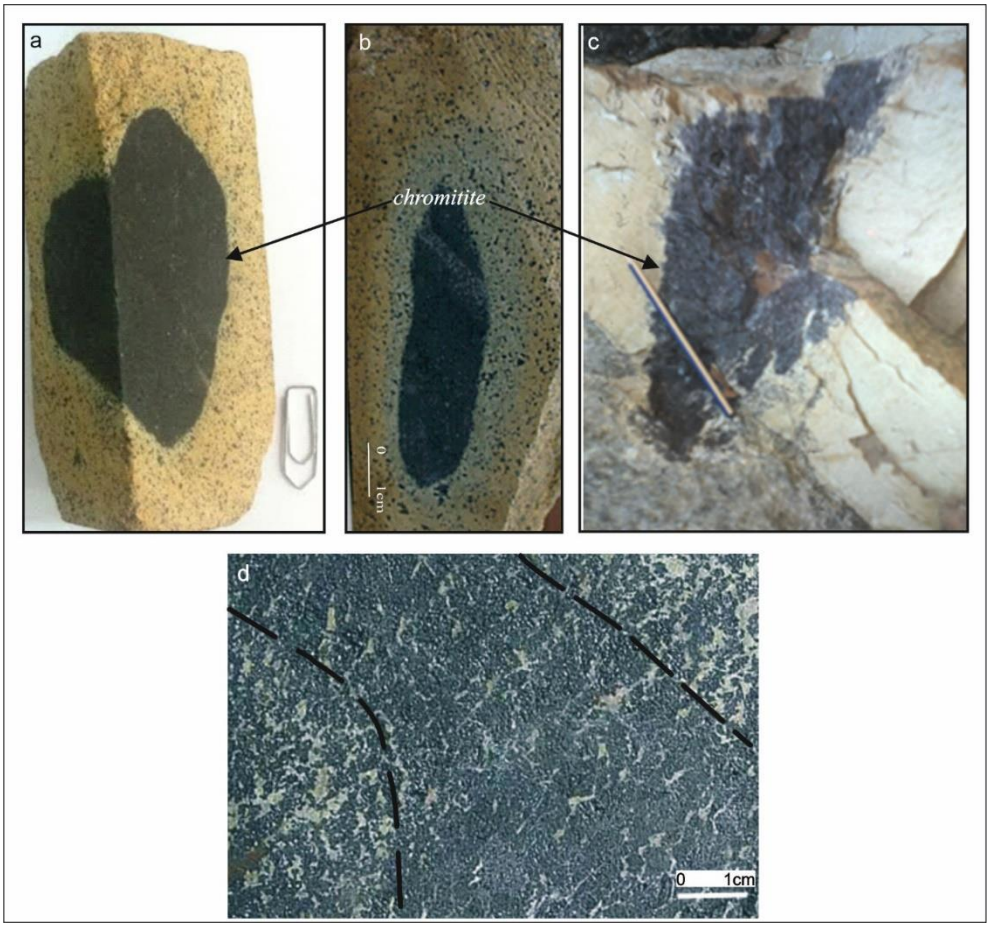

Figure 3. *Small-Scaled Massive Ore Samples,* ***a)*** *Sample Showing Deformation in One Direction,* ***b)*** *Deformation on Both Sides of the Massive Sample,* ***c)*** *Small-Scaled Massive ore Containing No Disseminated Ore* ***d)*** *Differences in Massive ore as a Result of Plastic Deformation*

Banded ore is located in the very limited areas. Chromitite ore composed of dunite-chromitite alternation. Both dunite and chromitite bands are not sterile and have gradual transitions. The thickness of the bands varies between a few mm and cm. There are 2-3 cm long pods and 1-2 mm thick dunite dikes in chromitite bands. Orientation of the pods are parallel to the bands. (Figure 4). Cr spinel crystals are also found in dunite pods and dykes.

Figure 4. *Dunite Pods and Dyke in Banded Chromitite Ore*
(Dunite Lenses are Parallel to Chromite Bands and Contain Cr spinels.
Dunite Dykes are Perpendicular to the Banded Chromitite and Contain Cr Spinels.)

Nodules of chromitite range from 10 to 30 mm in size and are approximately spherical, ovoid or cubic like. Nodules of different structures can coexist. The nodules are arranged parallel or oblique to the igneous layering. Irregular chromitite bodies are observed between some nodules and their size are smaller than 1cm. Nodules by the internal structure can be grouped by massive and skeletal olivine. Massive ones consist of 90-95 % and skeletal olivine ones consist of 85-90 % chromian spinel. Some nodules can be scattered with showing no contact to each other. Others can be found in the form of chain and get flatted (Figure 5a-f).

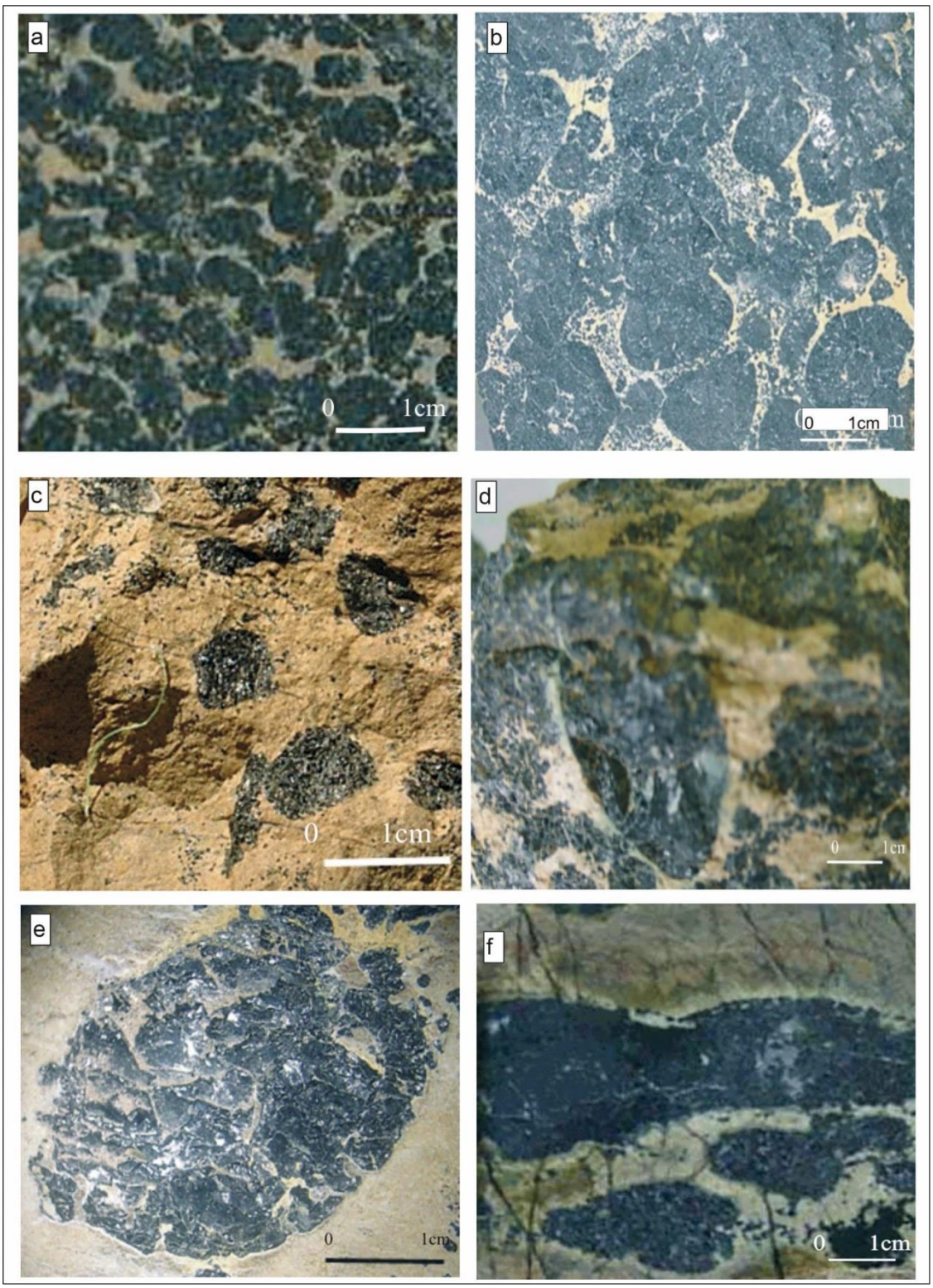

Figure 5. *Nodular Chromitite,* ***a)****,* ***b)*** *Different Size Nodular Chromitite,* ***c)****,* ***d)*** *Irregular Nodules,* ***e)*** *Skeletal Olivine Nodule Chromite,* ***f)*** *Chain and Get Flatted Nodules*

Disseminated chromitite are found with massive, nodular and banded type ores but also in the form of separate layers. Cr spinels founded disseminated in the olivines observed as one crystal or groups with 2-3 crystals. There is no orientation in chromite crystals and groups. The sizes of the crystals are quite different, ranging from 0.1 to 0.4 mm. (Figure 6a-b).

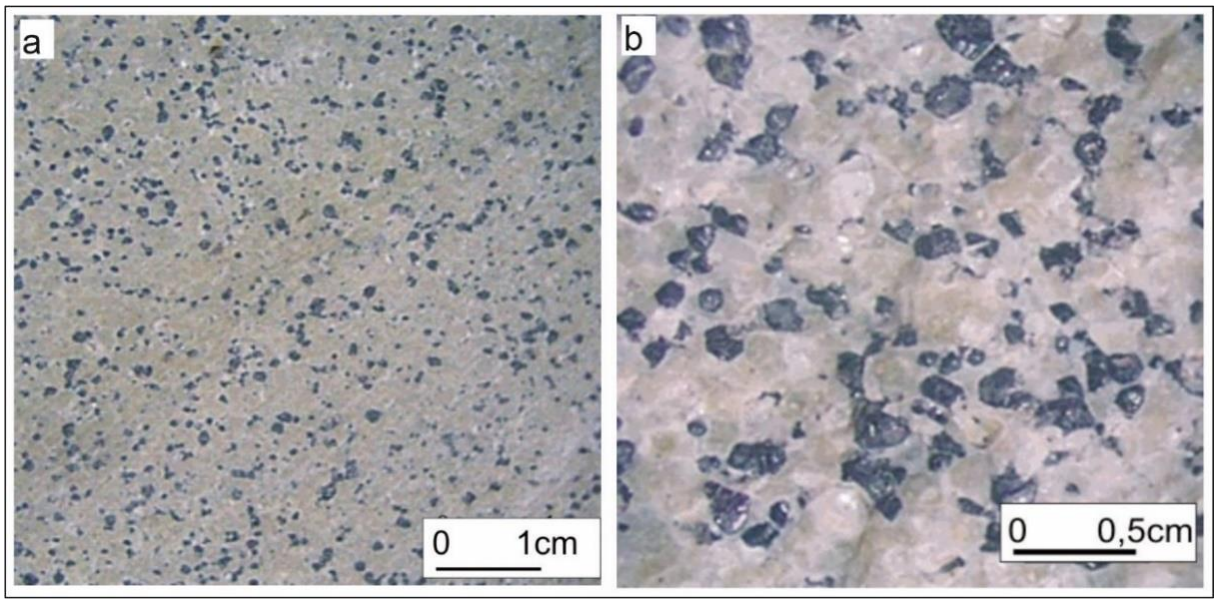

***Figure 6. a)**, **b)** Disseminated Chromitite Ore Sample*

4.2. Petrography

Chromitite in Mazmılı (PKO) area hosted in mantle peridotites section are harzburgite and dunite. Both harzburgites and dunites, which host the chromitite mineralization and deposits, were serpantinized, and they showed mesh texture. Harzburgites samples consist of partly serpentinized olivine (65-80 %), orthopyroxene (15-30 %), clinopyroxenes (3-5%), Cr-spinels (1-2 %) and accessory base metal sulphides.

Based on outcrop of dunite classified as thin envelopes around chromitite pods separating harzburgite and massive body. Mineralogy and textural observation are no disparity between these dunites. According to the descending order of quantity, dunite samples mainly composed serpentinized olivine (≥90%), ortopyroxene (<5%), clinopyroxene (<1-2%), Cr-spinels (<3-4%) and as accessory base metal sulphides. The serpentine minerals filled the fractures and spaces between crystals of Cr-spinel, relict olivine, pyroxene and accessory base metal sulphides (Figure 7a, b). Cr-spinel in the harzburgite and dunite are structure euhedral, subhedral to anhedral amygdaloidal are form host rocks. Cr-spinels within serpentinized dunite turned into magnetite rims along fractures and was characterized by dark red color (Figure 7c, d). Some Cr spinels in peridotites have a distinct orientation. (Figure 7e, f).

The Cr-spinel of chromitite are subhedral to euhedral in shape and vary in size from 0.01 to 0,5 mm (0.2-0,3 mm in average). Cr-spinel crystals showed high reflectivity, and dark to pale gray colors were typical in polished sections. The interstitial matrix of the chromitites consists of olivine, serpentine minerals and accessory base metal sulphide minerals (pentlandite, heazlewoodite and millerite). Most of Cr-spinel had characteristics of pull-apart break texture and micro faults by tectonics. However, samples from imbricate zones exhibited mylonitic and cataclastic textures (Figure 8a, b). Inclusions widely located in Cr-spinels as globular droplets were independent of each other. In certain instances, these droplets showed linear orientation (Figure 8c, d). Silicate inclusions, mainly olivine are interpreted as magmatic minerals based on their textural features by reflecting light microscopy. Base metal sulphide minerals, pentlandite, heazlewoodite and millerite occurred as inclusions in Cr-spinels and serpentine matrix. These inclusions were generally occurred only in trace amounts commonly as single isolated grains. Millerite was the most common base metal sulphides inclusion, according to the reflecting light microscopy studies, (Figure 9a, b).

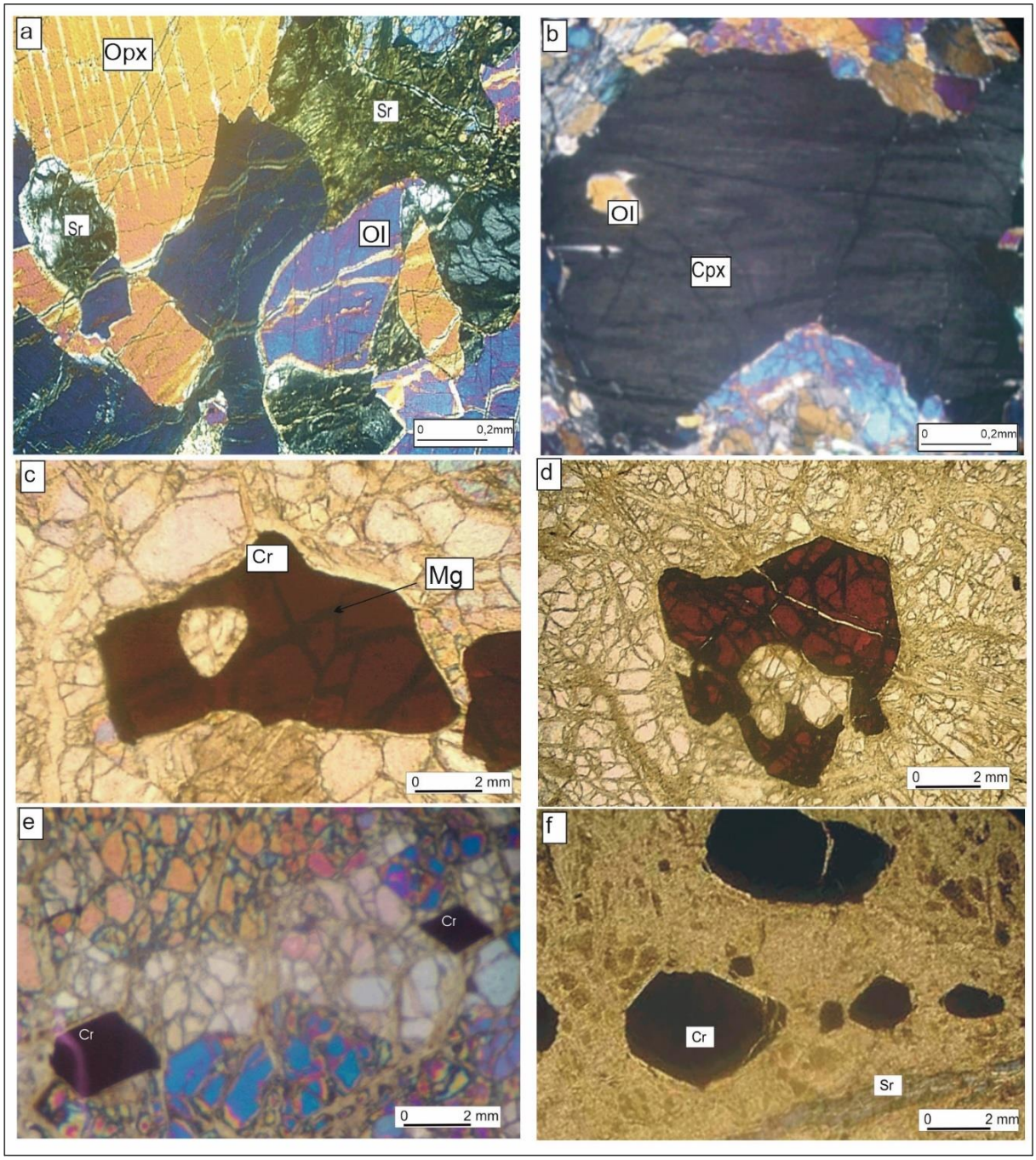

Figure 7. *Microphotos of Peridotite Thin Section,* ***a)***, ***b)*** *Peridotite Mesh Texture,* ***c)***, ***d)*** *Magnetite Rims of Magnetite in Amygdaloidal Cr Spinels in Peridotite,* ***e)*** *Euhedral Cr Spinesls in Olivine,* ***f)*** *Orientation of Cr Spinels (Opx: Ortopyroxene, Sr: Sepantine, Ol: Olivine, Cr: Cr Spinel, Mg: Magnetite).*

4.3. Geochemistry

4.3.1. Whole-Rock Analysis

Major oxides and trace element compositions of the semi-quantitative analysed by XR-F methods within oceanic mantle peridotite chromitites, massive, banded, nodular and disseminated are listed in Table 1. Major oxide concentrations are SiO_2 (3,81-46,91 wt%), Cr_2O_3 (7,05-50,84 wt%), MgO (15,10-40,09 wt%), Al_2O_3 (1,18-12,08 wt%) and FeO(t) (6,73-17,37 wt%). Trace elements concentrations are Ni (1140-2840 ppm), Ti (150-1740 ppm), Co (80-280 ppm), V (90-990 ppm), Zn (50-270 ppm), S (60-160 ppm) and Ca

(90-10790 ppm). However, Ga and Cl elements were not detected above the limit value in all analyses. Therefore, these samples were not taken excluded from the statistical evaluation.

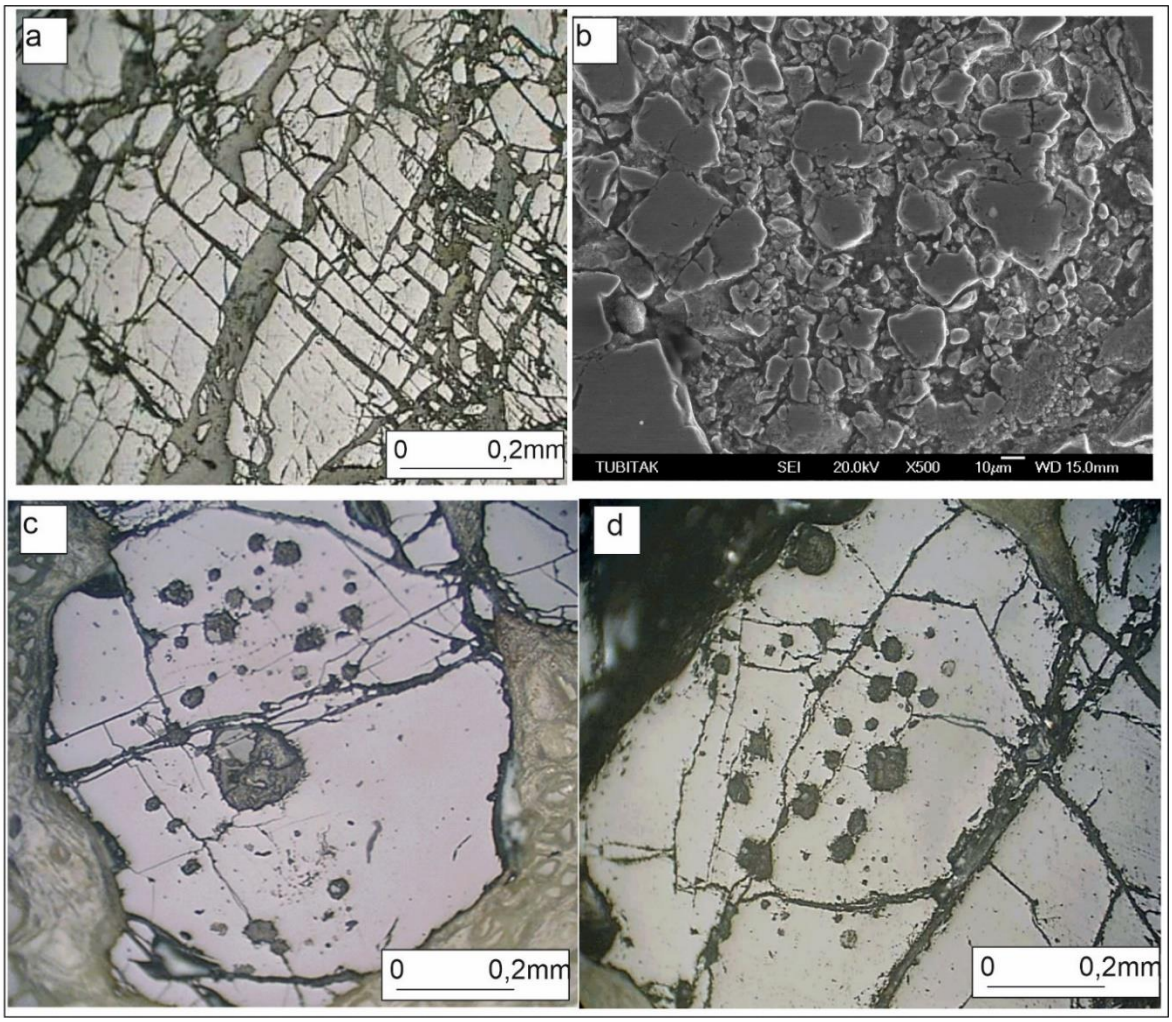

Figure 8. a) *Micro Faults and Pull-Apart Break Texture of Cr-Spinel,* ***b)*** *Scanning Electron Microscope Images of Samples from Imbricate Zones within Chromitites,* ***c)***, ***d)*** *Silicate Inclusions in Cr-Spinel as Droplets (****a****,* ***c****,* ***d****: Reflecting Light Microscopy,* ***b****: SEM)*

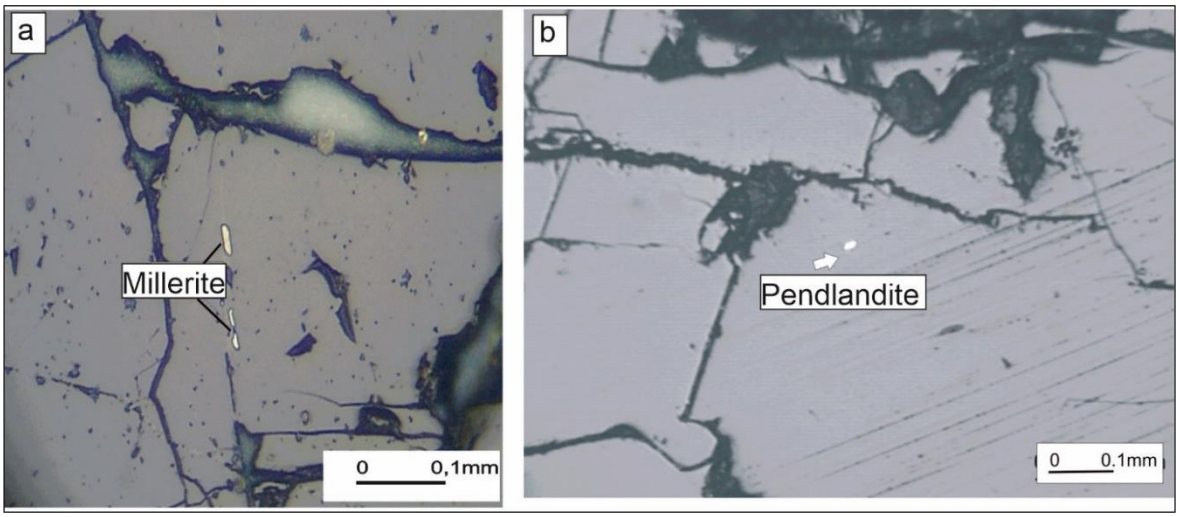

Figure 9. *Millerite and Pentlandite in Cr Spinels*

Olivine and Cr spinel are major components minerals of podiform chromitites. Cr spinel is an oxide with a spinel-type structure that might be expressed using the general formula AB_2O_4. The A site is occupied by Mg^{2+} and Fe^{2+} in tetrahedral coordination and the B site is usually occupied by Cr and Al in octahedral coordination; Cr and Al may be substituted by Fe3+ giving rise to ferrian chromite. Elements like Zn^{2+}, Co^{2+}, Mn^{2+} and Ni^{2+} can substitute Mg^{2+} and Fe^{2+} in A and V^{3+}, Ga^{3+} and Ti^{4+} can substitute Al and Cr in B. Type of nesosilicate or orthosilicate, Olivine is silicate with the general formula A_2SiO_4. The A site is occupied by Mg^{2+} and Fe^{2+} in tetrahedral coordination. Elements like Zn^{2+}, Co^{2+} and Ni^{2+} can substitute in A (Mg^{+2}, Fe^{+2}) (Table 2) (Colas et al., 2014).

Sulphur is major components inclusion minerals of millerite (NiS), heazlewoodite (Ni_3S_2) and pentlandite ($(Fe,Ni)_9S_8$) in Cr spinel and olivine. The low Ca contents are conformable with clinopyroxene abundance. Despite the different degree of serpentinization, the samples, major oxide and trace element concentrations do not appear to have been greatly modified and the major oxide and trace element contents are compatible with the mineralogical-petrological observations.

Table 1. *The Major Oxide and Trace Element Values of the Ore Samples Belonging to the Study Area (-: below detection limits, t: total)*

Major Oxides (wt %)										
	1	2	3	4	5	6	7	8	9	10
SiO_2	46,91	42,33	12,45	3,81	34,70	31,64	23,87	38,75	30,61	41,58
Cr_2O_3	11,26	14,24	40,88	50,84	16,67	26,53	34,91	14,96	20,80	7,05
MgO	33,57	33,85	23,36	15,10	37,03	28,99	25,40	35,22	35,11	40,09
Al_2O_3	1,18	1,77	11,44	12,08	3,27	4,25	5,46	1,93	4,61	1,81
$FeO_{(t)}$	6,73	7,18	11,34	17,37	7,56	8,10	9,79	7,01	8,19	8,65
Total	98,65	99,37	99,47	99,28	99,23	99,51	99,43	99,87	99,32	99,18
Trace elements (ppm)										
Ni	2840	2590	1710	1140	2630	1740	1890	2810	2380	2780
Ti	220	300	520	1740	370	560	600	300	540	150
S	100	150	80	60	110	90	60	160	120	130
Ca	5880	280	90	110	1540	190	180	10790	390	840
Co	80	110	200	280	110	110	130	90	110	130
V	120	170	700	990	210	290	400	190	290	90
Zn	50	70	200	270	80	110	160	60	110	60
Ga	-	850	20	20	-	-	-	-	-	-
Cl	490	-	-	230	760	230	50	980	870	840

Table 2. *Major, minor and trace element in Cr spinel and olivine mineral structures (Modified from ied from Colás et al., 2014; Huang & Deng, 2020).*

Mineral	IMA Classification	Formula	Position	Major element		Trace element	
				Element	Ionic Radius(Å)	Element	Ionic Radius(Å)
Chromite	Spinel subgroup	AB_2O_4	$A^{(IV)}$	Mg^{+2}	0,57	Zn^{+2}	0,6
						Co^{+2}	0,58
				Fe^{+2}	0,63	Ni^{+2}	0,55
			$B^{(IV)}$	Cr^{+3}	0,615	V^{+3}	0,64
				Al^{+3}	0,535	Ga^{+3}	0,62
				Fe^{+3}	0,645	Ti^{+4}	0,60
Olivine	Olivine group	A_2SiO_4	$A^{(II)}$	Mg^{+2} Fe^{+2}	0,57 0,63	Zn^{2+}, Co^{2+}, Ni^{2+}	0,6 0,68 0,55

Whole rock analysis of trace elements in the binary diagram drawn according to the amount of Cr_2O_3 and SiO_2 showed two different results, due to Cr and Si main component elements of Cr spinel and olivine. The whole rock Zn, V, Ti and Co contents had positive correlation but Ni, S and Ca negative with Cr_2O_3. While, Zn, V, Ti, and Co had negative correlation, Ni, S and Ca positive correlation with SiO_2 (Figure 10a-n).

The correlation coefficients between the contents of the trace elements and major oxides from Table 1 were calculated to examine the inter-trace element and major oxides relationships in the chromitite (Table 3). Inter trace element and major oxides positive correlation is found between Cr_2O_3, Al_2O_3, $FeO_{(t)}$, Ti, Co, V and Zn, V and Zn, implying a directly proportional relationship between them, furthermore negative correlation between these elements and MgO, SiO_2, S and Ca (Table 3).

Table 3*. Correlation Coefficients (r) for Selected Trace and Major Oxides in Chromitites from PKO Mantle Peridotite*

	SiO_2	Cr_2O_3	MgO	Al_2O_3	$FeO_{(t)}$	Ni	Ti	S	Ca	Co	V	Zn
SiO_2	1											
Cr_2O_3	-0,98	1										
MgO	0,89	-0,95	1									
Al_2O_3	-0,98	0,95	-0,85	1								
$FeO_{(t)}$	-0,91	0,87	-0,82	0,89	1							
Ni	0,92	-0,96	0,92	-0,89	-0,84	1						
Ti	-0,85	0,85	-0,84	0,79	0,93	-0,84	1					
S	0,79	-0,80	0,79	-0,71	-0,67	0,80	-0,63	1				
Ca	0,44	-0,42	0,40	-0,45	-0,40	0,55	-0,33	0,52	1			
Co	-0,90	0,85	-0,80	0,91	0,98	-0,82	0,86	-0,61	-0,44	1		
V	-0,97	0,96	-0,90	0,97	0,94	-0,90	0,89	-0,70	-0,37	0,95	1	
Zn	-0,99	0,98	-0,91	0,97	0,94	-0,94	0,88	-0,77	-0,48	0,93	0,98	1

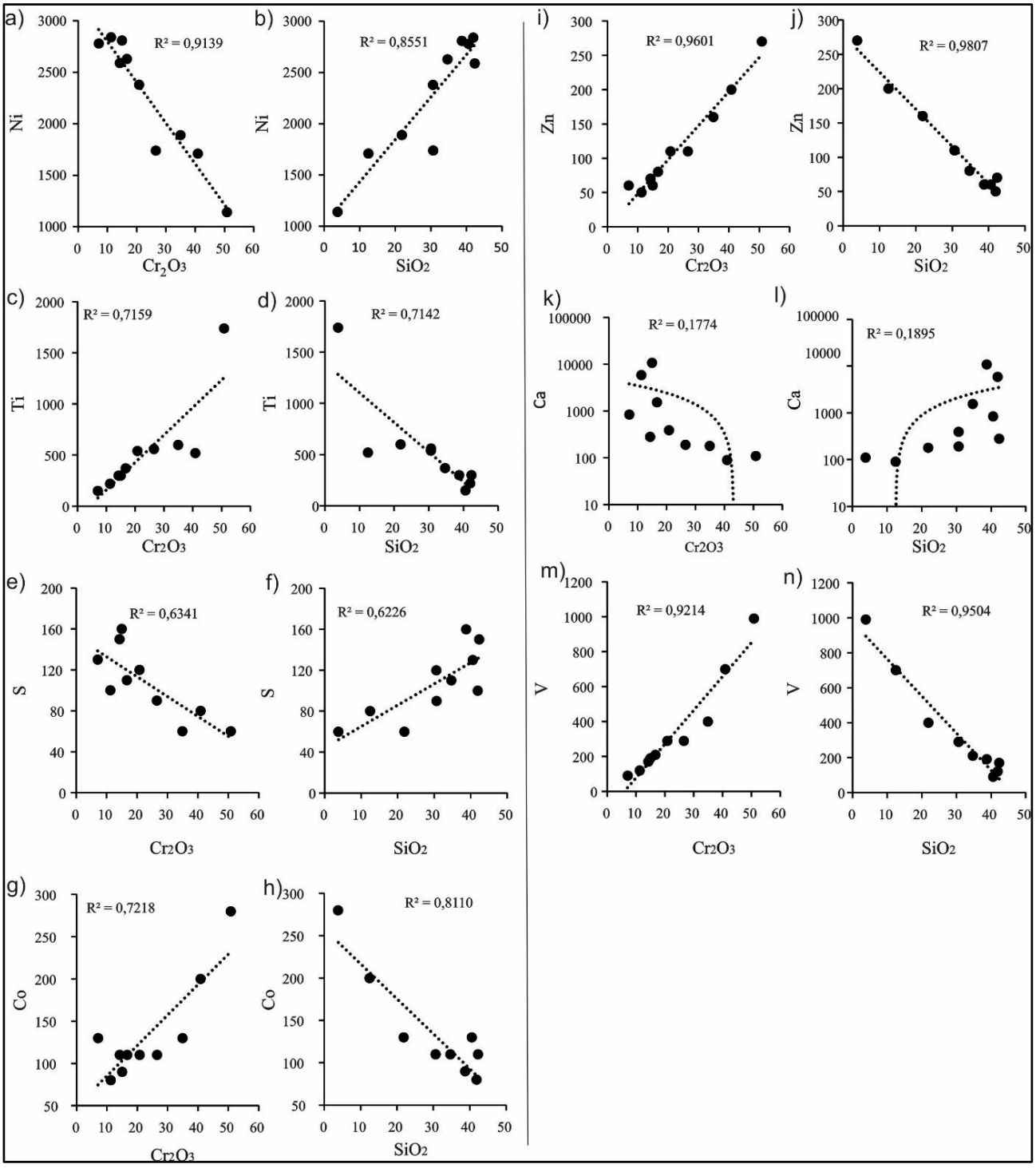

***Figure 10. a)**, **n)** Whole Rock Binary Diagrams of Cr_2O_3 and SiO_2 Versus Trace Elements*

5. DISCUSSION

Podiform Chromite deposits occur as autoliths in the upper mantle tectonites of harzburgite ophiolite types (HOT) (Pearce et al., 1984; Boudier & Nicolas, 1985; Roberts, 1988) and their sizes and distributions are difficult to predict other than their obvious orientation. (Dickey, 1976). By Cassard et al. (1981). They distinguish between congruent, discordant, and unconformable compartments depending on their attitude to the foliation-lineation reference frame in the surrounding plastically deformed peridotite. It is quite difficult to define the chromite ore types in ophiolites, but in general, disseminated, massive, banded, nodular and network structures are common (Thayer, 1964, 1969; Greenbaum, 1977; Brown, 1980; Leblanc, 1980; Duke,

1983). Some ore types are unique to ophiolites, these are nodular, orbicular and coarse crystalline ores (Thayer, 1964).

Podiform chromitites in the study area are massive, banded, disseminated and nodular. It was observed that the chromite masses were exposed to plastic deformation. The bodies forming the ore are under the influence of lateral forces and exhibit elastic behavior in the direction of the incoming force. Especially in the massive ore structure, these deformations are clearly observed. The nodular ore in the region has highly varying properties. Most of ore nodules have the ellipsoidal structure, there are also same cubic structures. The internal structure of the nodules is not homogeneous, and there are two different types of structures (skeletal and massive). The skeletal crystals within the nodules are single crystals that are surrounded by a rim of polycrystalline chromite. The nodules impinged on each other causing local deformation at points of contact (Prichard et al., 2015). There are olivine pods and micro dykes within the banded chromites. The long axes of dunite pods are parallel to each other and no crossing pods were encountered. Small-scale (5-10 cm) massive chromitite ore has plastic deformations applied by lateral forces. Plastic deformation traces are also seen in the nodular ore, in the bands formed by the nodules coming together, and in the aligning of the inclusions in the Cr spinel crystals in a certain direction. Accordingly, it can be said that chromite ore remained under the influence of lateral forces and showed plastic deformation before it solidified completely.

The lack of geochemical distinction between the different podiform type deposit suggests that they may have had similar origins (Cassard et al., 1981). The variation of minor and trace elements in podiform chromite can be used in petrography and environment interpretation of ores in tectonites (Yu et al., 2020). Limited exchange of elements does not substantially modify the original composition in chromite cores (Colas et al., 2014). Therefore, they help to clarify the trace element values of chromites in mineralogic-petrographic studies (Dare et al., 2009; Colás et al., 2014).

A total of 10 massive, nodular, disseminated and banded ore samples were analyzed chemically by XRF method. According to the results obtained in the main oxide and trace element values in the analyzed samples, their possible distributions in chromite and host rock were determined. While a positive relationship has detected between the trace elements Ti, Co, Zn and V and Cr_2O_3, there have a negative relationship between Ni, S and Ca. The detected Cr_2O_3 and trace element changes have an opposite relationship with olivine, the main mineral of dunites, which is the host rock of the chromite ore.

Compared to major elements, trace elements in chromites are more sensitive to formation conditions including pressure, temperature, oxygen fugacity and degree of partial melting and fractional crystallization (Dare et al., 2009; González-Jiménez et al., 2014). Especially, some trace elements (e.g., Ti, Ga, and V) can enter the octahedral site of the crystal structure of the chromite and replace the trivalent elements of Cr, Al, and Fe^{3+}, resulting in general varieties of chromites (Gervilla et al., 2012).

6. CONCLUSION

Chromite ore types in the study area are massive, banded, disseminated and nodular in accordance with the podiform chromite deposits. Chromite ores bear traces of plastic deformation under the influence of lateral forces developing in the lateral direction. Plastic deformation is also observed at the micro scale.

According to the chromite ore whole-rock geochemical analysis, there was a positive relationship between the amount of Cr_2O_3 and Zn, V, Ti, and Co, while a negative relationship was found between Ni, S and Ca. This situation is opposite with the dunites in which the chromite ore is located.

ACKNOWLEDGMENTS

This study was supported by FBE. 2001/021 of N. Omer Halisdemir University.

CONFLICT OF INTEREST

The authors declare no conflict of interest.

REFERENCES

Anıl, M. (l990). Pozantı-Karsantı, Mersin ve Kızıldağ (Hatay) Ofiyolitlerindeki Bazı Kromit Yataklarının Morfolojik Yapısal ve Jenetik Özellikleri ile Akdeniz Bölgesindeki Benzer Kromit Yataklarının Karşılaştırılması. Doğa, l4, 645-675, Ankara.

Blumenthal, M. (1946), Kilikya Toros'larının Çok Dikkate Değer Bir Parçası: Karanfildağ. MTA Mecmuası, 2. 257-286.

Boudier, F., & Nicolas, A. (1985) Harzburgite and lherzolite subtypes in ophiolitic and oceanic environments. Earth and Planet. Science Letters, 76(1-2), 84-92. doi:10.1016/0012-821X(85)90150-5

Brown, M. (1980). Textural and geochemical evidence for the origin of some chromite deposits in the Oman ophiolite. In: A. Panayiotou (Eds.) Ophiolites, Proceed. Intern. Ophiolite Symp. Cyprus, 714-721. Geol. Surv. Dep., Nicosia.

Cassard, D., Nicolas, A., Rabinovitch, M., Moutte, J., Leblanc, M., & Prinzhofer, A., (1981). Structural classification of chromite pods in southern New Caledonia. *Economic Geology*, *76*(4), 805- 831. doi:10.2113/gsecongeo.76.4.805

Choi, S. H., Shervais, J. W., & Mukasa, S. B. (2008). Supra-subduction and abyssal mantle peridotites of the Coast range ophiolite, California. Contributions to Mineralogy and Petrology, 156, 551–576. doi:10.1007/s00410-008-0300-6

Colás, V., González-Jiménez, J. M., Griffin, W. L., Fanlo, I., Gervilla, F., O'Reilly, S. Y., Pearson, N. J., Kerestedjian, T., & Proenza, J. A. (2014). Fingerprints of Metamorphism in Chromite: New Insights from Minor and Trace Elements. Chemical Geology, 389, 137–152. doi:10.1016/j.chemgeo.2014.10.001

Çakır, Ü. (1978). Petrologie Du Masisf De Pozantı-Karsantı (Taurus Cilicien, Turquie): Etude La Partie Centralla. These De Doctorat d'Ing. Univ. Satrasbourg. p. 251. (unpublished).

Dare, S. A. S., Pearce, J. A., McDonald, I., & Styles, M. T. (2009). Tectonic Discriminationof Peridotites Using fO2-Cr# and Ga-Ti-FeIII Systematics in Chrome-Spinel. Chemical Geology, 261(3-4), 199–216. doi:10.1016/j.chemgeo.2008.08.002

Dickey, J. S. (1976). A Hypothesis of Origin For Podiform Chromite Deposits. *Chromium: its Physicochemical Behavior and Petrologic Significance*, 1061-1074. doi:10.1016/B978-0-08-019954-2.50026-3

Dilek, Y., & Robinson, P. T. (Eds.) (2003). Ophiolites in Earth History. Geological Society, London, Special Publications, 218. doi:10.1029/2004EO440009

Dilek, Y., & Morishita, T. (2009). Melt migration and upper mantle evolution during incipient arc construction: Jurassic Eastern Mirdita ophiolite, Albania. Island Arc, 18(4), 551–554. doi:10.1111/j.1440-1738.2009.00692.x

Duke, J. M., (1983). Ore Deposit Models 7. Magmatic Segregation Deposits of Chromite. *Geoscience Canada*, *10*(1), 15–24.

Gervilla, F., Padro'n-Navarta, J. A., Kerestedjian, T., Sergeeva, I., González-Jiménez, J. M., & Fanlo, I. (2012). Formation of ferrian chromite in podiform chromitites from the Golyamo Kamenyane serpentinite, Eastern Rhodopes, SE Bulgaria: a two stage process. *Contributions to Mineralogy and Petrology*, *164*, 643-657. doi:10.1007/s00410-012-0763-3

Greenbaum. D. (1977). The chromitiferous rocks of the Troodos ophiolite complex, Cyprus. *Economic Geology*, *72*(7): 1175-1194. doi:10.2113/gsecongeo.72.7.1175

Huang, Y., & Deng, H. (2020) Geochemical Characteristics of Zoned Chromites in Peridotites from the Proterozoic Miaowan Ophiolitic Complex, Yangtze Craton: Implications for Element Mobility and Tectonic Setting. Journal of Earth Science, 31(2), 223–236. doi:10.1007/s12583-019-1278-x

Leblanc, M. (1980). Chromite growth, dissolution and deformation from a morphological view point: SEM investigations. *Mineralium Deposita*, *15*(2), 201-210. doi:10.1007/BF00206514

Lian, D., Yang, J., Dilek, Y., Wu, W., Zhang, Z., Xiong, F., Liu, F., & Zhou. W. (2017). Deep mantle origin and ultra-reducing conditions in podiform chromitite: Diamond, moissanite, and other unusual minerals in podiform chromitites from the Pozanti-Karsanti ophiolite, southern Turkey. American Mineralogist, 102(5), 1101–1113. doi:10.2138/am-2017-5850

Niu, Y., Langmuir, C. H., & Kinzler, R. J. (1997). The origin of abyssal peridotites: a new perspective. Earth and Planetary Science Letters 152, 251–265. doi:10.1016/S0012-821X(97)00119-2

Parlak, O., Höck, V., & Delaloye. M. (2002). The Supra-Subduction Zone Pozantı-Karsantı-Ophiolite Southern Turkey: Evidence For High-Pressure Crystal Fractionation of Ultramafic Cumulates. Lithos, 65(1-2), 205-224. doi:10.1016/s0024-4937(02)00166-4

Pearce, J. A., Lippard, S. J., & Roberts, S. (1984). Characteristics and tectonic significance of supra-subduction zone ophiolites. *Geological Society, London, Special Publications*, *16*, 77–94. doi:10.1144/GSL.SP.1984.016.01.06

Polat, A., & Casey, J. F. (1995). A Stuructural Record of The Emplacement of the Pozantı-Karsantı Ophiolite onto the Menderes-Taurus Block in The Late Cretaceus, Eastren Taurides, Turkey. Journal of Structural Geology, 17(12), 1673-1688. doi:10.1016/0191-8141(95)00061-h

Prichard, H. M., Barnes, S. J., Godel, B., Reddy, S. M., Vukmanovic, Z., Halfpenny, A., Neary, C. R., & Fisher, P. C. (2015). The structure of and origin of nodular chromite from the Troodos ophiolite, Cyprus, revealed using high-resolution X-ray computed tomography and electron backscatter diffraction. *Lithos*, *218-219*, 87-98. doi:10.1016/j.lithos.2015.01.013

Roberts, S. (1988). Ophiolitic chromitite formation: a marginal basin phenomenon. *Economic Geology*, *83*(5), 1034-1036. doi:10.2113/gsecongeo.83.5.1034

Takazawa, E., Frey, F. A., Shimizu, N., & Obata, M. (2000). Whole rock compositional variations in an upper mantle peridotite (Horoman, Hokkaido, Japan): are they consistent with a partial melting process? Geochemica et Cosmochimica Acta, 64(4), 695–716. doi:10.1016/S0016-7037(99)00346-4

Tekeli, O. (1981). Toros'larda Aladağ Ofiyolitli Melanjının Özellikleri. Türkiye Jeoloji Bülteni, 24, 57-64.

Tekeli, O., Aksay, A., Ürgün, B. M. & Işık, A. (1984). Geology of the Aladağ Mountains. Geology Of The Taurus Belt: Procedings Int. Sym., 26-29. September., 143-149. Ankara. Turkey.

Thayer, T. P. (1964). Principal Features and origin of podiform chromite deposits and some observations on the Guleman-Soridag District, Turkey. *Economic Geology*, *59*(8), 1497-1524. doi:10.2113/gsecongeo.59.8.1497

Thayer, T. P. (1969). Peridodite-gabbro complexes as keys to petrology of mid-ocean ridges. *Geological Society of American Bulletin*, *80*(8), 1511-1522. doi:10.1130/0016-7606(1969)80[1515:PCAKTP]2.0.CO;2

Uysal, I., Ersoy, E. Y., Karsli, O., Dilek, Y., Sadiklar, M. B., Ottley, C. J., Tiepolo, M., & Meisel, T. (2012). Coexistence of abyssal and ultra-depleted SSZ type mantle peridotites in a Neo-Tethyan Ophiolite in SW Turkey: Constraints from mineral composition, whole-rock geochemistry (major–trace–REE–PGE), and Re–Os isotope systematics. Lithos, 132–133, 50–69. doi:10.1016/j.lithos.2011.11.009

Yetiş, C. (1978). Geology of the Çamardı (Niğde) Region and the Characterics of the Ecemiş Fault Zone Between Maden Bogazı and Kamışlı. İstanbul Ünv. Fen Fak. Mecm. Seri E. 43, 41-61. (unpublished).

Yu, H., Zhang, H-F., Zou, H-B. & Yang, Y-H. (2019). Minor and trace element variations in chromite from the Songshugou dunites, North Qinling Orogen: Evidence for amphibolite-facies metamorphism. *Lithos*, *328-329*, 146-158. doi:10.1016/j.lithos.2019.01.009

Research Article / Araştırma Makalesi GU J Sci, Part A, 8(4): 551-569 (2021) https://doi.org/10.54287/gujsa.1030632

Gazi University
Journal of Science
PART A: ENGINEERING AND INNOVATION
http://dergipark.org.tr/gujsa

Determination of the Bed Hydrodynamics by MFIX-PIC in the Biomass Gasification Process of Circulating Fluidized Bed

Yelda ALTINSOY[1], Ahmet KEÇECİ[2], Hüseyin TOPAL[1*]

[1]*Gazi University, Department of Mechanical Engineering*
[2]*Doğuş University, Department of Mechanical Engineering*

Keywords

Fluidized Bed
Hydrodynamic Structure
MFIX-PIC
MP-PIC

Abstract

In this study, it was aimed to control the formation of flow regimes planned to be in the gasification process on the model, and the hydrodynamic structure of the circulating fluidized bed gasifier was obtained using the MFIX program. For this purpose, a model was established before pilot scale systems and hydrodynamic modeling was performed by entering the system dimensions that were calculated analytically. Because it is a necessary condition from the point of view of the chemical reaction to ensure the fluid bed regime of the gasifier, which is designated as a solid model, is a necessary condition. For this reason, the system whose geometry was determined and semi-empirical modeling was performed was modeled under previously determined operating conditions using the PIC (Eulerian-Lagrangian) model in the MFIX package program.

In this technique, while fluid behavior is resolved by the Euler structure, particle behaviour is considered by the Lagrangian structure. The numeral effects are in great arrangement with the empiric datum showing that MFIX-PIC methods are reasonable among concentrated gas-solid network simulation. The primary characteristics of gas-solid streams in CFB are qualitatively determined by an ordinary annular flux form inside the main bed. The pressure inclination formed in the gas phase inside the lower and upper zones of the CFB bed column indicated turbulent and irregular gas-solid streams in lower and upper zones. The increased superficial gas velocity conducts to a further dissymmetrical gas axial velocity model, which shows improved effect in the recycling frame for gas homogeneity due to the over gas velocity. The superficial gas velocity obtained as a result of the MFIX-PIC modelling was found to be 7m/s for 100 kW_{th} gas yield in the gasifier. The superficial gas velocity is the most basic parameter to be used both in the experimental parameter and in the thermochemical simulation.

Cite

Altınsoy, Y., Keçeci, A., & Topal, H. (20**). Determination of the bed hydrodynamics by MFIX-PIC in the biomass gasification process of circulating fluidized bed. *GU J Sci, Part A, 8*(4), 551-569.

Author ID (ORCID Number)

Y. Altınsoy, 0000-0002-5277-6981
A. Keçeci, 0000-0001-6502-3172
H. Topal, 0000-0001-7406-4398

Article Process

Submission Date 30.11.2021
Revision Date 22.12.2021
Accepted Date 30.12.2021
Published Date 31.12.2021

1. INTRODUCTION

Especially in energy sector, CFBs are extensively used in the several industrial application like, refinery, chemical, metal and environmental industries because of the transportation profits such as momentum, heat and mass transports parameters (Kunii & Levenspiel, 1991) However, due to the complicated CFB hydrodynamics structure, a comprehensive numerical and experimental investigation is needed. However, a detailed understanding of hydrodynamics structure and mass transport methods for gas-solid is needed to promote fluidized bed design, optimization and operation, especially when considering gasification. However, CFB in particular is intense sensitive gas/solid frameworks which carry out complex chemical reactions. At the same time, the fact that it provides high solid velocity, dense interaction between particles and significant heat and mass transfer makes it more important (Zhong et al., 2016). Because of numerical difficulties and intricacies in application estimates, fluidized bed studies are often qualified to a small-scale setup. Knowledge required for a minor size gasifiers are utilized to evaluate the hydrodynamic structure of a major scale gasifier.

*Corresponding Author, e-mail: htopal@gazi.edu.tr

Also, the gas/solid flows occurring in a major-scale gasifier are quite dissimilar compared in a minor-scale gasifier (Squires, 1982). Therefore, such an approach has not been found appropriate in the literature (Verma et al., 2015).

With the advancement of computational algorithms in recent years, numerical simulation modeling has become a powerful tool, especially in gas-solid two-phase flows (Gu et al., 2018; Liu & van Wachem, 2019; Stroh et al., 2019). It is important to study fluidized beds large enough to be able to solve industrial-scale problems using modeling. There are many studies on coarse grain models in CFD modeling studies. Because it is very important to enable modeling of gas/solid flows in large scale systems. Today, CFD studies are successfully used to obtain gas-solid hydrodynamic structure of fluidized beds. In order to model gas/solid flows [8] Euler-Lagrange Computational Fluid Dynamics-Discrete Element Model (CFD-DEM) (Tsuji et al., 1993; Deen et al., 2007) is based on the determination of micro and macro structural properties with a multi-scale approach. These two approaches have shown to give more accurate results for gas/solid flows. Usually, CFD approachment is separated to two types as E-E technique and E-L technique, which are based on solid phase processing. One of them considers it as a continuum in which the motion of the solid phase is solved by Euler's method. This approach is widely used to simulate large-scale CFBs because of its less precise resolution (Zhang et al., 2010; Nikolopoulos et al., 2013; Hamidouche et al., 2019).

However, the Eulerian-Eulerian method does not provide information on particle sizes for the solid phase and does not show the multiple distribution of the particle size distribution. The Eulerian-Lagrange approach, which is applied based on inter particle collision, has also found applications in more fields of CFD by combining DEM and multiphase particle in cell method (MP-PIC) methods (Alobaid, 2015). In the DEM technique, each particle is tracked and wall/particle/particle impact are resolved in the soft sphere impact technique (Cundall & Strack, 1979). However, studies in the literature on this subject are very few, especially for CFB simulations (Luo et al., 2015; Wang et al., 2017a, b; Xu et al., 2018; Yang et al., 2019). Comparing the MP-PIC modeling method with DEM, it uses a renewed method to simulate particle/particle impact. The purpose of this method is to reduce accounting costs. In other words, collecting particles with the same properties in a digital parcel provides a significant reduction in the number of particles that need to be monitored.

Also, solid compression stress is included in the MP-PIC technique to simulate information about inter particle impact. The weakness of the MP-PIC method lies in the simplification of the particle collision method, causing several particle scale features to be technically not accounted for in the simulation. However, in practice, in large-scale CFB simulations, the parameters of the particles, such as rotation and/or shape, can be neglected and supposed to be spherical (Shi et al., 2015; Liu et al., 2015; 2018). The Particle in Cell (PIC) approach has received great attention in industrial applications with gas-solid multicomponent flows. The methodology was first proposed by Andrews & O'Rourke (1996) for one-dimensional systems and extended to three-dimensional systems by Snider (2001).

In the PIC process (Snider, 2001; O'Rourke et al., 2009; O'Rourke & Snider, 2012; 2014), the gas phase is processed using an Euler framework, while the particles are grouped into computational plots and tracked as separate entities. Also, gas-solid streams, Andrews & O'Rourke (1996) proposed “Multiphase particle in cell” (MP-PIC) touch, that is the parcel touch and is widespread carried out in grain flow. This approach has also been widely used by Snider (2001), O'Rourke et al. (2009) and O'Rourke & Snider (2010), for granular flow. In particular, without solving particle collisions or governing Newtonian mechanics in any way, the PIC model generates a clustered solid stress momentum source term that directly affects the velocity of local solids (Snider, 2001). He defines this source term with a friction stress model, the friction stress model being driven by an assessment of the local solids volume ratio gradient and average area quantities. This statement implies that the model application is algebraic and thus computationally efficient. As a result, the PIC model can offer computational predictions for large industrial applications suitable for watchable wall time. Besides the friction stress model, the PIC can support auxiliary models (for example, a collision stress model, and wall friction models) that can contribute to the fidelity of the results. As with all combined computational fluid dynamics (CFD) simulations, these utility models will add time to the solution (Clarke & Musser, 2020).

Collisions between particles within parcels are not resolved but inter particle collisions are modeled using the stress term. Stress expression Auzerias et al. (1988) reported. Also, there are various numerical parameters used in conditional expressions within PIC routines, and their effects on results have not yet been measured. Despite these shortcomings, the PIC methodology has proven to model gas-solid systems quite well. While not as accurate as the discrete element modeling (DEM) approach, significant acceleration can be achieved using MFiX-PIC for large-scale systems. Instead of directly monitoring collisions between particles, PIC uses an ordinary "particle pressure" approach to avoid particles away being tightly wrapped. Patankar & Joseph (2001) investigated an Euler-Lagrange computational simulation (LNS) draft for particle stream and displayed which the parcel approach could catch the fundamental streams properties. However, this method is applicable where collisions occurring in the flow do not predominate, especially in dilute flow. In a model developed by Sakai & Koshizuka (2009), a coarse-grained model was determined by considering friction force and contact force. In this model, 3D piston flow is accurately modeled on a horizontal pipeline. However, the small number of calculated particles limited the system. However, in the DEM modeling is studied by Mokhtar et al. (2012), the similar particle assembly (SPA) model proposed for large-scale systems was verified. In Mokhtar et al. (2012) study, it is noteworthy that particles with the same properties (physical, chemical) are represented by a single particle. Bulk volume fractions were found to be independent of grain size (Bierwisch et al., 2009). It is important to know that second study is limited to dilute particulate systems that dual impacts occur only. It is unclear whether scaling applies in moderate to intense regimens.

Moreover, numerous modelling studies have demonstrated where the MP-PIC technique could evaluate intense gas-solid stream in major-scale CFBs using fairly great particle counts as accurately as they actually are. Jiang et al. (2014) investigated the gas-solid streams hydrodynamic structure of CFB which has six cyclone and determined that the computational consequent is similar as the ECT measurements. Wang et al. (2014) and Jiang et al. (2014) investigated the effect of simulating datas on the evaluation unity of the MP-PIC technique in his study. Liu et al. (2017) aimed to improve the solid circulation ratio for gas-solid stream in a binary CFB gasifier. Gu et al. (2018) studied parameters that may be important in CFB in a dual gasifier. As a result, the advantage of MFIX-PIC modeling compares to other modeling techniques can be explained as follows. The MFiX-PIC is best suited for industrial size and semi-intensive systems using multiphase flow simulations where precise parameters are paramount. The method mostly uses statistical averaging technique so that simulations can be run quickly and have minimal particle load.

2. MODELING STUDIES

This study constitutes the first step of modeling in the CFB gasifier. In order to determine the gas-solid contact properties required for the gasification mechanism, the MFIX open source package program was used. Numerical solution was performed with the particle-in-cell (PIC) model. For a highly efficient gasification process, it is necessary to create the necessary conditions, to fully understand the bed hydrodynamic structure and to determine the operating parameters under these hydrodynamic conditions.

The experimental system in which the biomass gasification study will be carried out is given in Figure 1. In this study, the solid-gas flow properties were numerically investigated as the first step in the circulating fluidized bed gasifier modeling. Fluid bed measurements were taken from the experimental system.

2.1. Overview of MFIX-PIC

The MFIX-PIC method was first proposed by Andrews & O'Rourke (1996) to see dense particle flows. Andrews & O'Rourke (1996) used the mass and momentum conservation equations accepted in TFM (Two Fluid Method) for gas phase motion. For the solid phase motion, it was solved by using Newton's second law of motion, by tracing the particles with the same properties on separate graphs. The MP-PIC model cannot resolve collisions directly. The Eulerian-Lagrange (E-L) method defines the gas phase as the continuum and the solid phase as the sum of the individual elements. The continuity equation is used for the gas phase, while the volume-averaged convection equations are used to solve the momentum balance. The MFIX-PIC technique’s equations are given below.

Continuity equation for gas phase:

$$\frac{\partial}{\partial t}\left(\varepsilon_g \rho_g\right) + \nabla.\left(\varepsilon_g \rho_g \vec{u}_g\right) = 0 \tag{1}$$

Gas phase momentum equation:

$$\frac{\partial}{\partial t}\left(\varepsilon_g \rho_g \vec{u}_g\right) + \nabla.\left(\varepsilon_g \rho_g \vec{u}_g \vec{u}_g\right) = -\varepsilon_g \nabla p + \nabla.\left(\bar{\bar{\tau}}_g\right) + \varepsilon_g \rho_g \vec{g} - \sum n_p \frac{V_p}{V_{cell}} \beta_p \left(\vec{U}_g(\vec{x}_p - \vec{U}_p\right) \tag{2}$$

Here;

Sub-symbol g symbolizes the gas phase, n_T, is liquid cell parcel number and n_p,is particles per parcel number. V_p and V_(cell) are particle and liquid cell volumes, one by one. βp is friction coefficient, U ⃗_g (x ⃗_p) is the superficial gas velocity at the parcel position, x ⃗_p and U ⃗_p parcel velocity τ ̿_g is stress tensor of gas phase :

$$\bar{\bar{\tau}}_s = 2\mu \bar{\bar{S}}_g \tag{3}$$

$$\bar{\bar{S}}_g = \frac{1}{2}[\nabla \vec{U}_g + (\nabla \vec{U}_g)^T] - \frac{1}{3}\nabla \vec{U}_g \vec{I} \tag{4}$$

Parcel motion equations

$$\frac{d\vec{x}_p}{dt} = \vec{U}_p \tag{5}$$

$$\frac{d\vec{U}_p}{dt} = \nabla \mathrm{p} - F_c.\vec{g} + \frac{\beta_g}{\rho_s}(\vec{U}_g(\vec{x}_p) - \vec{U}_g) \tag{6}$$

Here;

When the symbol "s" symbolizes solid phase, F_c interaction force of particle**.**

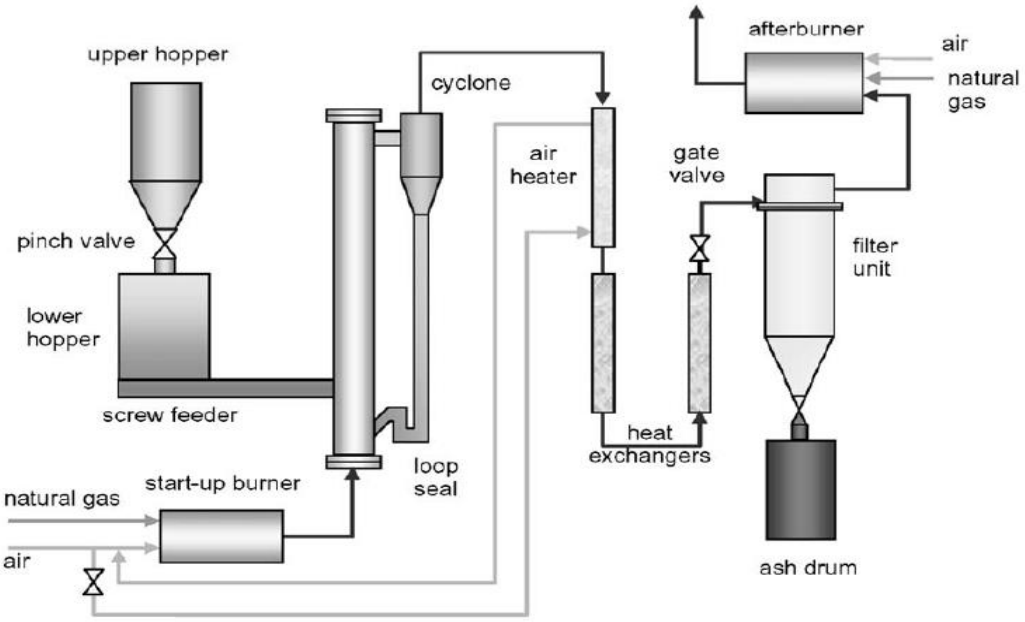

Figure 1. *Experimental Setup of CFB*

2.2. Gas-Solid Drag Model

In order to predict gas/solid flows in CFBs, the frictional force between gas and solid must be taken into account. The Gidaspow drag model (Gidaspow, 1994) is a widely used model. In this model, a model based on mono-dispersed particles was determined. In the simulation of gas/solid flows, the need for remodeling has emerged, especially for DEM poly disperse particles (Zhang et al., 2017, Lu et al., 2019). However, in many studies (Liu et al., 2015; Kallio et al., 2015; Thapa et al., 2016; Ma et al., 2017) mono-disperse drift model has been used in poly-disperse systems and very positive results have been obtained. In this study, the Gidaspow drag model, Wen & Yu (1966) and Ergun model (1952) were combined and used. The formulation of the Gidaspow drag model used in this study is as follows (Ding & Gidaspow, 1990),

$$\beta_{gm} = \begin{cases} \frac{3}{4} C_D \frac{\rho_g \varepsilon_g \varepsilon_m |U_g - U_m|}{\rho_p d_p} \varepsilon_g^{-2.65} & \varepsilon_g \geq 0.8 \\ \frac{150\varepsilon_s(1-\varepsilon_g)\mu_g}{\varepsilon_g d_{pm}^2} + \frac{1.75\rho_g \varepsilon_g |U_g - U_m|}{d_{pm}} & \varepsilon_g \geq 0.8 \end{cases} \quad (7)$$

$$C_D = \begin{cases} {}^{24}/_{Re}\,(1 + Re^{0.687}) & Re < 1000 \\ 0.44 & Re \geq 1000 \end{cases} \quad (8)$$

$$Re = \frac{\rho_g \varepsilon_g |U_g - U_m| d_{pm}}{\mu_g} \quad (9)$$

2.3. Modeling Parameters

Method: Particle-In-Cell (PIC)

Solid-Gas Drag Model: Gidaspow

Lattice cell size:

X: 1.24x10-2m,

H: 1.28x10-2m,

Z: 1.27x10-2m

(Cell sizes in the range of 20-30 times the particle diameter are compatible with the solutions used in the literature.)

Numerical Solution Parameters:

- Maximum 500 iterations for each time step

-Implicit Euler for temporal discretization, Superbee scheme for dimensional discretization

The simulation, which was run for -10 seconds, was started with 1.0x10-4 s time step, and it was adjusted depending on the CFL value in the range of $1.0x10^{-7}$ – $1.0x10^{-2}$ s time step. A time step factor of 0.9 is used for the time step adjustment.

2.4. Parameters required for simulation

In this study, the MFIX-PIC package program was used for the numerical solution in the experimentally created circulating fluidized bed (CFB). The circulating fluidized bed is composed of riser, cyclone, drop pipe, loop seal.

The three-dimensional geometry diagram of the bed and the lattice cells obtained as a result of the modeling are shown in Figure 2. The main bearing height is 5,500 m, the main bearing diameter and the drop pipe diameter are 0.100 m and 0.076 m, respectively. Superficial gas velocity (Ug) is 7.0 m/s from the distributor located under the main bearing.

Aeration mass flow rate (Qr) is given as 0.04 kg/s loop seal, which aims to transport particles from the fall pipe to the bearing column. At the same time, the other purpose of the aeration mass flow is to provide the returning solid flow to the cyclone bed by providing pressure balance. The CFB matter is silica sand using an average dp 0.530 mm (530 μm) and a concentration of 2500 kg/m3 belonging to Geldart group B particles. The grid cells in the model were first created with Cartesian grid cells. Afterwards, the solid model created with the CAD program to determine the wall conditions was converted into solution networks with the cut-cell method.

Boundary conditions must be set carefully before calculation. Specifically, the initial air inlet is defined as a unique mass flow limiting condition, while vent port inlet (return zone gas inlet) is defined as an main line limiting condition (point source). The pressure output limiting conditions are selected in which the cyclone outlet. Non-slip limiting condition are chosen for all walls are set. Solid matter primarily gather in the main column and loop seal by a space portion of 0.5.

1.0 × 10−4 s is an initial time step which set in the current modelling, and the time step is being automatically set throughout sum lean the Courant Friedrichs Lewy number (CFL). Volume fraction of closed packing is specified as 0.55. Another considerable modelling datas are shown in Table 1.

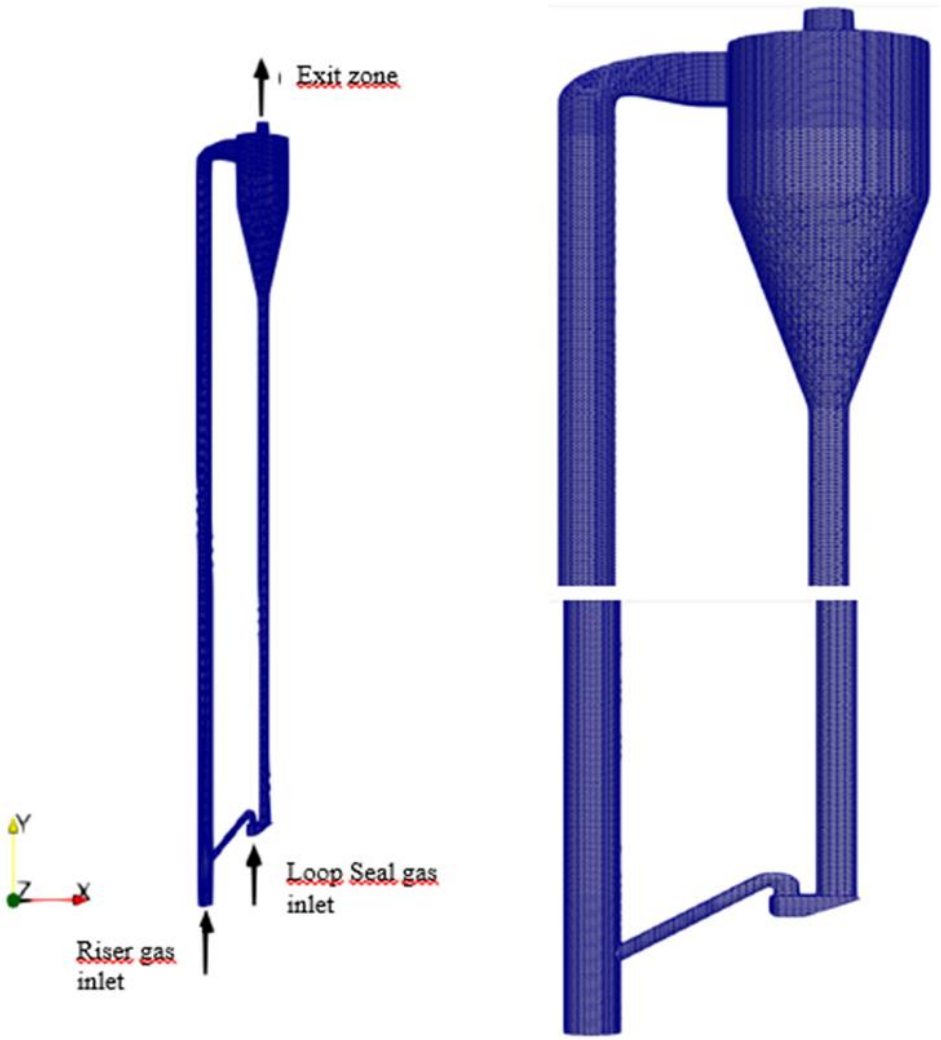

Figure 2. *CFB PIC Simulation Grid Cells*

Table 1. *Parameters Used in Simulation*

Parameters	**Data**
Riser Diameter D (m)	0.10
Riser Height H (m)	5.75
Gas Phase	
Average molecular weight of gas Mavg (kg/kgmol)	29.0
Viscosity μg (Pa.s)	1.80x10-5
Density ρg kg/m3	1.204
Solid Phase	
Particle diameter dp (μm)	530
Particle density ρs (kg/m3)	2500
Statistical weight (particle per parcel), np	100
PIC Parameters	
Solid volume fraction at close pack, εcp	0.55
Volume fraction exponential scale factor	3.0
Empirical dampening factor	0.85
Non-singularity constant	1.0x10-7
Time step interval	1.0x10-7 – 1.0x10-2
CFD initial time step, Δt (s)	1.0x10-4
Simulation time, t (s)	10
Maximum number of iterations	500
Time step factor	0.9
Solid-Wall Interaction Parameters	
Normal particle-wall restitution coefficient, ew	0.3
Tangential particle-wall restitution coefficient, eτ	0.995
Initial Conditions	
Initial riser bed height (m)	0.6
Initial loop seal bed height (m)	0.1
Operating temperature, Top (K)	293.15
Bed particle diameter distribution: 50% gas, 50% particle defined in Table 2.	
Boundary Conditions	
Wall-Boundary Condition	No-Slip
Primary Air Boundary Condition	
Gas volume fraction (%):	1.0
Y-axial superficial gas velocity (m/s):	7.0
Pressure (kPa):	101.325
Loop Seal Aeration Air Boundary Condition	
Gas volume fraction (%):	1.0
Mass flow rate (kg/s):	0.04
Pressure (kPa):	101.325
Outlet Boundary Condition	
Outlet pressure (kPa):	101.325

Table 2. *Solid Diameter Distribution and Solid Phases Suitable for Average Diameter are Defined*

Diameter (µm)	Quantity (%)
300	**0.1**
400	**0.1**
500	**0.5**
600	**0.1**
700	**0.1**
800	**0.1**

In this study, the program was run for a time period of 10 seconds. However, the results from the time until the simulation stability was reached in the modeling were not included in the calculation. Figure 3 represents the average pressure values in the lower region of the bed for each time step. It was observed that the statistical stability required for numerical solution improved after the first 2.5 seconds. Accordingly, the first 4 seconds of solution data are not included in the calculation.

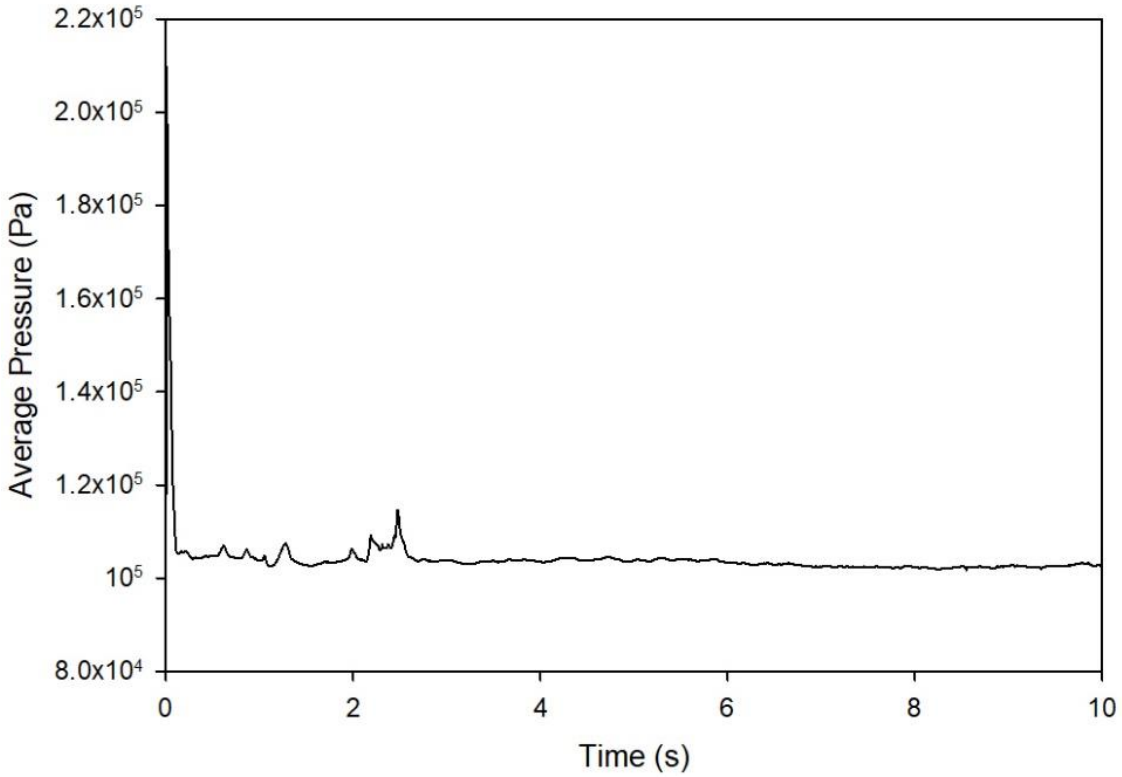

Figure 3 *Average Gas Pressure Results of Riser on Time Steps (H= 0.3m)*

Grid cell size, which is nearly concerned to MP-PIC simulation, is offset by an appropriate grid cell size setting of estimation accuracy and computational cost [50].In the PIC studies in the literature, it was seen that the lattice cell sizes of 20-30 times the particle diameter confirmed the solution. Therefore, a lattice cell size close to the solutions in the literature was chosen. It is given in Table 3.

Table 3. *Grid Analysis*

Condition	**Fine grid**
Cell number	854,400
Grid size (Δx×Δy×Δz)	1.24x1.28x1.27
Parcel Number (Cell Number/ Statistical weight np)	85,440

2.5. Modeling Results

In this section, the numerical results of the MFiX-PIC have been discussed.

While model validation; pressure graph, particle concentrations, and velocity distributions were taken into consideration and compared with the studies in the literature. Although there are changes in the numerical values depending on the parameters, the graphical shape and the distributions in the velocity contour are among the methods used for model verification in the literature.

The U-shape resemblance of the radial solid distribution and axial solid velocity, as seen in Figure 9b, is an important result for fluid bed modeling validation.

Models of gas-solid systems

Hydrodynamics structure of gas-solid in CFBs are depend on the macroscopic properties, especially gas velocity, pressure distribution, particle velocity, particle concentration (Wang et al., 2017a).

Figure 4 shows the time motion of particles variation in bed at Ug= 7.0 m/s. Solids are at first collected in the loop seal and riser. With the gas coming from the distributor, the solids begin to move from the column lower part to the upper part. Then the particles head into the cyclone with a superficial gas velocity of 7 m/s. Thanks to the geometric configuration of the cyclone, the particles separate from the gas solid phases and move towards the fall pipe. Gas particles which come from loop seal are carried back to main column. Thus, the cycle of particles in the bed is completed. Also, gas-solid flows change temporarily in the CFB amplifier. The solid phase height in the loop seal decreases as time increases. After 6 seconds solid phase height remains constant, indicating that the system has reached an equilibrium phase.

Figure 5 shows that a snap of the solid fraction of CFB at Ug= 7.0 m/s. Particles in the lower region of the riser accumulate in this region initially, and then the particle distribution increases with excessive gas-solid momentum exchange.

Figure 6 shows the distribution of solids and gas in the CFB at Ug= 7.0 m/s and the variation of particle and gas in the bed and cyclone from the top view.

The ascending particles accumulate above the riser, which is the riser upper zone, where there are strong collisions between the ascending particles and falling back particles. The particles irregular characteristics distribution can be seen in different riser zones.

This could be attributed to the distribution of unstable motion of particles through interphase and interactions of inter-particle in the main coloum. The gas flow affected due to wall confinement bend to push through the center zone of the amplifier (Luo et al., 2015; Shi et al., 2015; Wang et al., 2017b). So, a dilute distribution of ascending particles and intense falling particles are monitored in the middle and wall regions of the bed, resulting in an "annular flow" structure typical of flow model inside main coloum (bed column).

Also, as gas-solid flows are fully developed, the particle back mix close the wall slowly weakens throughout height of the main bed. Solids is based on to the helical motion of the gas phase. As shown in Figure 7, the gas phase entering the cyclone in a tangential direction rotates around the inner surface of the cyclone.

Because of reduction of the conic part, the gas phase moves back and moves axially centerline, eventually leaving a vortex finder. The outer vortex and inner vortex were found to have the same rotational direction for the cyclone, according to the experimental parameters (Wu et al., 2018). Moreover, the estimate outcomes for the CFB with MFIX-PIC method in this study are compatible with the studies which used the CFD-DEM in the literature (Luo et al., 2015; Ma et al., 2017; Wang et al., 2014a, b; Wu et al., 2018). In short applying MFIX-PIC in a pilot scale CFB in order to understand hydrodynamic structure is acceptable.

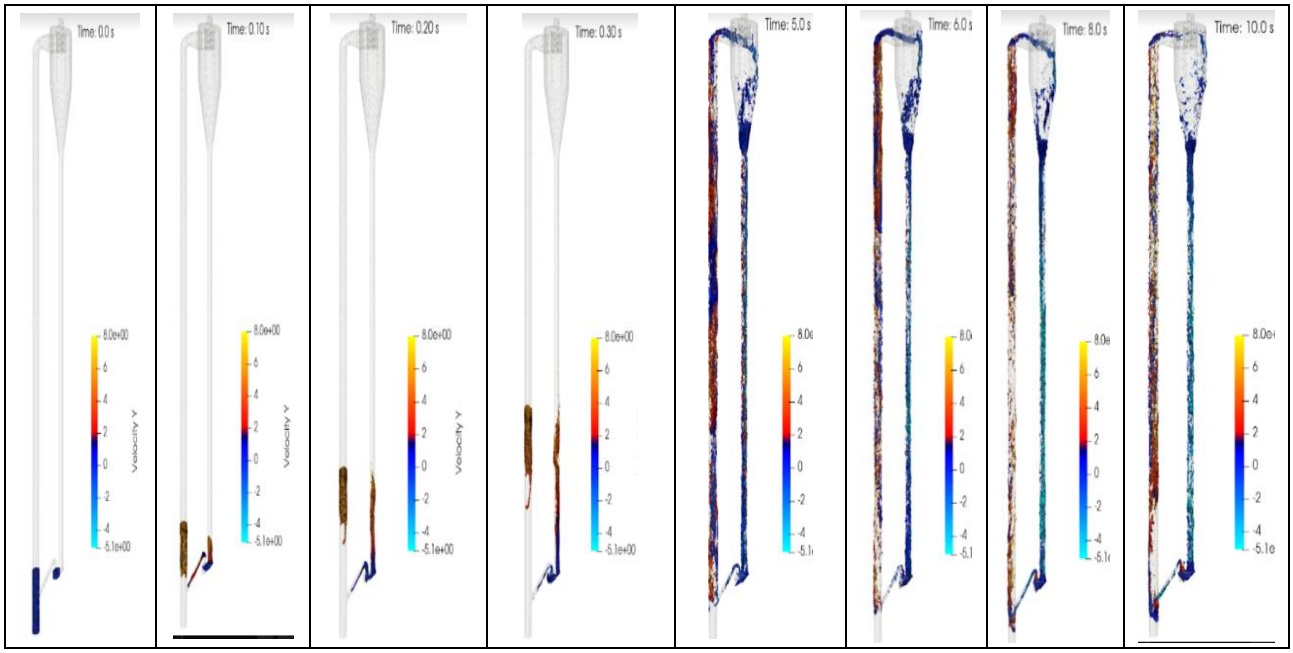

Figure 4. *Fluctuation of the Motion of the Particles in the CFB Versus Time Ug=7.0 m/s*

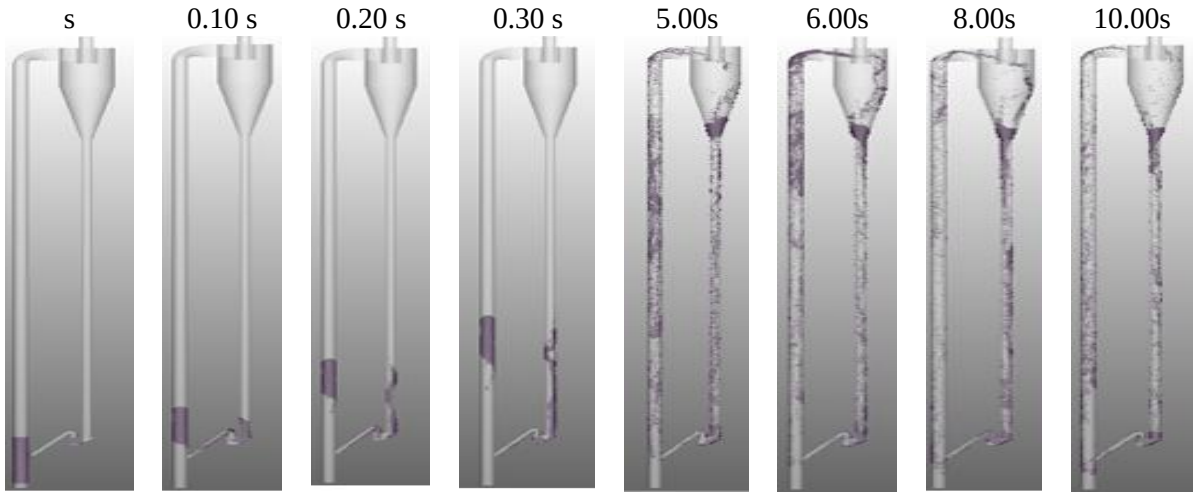

Figure 5 *Changes of Solid Distributions Over Time in a Circulating Fluidized Bed Gasifier Ug=7.0 m/s*

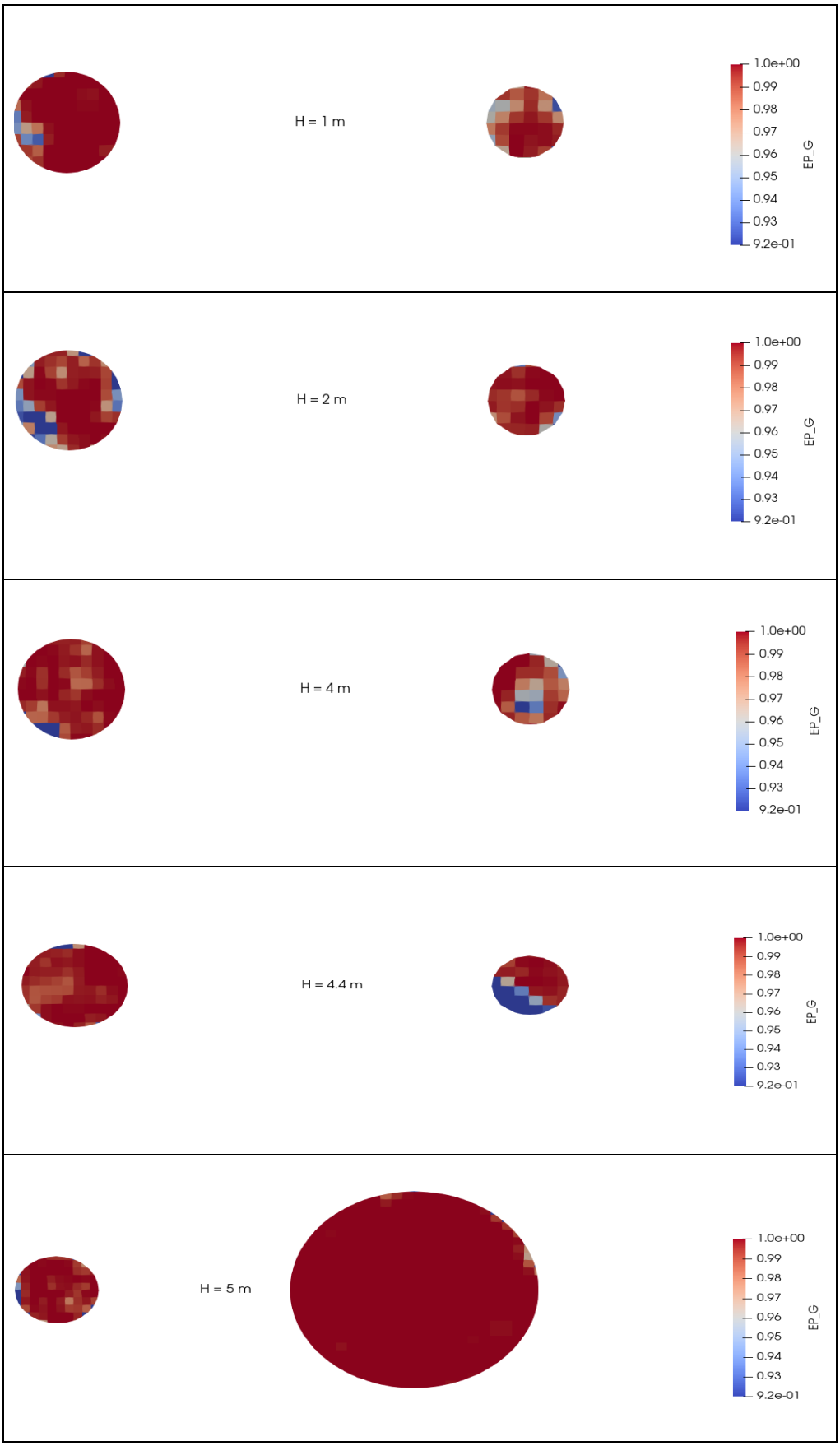

Figure 6. *Snapshot Variance of Particles and Gas in the Riser, t=10 s, Ug = 7.0 m/s Solid and Gas Fraction of CFB with Respect to Column Height*

Riser and cyclone solid circulation simulation

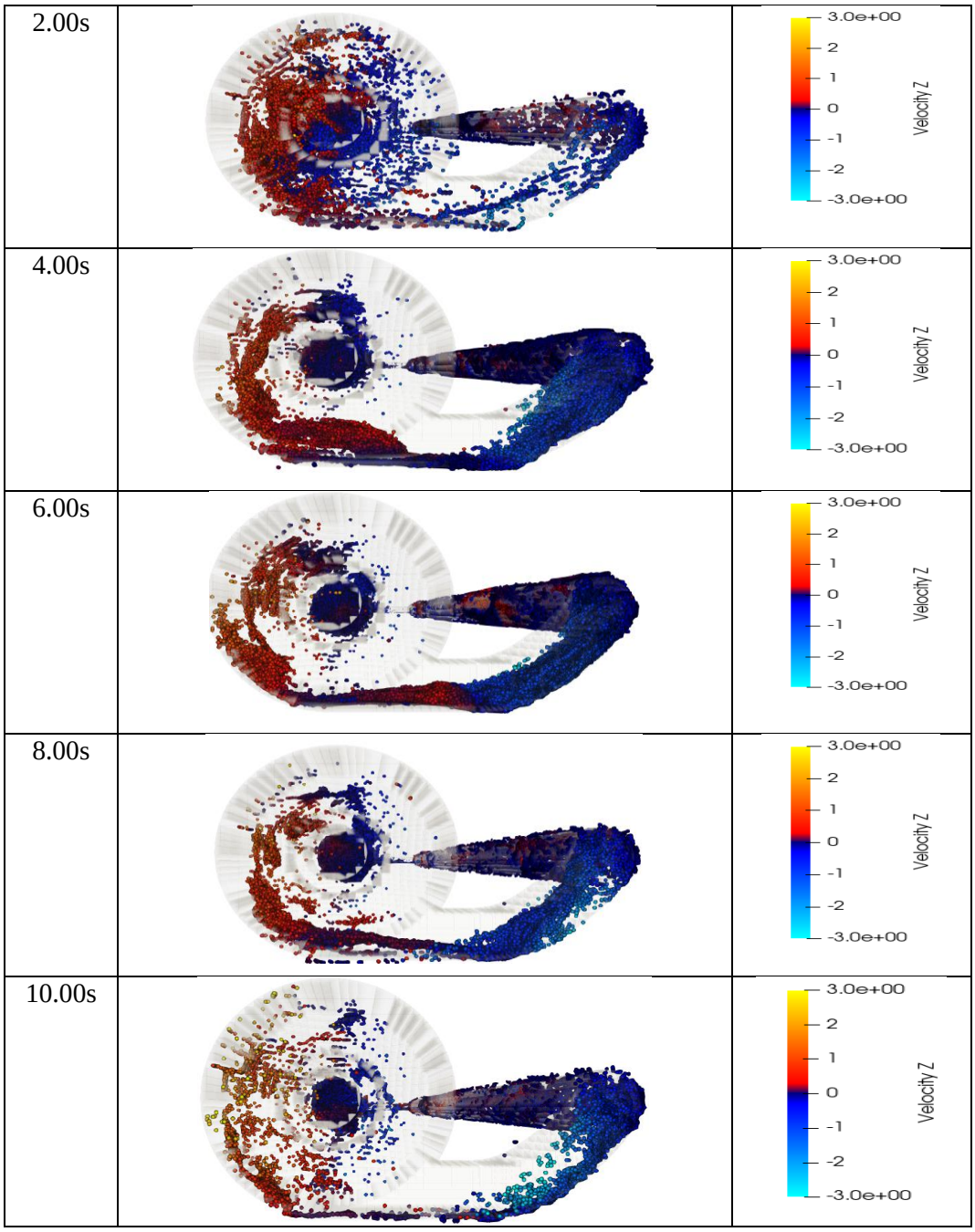

Figure 7. *Distribution of Solid Phase Velocity (Vz) in the Bed and Cyclone, t =10 s, Ug = 7.0 m/s*

Solid behaviour

Besides that the abrupt movements of the solid distribution, the solid hold up along the column height given in Figure 8 is shown as reported by Topal, 1999; Atimtay & Topal, 2004.

A large concentration of solids is concerned especially in side of lower zone of the riser and loop seal.

In addition, solid collect close column wall and on riser upper zone (Figure 8a). Throughout the riser height (Figure 8b), the solid distribution on the amplifier under several operational conditions provides a C-type distribution model suitable for experimental measurement (Jiradilok et al., 2008) and numerical prediction (Chen et al., 2017).

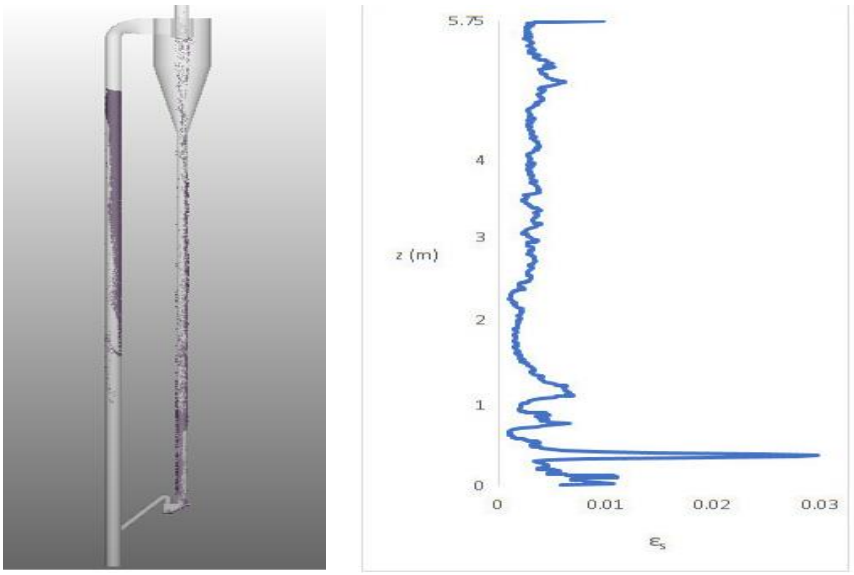

(a) (b)

Figure 8. *Solid Volume Fraction of Gasifier,* ***a)*** *Instantaneous Snapshot of Solid Volume Fraction,* ***b)*** *Time-Averaged Solid Volume Fraction Along Center-Line of Riser*

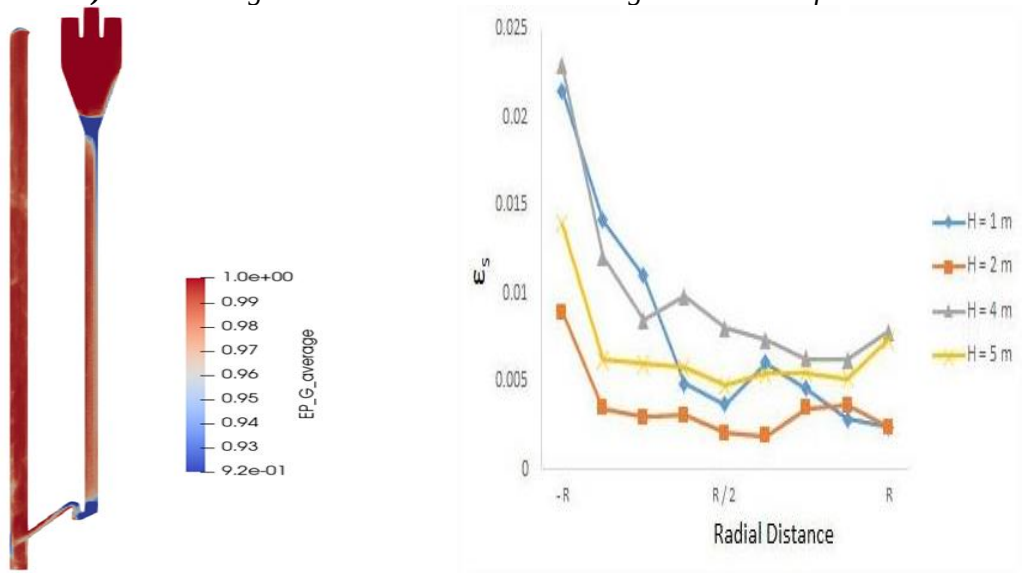

(a) (b)

Figure 9. *Gas Distribution Inside of CFB:*
a) *Ug=7.0 m/s,* ***b)*** *Radial Profiles Versus Solid Fraction According to the Height of Riser*

The dense solids concentration in the lower and upper regions depends on the input and output characteristics of the amplifier. As mentioned in the literature (Bai et al., 1992; Zhou et al., 1994), the bed column solids concentration in the radial direction varies from 0.005 to 0.1 independent of the column height, specifying that solids concentration evaluated by the MFIX-PIC model is appropriate. Also, as superficial gas velocity increases, on the contrary, the particle concentration slowly reduces, based on rised gas phase friction force on the increasing solids.

Figure 9 shows the variation profiles along the radial direction of the solids density occurring at several heights of the main column. The solids density is great close the wall but very low inside the middle region of the riser. In this case, the CFB amplifier also shows the core ring structure. Also, the particle concentration for different heights along the radial axis is not symmetrical due to unidirectional feeding.

Figure 10 shows that time averaged velocity contours of gas phase and comparison with Yang & Wang (2020). Gas velocity is decreased in near the wall because of gas-wall interaction. This situation in axial gas velocity can be shown as the reason for the formation of U-shape solid distribution as in Figure 9. The fact that the axial gas velocity slows down towards the walls also causes the solid velocities to slow down, as given in Verma & Padding (2020).

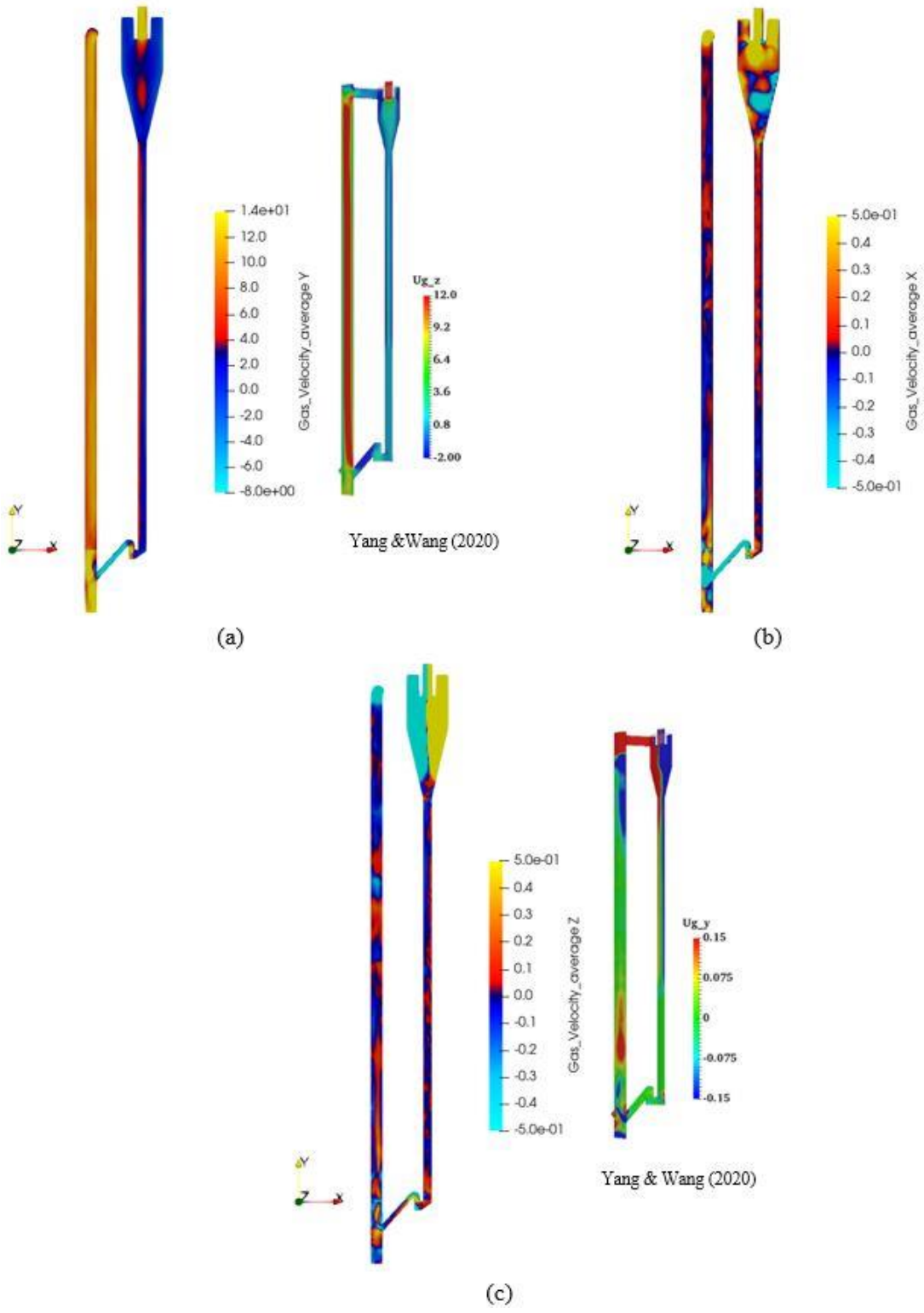

Figure 10. *Time-Averaged Velocity Contours of CFB Gasifier and Comparison with Yang & Wang (2020)* ***a)*** *z -direction,* ***b)*** *x-direction,* ***c)*** *y-direction*

When the z-direction gas velocity distribution in Figure 10c is examined, the structure of cyclone movement has been observed. As expected in the literature and theory, counter-directional velocity distribution in the cyclone region and deceleration towards the middle region of the cyclone were observed.

One way of correcting and symmetrical distribution of gas/solid flows in the bed is to perform a double feed (Wang et al., 2017b). In literature review, the results of the gas/solid flow simulation study conducted by Wang and Yang (2020) and the model outputs obtained from this study are compatible with each other. Meanwhile, our results for solid concentration distributions were also reported by Yang & Wang (2020) is consistent with their study.

3. CONCLUSIONS AND DISCUSSIONS

In this study, MFIX-PIC modeling method was used to determine the gas solid hydrodynamic structure which is basis of gasification in a circulating fluidized bed. In the circulating type fluidized bed model, the movements, solid concentration and velocity distributions of the solid particles in the column cyclone and return line were determined. Based on the numerical results obtained as a result of the modeling, the following conclusions were reached.

(1) Particles drop with a dense concentration close the riser wall, yet despite having a lower concentration, they increase significantly from the riser annular region, explaining as unique "core annulus" flowing model in the main column. Meanwhile, upward solids were monitored moving reverse and forth to the direction of radial aspect of the amplifier

(2) The variation of solid concentrations in the riser depends on the structural characteristics of the riser. However, although solids concentrations in the radial direction vary depending on the column height, generally vary slightly between 0.005 and 0.1 as indicated in the literature; this indicates that the particle concentration estimated by the existing MFIX-PIC simulation method is convenient.

(3) A large concentration of solids is noted in the loop seal and in the lower zone of the bed column.

(4) In addition, particles gather close the barrier together with the upper zone of the main column (Figure 7a). Alongside the riser height (Figure 7b), the particle concentration in the riser under several operational case presents a C-type dispersion model that is appropriate for experimental measurements (Jiradilok et al., 2008) as well as numerical estimation (Chen et al., 2017).

In summary, this study shows that the MP-PIC method gives acceptable results in modelling gas-solid hydrodynamics structure in 3D CFBs and can be used to determine the most basic operating parameters such as empty column gas velocity and bed material selection as well, which should be used in the design and process of CFBs shows.

Axial solid void fraction showed good agreement with the correlations of Yang & Wang (2020). Their study has mean error value which was calculated as 4%. The mean error value of this study showed as similar as the result of Yang & Wang (2020).

CONFLICTS OF INTEREST

The authors declare no conflict of interest.

REFERENCES

Alobaid, F. (2015). An offset-method for Euler-Lagrange approach. *Chemical Engineering Science, 138*, 173-193. doi:10.1016/j.ces.2015.08.010

Andrews, M. J., & O'Rourke, P. J. (1996). The multiphase particle-in-cell (MP-PIC) method for dense particulate flows. *International Journal of Multiphase Flow*, *22*(2), 379-402. doi:10.1016/0301-9322(95)00072-0

Auzerais, F. M., Jackson, R., & Russel, W. B. (1988). The resolution of shocks and the effects of compressible sediments in transient settling. *Journal of Fluid Mechanics*, *195*, 437-462. doi:10.1017/S0022112088002472

Bai, D. R., Jin, Y., Yu, Z. Q., & Zhu, J. X. (1992). The axial distribution of the cross-sectionally averaged voidage in fast fluidized beds. *Powder Technology*, *71*(1), 51-58. doi:10.1016/0032-5910(92)88003-Z

Chen, J., Meng, C., Wang, S., Yu, G., Hu, T., & Lin, F. (2017). Effect of solid mass flux on anisotropic gas-solid flowin risers determined with an LES-SOM model. *Particuology*, *34*, 70–80. doi:10.1016/j.partic.2016.12.003

Clarke, M., & Musser, J. (2020). The MFIX Particle-in-Cell Method (MFIXPIC) Theory Guide; DOE/NETL-2020/2115; NETL Technical Report Series; U.S. Department of Energy, National Energy Technology Laboratory: Morgantown, WV, 28. doi:10.2172/1630414

Cundall, P. A., & Strack, O. D. L. (1979). A discrete numerical model for granular assemblies, *Geotechnique*, *29*(1), 47–65. doi:10.1680/geot.1979.29.1.47

Deen, N. G., Van Sint Annaland, M., Van der Hoef, M. A., & Kuipers, J. A. M. (2007). Review of discrete particle modeling of fluidized beds. *Chemical Engineering Science*, *62*(1-2), 28-44. doi:10.1016/j.ces.2006.08.014

Ding, J., & Gidaspow, D. (1990) A bubbling fluidization model using kinetic theory of granular flow. *AIChE Journal*, *36*(4), 523-538. doi:10.1002/aic.690360404

Ergun, S. (1952) Fluid flow through packed columns. *Chemical Engineering Progress*, *48*(2), 89–94.

Gu, J., Shao, Y., Liu, X., Zhong, W. & Yu, A. (2018). Modelling of particle flow in a dual circulation fluidized bed by a Eulerian-Lagrangian approach. *Chemical Engineering Science*, *192*, 619–633. doi:10.1016/j.ces.2018.08.008

Gidaspow, D. (1994). *Multiphase Flow and Fluidization: Continuum and Kinetic Theory Descriptions*. Academic Press

Hamidouche, Z., Masi, E., Fede, P., Simonin, O., Mayer, K., & Penthor, S. (2019). Unsteady three-dimensional theoretical model and numerical simulation of a 120-kW chemical looping combustion pilot plant. *Chemical Engineering* Science, *193*, 102–119. doi:10.1016/j.ces.2018.08.032

Hu, C., Luo, K., Wang, S., Sun, L., & Fan, J. (2019). Influences of operating parameters on the fluidized bed coal gasification process: A coarse-grained CFD-DEM study. *Chemical Engineering Science*, *95*, 693-706.

Jiang, Y., Qiu, G., & Wang, H. (2014). Modelling and experimental investigation of the full-loop gas-solid flow in a circulating fluidized bed with six cyclone separators. *Chemical Engineering Science*, *109*, 85–97. doi:10.1016/j.ces.2014.01.029

Jiradilok, V., Gidaspow, D., Breault, R. W., Shadle, L. J., Guenther, C., & Shi, S. (2008). Computation of turbulence and dispersion of cork in the NETL riser. *Chemical Engineering Science*, *63*(8), 2135–2148. doi:10.1016/j.ces.2008.01.019

Kallio, S., Peltola, J., & Niemi T. (2015) Analysis of the time-averaged gas–solid drag force based on data from transient 3D CFD simulations of fluidized beds, *Powder Technology*, *274*, 227-238. doi:10.1016/j.powtec.2015.01.029

Kunii, D., & Levenspiel, O. (1991). *Fluidization Engineering*. Butterworth-Heinemann Inc.

Liu, H., Cattolica, R. J., Seiser, R., & Liao, C-h., (2015). Three-dimensional full-loop simulation of a dual fluidized-bed biomass gasifier. *Applied* Energy, *160*, 489–501. doi:10.1016/j.apenergy.2015.09.065

Liu, H., Cattolica, R. J., & Seiser, R. (2017). Operating parameter effects on the solids circulation rate in the CFD simulation of a dual fluidized-bed gasification system. *Chemical Engineering Science*, *169*, 235–245. doi:10.1016/j.ces.2016.11.040

Liu, D., & van Wachem, B. (2019). Comprehensive assessment of the accuracy of CFD- DEM simulations of bubbling fluidized beds. *Powder Technology*, *343*, 145–158. doi:10.1016/j.powtec.2018.11.025

Lu, L., Gao, X., Shahnam, M., & Rogers, W. A. (2019). Coarse grained computational fluid dynamic simulation of sands and biomass fluidization with a hybrid drag. *AIChE Journal*, *66*(4), e16867. doi:10.1002/aic.16867

Luo, K., Wu, F., Yang, S., Fang, M., & Fan, J. (2015). High-fidelity simulation of the 3-D full-loop gas-solid flow characteristics in the circulating fluidized bed. *Chemical Engineering Science*, *123*, 22–38. doi:10.1016/j.ces.2014.10.039

Ma, Q., Lei, F., Xu, X., & Xiao, Y. (2017). Three-dimensional full-loop simulation of a high-density CFB with standpipe aeration experiments. *Powder Technology*, *320*, 574–585. doi:10.1016/j.powtec.2017.07.094

Mokhtar, M. A., Kuwagi, K., Takami, T., Hirano, H. & Horio, M. (2012). Validation of the Similar Particle Assembly (SPA) Model for the Fluidization of Geldart's Group A and D Particles. *AIChE Journal*, *58*(1), 87–98. doi:10.1002/aic.12568

Bierwisch, C., Kraft, T., Riedel, H., & Moseler, M. (2009). Three-dimensional discrete element models for the granular statics and dynamics of powders in cavity filling. *Journal of the Mechanics and Physics of Solids*, *57*(1), 10–31. doi:10.1016/j.jmps.2008.10.006

Nikolopoulos, A., Nikolopoulos, N., Charitos, A., Grammelis, P., Kakaras, E., Bidwe, A. R. & Varela, G. (2013). High-resolution 3-D full-loop simulation of a CFB carbonator cold model. *Chemical Engineering* Science, 90, 137–150. doi:10.1016/j.ces.2012.12.007

O'Rourke, P. J., Zhao, P., & Snider, D. (2009). A model for collisional exchange in gas/liquid/solid fluidized beds. *Chemical Engineering Science*, *64*(8), 1784–1797. doi:10.1016/j.ces.2008.12.014

O'Rourke, P. J., & Snider, D. M. (2010). An improved collision damping time for MP-PIC calculations of dense particle flows with applications to polydisperse sedimenting beds and colliding particle jets. *Chemical Engineering Science*, *65*(22), 6014-6028. doi:10.1016/j.ces.2010.08.032

O'Rourke, P. J., & Snider, D. M. (2012). Inclusion of collisional return-to-isotropy in the MP-PIC method. *Chemical Engineering Science*, *80*, 39–54. doi:10.1016/j.ces.2012.05.047

O'Rourke, P. J., & Snider, D. M. (2014). New blended acceleration model for the particle contact forces induced by an interstitial fluid in dense particle/fluid flows. *Powder Technology*, *256*, 39–51. doi:10.1016/j.powtec.2014.01.084

Patankar N. A., & Joseph D. D. (2001). Modeling and numerical simulation of particulate flows by the Eulerian-Lagrangian approach. *International Journal of Multiphase Flow*, *27*(10), 1659-1684. doi:10.1016/S0301-9322(01)00021-0

Sakai, M., & Koshizuka, S. (2009). Large-scale discrete element modeling in pneumatic conveying. *Chemical Engineering Science*, *64*(3), 533-539. doi:10.1016/j.ces.2008.10.003

Shi, X., Sun, R., Lan, X., Liu, F., Zhang, Y., & Gao, J. (2015). CPFD simulation of solids residence time and back-mixing in CFB risers. *Powder Technology*, *271*, 16–25. doi:10.1016/j.powtec.2014.11.011

Snider, D. M. (2001). An Incompressible Three-Dimensional Multiphase Particle-in-Cell Model for Dense Particle Flows. *Journal of Computational Physics*, *170*(2), 523–549. doi:10.1006/jcph.2001.6747

Squires, A. M. (1982). Contribution towards a history of fluidization. In: Proceeding of the Joint Meeting of Chemical Engineering Society of China and AIChE, 322–353.

Stroh, A., Daikeler, A., Nikku, M., May, J., Alobaid, F., von Bohnstein, M., Ströhle, J., & Epple, B. (2019). Coarse grain 3D CFD-DEM simulation and validation with capacitance probe measurements in a circulating fluidized bed. *Chemical Engineering Science*, *196*, 37–53. doi:10.1016/j.ces.2018.11.052

Tsuji, Y., Kawaguchi, T., & Tanaka, T. (1993). Discrete particle simulation of two-dimensional fluidized bed. *Powder Technology*, *77*(1), 79–87. doi:10.1016/0032-5910(93)85010-7

Thapa, R. K., Frohner, A., Tondl, G., Pfeifer, C., & Halvorsen, B. M. (2016). Circulating fluidized bed combustion reactor: Computational Particle Fluid Dynamic model validation and gas feed position optimization. *Computers & Chemical* Engineering, *92*, 180–188. doi:10.1016/j.compchemeng.2016.05.008

Topal, H. (1999). Experimental Investigation of Hydrodynamic, Combustion and Emission Properties of Circulating Fluidized Bed. PhD Thesis, Gazi University, Ankara, Turkey. (In Turkish).

Atimtay, A. T. & Topal, H. (2004). Co-combustion of olive cake with lignite coal in a circulating fluidized bed. *Fuel*, *83*(7-8), 859–867. doi:10.1016/j.fuel.2003.09.015

Wang, Q., Yang, H., Wang, P., Lu, J., Liu, Q., Zhang, H., Wei, L., & Zhang, M. (2014a). Application of CPFD method in the simulation of a circulating fluidized bed with a loop seal, part I—determination of modeling parameters, *Powder Technol. 253*, 814–821. doi:10.1016/j.powtec.2013.11.041

Wang, Q., Yang, H., Wang, P., Lu, J., Liu, Q., Zhang, H., Wei, L., & Zhang, M. (2014b). Application of CPFD method in the simulation of a circulating fluidized bed with a loop seal part II—investigation of solids circulation. *Powder Technology*, *253*, 822–828. doi:10.1016/j.powtec.2013.11.040

Wang, S., Lu, H., Zhao, F., & Liu, G. (2014). CFD studies of dual circulating fluidized bed reactors for chemical looping combustion processes. *Chemical Engineering Journal*, *236*, 121-130. doi:10.1016/j.cej.2013.09.033

Wang, Q., Niemi, T., Peltola, J., Kallio, S., Yang, H., Lu, J., & Wei, L. (2015). Particle size distribution in CPFD modeling of gas–solid flows in a CFB riser. *Particuology*, *21*, 107–117. doi:10.1016/j.partic.2014.06.009

Wang, S., Luo, K., Yang, S., Hu, C., & Fan, J. (2017a) LES-DEM investigation of the time-related solid phase properties and improvements of flow uniformity in a dual-side refeed CFB. *Chemical Engineering Journal*, *313*, 858–872. doi:10.1016/j.cej.2016.10.130

Wang, S., Luo, K., Hu, C., & Fan, J. (2017b). CFD-DEM study of the effect of cyclone arrangements on the gas-solid flow dynamics in the full-loop circulating fluidized bed. *Chemical Engineering Science*, *172*, 199–215. doi:10.1016/j.ces.2017.05.052

Wang, S., Luo, K., Hu, C., Sun, L., & Fan, J. (2018). Effect of superficial gas velocity on solid behaviors in a full-loop CFB. *Powder Technology*, *333*, 91–105. doi:10.1016/j.powtec.2018.04.011

Wen, C. Y., & Yu, Y. H. (1966). Mechanics of fluidization. The Chemical Engineering Progress Symposium Series, 162, 100-111.

Wu, Y., Peng, L. Qin, L., Wang, M., Gao, J., & Lan, X. (2018). Validation and application of CPFD models in simulating hydrodynamics and reactions in riser reactor with Geldart A particles. *Powder Technology*, *323*, 269–283. doi:10.1016/j.powtec.2017.10.003

Xu, Y., Musser, J., Li, T., Gopalan, B., Panday, R., Tucker, J., Breault, G., Clarke, M. A., & Rogers, W. A. (2018). Numerical simulation and experimental study of the gas-solid flow behavior inside a full-loop circulating fluidized bed: evaluation of different drag models. *Ind. Eng. Chem. Res.*, *57*(2), 740–750. doi:10.1021/acs.iecr.7b03817

Verma, V. & Padding, J. T. (2020). A novel approach to MP-PIC: Continuum particle model for dense particle flows in fluidized beds. *Chemical Engineering Science: X*, *6*, 100053. doi:10.1016/j.cesx.2019.100053

Verma, V., Padding, J. T., Deen, N. G., & Kuipers, J. A. M. (2015). Effect of bed size on hydrodynamics in 3-D gas-solid fluidized beds. *AIChE Journal*, *61*(5), 1492–1506. doi:10.1002/aic.14738

Yang, S., Wang, S., Luo, K., Fan, J., & Chew, J. W. (2019). Numerical investigation of the backmixing and non-uniform characteristics in the three-dimensional full-loop circulating fluidized bed combustor with six parallel cyclones. *Applied Thermal Engineering*, *153*, 524–535. doi:10.1016/j.applthermaleng.2019.03.032

Yang, S., & Wang, S. (2020). Eulerian-Langrangian simulation of the full-loop gas-solid hydrodynamics in a pilot-scale circulating fluidized bed. *Powder Technology*, *369*, 223–237. doi:10.1016/j.powtec.2020.05.043

Zhang, N., Lu, B., Wang, W., & Li, J. (2010). 3D CFD simulation of hydrodynamics of a 150MWe circulating fluidized bed boiler. *Chemical Engineering Journal*, *162*(2), 821–828. doi:10.1016/j.cej.2010.06.033

Zhang, Y., Zhao, Y., Lu, L., Ge, W., Wang, J., & Duan, C. (2017) Assessment of polydisperse drag models for the size segregation in a bubbling fluidized bed using discrete particle method. *Chemical Engineering Science*, *160*, 106–112. doi:10.1016/j.ces.2016.11.028

Zhong, W., Yu, A., Zhou, G., Xie, J., & Zhang, H. (2016). CFD simulation of dense particulate reaction system: approaches, recent advances and applications. *Chemical Engineering Science*, *140*, 16–43. doi:10.1016/j.ces.2015.09.035

Zhou, J., Grace, J. R., Qin, S., Brereton, C. M. H., Lim, C. J., & Zhu, J. (1994). Voidage profiles in a circulating fluidized bed of square cross-section. *Chemical Engineering Science*, *49*(19), 3217–3226. doi:10.1016/0009-2509(94)E0125-A

JOURNAL OF SCIENCE

PART A: ENGINEERING AND INNOVATION

Correspondence Address

Gazi University
Graduate School of Natural and Applied Sciences
Emniyet Neighborhood, Bandırma Avenue
No:6/20B, 06560, Yenimahalle - ANKARA
B Block, Auxiliary Building

Yazışma Adresi

Gazi Üniversitesi
Fen Bilimleri Enstitüsü
Emniyet Mahallesi, Bandırma Caddesi
No:6/20B, 06560, Yenimahalle - ANKARA
B Blok, Ek Bina

e-mail | **e-posta**
gujsa06@gmail.com

web page | **web sayfası**
https://dergipark.org.tr/tr/pub/gujsa

e-ISSN 2147-9542